Reconstruction of climate variability
in Central Asia using lake sediments

Dissertation

Zur Erlangung des akademischen Grades

doctor rerum naturalium (Dr. rer. nat.)

vorgelegt dem Rat der Chemisch-Geowissenschaftlichen Fakultät der

Friedrich-Schiller-Universität Jena

von M. Sc. Roman Witt

Geboren am 31.05.1985 in Belzig

Gutachter:

1. apl. Prof. Dr. Gerd Gleixner

2. Prof. Dr. Roland Mäusbacher

Tag der Verteidigung: 25.09.2015

Table of Contents

List of Figures

List of Supplement Figures

List of Tables

List of Supplement Tables

List of Abbreviations

µXRF	micro X-ray Fluorescence
a.s.l.	above sea level
ACA	Arid Central Asia
ACL	Average Chain Length
AD	Anno Domini
AMS	Accelerator Mass Spectrometry
AP	Arboreal Pollen
ASE	Accelerated Solvent Extractor
BP	Before present
CAD	Central Asia Database
cal	calibrated
CK	Chatyr Kol
CPI	Carbon Preference Index
DACP	Dark Ages Cool Period
DJF	December, January, February
dw	dry weight
E/I	Evaporation to Inflow ratio
ELA	Equilibrium Line Altitude
ENSO	El Nino Southern Oscillation
FID	Flame Ionization Detector
GC	Gas-Chromatograph
GI-2	Greenland Interstadial-2
GISP2	Greenland Ice Sheet Project 2
GMWL	Global Meteoric Water Line
GPCC	Global Precipitation Climatology Centre
GRIP	Greenland Ice Core Project
GS-2	Greenland Stadial-2
H-2	Heinrich Event-2
IGRA	Integrated Global Radiosonde Archive
IOSM	Indian Ocean Summer Monsoon
IRMS	Isotope Ratio Mass Spectrometer
IS	Internal Standard
JJA	June, July, August
kyr	kilo years
LCAs	Long-Chain Alkenones
Leaf EL	Leaf Evaporation Line
LEL	Lake Evaporation Line
LGM	Last Glacial Maximum
LIA	Little Ice Age
LMWL	Local Meteoric Water Line
LPAZ	Local Pollen Assemblage Zones
LW	Lake Water
MAM	March, April, May
MAP	Mean Annual Precipitation
MAT	Mean Annual air Temperature
MAutT	Mean Autumn air Temperature
MCA	Medieval Climate Anomaly
MJJ	May, June, July
MRT	Mean Residence Time

MS	Mass Spectrometer
NAO	North Atlantic Oscillation
NAP	Non Arboreal Pollen
NC	Nam Co
NCEP	National Centers for Environmental Prediction
NGRIP	North Greenland Ice Core Project
NOAA	National Oceanic and Atmospheric Administration
NSIDC	National Snow and Ice Data Center
OIPC	Online Isotopes in Precipitation Calculator
OM	Organic Matter
OSC	Organic Sulphur Compounds
PC	Principal Component
PCA	Principal Component Analysis
POM	Particulate Organic Matter
rH	relative Humidity
SAR	Sediment Accumulation Rate
SK	Son Kol
Soil EL	Soil Evaporation Line
SON	September, October, November
SPEI	Standardized Precipitation Evapotranspiration Index
SST	Sea Surface Temperature
SW	Surface Water
TC	Total Carbon
TLE	Total Lipid Extract
TN	Total Nitrogen
TOC	Total Organic Carbon
UK	Unsaturation Ketone index
VPDB	Vienna Pee Dee Belemnite
VSMOW	Vienna Standard Mean Ocean Water
WET	Wet season
$\delta^{13}C_{carb}$	Stable Carbon Isotope Ratio of Carbonates
$\delta^{13}C_{org}$	Stable Carbon Isotope Ratio of Organic Matter
$\delta^{15}N$	Stable Nitrogen Isotope Ratio
$\delta^{18}O$	Stable Oxygen Isotope Ratio
$\delta^{18}O_{carb}$	Stable Oxygen Isotope Ratio of Carbonates
δD	Stable Hydrogen Isotope Ratio (D = Deuterium)

1 General Introduction

1.1 Motivation

Current warming as threat for Central Asian water allocation

One of the major recent problems of human population is the current global warming, seriously impacting the environment, economy and also politics. A focal point is Central Asia, rich in mineral resources but poor in sufficient water supply due to a semiarid to arid climate. The basis of primary care is irrigated agriculture, which exclusively relies on water supply and, therefore, first notices the decreasing water availability during summer. The origin of rivers in Central and High Asia is the world third largest headwater area ("Third Pole") with huge numbers of glaciers, snowfields and lakes located in mountain ranges of the Tian Shan, Pamir, Karakorum, Himalaya and the Tibetan Plateau known as "water towers of Asia". Since river pathways cross borders of several Central Asian countries, they already compete in water, energy (hydropower plants) and development. This issue needs to be addressed soon to prevent potential conflicts in this region and their neighboring countries. The understanding of responses of glacier runoff during summer, variability of precipitation and temperature extremes to climatic change is necessary to educate and support political decisions. In this case, the policymaker relevant IPCC report 2013 predicts "that Northern Hemisphere spring snow cover will decrease during the 21st century as global mean surface temperature rises and global glacier volume will further decrease" (Stocker et al. 2013). Climate change scenarios are still unreliable, with unknown total changes in precipitation and temperature for Central Asia, but changes in precipitation distribution and occurrence of weather extremes are already visible. To optimize future climate predictions and possible environmental reactions globally and particularly in Central Asia, long-term data from the past climate changes, by proxy reconstruction using high-resolution archives are essential.

The general warming trend in Central Asia with the retreat and shrinkage of glacier is observed, but responses of catchments and lakes to changes remain unclear (Unger-Shayesteh et al. 2013). It is supposed that areas influenced by glaciers show less seasonal runoff variability than e.g. rivers without deglaciation influence. Large uncertainties still exist about glacier changes and impact in the Tian Shan and Pamir mountain ranges. The decreasing summer runoff holds massive conflict potential for upstream and downstream countries, which are using Tian Shan meltwater (Sorg et al. 2012). One example of excessive irrigation plus reduced runoff is the progressive desiccation of the Aral Sea since the 1960s (Karthe et al. 2015).

Reconstruction of the Westerlies in Central Asia

A climate parameter tightly connected to temperature is the precipitation, which could be influenced in its amount and seasonal distribution. Climate models perform poorly at Tian Shan and tend to overestimate precipitation (Solomon et al. 2007). Precipitation in form of rain or snow in the Tian Shan strongly depends on the strength and pathway of the Westerly atmospheric circulation system (Chen et al. 2010). As this system naturally interplays with Asian monsoons and the Siberian Anticyclone, changes in its source region lead to fluctuations and shifts in circulation pattern. The Atlantic Ocean is the primary moisture source for the Westerlies, while the Pacific and Indian Ocean are sources for the East and South Asian Monsoon, respectively. They further show ocean-atmospheric teleconnections e.g. North Atlantic Oscillation (NAO) and El Nino Southern Oscillation (ENSO), thus influencing the intensity and dominance of the circulation systems (Hurrell and Deser 2009). These factors hinder a precise climate prediction for Central Asia in a global warming scenario. Moisture variability on short timescales is mainly determined by the combination of North Atlantic sea-surface temperatures (SSTs) and summer insolation; however, impact of secondary feedback mechanisms possibly play another important role.

The mid-latitude Westerlies bring moisture to a lesser fraction directly from the North Atlantic (13 %), and a major fraction recycled via Aral-Caspian basin, eastern Mediterranean and Black Seas (87 %) to the east (Aizen et al. 1997; Aizen et al. 2006). Most of the precipitation at the Tian Shan falls during late spring and summer, when low pressure systems develop over the eastern Mediterranean (Lioubimtseva et al. 2005; Chen et al. 2010). Total amounts are significantly lower compared to the Indian Ocean Summer Monsoon (IOSM) resulting in the term "Arid Central Asia" (ACA). However, regional delivery can be very heterogeneous at spatial and temporal scale. Water transport can reach far east regions like the Mongolian and Tibetan Plateau (Sato et al. 2007), so that the core zone of the westerly-dominated climatic regime was defined between 35°–53°N and 50°–90°E (Huang et al. 2015). It is even assumed that North Atlantic signal prominently penetrated more eastwards during full glacial periods, so reaching the Southern Tibetan Plateau (Günther et al. 2015) and most western Chinese Loess Plateau, because of the steeper meridional thermal gradient (Vandenberghe et al. 2006). Additionally, also the Siberian High became stronger in glacial periods, due to enhanced surface cooling of Eurasia. The westerly mean wind speeds were higher by 60 % in glacial times compared to interglacial ones. The effective moisture in Arid Central Asia during the Holocene, the subsequent period of the Last Glacial, is temporally very inconsistent (Figure 1).
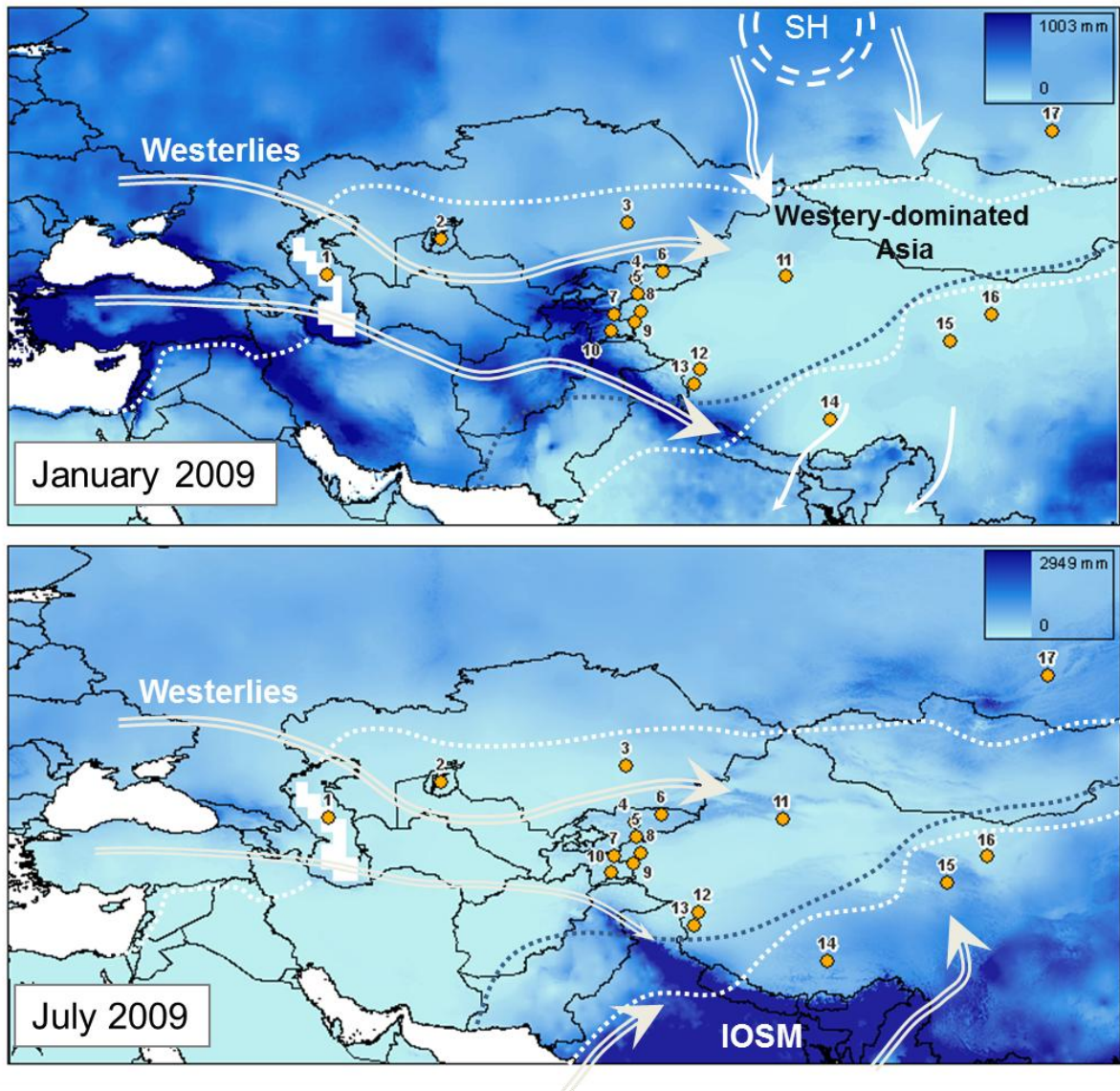
Figure 1: Atmospheric circulation systems influencing Arid Central Asia and the Tibetan Plateau in summer (July) and winter (January) month and mean annual precipitation from 2009 AD.

Precipitation data are provided by CGIAR-CSI (http://www.cgiar-csi.org/data/uea-cru-ts-v3-10-01-historic-climate-database). Palaeoenvironmental records in Asia are marked with IDs and orange circle: (1) Caspian Sea (Rychagov 1997); (2) Aral Sea (Sorrel et al. 2009); (3) Lake Balkash; (4) this study, Lake Son Kol; (5) this study, Lake Chatyr Kol; (6) Lake Issyk Kul (Ricketts et al. 2001); (7) Lake Karakul (Mischke et al. 2010); (8) Kashgar (Zhao et al. 2012); (9) Lake Karakuli (Aichner et al. 2015); (10) Lake Sasi Kul (Lei et al. 2014); (11) Lake Bosten (Wünnemann et al. 2006); (12) Lake Sumxi Co (Vancampo and Gasse 1993); (13) Lake Bangong Co (Gasse et al. 1996); (14) this study, Lake Nam Co; (15) Lake Qinghai (Lister et al. 1991); (16) Lake Zhuyeze (Chen et al. 2006) and (17) Lake Baikal (Tarasov et al. 2009). White arrows indicate air masses (Indian Ocean Summer Monsoon = IOSM; Siberian High = SH); area enclosed by the white dashed line is Westerlies-dominated arid Asia (Huang et al. 2015) and blue dashed line indicates the modern limit of the summer monsoon (Chen et al. 2008).

The relative influence of the main moisture sources for Central Asia (Westerlies and Asian Monsoon) has showed considerable variations in intensity and spatial extent in the past. The international community debate about regional moisture history in ACA and Monsoonal Asia (Herzschuh 2006; Chen et al. 2008; Chen et al. 2010; Ran and Feng 2013) indicating that (1) the "Holocene Thermal Optimum" of monsoonal influenced Tibetan Plateau was reached in the Early Holocene and of Westerlies influenced north-western China during the Mid-Holocene; (2) the "Holocene Moisture Optimum" of the Tibetan Plateau occurred during the Early Holocene, while in Xinjiang (north-west China) at the Late Holocene; (3) during the last 2000 years moisture shows inverse relationship to temperature in ACA. With these insights of asynchronous inter-regional and synchronous intra-ACA moisture changes along a dry Early-, a less dry Mid- and moderately wet Late Holocene, the effective moisture evolution of ACA is seen as "out-of-phase" to monsoonal Asia (Chen et al. 2008).

Climatic and environmental relevant proxies

To understand the seasonal impact of climate change on regional hydrology we have to reduce the uncertainties in climate predictions. As already mentioned, meteorological data would display the ultimate data source, however data collection before their installation in 1890 AD and after breakdown of former Soviet Union in 1991 AD has become complicated in Central Asia. Therefore, alternative long-term high-resolution archives like lacustrine varved sediments, speleothems, tree-rings, ice cores or loess can be utilized for this purpose. Lacustrine sediments from numerous large lakes in the Tian Shan provide detailed information of past changes in their organic matter and mineral composition. Various proxies, recording the relative climate signal have been investigated and successfully used to reconstruct palaeoclimate.

Molecular organic geochemical proxies are increasingly being utilized reviewed by Castaneda and Schouten (2011), with compound-specific isotope analysis using isotope ratio mass spectrometry as one of the newly established methods. The use of leaf wax biomarkers like *n*-alkanes, with a high chemical inertness, insolubility and resistance to biodegradation qualify them as excellent molecular fossil to be used for palaeoclimate investigations. Their simple molecular structure strongly binds carbon and hydrogen atoms, therefore keeping their isotopic content inviolate during time. Since it is known, that the hydrogen-isotopic composition (δD) of terrestrial and aquatic *n*-alkanes records the isotopic signal of their environmental water, they gain increased importance as palaeoclimate proxy (Sachse et al. 2012). Nevertheless, isotopic fractionation between source water and lipid hydrogen is exposed to biochemical, physiological and environmental influences, which has to be understood to clarify interpretations. Environmental factors like temperature, amount and source of precipitation, evapotranspiration or relative humidity clearly modify the δD signal (Sachse et al. 2006; Hou et al. 2008; Polissar and Freeman 2010). The contemplation of terrestrial and aquatic derived signals can qualify the ecosystem

evapotranspiration (Sachse et al. 2006), since terrestrial plants use the meteoric water and aquatic organism the lake water for *n*-alkane biosynthesis. Further investigations raise the possibility to use the isotopic difference to estimate evaporation to inflow ratios and reconstruct water balances (Mügler et al. 2008), but still controversy exist about the type of setting (Aichner et al. 2010b).

Additional information on past lake/sea surface temperature can be determined using the unsaturation ketone index (U^K_{37}) from haptophyte-produced long-chain alkenones (LCAs), one of the oldest organic geochemical proxy (Brassell et al. 1986). The application of a universal temperature calibration is possible in the marine sector (Conte et al. 2006), whereas lacustrine settings need individual calibrations due to unknown haptophyte phylotypes and poor knowledge about how multiple species influence the alkenone variability. Therefore, investigations of (1) the source of alkenones, (2) the proportion of dominant species to the alkenone distribution and (3) the response of haptophyte species to environmental parameters like temperature, salinity and nutrient availability are necessary to create and understand lake-specific LCA calibrations. Some studies reported better correlations of seasonal temperatures rather than mean annual temperatures (Zink et al. 2001; Pearson et al. 2008), which has to be investigated for individual sites with seasonal climate. Since seasonal conditions in lake systems could lead to dramatic changes in boundary conditions for haptophyte productivity and vitality, the preservation and stability of alkenones could also be influenced (Rontani et al. 2013). Few palaeoclimate studies so far investigated alkenones, and even less knowledge is available to interpret past periods of degraded LCA signatures.

To optimize the palaeoenvironmental reconstruction using organism-specific organic compounds, since they are influenced by additional factors and processes, multi-proxy and interdisciplinary investigations should be applied. The additional acquisition of bulk organic and inorganic carbon, oxygen- and nitrogen elemental, isotopic and molecular composition provide evidences of organic matter delivery and accumulation (Meyers 2003). Catchment related minerogenic input to lake systems as well as lake internal precipitation and redox processes inferred from bulk elemental compositions via X-ray Fluorescence scanning (XRF) give further insight into factors influencing the sedimentary record to decipher the limnological history of a lake system. To overcome the problem that certain proxies may record different information at different regions and even lakes, we combined the supporting approach of multi-proxy investigations with multi-location comparisons to strengthen the palaeoenvironmental and palaeoclimatic reconstruction in the heterogeneous Tian Shan region.

Generally, still incomplete understanding exist about (a) the relative distribution of seasonal precipitation (winter/summer) to the regional hydrology, (b) the general role of glaciers to environments and lake systems in case of runoff, water balance and buffering capacity, (c) the teleconnection of dominant climate regimes and their variability in space and time, (d) the past patterns of the Westerlies in ACA and the interplay with Asian monsoons. To

discover these topics long-term high-resolution palaeoclimate records with transfer functions linked to transect and process studies are essential.

1.2 Objectives

This thesis is part of the BMBF funded joint research project CADY "Central Asian climate dynamics" within the research program CAME "Central Asia and Tibet: Monsoon dynamics and geo-ecosystems". This project aims to reconstruct the Holocene climate variability and regional hydrology in Central Asia to provide an overview of seasonality, extreme climate events and teleconnections of Asian atmospheric circulation systems.

The aim of this thesis was to reconstruct and qualify the past changes in the seasonality and isotopic composition of precipitation over the Asian region using lake sediments from Kyrgyzstan. Increasing the number of palaeoclimate records from Kyrgyzstan will help to understand spatial patterns of precipitation and temperature dynamics over Central Asia and neighboring regions like the Tibetan Plateau. Additional information are needed of glacier responses to climate changes to better predict meltwater supply during the current "global warming scenario". Therefore, understanding of past time intervals with similar conditions like Early Holocene warming or deglaciation at the end of the Last Glacial Maximum (LGM) is essential.

I wanted to discuss the following research hypothesis:

1. Regional hydrology during the Holocene was strongly influenced by changes in the intensity and spatial extent of the Westerlies, Siberian High and Asian monsoon.
2. Climate change has strong impact on glaciation and runoff, which could influence limnological and environmental conditions at related aquatic systems.
3. Warming is causing changes in ocean-atmospheric teleconnections and their regional impact.

In detail, my specific objectives are:

1. Evaluate the current hydrological situation of two Kyrgyz lakes using stable oxygen/hydrogen isotopic composition approach.
2. Identify the biological source of lacustrine sedimentary *n*-alkanes as well as source waters for their biosynthesis in Central Kyrgyzstan lake systems.
3. Undertake qualification of climate relevant parameters controlling isotopic composition of *n*-alkanes based on meteorological data.
4. Investigate the applicability of alkenones as palaeoclimate/limnology proxy in Central Asian lakes.
5. Assess the impact of glacier to lacustrine systems and their water isotope fractionation.
6. Identify changes in seasonality/intensity of precipitation with special focus on summer/winter signature in stadial and inter-stadial periods.

7. High resolution reconstruction of past changes in spatial and temporal climate/hydrology variability during the Holocene using lacustrine sediments.
8. Identify spatial and temporal changes in past global teleconnections.

Therefore, an inventory of lake/catchment hydrology during late-summer was accomplished at Lake Son Kol and Chatyr Kol inferred from lake-, inflow-, precipitation-, soil-, plant- and compound-specific sedimentary hydrogen/oxygen isotopic composition data (1). Comparison of *n*-alkane signatures from terrestrial and aquatic plants with lacustrine sediments was carried out to decipher local *n*-alkane sources in the lake systems (2). Subsequently, compound-specific hydrogen isotopic composition from recent surface sediments was directly compared with measured temperature and precipitation data from local meteorological stations to qualify their impact on isotope fractionation (3). Detailed investigations of temperature-sensitive proxies have been performed to characterize their application in continental lake sites (4). The relative influence of glaciers on lake systems was investigated by comparing two lakes on different spatial and temporal scales (5). Recently investigated climate-sensitive proxies were applied on Kyrgyz sedimentary records spanning the Holocene period to reconstruct ancient climate variability (6–8).

1.3 Thesis Organization

The thesis is organized into 10 chapters. The following Chapter 2 explains the general methods in all studies and a detailed description of the sampling sites. Chapter 3 evaluates the surface sediment compound-specific stable hydrogen isotope composition from Kyrgyz Lakes Son Kol and Chatyr Kol with modern observational climate data. Chapter 4 is a peer-reviewed published article in *The Holocene* (Lauterbach et al. 2014) investigating the climatic imprint of the mid-latitude Westerlies in Kyrgyzstan and local climate variability during the last 6000 years inferred from Lake Son Kol sediments. Chapter 5 depicts the entirely Holocene climate variability and consequences on glacier melt and lake level changes using Lake Chatyr Kol sediments. The thesis ends with a synthesis in Chapter 6, a summary in English (Chapter 7) and German (Chapter 8). The references are listed in Chapter 9. An additional manuscript, as part of the supplementary material (Chapter 10) is under revision in the *Journal of Paleolimnology* (Witt et al. 2015) and additionally discusses the influence of the Westerlies at the Tibetan Plateau during the Last Glacial Maximum using Lake Nam Co sediments.

2 Study Sites and Methods

2.1 Study Sites
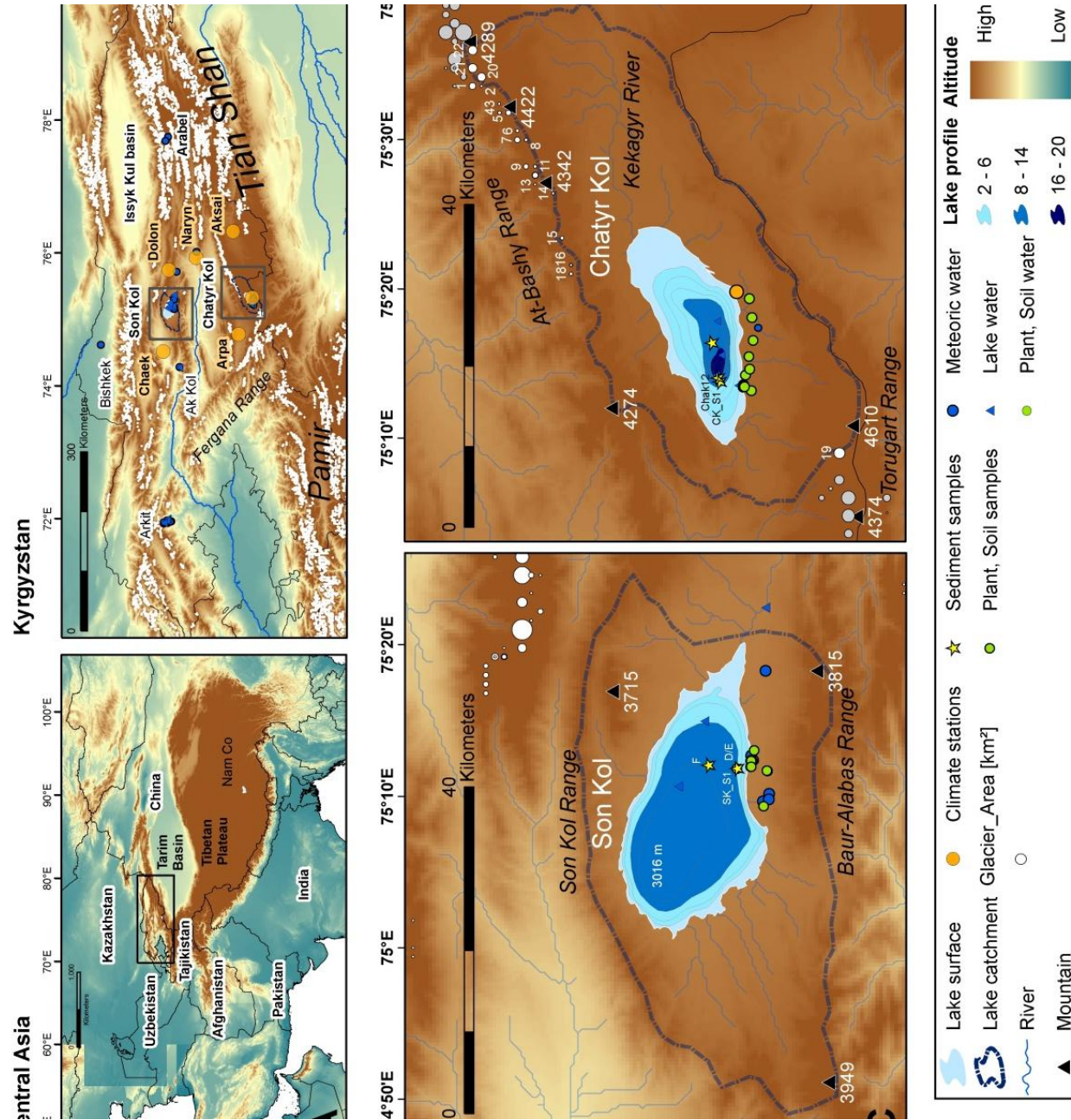
Figure 2: The study region.
Location of Lake Son Kol (C) and Chatyr Kol (D) within the Tian Shan mountain range in Kyrgyzstan (B), Central Asia (A). The lakes include isobaths with corresponding water depth in m below lake surface level after (Romanovsky 2007; Lauterbach et al. 2014). The topographic map of Kyrgyzstan and neighboring countries is based on Digital Elevation Model provided by HydroSHEDS (http://hydrosheds.cr.usgs.gov) (Lehner et al. 2006). Glaciers are marked as white circles, while glaciers influencing the Chatyr Kol catchment are shown as white circles with

specific IDs (Supp. Table 1). They are based on the World Glacier Inventory by WGMS and NSIDC updated 2012. Meteorological stations provided by Central Asia Database (CAD) (Univ. of Idaho at www.sci.uidaho.edu/cae) are marked as orange circles. During field campaigns in 2011/12 AD several plant-, soil- (green circles) and meteoric water samples (blue circles) were taken from the southern catchments. Lake surface- and profile water samples are indicated by blue triangles. Sediment cores are marked by yellow stars.

2.1.1 Lake Son Kol

Lake Son Kol (41°45'32''N–41°55'34''N, 75°1'7''E–75°20'10''E) is located at 3016 m above sea level (a.s.l.) in the Central Tian Shan of Kyrgyzstan, about 80 km northwest of the town Naryn (Figure 1B). The lake is at maximum ~29 km long and ~18 km wide (surface area ~283 km², maximum depth ~13 m) and occupies the central part of an about 60 x 30 km large high-alpine valley (catchment area ~1116 km²). The resulting lake volume is 3.7-times larger for Chatyr Kol (2.28 x 10^9 m³). The catchment is surrounded by the mountains of the Son Kol Range and Baidula Ranges in the north and the Baur-Alabas Range and Moldo Range in the south, reaching elevations of 3800 – 4000 m a.s.l. (Shnitnikov 1980). These mountain ranges are composed of Cambro-Ordovician, Carboniferous and Permian granitoids, gabbros, metamorphites, and sedimentary rocks (De Grave et al. 2011), while the extensive pasture-covered plains around the lake mainly consist of Quaternary erosional material from the mountains. Besides receiving water from groundwater inflow and precipitation on its surface, the lake is predominantly fed by rainfall and snowmelt runoff, provided by several mostly perennial tributaries. The lake is drained by a single outlet at its eastern end, which discharges into the Naryn River and finally into the Syr Darya. The measured salinity in summer 2012 AD was low compared to Chatyr Kol (0.34 g l^{-1}) declaring it as largest fresh water lake in Kyrgyzstan. The heterogeneous spatial distribution of precipitation in the region is clearly displayed by recent data: while at the Dolon station (41°48'N, 75°48'E, 3040 m a.s.l.), about 50 km east of Son Kol, the average annual precipitation amounts to 380 ± 92 mm between 1961 and 1990 AD (National Snow and Ice Data Center (NSIDC) (Williams and Konovalov 2008), it is clearly higher at lake Son Kol itself (500–600 mm) (Academy of Science of the Kyrgyz SSR 1987). Nevertheless, the lowest precipitation appears in DJF with only 5.5 % of the mean annual total precipitation (Figure 3). The highest amount of precipitation is falling in July (21 %) and generally in the summer month (MJJ) with 56 %. Regional water isotope composition (δD, δ^{18}O) of precipitation is more enriched in summer month confirmed by Online Isotopes in Precipitation Calculator (OIPC) data from Dolon station and event sampling in Bishkek (Morris et al. 2006). The local high-alpine climate is characterized by short temperate summers and severely cold winters with snow cover between November and April. The dominance of cold moist Westerlies air masses results in low mean annual air temperatures of -1.6 ± 0.9 °C at Dolon (1961–88 AD, NSIDC) and mean annual relative humidity of 55.4 ± 23 % at Naryn station (1972–80 AD, NOAA IGRA). Own temperature measurements confirm January and July means of about −20 °C and 10 °C, respectively

(Figure 3). Lake water temperature ranges between ~16 °C in summer and 0–2 °C in winter (ice cover usually between October and late April) with almost no vertical variations (< 2 °C) throughout the water column (Figure 5A). Since the surrounding ranges fall below the present equilibrium line altitudes (ELAs), no glaciers occur in the catchment.

Owing to the high altitude and the associated extreme climate conditions, the local vegetation is characterized by montane steppe and meadow communities, dominated by Poaceae (e.g. *Festuca*), *Artemisia*, and alpine elements (e.g. *Gentiana*). Resulting from high grazing pressure, dwarfed individuals of most taxa and grazing-resistant species (e.g. *Leontopodium*) dominate. Local tree-stands (mainly *Picea schrenkiana*) occur only beyond the surrounding mountain ranges up to altitudes of ~3000 m a.s.l. Most of the shore areas are covered by sedge marsh (mainly *Carex* and *Kobresia*), and large parts of the lake bottom down to water depths of at least 7–8 m are covered by submerged macrophytes (e.g. *Myriophyllum*) and algae (e.g. *Chara*).
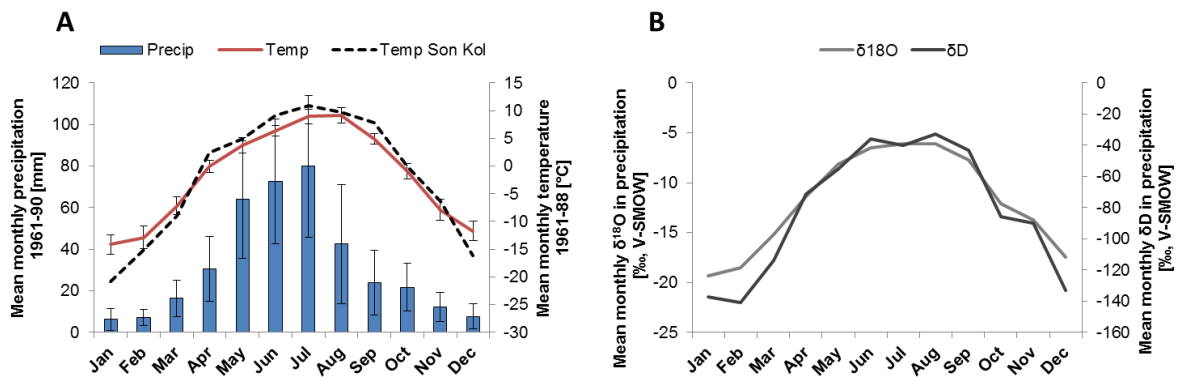
Figure 3: (A) Seasonal variation in mean monthly precipitation amounts (1961–90 AD) and temperatures (1961–88 AD) from the meteorological station "Dolon" (41°48'N, 75°48'E) provided by NSIDC. Black dashed line represents mean monthly air temperature values carried out 2 m above ground surface at a sun-shielded, north facing site at Son Kol between Sep 2011 and July 2012 AD. (B) Calculated mean monthly stable isotope composition ($\delta^{18}O$, δD) in precipitation at 41°N, 75°E and 3545 m altitude provided by the OIPC.

2.1.2   Lake Chatyr Kol

The closed-basin Lake Chatyr Kol (40°34'32''N–40°42'29''N, 75°9'33''E–75°24'4''E) is located in the Southern Tian Shan Mountains of Kyrgyzstan (Central Asia) at 3545 m a.s.l., about 140 km south of Lake Son Kol (Figure 2B). Lake Chatyr Kol has a surface area of 159 km², an expansion of 10–12 km wide and ~23 km length, a maximum depth of 20 m but a more frequently depth of 1–4 m. Thus the water volume is rather small with 0.61 x 10^9 m³, compared to its area. It is surrounded by the At Bashy range (~4600 m) in the north and the Torgurat range (> 4800 m) in the south (continuing north-westward as Fergana range). The closed Chatyr Kol catchment (area 1084 km²) is part of the meso-cenozoic Ak Sai Basin (De Grave et al. 2011). Separated by postglacial formations it is enclosed by basins of the Naryn River (flows into the Aral Sea) in the west and Kokshaal-Tarym (into the Lopnor Lake) in the east (Shnitnikov et al. 1978). The extensive plains around the lake, which are covered by extensive pastures, are composed of Quaternary deposits, consisting of eroded material from the mountain ranges. Lake Chatyr Kol is fed by several, partly perennial, small tributaries and drained by one major inflow (Kekagyr River) at its north-eastern end deliver half of the annual inflow amount. In consideration of the shallow ground in the east, it is clear that the Kekagyr River promotes the most allochthonous material. After Romanovsky (2007) this freshwater supplied area has a lower salinity (0.24 g l^{-1}) than the western deeper area (1.06–1.15 g l^{-1}). The measured salinity in summer 2012 AD in the western area was 1.19 g l^{-1}. The additional inflow is delivered by spring melting of snow and summer storm precipitation, while groundwater has an insignificant proportion. A non-negligible part is coming from the short-term summer thawing of glaciers as a key member of Chatyr Kol's water balance. The recent ELA of the southern Torgurat range is 4340 m, whereas at the northern At Bashy range it is lower at ~4010 m (Koppes et al. 2008). Thus, modern glaciers of both ranges influences Chatyr Kol having total areas between 0.1 and 1.4 km² with mean elevations from 3910 to 4430 m (Supp. Table 2). Generally they are classified as Mountain- and Valley Glaciers with snow as their source of nourishment. Due to the location east of the north-westward Fergana range, moisture delivered mainly by the mid-latitude is strongly blocked and results in very dry conditions at Chatyr Kol. Therefore, the mean annual relative humidity is only 43.5 ± 21.6 % (1971–2011 AD, Kashi station, NOAA IGRA). The resulting northwest to southeast continentality gradient of decreasing precipitation rates and temperatures of Kyrgyzstan makes Chatyr Kol catchment to one of the driest regions. By referring to the meteorological station (Chatyr Kol, 40°36'N, 75°48'E) the mean annual precipitation amounts are 236.5 ± 86.9 mm (1961–90 AD, NSIDC). The general influence of the Siberian Anticyclone in winter, which would decrease the amount of winter precipitation like at the Northern Tian Shan ranges, is not effective at the southern ranges like Ak Sai Basin. Identical to Son Kol, the lowest precipitation appears in DJF with only 5.5 % of the mean annual total precipitation (Figure 4A). The highest amount of precipitation is falling in May, but generally in the summer month (JJA) with 47 %, when unstable atmospheric

stratifications increase (Aizen et al. 1995). Regional water isotope composition (δD, δ^{18}O) of precipitation is more enriched in summer month confirmed by OIPC data on site (Figure 4B). The dominance of cold moist Westerly air masses results in very low mean annual air temperatures of –5.2 ± 0.8 °C at Chatyr Kol, with highest values in July and August (1961–88 AD, NSIDC). Nevertheless, warmer Mid-Holocene conditions must have resulted in higher precipitation and/or meltwater rising the lake level, supported by investigated terraces of a height up to 32 m (Shnitnikov et al. 1978). Lake surface is covered with ice (thickness: 0.25 to 1.5 m) from October to April. Permafrost soils were found at depth between 2 to 3 m (Shnitnikov et al. 1978). Thus the close timing of glacier accumulation in spring/summer and the glacier ablation in summer characterize the glaciers in the Southern Tian Shan as "summer-accumulation type" (Ageta and Higuchi 1984). The cold and dry conditions as well as the high altitude at Chatyr Kol lead to smaller glacier area losses compared to the Northern ranges under current rising temperatures, showing the regional differences in glacier area changes (Narama et al. 2010; Sorg et al. 2012).

Regional climatic conditions and high altitudes determine the desert and semi-desert vegetation (Shnitnikov et al. 1978). Under the dominance of montane grassland no trees can be found (Taft et al. 2011). *Potamogeton* and *Myriophyllum* are the most abundant lake aquatic plants at southern lagoon with < 0.5 m depth. Lake Chatyr Kol is not inhabited by fish, because during winter thick ice cover caused oxygen deficit, which even is relatively low in summer (Figure 5B). Additional CO_2 and H_2S degassing from groundwater and sediment respectively prevent a fish stock. One side effect of missing fish is the large number of amphipoda *Gammarus alius sp. nov.* newly discovered at Chatyr Kol (Sidorov 2012).
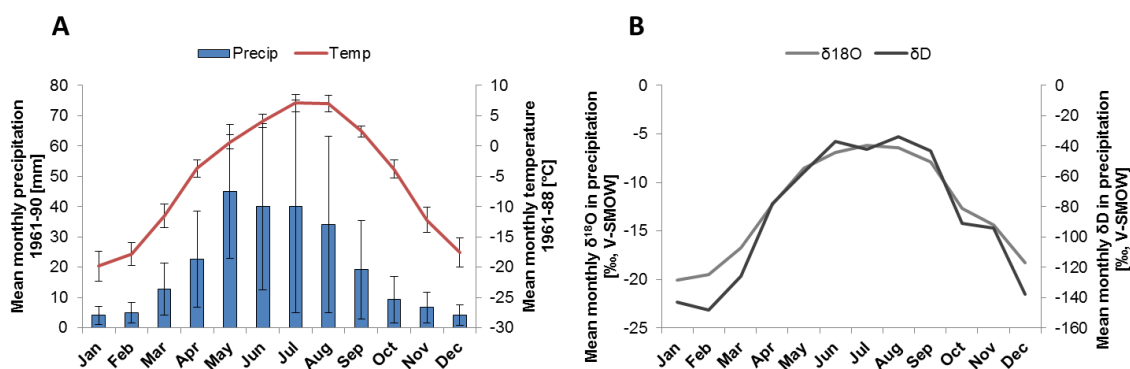
Figure 4: (A) Seasonal variation in mean monthly precipitation amounts (1961–90 AD) and temperatures (1961–88 AD) from the meteorological station "Chatyr Kol" (40°36'N, 75°48'E) provided by NSIDC. (B) Calculated mean monthly stable isotope composition (δ^{18}O, δD) in precipitation at 40°N, 75°E and 3545 m altitude provided by the OIPC.
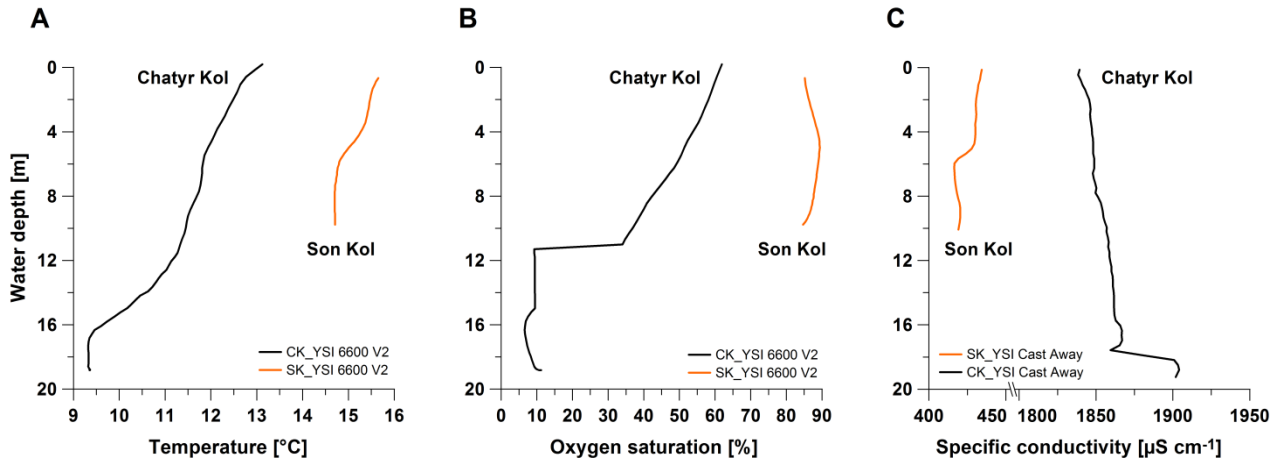
Figure 5: Point measurements of (A) water temperature, (B) water oxygen saturation and (C) water specific conductivity. Data collection was carried out at 23rd July 2012 AD at Chatyr Kol coring site "Chak12_comp2" as well as at 31st July 2012 AD at Son Kol coring site D across the water column by using YSI 6600 V2 and YSI Cast Away CTD multi-parameter water probes.

Table 1: Main physical and climatological characteristics of Lake Chatyr Kol and Son Kol.

	Chatyr Kol	Son Kol
Location	40°37'42"N, 75°17'30"E	41°50'41"N, 75°9'21"E
Altitude [m a.s.l.]	3545	3016[a]
Lake area [km²]	159	283
Catchment area [km²]	1084	1116
Lake/catchment ratio	1 : 6.8	1 : 3.9
Glacier influence	yes	no
Max depth [m]	20	13[a]
Volume [m³]	0.61×10^9	2.28×10^9
Mean residence time [a][b]	2.4	5.3
Mean annual temperature [°C]	-5.2 ± 0.8[c] (Chatyr Kol)	-1.6 ± 0.9[c] (Dolon)
Mean annual precipitation [mm]	236.5 ± 86.9[d] (Chatyr Kol)	382.9 ± 92.35[d] (Dolon)
Mean annual relative humidity [%]	43.5 ± 21.6[e] (Kashi)	55.4 ± 23.1[f] (Naryn)
Specific conductivity [µS cm^{-1}][g]	1860	530
Salinity [g l^{-1}]	1.19	0.34

[a] (Lauterbach et al., 2014).

[b] (Gibson et al., 2002).

[c] (1961-88 AD; NSIDC) Chatyr Kol (40°36'N, 75°48'E), Dolon (41°48'N, 75°48'E).

[d] (1961-90 AD; NSIDC) Chatyr Kol (40°36'N, 75°48'E), Dolon (41°48'N, 75°48'E).

[e] (1971-2011 AD; NOAA IGRA) Kashi (39°28'12"N, 75°58'48"E).

[f] (1972-80 AD; NOAA IGRA) Naryn (41°25'48"N, 76°E).

[g] Measured in July/August 2012 AD.

2.2 Materials and Methods

2.2.1 Fieldwork and Sampling

2.2.1.1 Surface Sediments

Surface sediments (0–5 cm) were collected from 10.5 m water depth ("SK_S1"; 41°47'39''N, 75°11'49''E) at Lake Son Kol and from 20.5 m water depth ("CK_S1"; 40°36'22''N, 75°14'1''E), 20.2 m water depth ("CK_S2"; 40°36'15''N, 75°13'46''E) and 15.4 m water depth ("CK_S3"; 40°36'47''N, 75°16'22''E) at Chatyr Kol using a 90-mm UWITEC gravity corer. Each sample of 1-cm was sliced and packed in plastic bags. For following investigations all sediment samples were freeze dried (P25, Piatkowski, Munich, Germany) and coarse vegetation pieces were removed.

2.2.1.2 Composite profiles from Son Kol

Five gravity cores of about 120–165 cm length were obtained in August 2011 AD from three different sites in the eastern part of Son Kol (D: 41°47'38''N, 75°11'49''E, 10.5 m water depth; E: 41°47'4''N, 75°11'4''E, 11.5 m water depth; F: 41°49'31''N, 75°12'03''E, 12.5 m water depth; (Figure 2) by using a 90-mm UWITEC gravity corer with additional hammer weight. Despite the large distances between the sites and likely associated spatial differences in sediment distribution within the lake basin, all cores reveal a generally similar sediment composition (Figure 6a). As the two cores from site D (SONK_11_D1 and SONK_11_D2), which is located ~2 km off a large fluvial fan at the southern lake shore (

Figure 2C), contained the longest sediment sequence, a ~175-cm-long composite profile (SONK_11_D1/2) was constructed from these cores by correlating them via distinct lithological marker layers (Figure 6b). Following core opening, photographing, and lithostratigraphical description, one half of the composite profile was kept for non-destructive core-scanning analyses, while the second was subsampled for sedimentological, isotopic, (bio)-geochemical, and micro-palaeontological analyses as well as for radiocarbon dating.
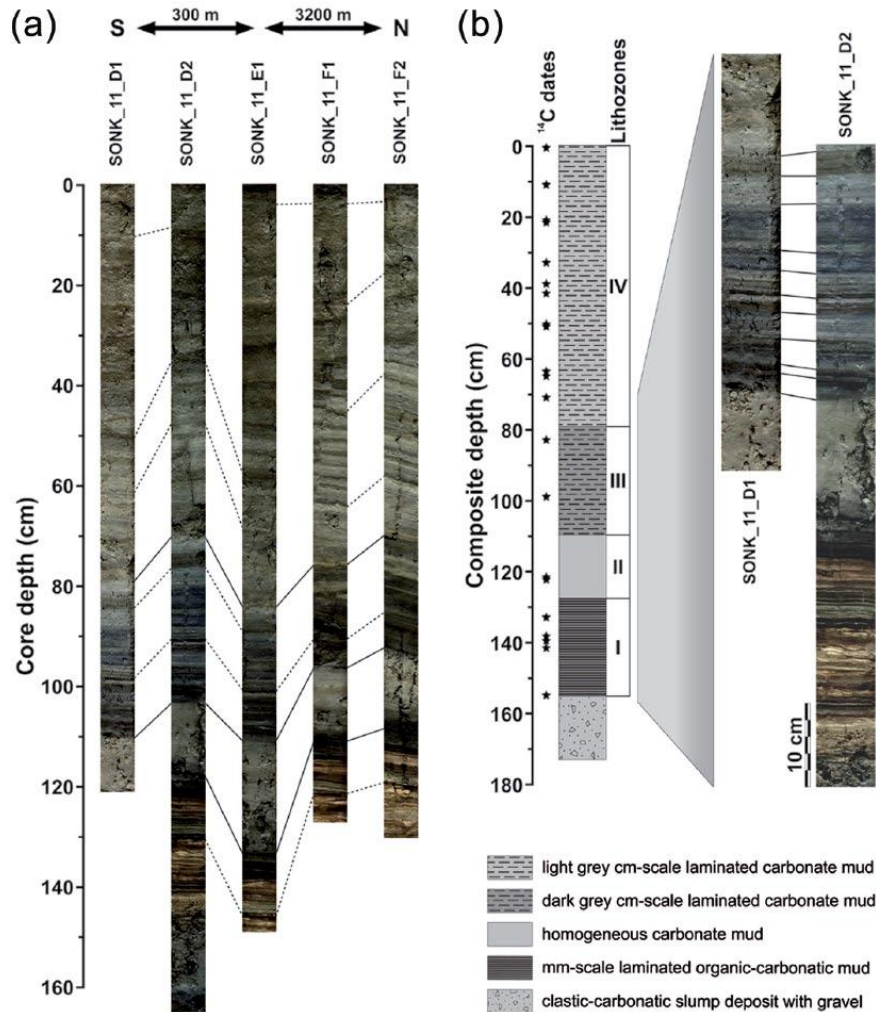
Figure 6: Sediment lithology from Son Kol.
(a) General correlation between the five sediment cores obtained from Son Kol. Solid lines indicate boundaries of major lithostratigraphical units, dashed lines further correlation layers. (b) Schematic lithological profile and corresponding lithostratigraphical units of the composite profile SONK_11_D1/2. Detail photographs of the two sediment cores SONK_11_D1 and SONK_11_D2 illustrate the close agreement between both cores and the correlation through distinct lithological marker layers.

2.2.1.3 Composite profiles from Chatyr Kol

Four overlapping 60 mm piston cores of 6-m length from 20 m water depth were taken in July/August 2012 AD from the deepest south-western part of Chatyr Kol (40°36.37'N, 75°14.02'E). For determination of the deepest lake position an echo-sounder was used. After correlating distinct lithological marker layers of piston cores, the 623.5-cm long composite profile "Chak12_comp2" consisting of eight sub-cores (B2o, B2u, A3o, A3u, B1o, A4o, A2o and A2u) was constructed.
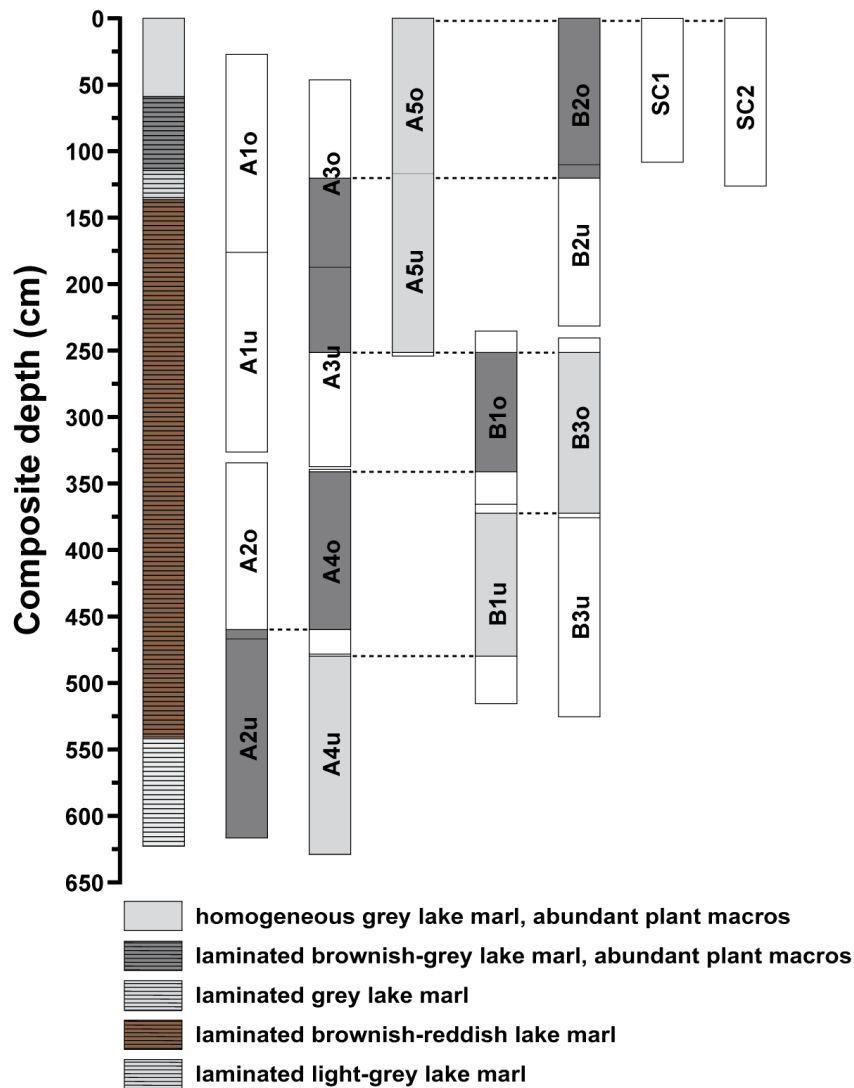
Figure 7: Construction of composite profile "Chak12_Comp2" obtained from Chatyr Kol. Dashed lines indicate connection points between gravity cores (dark grey).

2.2.1.4 Organic matter

To identify the imprint of different types of organic matter (OM) in the lake sediments, several samples of terrestrial and aquatic plants, algae, and dung from different herbivores, representing the digested residue of terrestrial plant material, were collected from the lake and its catchment during field campaigns in summer 2011 and 2012 AD. In addition, several samples of catchment soils were taken from different depth intervals. All samples were air-dried in the field, and soil samples were additionally sieved at 2 mm mesh size.

2.2.1.5 Water

To investigate isotopic composition of different water sources we collected roots, leaves and soil for water extraction in July/August 2012 AD as well as lake surface water, lake profile water, river water and precipitation from rainfall events in August 2011 AD and July/August 2012 AD mainly from Lake Chatyr Kol and Son Kol. Regional water samples from Lake Ak Kol (77 km west of Son Kol), Lake Aram Kol, Lake Irik Kol, Lake Kyle Kol, Lake Sary Chelek and River Arkit (270 km west of Son Kol) as well as River Arabel (210 km east of Son Kol) were collected in June 2012 AD (Figure 2B). Note that these sampling sides are located on the same latitude like Son Kol. Plant compartments like roots and leaves were collected at early afternoon by sampling different individuals of a species. After cutting with scissors they were enclosed in 30-ml screw cap vials (PE) separately and sealed with plastic paraffin film. The ambient soil at 0–5 and 5–10 cm depth was sieved at 2-mm mesh size, enclosed in 30-ml vials and tightly sealed. River-, lake water and precipitation were directly filled in 30-ml vials and sealed without having air bubbles on top.

2.2.2 Radiometric dating

2.2.2.1 Composite profile "Sonk11_D1/2"

In order to establish a chronology for the composite profile from Son Kol, 28 samples of organic material (plant macrofossils, shells, bulk sediment) collected from the sediments as well as from recent algae (

Table **2**) were dated by accelerator mass spectrometry (AMS) ^{14}C dating at the Poznań Radiocarbon Laboratory. The resulting conventional radiocarbon ages were calibrated using OxCal 4.1 (Ramsey 1995, 2001; Ramsey 2009) with the IntCal09 calibration data set (Reimer et al. 2009). To further constrain the chronology, activity measurements for the short-lived radionuclides ^{137}Cs and ^{241}Am were carried out on dried and homogenized sediment samples, taken continuously at 0.5-cm-steps from the uppermost 10 cm of the sediment core. Measurements were conducted by gamma spectrometry using a high-efficiency, low-background well-type germanium detector (Canberra Industries GWC 2522-7500 SL) and processed with the software GENIE 2000 3.0. Counting statistics were

better than 5 % for ^{137}Cs (661 keV) and better than 20 % for ^{241}Am (59.5 keV), except for samples with very low activities (< 0.002 Bq g^{-1} ^{241}Am). The measurement accuracy was validated using the standard reference materials IAEA-384 and IAEA-385, and a correction was applied for filling height (1.3–2.7 cm) and sample weight (0.8–2.0 g). The resulting mean sediment accumulation rate is 0.2 mm yr^{-1} (1 cm = ~41 yr).
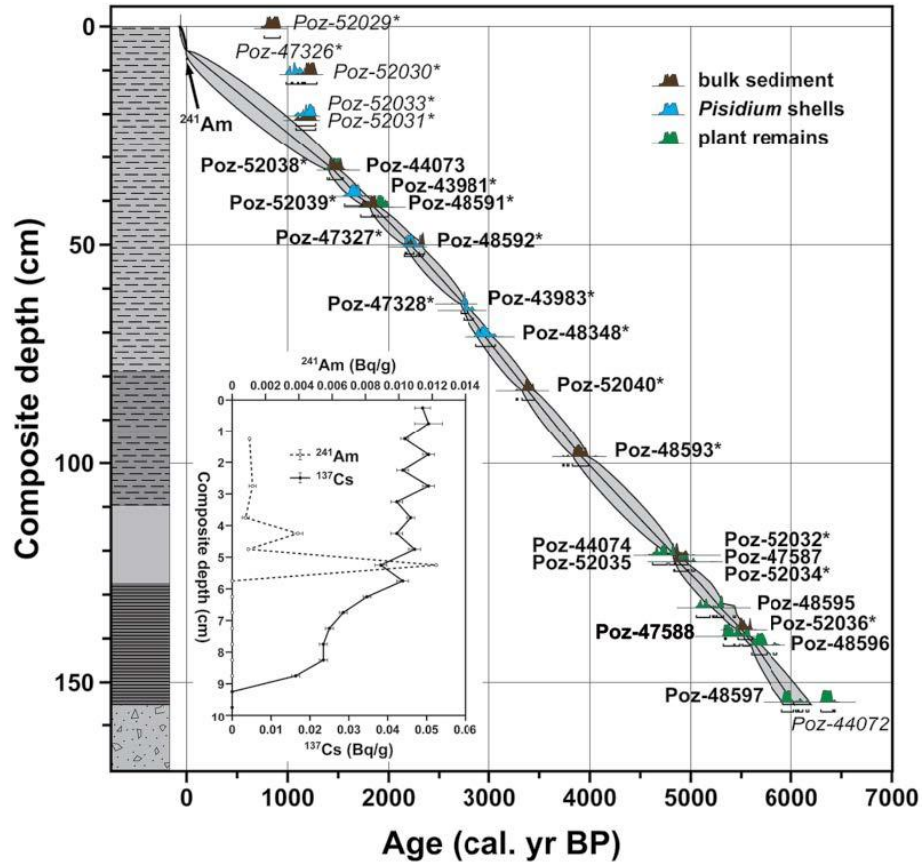
Figure 8: Age model of composite profile SONK_11_D1/2.
Results derived from the P_Sequence depositional model (model parameter k = 2) implemented in OxCal 4.1 (Ramsey 1995, 2001; Ramsey 2008). The solid line between individual radiocarbon dates represents the age model and the grey shading represents the 2σ probability range. Individual AMS ^{14}C dates obtained from bulk sediment OM, Pisidium nitidum shells and terrestrial plant remains are displayed as calibrated 2σ probability functions. Aquatic samples with asterisks were corrected for the hardwater effect prior to calibration and italicized samples were omitted from the age modelling procedure. The inset shows results of ^{137}Cs and ^{241}Am activity measurements on the uppermost 10 cm of the composite profile.

Table 2: AMS ^{14}C dates obtained from macrofossils and bulk sediment OM from composite profile SONK_11_D1/2.
Conventional ^{14}C ages were calibrated using OxCal 4.1 (Ramsey 1995, 2001; Ramsey 2009) with the IntCal09 calibration data set (Reimer et al. 2009). Conventional ^{14}C ages obtained from aquatic material and bulk sediment OM were corrected by -150 years before calibration to consider the hardwater effect. Samples attached with hash (#) were not considered for age modelling.

Sample code		Composite depth [cm]	Dated material	AMS ^{14}C age [yr BP ± σ]	Corr. AMS ^{14}C age [yr BP ± σ]	Calibrated age [cal. yr BP, 2σ]
Poz-47591		–	recent *Chara sp.*	155 ± 30	–	0–285
Poz-53029	#	*0.5*	*bulk sediment*	*1070 ± 30*	*920 ± 30*	*765–923*
Poz-47326	#	*11*	*shells[1]*	*1310 ± 25*	*1160 ± 25*	*983–1172*
Poz-53030	#	*11*	*bulk sediment*	*1420 ± 30*	*1270 ± 30*	*1095–1286*
Poz-52033	#	*20.5*	*shells[1]*	*1400 ± 30*	*1250 ± 30*	*1081–1274*
Poz-53031	#	*21.5*	*bulk sediment*	*1400 ± 30*	*1250 ± 30*	*1081–1274*
Poz-44073		33	terrestrial plant remains[2]	1575 ± 35	–	1389–1537
Poz-52038		33	bulk sediment	1750 ± 30	1600 ± 30	1410–1546
Poz-43981		39	shells[1]	1900 ± 30	1750 ± 30	1561–1734
Poz-48591		41.5	terrestrial plant remains[2]	2120 ± 35	1970 ± 35	1830–1995
Poz-52039		41.5	bulk sediment	2030 ± 35	1880 ± 35	1721–1891
Poz-48592		50	bulk sediment	2430 ± 30	2280 ± 30	2159–2351
Poz-47327		50.5	shells[1]	2385 ± 30	2235 ± 30	2153–2338
Poz-43983		63.5	shells[1]	2760 ± 30	2610 ± 30	2715–2777
Poz-47328		65	shells[1]	2815 ± 35	2665 ± 35	2744–2845
Poz-48348		71	shells[1]	2995 ± 30	2845 ± 30	2870–3063
Poz-52040		83.25	bulk sediment	3305 ± 35	3155 ± 35	3271–3450
Poz-48593		98.5	bulk sediment	3740 ± 35	3590 ± 35	3732–3985
Poz-44074		121	terrestrial plant remains	4200 ± 35	–	4620–4846
Poz-52032		121	bulk sediment	4465 ± 35	4315 ± 35	4835–4969
Poz-47587		122.5	terrestrial plant remains[2]	4340 ± 40	–	4839–5036
Poz-52034		122.5	bulk sediment	4455 ± 35	4305 ± 35	4831–4965
Poz-52035		122.5	terrestrial plant remains	4320 ± 35	–	4836–4971
Poz-48595		133	terrestrial plant remains	4560 ± 35	–	5053–5439
Poz-52036		138	bulk sediment	4950 ± 40	4800 ± 40	5333–5607
Poz-47588		139.5	terrestrial plant remains[2]	4700 ± 40	–	5320–5581
Poz-48596		141.5	terrestrial plant remains[2]	4960 ± 40	–	5600–5858
Poz-48597		154.5	terrestrial plant remains	5220 ± 40	–	5908–6176
Poz-44072	#	154.5	terrestrial plant remains	5580 ± 35	–	6297–6436

[1]*Pisidium nitidum*

[2]Sample with small size (<1 mg C)

2.2.2.2 Composite profile "Chak12_Comp2"

Regarding the still unpublished chronology of Chak12_comp2 sediment, we only present a preliminary age model made from 7 samples of terrestrial plant macrofossils collected from this sediment core (Figure 9). Dating was done with AMS ^{14}C at the Poznan Radiocarbon Laboratory. The investigated core covers a time span of ~11,170 years from 0 to 625.5 cm. The resulting mean sediment accumulation rate is 0.55 mm yr^{-1} (1 cm = 17.87 yr) (Table 3).

Age [cal. yr BP]

y = 0.0557x
R² = 0.988
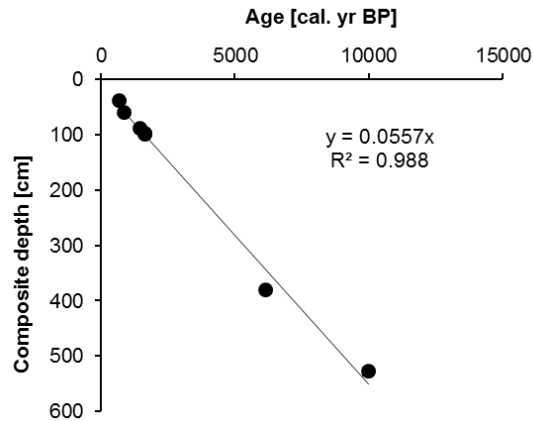
Figure 9: Preliminary age model of the composite profile "Chak12_comp2".
The core from 0 to 625.5 cm includes 7 AMS ^{14}C ages obtained from terrestrial plant remains (Table 3).

Table 3: AMS ^{14}C dates from terrestrial plant remains from composite profile Chak12.

Sample code	Composite depth [cm]	Dated material	AMS ^{14}C age [yr BP ±σ]	Calibrated age [cal. yr BP ±σ]
Poz-54282	38.5	Terrestrial plant remains	755 ± 35	697.5 ± 36
Poz-54283	59.5	Terrestrial plant remains	995 ± 30	881 ± 82
Poz-54286	88	Terrestrial plant remains	1595 ± 30	1479 ± 69
Poz-54284	98	Terrestrial plant remains	1715 ± 35	1629 ± 77
Poz-56614	98.7	Terrestrial plant remains	1730 ± 30	1636 ±72
Poz-63307	380.5	Terrestrial plant remains	5360 ± 40	6140 ± 137
Poz-54302	528	Terrestrial plant remains	8890 ± 50	9988 ± 203

2.2.2.3 Surface Sediments

The determination of calibrated radiocarbon ages for CK_S1 surface sediments was accomplished using the chronology of the composite profiles "Chak12_comp2" from Chatyr Kol based on AMS ^{14}C dates (40°36.37'N, 75°14.02'E, 20 m water depth), whereas the ages for SK_S1 are based on [241]Am dating at "Sonk_11_D1/2" from Son Kol (41°47'3''N, 75°11'4''E, 10.5 m water depth), respectively.

2.2.3 Sediment microfacies

Sediment microfacies analysis was carried out on large-scale petrographic thin sections, prepared according to Brauer et al. (1999), by using a ZEISS Axiophot polarization microscope at 25–400× magnification. High-resolution major element scanning was performed on the foil-covered fresh surface of the split sediment cores by using a vacuum-operating Itrax µXRF core scanner (Croudace et al. 2006) equipped with a Cr x-ray tube (tube voltage 30 kV, tube current 30 mA, 200 µm resolution, 10 s exposure time, single scan line). Measured element intensities (e.g. Ti and K) are reported as counts per 10 s, semi-quantitatively representing relative changes in element concentration. To further characterize the composition of the lake sediments, selected freeze-dried and homogenized samples were analyzed by x-ray diffractometry using a PANalytical Empyrean diffractometer with a Cu Kα x-ray tube operating at 40 kV and 40 mA. Diffraction data were recorded from 5° to 85° (2θ) with a continuous step width of 0.013° (60 s scan time per step) and analyzed with the Rietveld algorithm Autoquan/BGMN (Bergmann et al. 1998).

2.2.4 Pollen and Diatom analyses

For pollen analyses at Senckenberg Research Institute in Weimar, 1 cm^3 sediment samples were taken from the composite profile (average increment 5 cm) and prepared with HCl, KOH, HF, and hot acetolysis mixture, following standard methods (Wright 1986). A defined quantity of *Lycopodium* spores was added to each sample to calculate the pollen concentration as pollen grains per cm^3 dry sediment (Stockmarr 1971). Sample residues were stained with safranin and mounted in glycerine, and on average 1000 terrestrial pollen grains per sample were counted and identified using the reference collection of the Senckenberg Research Station of Quaternary Palaeontology and pollen atlases of Reille (1992) and Beug (2004). Pollen percentages were calculated based on the sum of trees/shrubs (Arboreal Pollen; AP) and herbs (Non Arboreal Pollen; NAP), excluding aquatics and non-pollen palynomorphs. Local pollen assemblage zones (LPAZ) were defined by constrained incremental sum of squares cluster analysis (CONISS) with the software PAST (Hammer et al. 2001).

Diatom sample preparation and determination of concentration were processed following standard procedures at the TU Braunschweig (Kalbe and Werner 1974; Battarbee and Kneen 1982).

2.2.5 Geochemical/isotopic analyses at Son Kol and Chatyr Kol

For geochemical/isotopic analyses, 0.5-cm-thick sediment slices were taken continuously from the composite profile, followed by freeze-drying and homogenization. For analysis of the total organic carbon (TOC) content and the stable carbon isotope ratio of the organic fraction ($\delta^{13}C_{org}$), 1–3 mg sediment were placed in Ag capsules, treated with 20 % HCl at 75 °C, and subsequently processed in a Carlo Erba CN 2500 elemental analyzer coupled to a Finnigan DELTA^{plus}XL isotope ratio mass spectrometer (IRMS) at the GFZ Potsdam. Total nitrogen (TN) content and stable nitrogen isotope ratio ($\delta^{15}N$) measurements were carried out with the same analytical facility (15–50 mg sediment in Sn capsules, no acid treatment). Geochemical and isotopic analyses of plant-, soil- and dung samples were carried out in a similar manner as for the lake sediments with 10–15 mg sample material for TOC, TN, and $\delta^{15}N$ analyses and ~0.5 mg for $\delta^{13}C_{org}$ analyses being used. For all analyzed samples, the TOC and TN contents were used to calculate the atomic C/N ratio. Results of the TOC and TN analyses are expressed as percent of dry weight (dw), while those of the $\delta^{13}C_{org}$ and $\delta^{15}N$ measurements are expressed in the conventional δ-notation relative to the Vienna Pee Dee Belemnite (VPDB) and atmospheric nitrogen (AIR) standards, respectively. Based on repeated measurements of international reference standards relative (IAEA CH-7, N-1, N-2 and USGS-24), the precision of the elemental and isotopic analyses is < 0.2 % and < 0.2 ‰, respectively.

The stable isotope composition of carbonates ($\delta^{13}C$ and $\delta^{18}O$) was determined at the GFZ Potsdam using a Thermo Finnigan GasBench II with carbonate option coupled to a DELTA^{plus}XL mass spectrometer. From each sample, about ~0.5 mg were loaded into 10 ml Labco Exetainervials. After automatically flushing with He, the carbonate samples were reacted in phosphoric acid (100 %) at 75 °C for 60 min, following the analytical procedure described in Spotl and Vennemann (2003). The isotope compositions were given relative to the VPDB standard in the conventional delta notation, and were calibrated against two international reference standards (NBS-19 and NBS-18). The standard deviation (1 sigma) for reference analyses was 0.06 ‰ for $\delta^{13}C$ and 0.08 ‰ for $\delta^{18}O$.

2.2.6 Analyses of sedimentary lipids (*n*-alkanes and alkenones)

To determine the *n*-alkane composition of the lake sediments, 0.3–1.3 g dried and homogenized sediment (sample increment 1 cm) were processed in a DIONEX ASE-200 accelerated solvent extractor, operating at 100 °C and 137 bar for 15 min in two cycles and using a 9:1 (v/v) CH_2Cl_2/CH_3OH solvent mixture. For quantification and loss correction an Internal Standard (IS) of Androstan (50 ng μl^{-1}) was added to the Total Lipid Extract (TLE) prior to chromatography. The TLE was separated into aliphatic, aromatic and polar fractions using solid phase extraction on silica gel (0.040–0.063 mm mesh; Merck, Darmstadt, Germany) according to Rach et al. (2014). The aliphatic fraction containing *n*-alkanes was eluted by adding 12 ml *n*-hexane and subsequently desulphurized by elution

through HCl-activated (15 %) copper. The aromatic fraction containing alkenones and the polar fraction were extracted by using 12 ml of hexane/dichloromethane (1:1, v/v) and 12 ml of dichloromethane/methanol (1:1, v/v), respectively.

Biogeochemical analyses of "Sonk11_D1/2" and "Chak12_comp2" was accomplished using different identification and quantification methods. Therefore, in the following "SK-Method" and "CK-Method" represent the individual methods used for "Sonk11_D1/2" and "Chak12_comp2/surface", respectively.

SK-Method:

n-Alkanes were quantified using a ThermoQuest TRACE GC 2000 gas chromatograph (GC), equipped with a flame ionization detector (FID), Identification was done with an external *n*-alkane standard mixture (*n*-C10 to *n*-C34). The PTV injector was operated in splitless mode with an initial temperature of 45 °C for 0.1 min, then heated up with 14.5 °C s^{-1} to 300 °C and held there for 3 min. The GC oven was held at 90 °C for 1 min, raised with 10 °C min^{-1} to 300 °C, held there for 9 min, and finally heated with 30 °C min^{-1} to 335 °C and held there for 3 min. The helium carrier gas flow was held constant at 2 mL min^{-1}. The FID was operated at 300 °C and with gas flows of 40, 45, and 450 mL min^{-1} for synthetic air, H_2 and N_2, respectively.

CK-Method:

n-Alkanes were quantified and identified using a GC system 7890A interfaced to an Ion Trap MS 220 (both Agilent Technologies, Santa Clara, USA). The GC was operating with a DB-1ms column (30 m length, 0.25 mm ID, 0.25 µm film thickness, Agilent). The PTV-injector in splitless mode had a constant temperature of 250 °C. The initial GC oven temperature of 120 °C was held for 1 min, raised to 325 °C at 5 °C min^{-1}, held there for 10 min and finally increased with 30 °C min^{-1} to 340 °C and held for 3 min. Helium was used as carrier gas at constant flow of 1.3 ml min^{-1}. Mass spectrometer worked in EI-Mode under following operating conditions: transfer line 280 °C, ionization energy 70 eV, emission current 50 µA, 0.7 scans s^{-1}, mass range 50-650 m/z. Sedimentary *n*-alkanes were identified via reference mass spectra and retention times of an external *n*-alkane standard mixture (*n*-C$_{15}$ to *n*-C$_{33}$). The MS Workstation Software "MS Data Review 7.0.1" (Agilent) was used for calibration function with the external *n*-alkane mixture peak areas/amounts (nine different concentration level 5–200 ng µl^{-1}) including external Androstan (constantly 50 ng µl^{-1}) relative to the sample *n*-alkane peak areas/amount with an internal Androstan (50 ng µl^{-1}).

Detection and quantification of alkenones was performed at the University of Glasgow using a GC-MS (QP2010 plus) and GC-FID system (GC-2010, Autosampler AOC-20i; all Shimadzu, Kyoto, Japan). Prior to measurements an internal C$_{37}$ alkane standard was added to the alkenone fraction. The GC-MS and the GC-FID were equipped with a BP1 column (60 m length, 0.25 mm ID, 0.25 µm film thickness, SGE Analytical Science, Melbourne, Australia). The GC-MS oven temperature program was initially held at 60 °C for 2 min,

ramped to 120 °C at 30 °C min^{-1}, then to 340 °C at 3 °C min^{-1} held 20 min. Compound identification was based on m/z values for methyl LCAs. Mass spectrometer worked in EI-Mode. The GC-FID injector in splitless mode was constantly at 340 °C. After injection of 1 µl sample the initial GC oven temperature of 60 °C was held for 2 min, raised to 120 °C at 30 °C min^{-1}, raised to 300 °C at 5 °C min^{-1} and finally increased with 5 °C min^{-1} to 350 °C and held for 10 min. Hydrogen was used as carrier gas at constant flow of 3.3 ml min^{-1} with a pressure of 190.7 kPa. The FID was operated constantly at 350 °C with gas flows of 400, 40 and 30 ml min^{-1}, for synthetic air, H$_2$ and He, respectively. The quantification was based on an external calibration of n-alkane C$_{37}$ having similar properties than LCA and peak areas of the FID.

Alkenone unsaturation indices (U$_{37}^{K}$, U$_{38}^{K}$ and U$_{3738}^{K}$) were calculated after (Brassell et al. 1986) and (Pearson et al. 2008), while % C$_{37:4}$ was calculated after (Rosell-Mele 1998):

$$U_{37}^{K} = ([MeC_{37:2}] - [MeC_{37:4}]) / ([MeC_{37:2}] + [MeC_{37:3}] + [MeC_{37:4}]) \qquad [1]$$

$$U_{37}^{K\prime} = ([MeC_{37:2}]) / ([MeC_{37:2}] + [MeC_{37:3}]) \qquad [2]$$

$$U_{38}^{K} = ([EtC_{38:2}] - [EtC_{38:4}]) / ([EtC_{38:2}] + [EtC_{38:3}] + [EtC_{38:4}]) \qquad [3]$$

$$U_{38}^{K\prime} = ([EtC_{38:2}]) / ([EtC_{38:2}] + [EtC_{38:3}]) \qquad [4]$$

$$U_{3738}^{K} = ([EtC_{38:2}] - [EtC_{38:4}] + [MeC_{37:2}] - [MeC_{37:4}]) / ([EtC_{38:2}] + [EtC_{38:3}] + [EtC_{38:4}] + [MeC_{37:2}] + [MeC_{37:3}] + [MeC_{37:4}]) \qquad [5]$$

$$K37/K38 = ([MeC_{37:4}] + [MeC_{37:3}] + [MeC_{37:2}]) / ([EtC_{38:4}] + [EtC_{38:3}] + [EtC_{38:2}]) \qquad [6]$$

$$\% \ C_{37:4} = [MeC_{37:4}] / ([MeC_{37:2}] + [MeC_{37:3}] + [MeC_{37:4}]) \times 100 \qquad [7]$$

2.2.7 Measurement of n-alkane δD values

SK-Method:

Stable hydrogen isotope ratios of the n-alkane n-C$_{29}$ (δD$_{C29}$) were analyzed using a coupled GC-IRMS system. Samples were injected into an Agilent Technologies HP5890 Series II GC system equipped with a SGE BP1 column (60 m, 0.32 mm ID, 0.50 µm film thickness). The injector was operated at 280 °C in splitless mode. The oven was maintained for 1 min at 60 °C, heated with 10 °C min^{-1} to 300 °C, and held there for 28.5 min. The final ramp heated with 20 °C min^{-1} to 340 °C, where it was held for 3 min. The column flow was constant at 2 mL min^{-1}; 5 % of the gas flow was transferred to a ThermoElectron GCQ ion trap mass spectrometer for identifying mass fragments and 95 % went to a Finnigan DELTAplusXL IRMS. The H$_3^+$ factor was determined daily and stayed constant within the analytical error at 10.78 (SD = 1.61, n = 19) during the measurement period.

CK-Method:

Stable hydrogen isotope ratios (δD) were analyzed using a coupled GC-IRMS system. Samples were injected into a GC system 7890A (Agilent Technologies, Santa Clara, USA) equipped with a BP1 column (60 m, 0.32 mm ID, 0.50 µm film thickness; SGE GmbH, Darmstadt, Germany). The injector was operated at constant temperature of 280 °C in splitless mode. The oven was maintained for 1 min at 110 °C, heated at 5 °C min^{-1} to 320 °C and held for 8 min. The final ramp heated at 30 °C min^{-1} to 350 °C and held for 2 min. The column flow was constant at 1.3 ml min^{-1}. The GC system is linked via GC Isolink and ConFlo IV interface to the isotope ratio mass spectrometer Delta V Plus (Thermo Scientific, Waltham, USA). The H_3^+ factor was determined on a daily basis (4.14 ± 0.24; n = 25). The hydrogen isotope fractionation (ε) between δD values of the product (here: *n*-alkanes) and the source water was calculated using the equation from Günther et al. (2013).

The hydrogen isotope content was determined in triplicate and reported concerning to conventional δ-notation, in per mil [‰] relative to the Vienna Standard Mean Ocean Water (V-SMOW) scale.

$$\delta D \, [‰] = ((D_{sample}/H_{sample})/(D_{standard}/H_{standard}) - 1) \qquad [8]$$

A general offset calculation was accomplished using H_2 reference gas and a standard mixture containing several *n*-alkanes (C_{15} to C_{33}). Drift corrections were applied, determined by standards after every three samples (Werner and Brand 2001).

n-Alkane and Alkenone concentrations are reported in microgram per gram of dry sediment (µg g^{-1} dw), where total *n*-alkane amount is the sum of *n*-C_{17} till *n*-C_{31} and total alkenone amount is the sum of MeC_{37} and EtC_{38}.

Cluster analysis of the sedimentary *n*–alkane and alkenone distribution was performed with the PASW statistics 18 software, using K–means clustering. Resulting Final Cluster Centers composition defined as the mean *n*-alkane/alkenone composition of the individual samples within the same cluster were used to visualize the *n*-alkane as well as alkenone distribution pattern of certain cluster discussed in sediment profiles.

2.2.8   Calculation of evaporation to inflow ratio (E/I)

E/I ratio was calculated to determine the influence of evaporation and water inflows on the water balance of Lake Chatyr Kol and Son Kol. We used water δD and $\delta^{18}O$ values from the spatial surveys in 2011/12 AD, local climate parameters and experimental determined fractionation factors.

Regarding the available parameter, we choose the stable isotope approach by Gat and Levy (1978) to calculate the evaporation/inflow ratio with equation [9].

$$E/I = ((1-h) / h) \times ((\delta D_{LW} - \delta D_{IW}) / (\delta D^* - \delta D_{LW})) \qquad [9]$$

It includes the mean annual relative humidity (h), δD values of the lake water (δD_{LW}) and inflow water (δD_{IW}). The δD value for the water body under local meteorological conditions (δD^*) was calculated using equations in Gat and Levy (1978) and Fritz and Fontes (1980).

If only sedimentary δD values are available, which is the case in our palaeo-hydrological study with sediment cores, we used global transfer functions by Günther et al. (2013) to reconstruct δD_{LW} and δD_{IW} values. Here, n-alkane δD values of sedimentary n-C_{23} represent the isotopic composition of the lake water [10] and δD of sedimentary n-C_{29} represent the inflow water isotopic composition [11].

$$\delta D_{LW} [‰] = 0.582 \times \delta D_{C23} + 38.021 \text{ (global)} \qquad [10]$$

$$\delta D_{IW} [‰] = 1.077 \times \delta D_{C29} + 124.19 \text{ (global)} \qquad [11]$$

2.2.9   Water extraction and determination of $\delta D/\delta^{18}O$

The bulk water extraction of leaves, roots and soils was performed at the Paul Scherrer Institute in Villigen, Switzerland using cryogenic vacuum distillation (Ehleringer et al. 2000). The frozen samples were heated up to 80 °C for 2 h in an evacuated system running with 0.03 mbar, while the evaporated water was collected in glass U-tubes. These were cooled in liquid nitrogen to freeze the water vapor. After extraction, all melted water was transferred into 2-ml microvials.

Water δD and $\delta^{18}O$ of the extracted plant- and soil water (n = 31) as well as river-, lake- and precipitation water (n = 21) from Chatyr Kol and Son Kol were determined using a high-temperature reactor (TC/EA) coupled online via ConFlo III to a Delta$^+$ XL isotope ratio mass spectrometer (Thermo Fisher Scientific, Bremen, Germany) at the Max Planck Institute for Biogeochemistry (Gehre et al. 2004). Water δD and $\delta^{18}O$ from Son Kol samples taken in August 2011 AD (n = 18) were measured at the Alfred Wegener Institute for Polar and Marine Research in Potsdam. The samples were processed in a Finnigan MAT Delta-S IRMS (Thermo Fisher Scientific), following the gas equilibration technique described by Meyer et al. (2000). Results are given relative to the VSMOW standard in the

conventional δ-notation. The analytical precision is < 0.1 ‰ for $\delta^{18}O$ and < 0.5 ‰ for $\delta^{2}H$ measurements.

2.2.10 Meteorological Data

The OIPC reflects global statistical relations between latitude, elevation and $\delta^{18}O/\delta D$ values of precipitation with empirical spatial corrections based on measured values (from waterisotopes.org (Bowen and Revenaugh 2003)). In consequence, this location-specific database provides inter-annual stable isotope distribution of precipitation.

The detection of spatial and temporal climate pattern requires robust and continuous observational data, which are hard to obtain since the number of available stations degraded in Kyrgyzstan from n = 83 in 1985 AD to n = 30 in 2000 AD due to the breakdown of the Soviet Union in 1991 AD (Unger-Shayesteh et al. 2013). Since the distribution of meteorological stations in Kyrgyzstan is inhomogeneous, even the location within the heterogeneous orography complicates the reliability of these data. Six stations (Aksai, Arpa, Chaek, Chatyr Kol, Dolon and Naryn) located in Central Tian Shan close to the investigated lake sites with monthly resolution of temperature and precipitation values within the period 1891–2005 AD were used to average the regional mean annual air temperature (MAT) and mean annual precipitation (MAP) (Table 4). The stations Naryn and Chaek represent intramontaneous valley and basin locations in the Tian Shan, while the category mountain and high mountain regions of different exposition is represented by the stations Dolon, Arpa, Aksai and Chatyr Kol. The closest station representing Lake Chatyr Kol is located within its catchment, while Son Kol`s closest one is the 50 km eastwards located Dolon station.

Additionally, the standardized precipitation evapotranspiration index (SPEI) was used as comparison to measured δD values. The SPEI is based on mean temperature data obtained from the National Oceanic and Atmospheric Administration/National Centers for Environmental Prediction (NOAA NCEP) and monthly precipitation sums obtained from Global Precipitation Climatology Centre (GPCC) and uses the climatic water balance to work as a drought index (Vicente-Serrano et al. 2010; Begueria et al. 2014). The SPEI data were calculated for the 24-month time scale between 1950 AD and 2014 AD using the SPEI Global Drought Monitor (http://sac.csic.es/spei) for the Son Kol area (upper left: 41.25, 76.25; lower right: 42.25, 74.25) and Chatyr Kol area (upper left: 40.25, 76.25; lower right: 41.25, 74.25) including their neighboring climate stations. To evaluate the climate data and the calculated SPEI data, bivariate Pearson correlations were applied within overlapping periods using PASW Software. Correlations marked with "**" and "*" are significant at 0.01 and 0.05 level (2-tailed), respectively.

Table 4: Meteorological stations in the Central Tian Shan close to Lake Son Kol and Chatyr Kol provide long-term terrestrial observational data in weakly resolution of temperature and precipitation (see Figure 2).

Climate Station	Latitude N	Longitude E	Elevation [m a.s.l]	Source	Parameter	Record [Year AD]
Aksai	40.88	76.32	3135	CAD[a]	Temp	1952-1997
Arpa	40.79	74.78	2862	CAD	Temp	1961-1990
				CAD	Precip	1954-1988
Chaek	41.93	74.52	1563	CAD	Temp	1961-2005
				CAD	Precip	1980-2005
Chatyr Kol	40.59	75.33	3540	CAD	Temp	1961-1988
				CAD	Precip	1961-1988
Dolon	41.84	75.75	3040	CAD	Temp	1961-1988
				CAD	Precip	1961-1988
Naryn	41.43	75.93	2039	CAD	Temp	1926-2005
				CAD	Precip	1891-2005

[a] Central Asia Database (provided by Univ. of Idaho at www.sci.uidaho.edu/cae)

3 Modern hydrological situation at mid-latitude Westerlies influenced Lake Chatyr Kol and Son Kol, Kyrgyzstan, Central Asia

3.1 Abstract

Lakes in the Tian Shan Mountains, associated to arid climate under Westerlies influence, have the potential to store palaeoclimate relevant information in their sediments. The lake water isotopic composition, either indirectly recorded in sediment proxies or directly determined retains important information about the lake hydrology and water balance. Thus, interpretation of compound-specific stable hydrogen isotope composition from lacustrine sedimentary records (δD_{C23}, δD_{C29}) requires knowledge about recent hydrology and fractionation processes. Therefore, we investigated the modern isotope hydrology of Kyrgyz lakes Chatyr Kol and Son Kol by determining water isotope composition ($\delta^{18}O$, δD) of recent meteoric-, lake-, plant-, soil- and surface sediment samples. We found, that summer inflow represents a mixture of summer precipitation and snowmelt, and therefore balance out the evaporative enrichment of the lake water. The proportion of glacier and snowfields in a catchment strongly influences the lake water isotopic signal and the response to warming/evaporation. Here, Chatyr Kol with large glacier impact reacts delayed to climate changes than Son Kol without glacier influence, visible in asynchronous E/I ratio since 1975 AD. To evaluate the signal recorded in sedimentary proxies, we correlated compound-specific δD values from Chatyr Kol and Son Kol with meteorological temperature and precipitation data of Kyrgyzstan. Highest correlation was obtained between δD_{C29} and MAT ($r = 0.966$, $p < 0.01$), resulting in the transfer function: MAT [°C] = 0.0437 x δD_{C29} + 10.602, indicating temperature as main driver for terrestrial isotope fractionation in Westerlies controlled arid regions. Since the E/I ratio as combination of δD_{C23} with δD_{C29} correlates best with SPEI, this proxy should be applied in upcoming palaeoclimate applications on the last 100 years.

3.2 Introduction

The Tian Shan Mountain Range with an extension of 1500 km in southwest-northeast direction from Kyrgyzstan to Xinjiang (China) is an essential part of Central Asia's water tower. With more than 6000 modern glaciers and snowfields ranging in altitude from 3000 to > 7000 m, it continuously supplies their surrounding areas with water also during summer periods. As reaction to the India-Eurasia collision 52 to 35 myr ago, intracontinental mountain ranges and intramontane basins were formed in Central Asia (

Figure 2). The Kyrgyz Tian Shan Mountains are located between active structures of the Pamir Block and the Tarim Plate in the South and the stable Kazakhstan Shield in the North (Buslov et al. 2007). As the first orographic and very heterogeneous E-W-trending barrier for south- and eastward moving air masses from Siberia (Siberian anticyclonic circulation) and the North Atlantic Ocean (cyclonic activity), it is characterized by a precipitation and

temperature gradient as well as various grades of storminess from northwest to southeast under continental conditions (Aizen et al. 1997; Aizen et al. 2001). The mid-latitude Westerlies bring moisture to a lesser fraction directly from the North Atlantic (13 %), and a major fraction recycled via Aral-Caspian basin, eastern Mediterranean and Black Seas (87 %) to the west (Aizen et al. 1997; Aizen et al. 2006). In contrast, the Asian summer monsoon does not directly influence the region at present and most likely had only negligible impact since the Mid-Holocene (Cheng et al. 2012). Observations on meteorological stations clearly show significant variations in the seasonal and annual precipitation throughout the Tian Shan owed to orographic effects (Bohner 2006; Narama et al. 2010). This climatic and orographic heterogeneity subdivides the Tian Shan region into four sub-regions with certain characteristic (Aizen et al. 1997). The Western Tian Shan is moderately influenced by the south-western cyclonic circulation and weakly influenced by the Siberian circulation resulting in moist climate with maximum precipitation amounts in spring (March to June) and moderate amounts in autumn and winter (November to February). The Northern Tian Shan has a lower winter precipitation due to strong influence of the Siberian anticyclonic circulation. Its maximum precipitation occurs during spring and summer (April to August). The winter precipitation in the Central and Eastern regions is minimized by its isolation due to surrounding ranges. Most of the precipitation in the area occurs as convective rainfall during summer, driven by moist westerly air masses (Aizen et al. 2001). Recent climate investigations already detected decreasing precipitation amounts in certain regions (Central Kyrgyzstan) from 1961 to 2000 AD, while regional precipitation changes are not consistent (Unger-Shayesteh et al. 2013). Despite study specific uncertainties, temperatures are generally increasing since 1970 AD (Narama et al. 2010), with stronger warming during cold seasons and in lower elevations. Additionally, warming is less pronounced in the Northern Tian Shan (Unger-Shayesteh et al. 2013). In consequence of these climate changes also glaciers in Central Asia retreat, with larger shrinkage in the Northern Tian Shan (Narama et al. 2010; Sorg et al. 2012). Due to the increased air temperatures, the maximum snow depth decreased and the snow cover was reduced (Unger-Shayesteh et al. 2013). The observation of spatial and temporal climate pattern or simply climate changes throughout the Tian Shan requires robust and continuous historical and meteorological climate data. Since these properties are rarely fulfilled in Kyrgyzstan because climate stations recorded earliest in the 1890s AD, alternative long-term proxy data have to be used as input for climate models. Long-term climate reconstructions already exist for Central Asia derived from lacustrine sediments (Ricketts et al. 2001; Mischke et al. 2010; Mathis et al. 2014), tree rings (Esper et al. 2002; Esper et al. 2003; Chen et al. 2013) and speleothems (Cheng et al. 2012). Nevertheless, the evaluation of proxy-data records is essential to understand the processes transforming the climate signals into the proxy. The use of compound-specific stable hydrogen isotopes (δD) in lacustrine sediments especially in the Westerly-influenced Tian Shan is not establishes until today, but was already successfully implemented in multi-proxy approaches on the Tibetan Plateau (Mügler et al. 2010). For correct palaeo-hydrological interpretations of lipid δD values spatial transect studies investigated correlations to environmental variables

influencing the isotopic signal (Sachse et al. 2004; Garcin et al. 2012; Günther et al. 2013). In this study we use sediment cores from two Kyrgyz lakes to compare their compound-specific δD signal with meteorological data to evaluate the reaction of lipids to the local climatic changes in Central Tian Shan on a temporal scale.

3.3 Results

3.3.1 Water isotopic composition (δD, $\delta^{18}O$)

Stable hydrogen and oxygen isotopic composition (δD, $\delta^{18}O$) of Kyrgyz summer meteoric- (river, tap, inflow), precipitation- and lake water samples are plotted against the Global Meteoric Water Line (GMWL, $\delta D = 8 \times \delta^{18}O + 10$ (Craig 1961)) as a Local Meteoric Water Line (LMWL, $\delta D = 7.8 \times \delta^{18}O + 12$; $R^2 = 0.99$) and two Lake Evaporation Lines (LEL) (Figure 10A). The LMWL is close to the GMWL, while the LEL differs from them. Additionally Lake Son Kol (SK) and Chatyr Kol (CK) water samples differ amongst each other due to their individual hydrological character (throughflow vs. terminal), resulting in LEL_{SK}: $\delta D = 5.5 \times \delta^{18}O - 15.25$ ($R^2 = 0.99$) and LEL_{CK}: $\delta D = 5.6 \times \delta^{18}O - 12.4$ ($R^2 = 0.93$). Water isotope values from other lakes (i.g. Ak Kol, Aram Kol, Irik Kol, Kyle Kol and Sary Chelek) located in the Eastern and Western Tian Shan plot on the LMWL, close to the intersection of the LEL. Calculated mean annual precipitation values for Chatyr Kol (–85.9; –12.5 ‰) and Son Kol (–81.6; –11.9 ‰) using the OIPC plot in the same range. OIPC values for July and August show higher values (CK: –38; –6.3 ‰; SK: –36.5; –6.1 ‰) and are close to collected precipitation samples at Son Kol (–28.3; –5.1 ‰) during the July/August campaign in 2012 AD. Precipitation values at Chatyr Kol show higher enrichment (–10.4; –3.2 ‰). By using measured water isotope data from 2011/12 AD the calculated E/I ratios of Son Kol (0.93) and Chatyr Kol (8.07) clearly differ.

Extracted leaf- and soil water values plot on specific Leaf- and Soil Evaporation Lines (Leaf EL, Soil EL) with different slopes in dependency of the lake and its local climatic conditions (Figure 10B). The enrichment of leaf and soil samples from the catchment of Chatyr Kol is generally higher than from Son Kol. The enrichment of leaf water (Chatyr Kol: $\delta D = 2.4 \times \delta^{18}O - 35.8$; $R^2 = 0.81$; Son Kol: $\delta D = 4.4 \times \delta^{18}O - 15.4$; $R^2 = 0.89$) is clearly higher than from soil water (Chatyr Kol: $\delta D = 5.1 \times \delta^{18}O - 32.7$; $R^2 = 0.78$; Son Kol: $\delta D = 5.5 \times \delta^{18}O - 23.2$; $R^2 = 0.96$).
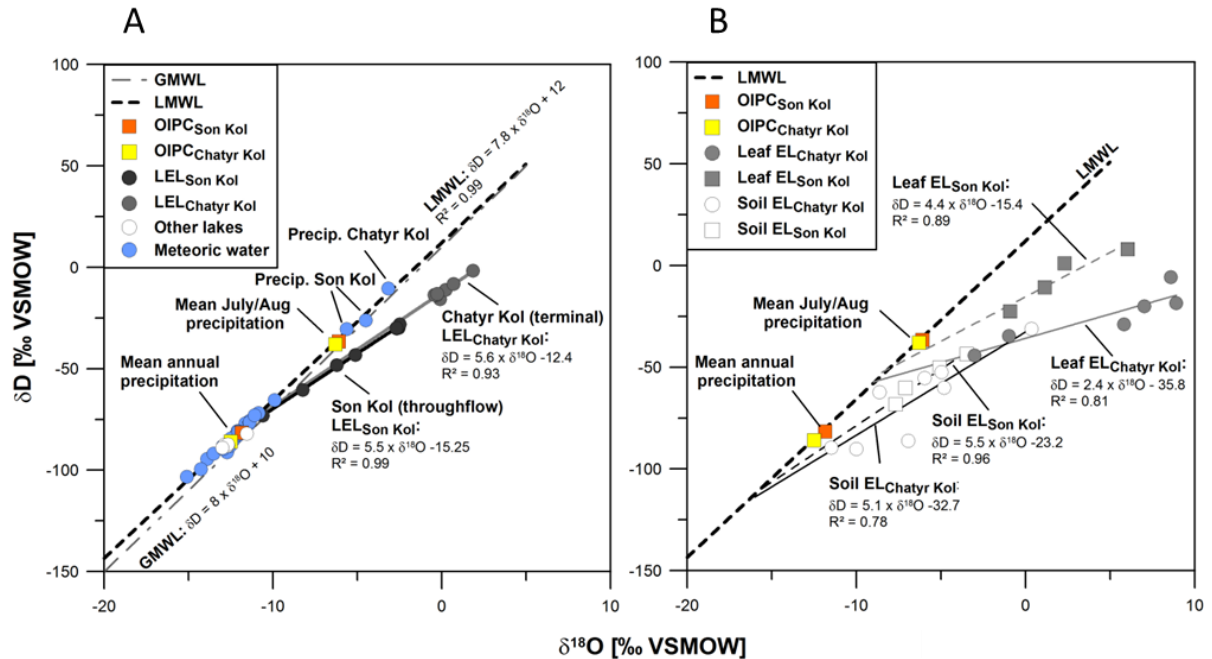
Figure 10: (A) Correlation between δD and δ¹⁸O values for lake-, meteoric- and precipitation water from Kyrgyzstan for September 2011 AD and July/August/September 2012 AD.
The GMWL is plotted as reference (grey dashed line) to the Kyrgyz water isotope composition, forming the LMWL (blue circles/black dashed line). Summer (July/August) and mean annual precipitation values were calculated using the OIPC (orange/yellow squares). LEL include Lake Son Kol (black circles) and Lake Chatyr Kol (grey circles), while other lakes like Ak Kol, Aram Kol, Irik Kol, Kyle Kol and Sary Chelek (white circles) are plotting on the LMWL. (B) Correlation between δD and δ¹⁸O values for extracted soil- and leaf water samples. Values from Chatyr Kol catchment (circles) are generally more enriched than Son Kol catchment values (squares), moreover leaf water values (grey symbols) are more enriched than soil water values (white symbols). Each Lake has its specific Leaf- and Soil Evaporation Lines (Leaf EL, Soil EL).

3.3.2 δD values within lake catchments

Stable hydrogen isotope composition (δD) of meteoric-, lake- and extracted soil-, root- and leaf water samples from Chatyr Kol- and Son Kol catchments are plotted against each other to visualize the different isotopic fractionations between these lake systems (Figure 11). The inflow water at both locations is relatively similar with –77.2 ‰ at Chatyr Kol and –74.9 ‰ at Son Kol. The MAP values, calculated from the intercept of LEL and LMWL (CK: –76.2 ‰; SK: –79.3 ‰), are also close to measured inflow values. Close relation also occur between the deeper soil water (–75.5 ‰) at Chatyr Kol and the MAP as well as inflow values. Following the water isotopic signal from deeper soil via the roots (–65.6 ‰) to the leaves (–25.3 ‰), δD values become stepwise enriched. The upper soil water is slightly depleted in deuterium (–56.3 ‰) compared to the roots. At Son Kol catchment, deeper soil water values show slightly differences to the inflow water (p = 0.17). Here, the water signal cascade shows stepwise enrichment from the deeper soil (–64.3 ‰), to the

upper soil (−46.9 ‰) via roots (−28.1 ‰) to the leaves (−6 ‰). After biosynthetic fractionation compound specific δD values of n-alkanes C_{23} in aquatic plant leaves (SK: −194.2 ‰) and C_{29} in terrestrial plant leaves (SK: −136.2 ‰) as well as their sedimentary organic matter from 1–5 cm depth (SK_S1: n-C_{23} −114.9 ‰; n-C_{29} −185.4 ‰, CK_S1: n-C_{23} −133.5 ‰; n-C_{29} −190 ‰) are highly depleted. Compound-specific isotope enrichment (ΔδD$_{C29-C23}$) in the sediments vary during the core profiles ranging at Chatyr Kol from −50 to −66 ‰ (mean: −56.5 ‰) and at Son Kol between −62 and −80 ‰ (mean: −65.5 ‰). Comparing lake water- and meteoric water values, they are similar within each location. At Chatyr Kol δD values of the lake water (−11 ‰) and the meteoric water (−10.4 ‰) have the highest enrichment of all catchment samples. However at Son Kol, δD values of the lake water (−34.8 ‰) and the meteoric water (−28.3 ‰) are comparably more depleted.
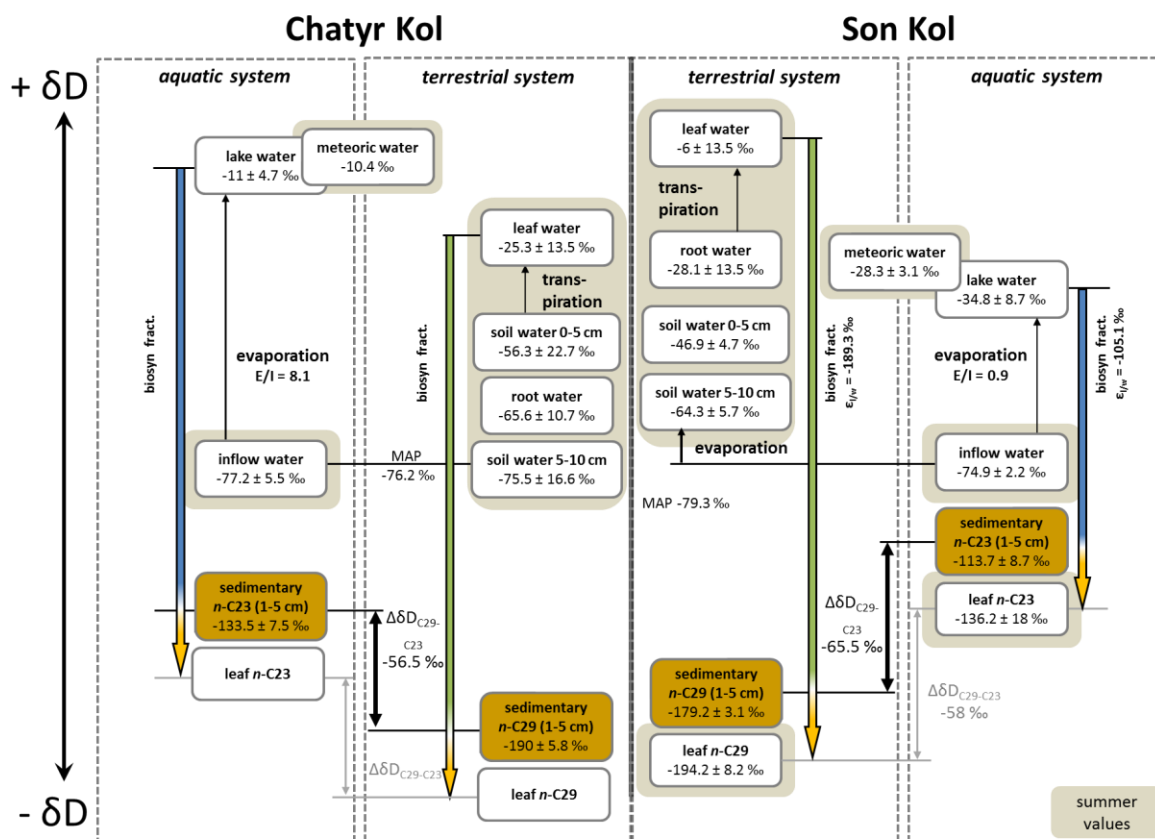
Figure 11: Stable hydrogen isotope relationship between source water and n-alkanes from aquatic and terrestrial systems at Lake Chatyr Kol and Son Kol.

Summer values from 2012 AD are shown with a grey background. Biosynthetic fractionation (biosyn fract.) describes the change from source water for alkane synthesis to their leaf products. The difference between terrestrial C_{29} alkane and aquatic C_{23} alkane (ΔδD$_{C29-C23}$) in lacustrine sediments displays the ecosystem evapotranspiration. δD values represent the averages from several combined samples. Figure is not to scale.

3.3.3 Alkane distribution of surface sediments

Surface sediment samples from Lake Chatyr Kol and Son Kol differ in their *n*-alkane distribution and concentration. The odd mid-chain *n*-alkanes C_{23} and C_{25} as well as the odd long-chain *n*-C_{27}, *n*-C_{29} and *n*-C_{31} dominate the Chatyr Kol alkane distribution with highest amounts for *n*-C_{23} (4.7 ± 1.1 µg g^{-1} dw) and *n*-C_{29} (5.8 ± 1.5 µg g^{-1} dw). In contrast, the distribution in Lake Son Kol surface sediments is dominated in first order by the short-chain *n*-C_{17} (20.8 ± 5.2 µg g^{-1} dw) and in second order by the long-chain *n*-C_{29} and *n*-C_{31} ($12 \pm 2.6/2.7$ µg g^{-1} dw, respectively). In consequence, the general concentrations in Son Kol samples are 2.5-times higher than in Chatyr Kol.
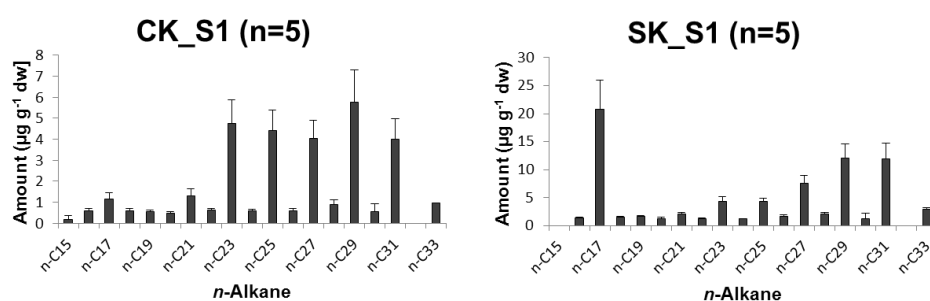
Figure 12: Distribution and amounts of *n*-alkanes in surface sediment samples at Chatyr Kol (CK_S1) and Son Kol (SK_S1). Error bars represent the standard deviation between short-core samples (n = 5).

3.3.4 Compound specific δD values of surface sediments

Isotope composition of surface sediments CK_S1 and SK_S1 reveal lake and catchment information. Surface sediment δD values of mid-chain *n*-alkanes C_{23} are generally more enriched compared to the long-chain *n*-alkanes C_{29} independent from lake-specific characteristics (Figure 13A). Nevertheless, the pattern became asynchronous after 1975 AD, resulting in different $\Delta\delta D_{C29-C23}$ values (Figure 13B) and E/I ratios (Figure 13C). From 1954 to 1975 AD the isotope difference between mid-and long-chain *n*-alkanes remains constant, while until today at Chatyr Kol the trend is going to smaller differences ($\Delta\delta D_{C29-C23}$ values became more positive), while at Son Kol it is reverse with decreasing trend to more negative $\varepsilon_{C29-C23}$ values. Since $\Delta\delta D_{C29-C23}$ and E/I represent the isotope difference of C_{29} and C_{23}, their correlation is significantly high (r = –0.99**). However, the calculation of E/I additionally includes lake-specific factors and therefore represents a more detailed pattern, Son Kol had a lower E/I ratio until 1984 AD. Responsible for the opposite behavior are the mid-chain *n*-alkanes C_{23}, while C_{29} remain rather synchronous. Both lakes have an identical mean E/I ratio of 1.36 between 1937 and 2008 AD.
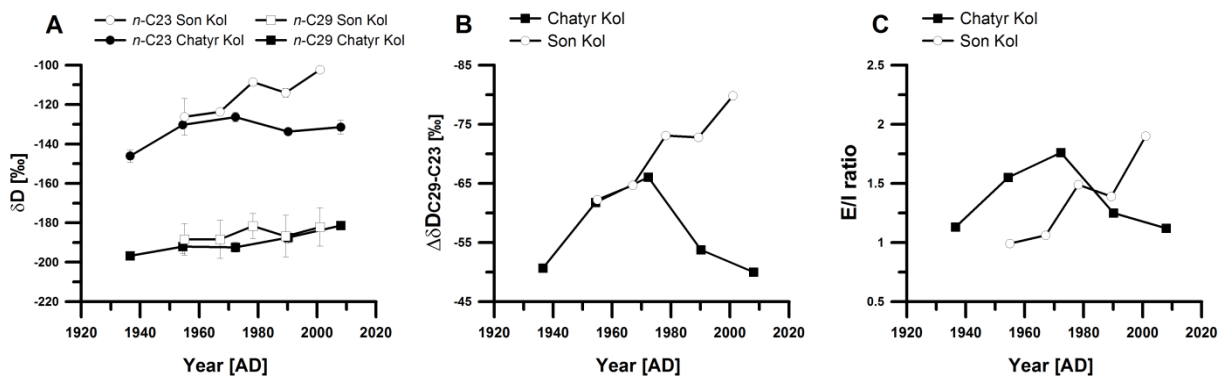
Figure 13: Age-profile of surface sediment cores reveal different compound specific δD values of surface sediments at Chatyr Kol (CK_S1) and Son Kol (SK_S1).
(A) Mid- and long-chain *n*-alkanes C_{23} and C_{29} have a general clear separation in both lakes. (B) Isotope difference between *n*-alkanes visualized as $\Delta\delta D_{C29-C23}$ values shows lake specific separation after 1975 AD resulting in more depleted values at Son Kol. (C) The calculated E/I ratio disclosed a lake separation at 1984 AD resulting in higher evaporation at Son Kol.

Table 5: Compound-specific δD values within short core SK_S1 (Son Kol) and CK_S1 (Chatyr Kol) and their calculated $\Delta\delta D_{C29-C23}$ and E/I values.

Sample	Depth [cm]	Year [AD]	δD_{C23} MW [‰]	Std [‰]	δD_{C29} MW [‰]	Std [‰]	$\Delta\delta D_{C29-C23}$ [‰]	E/I
SK_S1	1	2001	-102	5	-182	4	-80	1.9
SK_S1	2	1989	-114	8	-187	1	-73	1.4
SK_S1	3	1978	-109	7	-182	3	-73	1.5
SK_S1	4	1967	-124	8	-188	1	-65	1.1
SK_S1	5	1955	-126	3	-188	2	-62	1.0
SK_S1	**Mean**		**-114**		**-179**		**-65**	**1.4**
	Std		**9**		**3**		**7**	
CK_S1	1	2008	-131	3	-181	1	-50	1.1
CK_S1	2	1990	-134	0.5	-187	3	-54	1.3
CK_S1	3	1972	-126	3	-192	2	-66	1.8
CK_S1	4	1954	-130	1	-192	3	-62	1.6
CK_S1	5	1937	-146	3	-197	2	-51	1.1
CK_S1	**Mean**		**-134**		**-190**		**-56**	**1.4**
	Std		**7**		**6**		**7**	

3.3.5 Geochemical/isotopic composition ($\delta^{13}C_{org}$, TOC and TN) of catchment samples

Soils reveal a characteristic geochemical/ isotopic signature with $\delta^{13}C_{org}$ of −24.3 ± 0.7 ‰ (SK) and −23 ± 1.1 ‰ (CK) and C/N ratios of 11.5 ± 1.4 (SK) and 6.9 ± 1.5. In contrast, modern terrestrial plants show comparatively low $\delta^{13}C_{org}$ values (SK: −26.9 ± 2.2 ‰, CK: − 26.2 ± 1.9 ‰), but clearly higher C/N ratios (SK: 35.3 ± 15.8, CK: 17.4 ± 6.9). Animal dung is characterized by $\delta^{13}C_{org}$ ranges between their source material (SK: −27.7 ± 0.3 ‰, CK: −27.1 ± 1.3 ‰) as well as C/N ratios (SK: 26.5 ± 2.1, CK: 29.1 ± 9.2). Submerged aquatic macrophytes and algae reveal relatively low C/N ratios (SK: 20.4 ± 6, CK: 19.4 ± 8) similar to the terrestrial material, but overall higher $\delta^{13}C_{org}$ values (SK: − 15 ± 3.5 ‰, CK: −11 ± 1.3 ‰) clearly separate them from other materials.
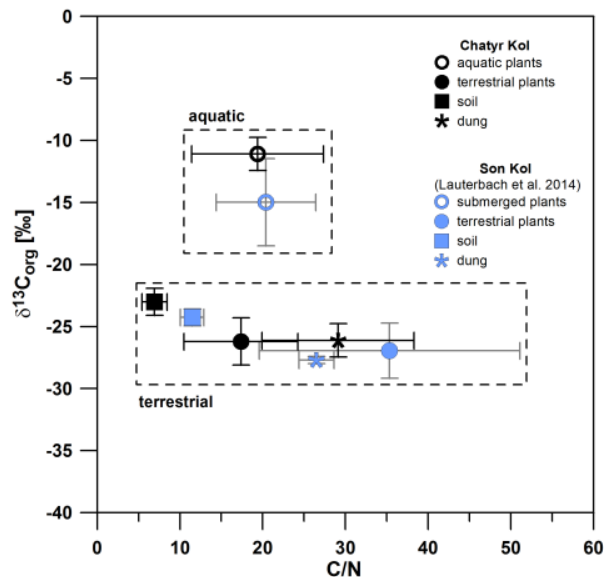
Figure 14: Sources of organic matter according to the $\delta^{13}C_{org}$ composition and C/N ratio from Chatyr Kol and Son Kol (Lauterbach et al. 2014).

3.3.6 Climatological analysis

3.3.6.1 Mean annual and seasonal meteorological data

We present long-term meteorological data from Kyrgyz climate stations between 1891 and 2005 AD (Figure 15). The longest and most continuous MAP record since 1891 AD and MAT record since 1926 AD is provided by the station Naryn.

The observation disclosed a positive linear trend of the MAT since 1950 AD with a warming of +0.38 °C per decade (Figure 15A). Since the data availability at the other sites is not sufficient or their individual locations/altitudes reduce the climate sensitivity, general temperature trends are not recognizable at Chatyr Kol, Arpa and Aksai or they are smaller

at Dolon and Chaek compared to Naryn. Therefore, Naryn`s correlation with Chaek (r = 0.7**) is significantly high, while with Aksai (r = 0.4**) and Dolon (r = 0.4*) is smaller but still significant (Figure 16B). On seasonal level temperature changes during winter month were higher compared to summer month.

The correlations of Naryn MAP with Arpa (r = 0.73**), Chatyr Kol (r = 0.78**), Chaek (r = 0.72**) and Dolon (r = 0.53**) are significantly high (Figure 15B). Assuming Naryn climate station as the representative dataset for Central Kyrgyzstan (Inner Tian Shan), the long-term precipitation record from 1891 to 2005 AD reveals irregular cyclic variations and a rather negligible general increasing trend depending on the time-interval (+4.6 mm per decade). Conspicuously, from 1891 to 1950 AD the precipitation shows an increasing trend with +6.3 mm per decade. On short-term scales this time series exhibit very strong shifts from either positive or negative trends. With a cyclicity of ~40 years for increasing trends and ~20 years for decreasing trends, the turning points were reached at 1917, 1954 and 1975 AD. Since the dataset does not extend until today, the increasing trend did not reach its turning point so far. Considering also neighboring climate stations, the relative short-term precipitation changes are synchronous and therefore independent from elevation. Nevertheless, the absolute amounts of mean precipitation calculated for the time-interval 1980 to 1988 AD vary depending on elevation and exposition (Figure 15B).
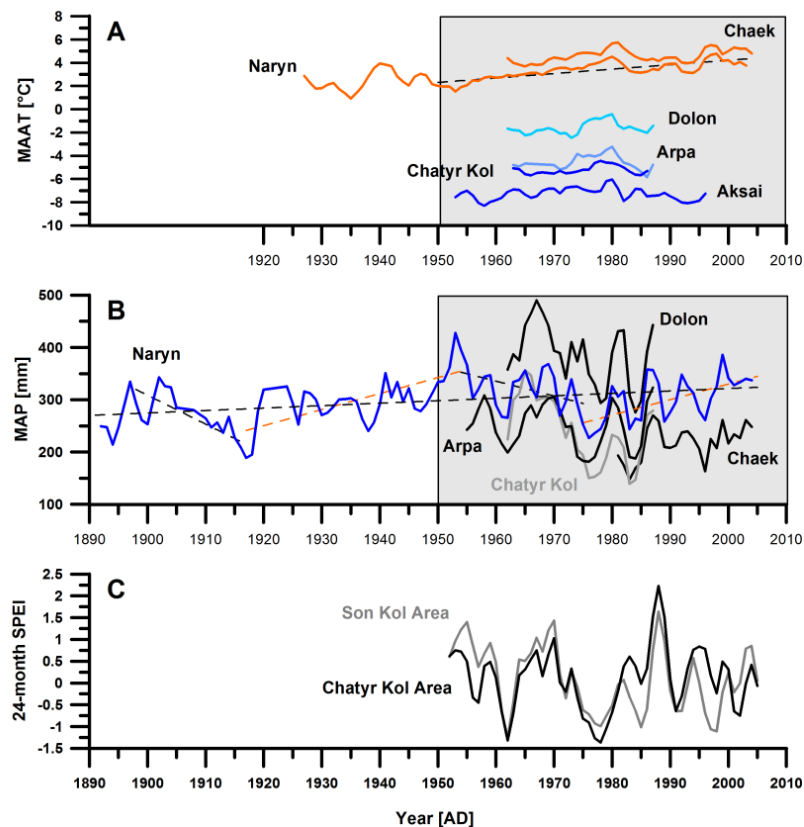
Figure 15: Time series of meteorological data from six climate stations (Aksai, Arpa, Chaek, Chatyr Kol, Dolon and Naryn) in Central Tian Shan provided by the University of Idaho in the CAD.

(A) Records for the mean annual air temperature between 1926 and 2005 AD reveal altitude dependent absolute values with warming trends since 1950 AD only at lower altitudes (e.g. Naryn) (dashed line). (B) Long-term records of the mean annual precipitation between 1891 and 2005 AD are synchronous, but different in absolute amounts due to altitude and exposition. (C) The SPEI calculated for the 24-month time scale at Son Kol and Chatyr Kol area is different in some periods and available using the SPEI Global Drought Monitor (http://sac.csic.es/spei). Grey boxes represent time frame of interest for correlation with SPEI data.
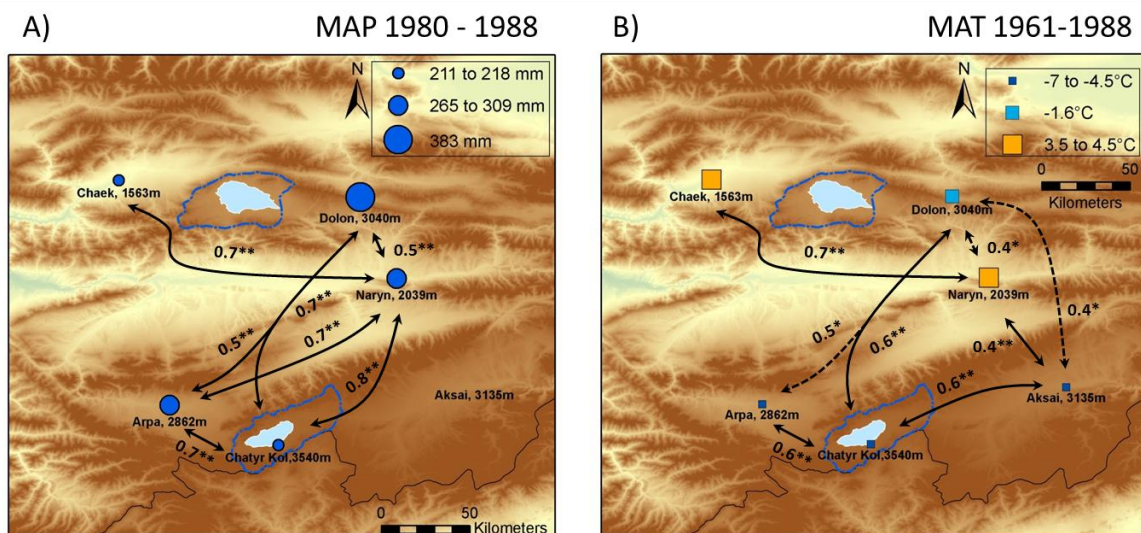
Figure 16: Correlations of precipitation and temperature climatic data visualized in relation to geographical location of source stations. Observational data from the CAD for 6 meteorological stations with different (A) mean annual precipitation (MAP) values between 1980 and 1988 AD (circles) and (B) mean annual air temperature (MAT) values between 1961 and 1988 AD (squares). All shown correlations (black arrows) between the datasets in the period 1891 until 2005 AD are significant at 0.01 level (**) or 0.05 level (*) (2-tailed) using the Pearson (r) bivariate correlation.

3.3.6.2 Correlation of sedimentary δD values with temperature

The MAT at the station Naryn shows positive correlations with the hydrogen isotope composition of the long-chain n-alkane C_{29} from Son Kol surface sediments SK_S1 (r = 0.85*) and Sonk11 D1/2 (r = 0.966**) and Chatyr Kol surface sediments CK_S1 (r = 0.83). Here, δD_{C29} from Son Kol follows short-term MAT values, while δD_{C29} from Chatyr Kol rather follows the long-term trends (Figure 17A). After using seasonal temperature values for winter (DJF), spring (MAM), summer (JJA) and autumn (SON) we calculated different patterns for both lake sediments. The SK_S1 δD_{C29} values are highly correlated with Naryn temperatures in the winter (r = 0.86), spring (r = 0.8) and summer (r = 0.8) season. On the other hand, CK_S1 is only highly correlated with winter (r = 0.85) and autumn (r = 0.9*). Interestingly, the mid-chain n-alkane C_{23} also shows high correlations with the seasonal temperatures at Naryn. At SK_S1 the winter- (r = 0.95*),

summer- (r = 0.87) and autumn (r = 0.88*) temperatures are higher correlated to δD_{C23} than for δD_{C29}. At CK_S1 only the spring temperature (r = 0.8) has a high correlation coefficient with δD_{C23}. Resulting from these correlations, the calculated isotope difference between mid- and long-chain *n*-alkanes ($\Delta\delta D_{C29-C23}$) and Naryn MAT correlates highly significant only at Son Kol (SK_S1; r = –0.92*).

3.3.6.3 Correlation of sedimentary δD values with precipitation

The mean annual precipitation data of Naryn generally show no significant correlation with any δD data. However, the mean precipitation during the WET season (April to August) is significantly correlated with CK_S1 δD_{C29} values (r = 0.9*). Also δD_{C29} values from Son Kol obviously following the WET season precipitation trend, but here the influence by MAT between 1925 and 2001 AD is more apparent (r = 0.8* to 0.97**). Since δD_{C23} data are synchronous with C_{29} at Son Kol, trend correlations with MAT and WET precipitation from Naryn are detected. Regarding the C_{23} isotope composition of Chatyr Kol, other factors possibly lead to a lower correlation (r = 0.6) since 1970 AD.
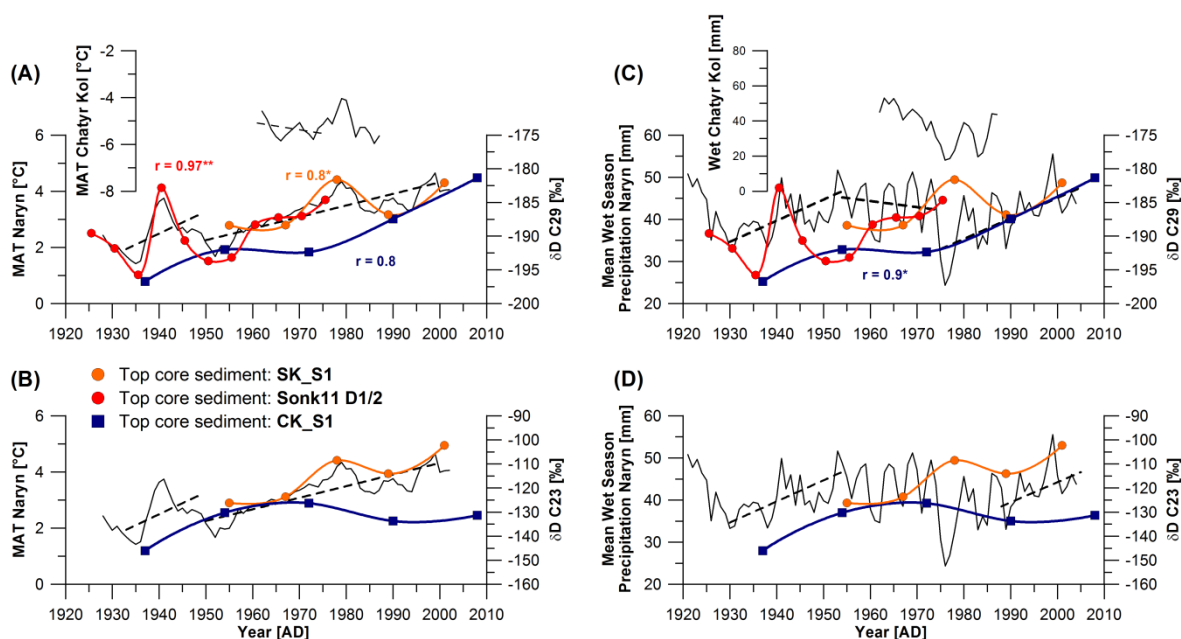
Figure 17: Correlation of measured surface sediment compound-specific stable hydrogen data (δD_{C23}, δD_{C29}) from Son Kol (SK_S1, Sonk11_D1/2) and Chatyr Kol (CK_S1) with meteorological temperature and precipitation data provided by CAD. (A) δD_{C29} values of CK and SK significantly correlate with Naryn MAT. (B) δD_{C23} values rather follow linear trends of Naryn MAT. (C) δD_{C29} values of CK and SK correlate with mean WET season precipitation from Naryn. (D) δD_{C23} values against Naryn WET precipitation show limited correlation at trends.

3.3.6.4 Correlation of sedimentary δD values with SPEI

Since the SPEI uses regional measured temperature and precipitation data as source for the drought intensity calculation, correlations with δD_{C29} values from both cores are negative but as significantly high (SK: $r = -0.8$; CK: $r = -0.92^*$) as with MAT and WET precipitation of Naryn (Figure 18A). On the other hand, SPEI could also be used to explain opposite behavior of δD_{C23} values. The use of local SPEI (SK, CK) seems to be helpful, because they differ in their drought intensity especially between 1970 and 1990 AD. Here, δD_{C23} follow the negative excursion of the SPEI from Son Kol area. Values from CK_S1 rather change slowly in the opposite direction reacting to the more humid SPEI from the Chatyr Kol area. Calculated E/I ratios show the intersection of both lake curves at 1984 AD, indicating higher evaporation at Chatyr Kol earlier. This also implies that evaporation at Chatyr Kol is lower in recent years.
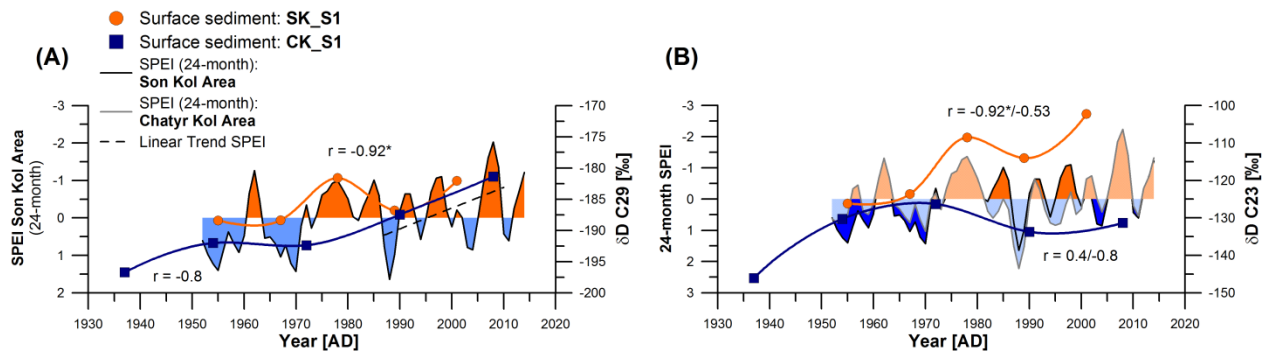
Figure 18: Correlation of measured surface sediment (A) δD_{C29} and (B) δD_{C23} data from SK_S1 (orange line) and CK_S1 (blue line) with the calculated SPEI from the Son Kol- (black line) and Chatyr Kol (grey line) area. Correlation coefficients are dependent as follows: r = SK SPEI/CK SPEI.
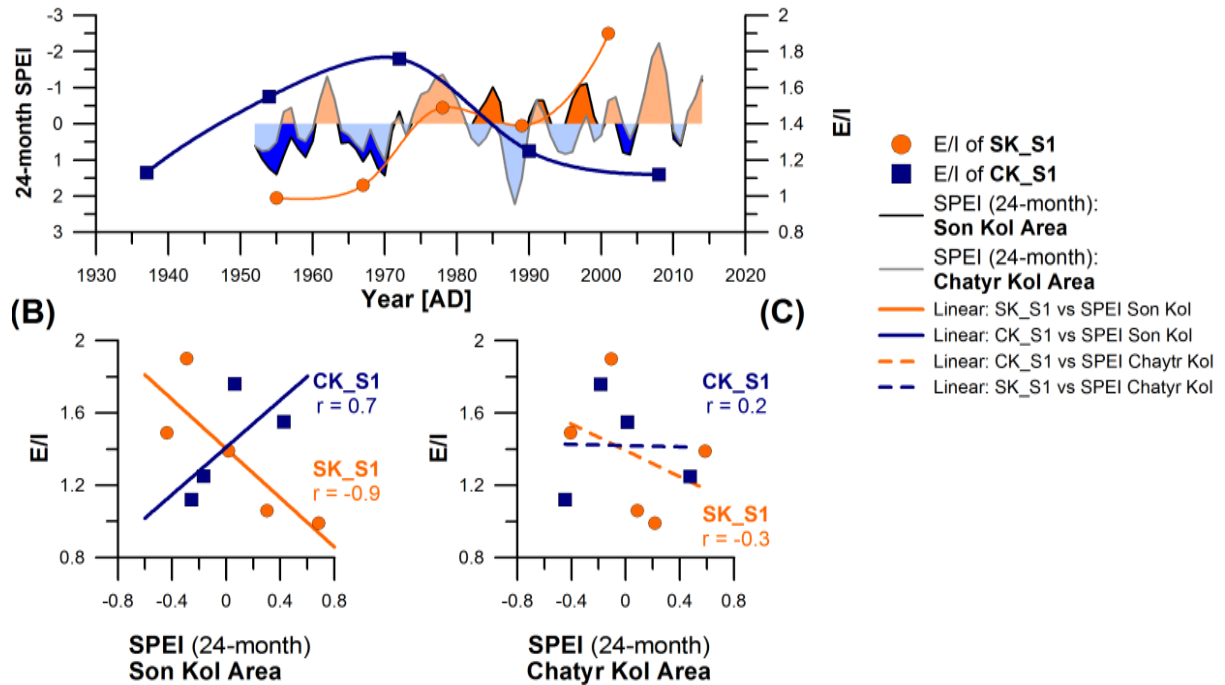
Figure 19: Correlation of calculated E/I ratios with 24-month SPEI using the same nomenclature as in Figure 18. (A) XY-plot of E/I ratios from SK_S1 and CK_S1 and site specific SPEI data shows better correlation with (B) Son Kol area than (C) Chatyr Kol area.

3.4 Discussion

3.4.1 Recent hydrological situation at Chatyr Kol and Son Kol

Using the isotope composition of water from lakes and their catchments enables the comparison and classification of hydrological regimes in a quantitative way (Gibson et al. 2002) (Figure 10). Because δD and δ^{18}O values of meteoric water generally follow the rules of fractionation and Rayleigh distillation processes as well as temperature, this pattern results in a GMWL defined as δD = 8 x δ^{18}O + 10 (Craig 1961; Gat and Gonfiantini 1981). Nevertheless, local variations slightly influence the isotope composition of inflow waters especially in endorheic basins like Chatyr Kol and generate a more specific Meteoric Water Line. This LMWL for Kyrgyz water samples differs in minor degree from the GMWL (Ingraham 1998). An inter-annual difference between the two sampling years 2011 and 2012 AD was not detected, indicating unchanged weather conditions during the late summer month in both years (July, August, September). Shifts along the LMWL indicate seasonal variation due to temperature-dependent summer (enriched) and winter precipitation (depleted) (Jonsson et al. 2009). The local summer precipitations of Chatyr Kol and Son Kol are more enriched than the calculated OIPC summer precipitation, showing that this selective sampling represents a date with rather higher temperatures (CK: 20 °C, 40 % rH) than the mean summer temperature. The even higher enrichment of Chatyr Kol precipitation could be explained with the higher evaporation of falling precipitation under lower humidity (Dansgaard 1964) and/or stronger convective rain due to local

moisture recycling under relative dry conditions (Mügler et al. 2008). Nevertheless, inflow water from Chatyr Kol and Son Kol as well as other Kyrgyz lakes, which are close to the mean annual precipitation value calculated by the OIPC, suggest that inflow water is a mixture of summer precipitation and spring melting of snow mostly accumulated during spring and summer. Samples which plot on the LMWL are isotopically identical with the local precipitation, meaning that lakes on LMWL have not experienced evaporative enrichment. These lakes, Ak Kol, Aram Kol, Irik Kol, Kyle Kol and Sary Chelek, located in the Eastern and Western Tian Shan seem to have short residence times either due to high precipitation or lake stratification (Tyler et al. 2007) and underwent no enrichment during summer. This is not the case for Chatyr Kol and Sol Kol plotting on individual LEL indicating strong evaporative enrichment of the remaining lake water (Craig and Gordon 1965). The slope of the individual LEL strongly depends on local atmospheric conditions like relative humidity and temperature during the evaporation period and even seasonality (Clark and Fritz 1997; Gibson et al. 2005; Gibson et al. 2008). Generally, LEL slopes range between 4 and 7 in most regions (Gibson et al. 2005). Studies by Gibson et al. (2008) showed that typical LEL slopes of mid-latitude lakes are between 5 and 6 if the lake is not at isotopic steady state. Here, the evaporative flux is clearly distinguished from the transpiration flux. While LEL slopes at Chatyr Kol and Son Kol have values of 5.6 and 5.5, the seasonal climate of Kyrgyzstan conforms to the mid-latitude scenario. The intersection of the LEL with the LMWL can be used as approximation of the mean isotope composition of the input water (Gibson et al. 2005; Jonsson et al. 2009). Therefore, the measured inflow, the calculated OIPC mean annual precipitation and the LEL-LMWL intersect of Chatyr Kol and Son Kol show similar individual δD and $\delta^{18}O$ values, indicating that isotopic composition of regional mean annual precipitation is identical. Additional information about the water balance derives from the displacement of the lake water isotope values along the LEL (Gibson et al. 2005). The larger the distance from the LEL-LMWL intersect, the higher the water was affected by evaporative enrichment. The sampling campaigns took place in the late summer month, where evaporation is expected to be highest and precipitation amounts are low, so that the seasonal cycle has not been fully detected by our data. An annual dataset would also show an opposite effect of snowmelt dilution along the LEL closer to the LMWL during spring (Edwards et al. 2004). The minor difference of the LEL between Chatyr Kol and Son Kol arise from variations in snowmelt isotope composition and/or different contributions from precipitation. In detail, lake water samples at Son Kol show higher LEL-parallel shifts than Chatyr Kol, indicating a higher contribution of periodic input of isotopically depleted inflow water and precipitation regardless of water source (Edwards et al. 2004). These shifts can directly be transformed into fluctuations of the water balance semi-quantitatively expressed by the calculated E/I ratio. The E/I determines the degree to which isotopic enrichment is attenuated by dilution (Gibson and Edwards 2002). An E/I > 1 indicates a lake desiccating towards its theoretical limiting isotopic enrichment, while E/I < 1 represent a lake where inputs exceed evaporative losses (Pham et al. 2009). The present high E/I ratio of 8.1 at Chatyr Kol results of the strongly enriched lake water value (−11 ‰), which would display in this case

an extreme influence of evaporation on the lake hydrology during late summer. However, we advise not to over-interpret this pattern calculated from one-time sampling, which probably simply reflects a sensitive response of the lake to a low water input by precipitation and snowmelt under higher daytime temperatures and evaporations. Since the E/I ratio of Son Kol is much smaller (0.93) than Chatyr Kol and even < 1, the inflow derived from precipitation was stronger in 2011/12 AD. The general higher annual precipitation amount of the Son Kol area is proven by meteorological data of the last century (Figure 15). Water profile investigations during the field campaign disclosed relatively well mixed water bodies with no distinct thermo- and halocline at Son Kol (Figure 5). Here, bottom water (12 m) was characterized by oxic conditions. At Chatyr Kol we measured no obvious thermocline, while anoxic conditions dominate the bottom water unless only in the central basin. Consequently, these shallow lakes are well mixed during the open water period and allow the use of single sampling events to characterize the lake water isotope composition. Once no stratification appears the calculation of water balance parameters like mean residence time (MRT), throughflow and catchment runoff become suitable for the inference of catchment-lake connections. Jonsson et al. (2009) showed that lake water residence times strongly effect the amplitude of the seasonal isotope variation in sub-arctic lakes. Lakes with short residence times react more sensible to snowmelt or summer precipitation visible in their isotope composition. The MRT of Chatyr Kol (2.4 a) is only half of Son Kol (5.3 a), contrary to the higher salinity and more enriched lake water isotope composition. Further, the higher catchment/lake ratio of 1:6.8 compared to Son Kol (1:3.9) could not balance out the obviously high evaporation intensity, since this region receives insufficient precipitation to diminish the effects of summer evaporation. The most striking fact strengthens Chatyr Kol enrichment during summer 2011/12 AD is its hydrological character. This terminal lake, where the evaporation is the only factor balancing the inflow, is primarily in a negative water balance in Arid Central Asia. In contrast, the low E/I ratio of Son Kol is a result of its throughflow character limiting the isotopic enrichment. Beside the hydrological character also glacier occurrence significantly determines the lake water balance.

The higher elevation of Chatyr Kol (3545 m) results in a lower mean annual temperature compared to Son Kol, so that the longer-lasting ice cover season from November till May comparable with Lake Karakul (3928 m), Tajikistan (Mischke et al. 2010) suppresses lake water evaporation and atmospheric exchange (Gibson et al. 2002). As a result, also the significant snow/glacier-melt is later in spring/summer leading to spontaneous depletion of the lake water isotopic composition. Snow accumulation in the neighboring mountains was probably not recorded at lower-elevated climate station "Chatyr Kol" providing data for MRT calculations. Falatkova et al. (2014) mentioned an underestimation of solid precipitation amounts (snow) in mountainous areas. We therefore consider Lake Chatyr Kol having a shorter MRT than expected indicating a larger seasonal variation in the isotope composition of the water and a faster response on seasonal changes in precipitation/inflow (Jonsson et al. 2009). We confirm with findings by Gibson et al. (2002), that the lake

volume is an important factor in estimation of response sensitivity to short-term perturbations, where Chatyr Kol should react faster to climate changes (temperature, precipitation). But the occurrence of glaciers within the catchment enables a lake to buffer climate events like larger lakes do. Due to variation in the duration of ice-free period, water balance becomes shifted as well.

3.4.2 Plant and soil water isotopic composition

Since evaporation also influences soil and leave surfaces, their water become enriched as well. Generally, evaporation of soil water occurs in the upper 20 cm with intensity influenced by several processes like water movement, residence time and soil matrix affecting vapor transport (Gazis and Feng 2004; Gibson et al. 2008). The evaporative influence decreases with depth, resulting in highest enrichment at soil surface layer (Barnes and Allison 1988) also observed in this study. Their isotope enrichment at unsaturated condition results in slopes (~3) below the ones from open water bodies (Allison et al. 1983; Flanagan et al. 1991). If the soil is rather saturated, its slope becomes higher between 4 and 6 (Allison 1982). Depending on the evaporation intensity, a lowering of the soil water slope is the result especially in soils of arid or seasonally arid regions without full vegetation cover (Allison and Hughes 1983). Therefore, soils at Chatyr Kol and Son Kol with slopes of 5.1 and 5.5 were probably influenced by relatively high water content during sampling and were protected against too high evaporation due to a moderate vegetation cover. Nevertheless, Chatyr Kol experienced much higher evaporation. Plants taking up soil water mostly recharged by precipitation rather than by groundwater. Groundwater was not directly investigated in this study but should be of minor importance at Son Kol sampling location due to elevated and sloping catchment topography. Groundwater situation at Chatyr Kol sampling site is expected to be of larger importance since meltwater streams and/or mountain runoff infiltrate to higher extent at the southern plain. The isotope composition of plant water reveals information about the soil depth used for water assimilation (Chimner and Cooper 2004). The water uptake by plants is not accompanied by significant isotope fractionation, so at least root water should retrace the soil water source signal (Ehleringer and Dawson 1992), also detected but generalized on a Tibetan Plateau transect study by Günther et al. (2013). Conversely, if soil undergoes water loss by plants transpiring moisture to the atmosphere, fractionation is not occurring as well, since it is a quantitative process (Gibson and Edwards 2002). Further water transport to the leaves via stem (xylem water) also does not change the original isotope composition. Generally, roots in both catchments have mean length of 10 cm; however major variability in their water isotope composition could be detected. Isotope composition of root water at Chatyr Kol is not significantly different from upper and deeper soil water ($p = 0.48$ and $p = 0.34$, respectively), but it preferentially originates from the upper soil (0–5 cm). Because deep soil water isotope composition (–75.5 ‰) is identical with inflow (–77.2 ‰) and calculated MAP (–76.2 ‰), we assume that inflow water from streams also influence local soil

profiles. The proportion of deep soil water becomes strongly minimized at Son Kol, were root water significantly differs from deep soil water (p = 0.01) and even upper soil water shows differences (p = 0.06), indicating water uptake rather originates from upper soil layer but more likely from direct summer precipitation events. This assumption is supported by identical meteoric water hydrogen isotope values (–28.3 ‰) to root values (–28.1 ‰). Another assumption explaining the difference between root and depleted soil water at Son Kol is derived by Araguasaraguas et al. (1995), where soil water extracted with vacuum distillation could include proportions of the more tightly bound isotopically depleted water molecules. Generally, the most likely assumption is that soil water rather correlates with the mean annual inflow (see intersection of Soil EL), while plants compensate water stress with a higher proportion of meteoric water during late summer. Only processes like leaf water evaporation depending on humidity, leaf transpiration rate and isotope composition of the atmospheric water, lead to isotopic enrichment of the Chatyr Kol and Son Kol leaf water (Dongmann et al. 1974). Differences of leaf water enrichment between our sites are hard to interpret either due to leaf physiology changing even within C_3 plants of the same genus (Kahmen et al. 2008) or changes in vapor pressure gradients between atmosphere and leaf (Barbour and Farquhar 2000). Another uncertainty is the source water for plant wax lipid biosynthesis. Here, the extracted bulk leaf water does not necessarily have to be the cellular water pool for *n*-alkanes (Sachse et al. 2009).

3.4.3 Hydrogen source for *n*-alkane biosynthesis

Sedimentary *n*-alkanes, synthesized as cuticular wax layers in plants, occur in different chain-length depending on the need of water protection against evaporation. The long-chain *n*-alkanes with more than 27 carbon atoms are mainly produced by higher terrestrial plants (Eglinton and Hamilton 1967; Maffei 1996). Aquatic submerged macrophytes produce mid-chain odd *n*-alkanes C_{21} to C_{25} (Ficken et al. 2000), while algae and photosynthetic bacteria are thought to be producer of short-chain *n*-alkanes like C_{17} (Gelpi et al. 1970). The lake systems investigated here are characterized by organic matter input from different sources. Surface sediments from Chatyr Kol integrating the last 75 years identify a dominant input of aquatic as well as terrestrial organic matter in a moderate concentration, indicating lake productivity and catchment properties promote an equal accumulation. On the other side, Son Kol sediment OM underrepresents aquatic plant signals, while algae blooms apparently dominate the *n*-alkane distribution likely due to lower salinity. Terrestrial input is of major importance as well, rather favored by longer vegetation period and higher productivity than Chatyr Kol.

The use of *n*-alkane stable hydrogen isotope compositions (δD) for palaeoclimate reconstructions is already an established tool, since they record the isotope value of their source water investigated in transect studies (Huang et al. 2004; Sachse et al. 2004; Garcin et al. 2012; Günther et al. 2013). Generally, the δD values of aquatic plant derived *n*-C_{23} correlate with the lake water δD values, while δD of terrestrial *n*-C_{29} rather correlate with

the meteoric water isotope composition (precipitation/inflow). The excessive evaporative effect in arid regions especially for terminal lakes would lead to enriched lake water δD values compared to precipitation δD values also indicated by Hou et al. (2008) for south-western USA and by Günther et al. (2013) for the Tibetan Plateau. The summer situation in Kyrgyzstan could not confirm these findings, whereas δD values of sedimentary n-C$_{23}$ were more enriched than n-C$_{29}$ as expected. Therefore, recent hydrological data from summer 2011/12 AD are not suitable for sedimentary compound-specific isotope composition modelling. Because even if both lake sites match in vegetation composition, supported by stable carbon isotope composition (Figure 14), several other factors like soil water evaporation, leaf water transpiration and biosynthetic fractionation have an influence on the apparent fractionation from source water to plant-wax lipids and finally sedimentary n-alkanes (Sachse et al. 2012).

3.4.4   Isotopic fractionation

In order to evaluate fractionation processes on a global scale, we compared data of apparent fractionations between δD$_{C23}$ and δD lake water (εC$_{23}$/LW), δD$_{C29}$ and δD inflow water (εC$_{29}$/SW), and the isotopic differences between sedimentary n-C$_{23}$ and n-C$_{29}$ (ΔδD$_{C29-C23}$) from global transect studies with climate and water parameters like temperature, precipitation, pH, conductivity and even glacier influence (Sachse et al. 2004; Garcin et al. 2012; Günther et al. 2013). Here, the apparent fractionation of the terrestrial system (εC$_{29}$/SW) significantly negatively correlates with the MAT (r = –0.56**) and minor with MAP (r = –0.3), but it significantly correlates best with SPEI (r = 0.62**) (

Figure 20). We confirm, that εC29/SW values increase with decreasing MAT and MAP, similar to decreasing relative humidity (Sachse et al. 2012). This indicates that εC$_{29}$/SW is mainly controlled by climate. Since the aquatic proxy εC$_{23}$/LW does not correlate with εC$_{29}$/SW (r = 0.2; p = 0.3), but significantly with ΔδD$_{C29-C23}$ (r = –0.87**) describing the E/I, it is rather controlled by the lake hydrology. However, previous studies only discussed the fractionation pattern under "dry and/or warm" as well as "wet and/or cool" conditions, where in the latter the lake water δD represents δD of MAP, finally resulting in positive ΔδD$_{C29-C23}$ values (Huang et al. 2004; Sachse et al. 2004, 2006; Hou et al. 2008). Even under generally arid conditions, when evaporation exceeds precipitation and ΔδD$_{C29-C23}$ values become reversely negative, fractionation intensities are not constant. We could show that fractionation pattern in Central Asia under dry and cold conditions are different compared to the Tibetan Plateau (dry/cool) and are additionally influenced by several lake specific conditions. One fundamental factor controlling these pattern is most probably the influence either by monsoonal or westerlies air-masses, but on secondary order it could be the occurrence of glaciers. Hou et al. (2008) proposed, that δD values of terrestrial leaf waxes (n-C$_{29}$) in dry regions and from a catchment with glacier influence may be the better proxy for δD of precipitation. For palaeoclimate reconstructions we therefore want to examine their hypothesis by first comparing meteorological data including temperature and

precipitation with measured sedimentary compound specific stable hydrogen isotope data. Yet it was not totally clear which climate parameter to which proportion influences sedimentary δD n-C_{23} and n-C_{29} in arid and cold environments. Quantitative investigations could help to resolve the conflicting interpretations.
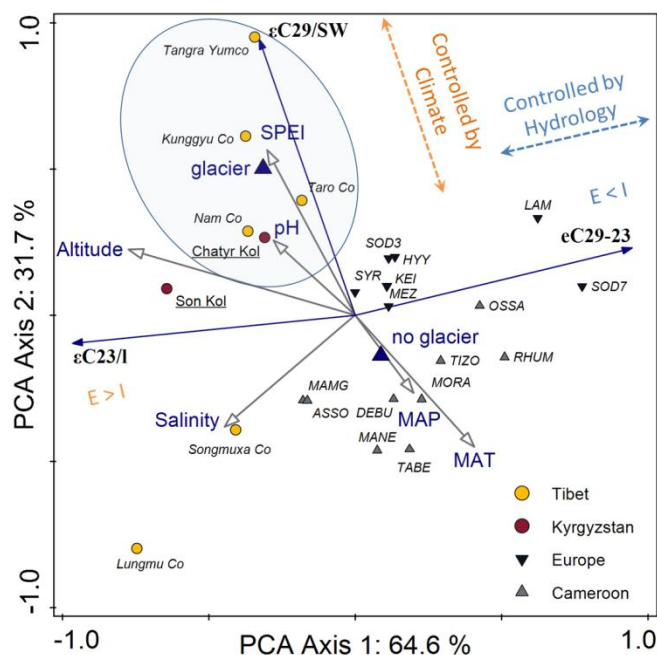
Figure 20: Principal Component Analyses of lakes from transect studies distributed by their aquatic- (εC_{23}/LW) terrestrial (εC_{29}/SW) apparent fractionation and enrichment ($\Delta\delta D_{C29-C23}$) (blue arrows) and possible environmental (climate/water) parameters (grey arrows) influencing hydrogen isotopic fractionation of plant wax lipids. Lakes within the blue circle are subject to glacier influence. Further details available in Supp. Table 2.

3.4.5 Palaeoenvironmental implications

Several studies already discussed the application of $\Delta\delta D_{C29-C23}$ as palaeohydrology/-climate indicator in surface sediment transects (Mügler et al. 2008; Günther et al. 2013) and deep core investigations (Aichner et al. 2010b; Rach et al. 2014; Rao et al. 2014). The simple calculation of $\Delta\delta D_{C29-C23}$ does not include lake specific parameters making absolute inter-lake comparisons problematic. As a consequence, correlations between $\Delta\delta D_{C29-C23}$ and environmental parameters could not always be detected (Aichner et al. 2010b; Rao et al. 2014). We rather suggest the calculation of the E/I ratio, which includes climate parameter like relative humidity and MAT as well as source water isotope values (δD_{LW}, δD_{SW}) and even highly correlates with $\Delta\delta D_{C29-C23}$ (r = –0.99**). In order to evaluate the factors influencing the difference between terrestrial and aquatic systems, we need to understand the controlling factors for the individual biomarker on a quantitative level. Since we know that different climatic regimes have certain fractionation pattern, we use meteorological

data from ACA to compare also intra-regime responses to temperature and precipitation changes.

The observational data disclosed a positive linear trend of the MAT since 1950 AD with a warming of +0.38 °C per decade, also matching with global surface air temperature observations (Trenberth et al. 2007). The intra-montane valley location and the low elevation of the Naryn meteorological station reinforce this temperature increase. Many studies correlated the increasing Central Tian Shan MAT with higher increases in winter and autumn temperatures possibly due to a weakened Siberian Anticyclone (Giese et al. 2007; Siegfried et al. 2012; Kriegel et al. 2013). Sedimentary δD *n*-C$_{29}$ values from Son Kol follow short-term MAT values (r = 0.85* to 0.97**), while δD$_{C29}$ from Chatyr Kol rather follows the long-term trends (r = 0.83). The intensity of temporal integration of these sedimentary records could be possibly declared by different sediment accumulation rates, which is higher at Son Kol during the last 60 years ending up in the integration of shorter time intervals. Consequently, response to climate changes is more visible at Son Kol at least during the last century. Therefore, based on the measured δD values of *n*-C$_{29}$ at Son Kol, the MAT of this region (Naryn) can be reconstructed following equation [12] (Figure 21).

$$\text{MAT}_{\text{Naryn}} \, [°C] = 0.0437 \times \delta D_{C29} + 10.602 \quad\quad\quad\quad\quad\quad [12]$$
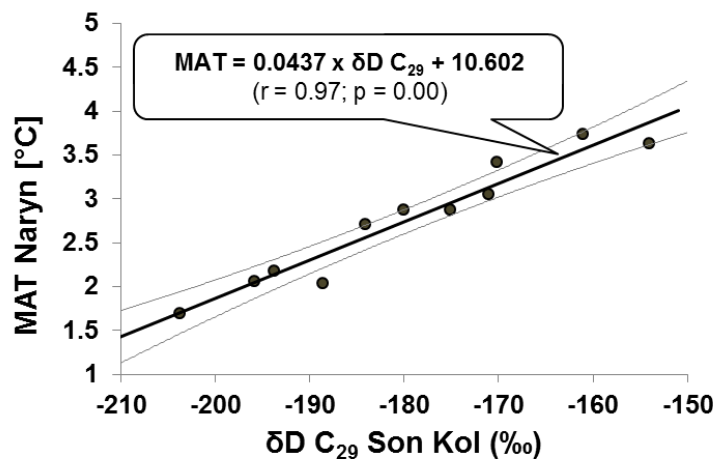
Figure 21: δD of sedimentary *n*-C$_{29}$ from Son Kol vs. MAT measured at Naryn station.
The thick line represents the regression and the thin lines are the 95 % confidence interval of the regression line.

The general warming trend since 1950 AD does not necessarily induce a decreasing MAP trend as discovered in some regions of Central Kyrgyzstan. At Naryn region warming correlates with higher precipitation since 1980 AD. Not limited to this timeframe, MAP signal is extremely high recorded in the δD$_{C29}$ values from Chatyr Kol (r = 0.9*). Since MAT and MAP data are included in SPEI calculations, this precipitation/evaporation index

could obviously best explain changes in terrestrial isotope composition (δD_{C29}) of Son Kol (r = –0.8) and Chatyr Kol (r = –0.92*) and should be applied in palaeoclimate reconstructions of the last 60 years, especially if only terrestrial *n*-alkanes are present in sedimentary records. The interpretation of the aquatic δD_{C23} is just rudimentary possible with MAT, MAP and even SPEI data. Since δD_{C23} values record the lake water isotope composition, which also indicates salinity, become enriched due to higher evaporation (high summer air temperatures) and could be depleted due to increased inflow (precipitation/meltwater). The hydrology (water balance) of the throughflow Lake Son Kol is limited to precipitation (inflow) and outflow during summer to prevent evaporative enrichment. As expected, δD_{C23} values of Son Kol become clearly enriched at ~1977 AD under warmer and drier conditions. However, the increased MAP since 1980 AD was not able to counterbalance the evaporation forced by higher MAT, leading to δD_{C23} enrichment. These enrichment patterns could not be detected at the terminal Chatyr Kol, where a general depletion of δD_{C23} values occurs under warmer conditions. The key factor balancing the lake water isotope composition seems to be the occurrence of glaciers. The inflow from glacier surface melting is the main water source during summer and depends mainly on air temperature and radiation (Falatkova et al. 2014). The glacial contribution is 1.5-times larger during the melting season (summer) at Chatyr Kol. Günther et al. (2015) tried to include the effect of thresholds to the response of systems. The MAT at Chatyr Kol (–5.2 °C) is generally lower than at Son Kol (–1.6 °C) partly depending on altitude, and therefore climate change in colder regions may lead to faster snow accumulation under increased winter precipitation since they do not exceed the threshold. The average annual shrinkage rate of Chatyr Kol glacier between 1960 and 2000 AD was lowest (0.17) compared to other glaciers in the inner ranges of Tian Shan mountains (Sorg et al. 2012). Other satellite investigations also detected only small decreases in the glacier area for Fergana-region and At Bashy between 1970 and 2000 AD (9 % and 12 %, respect.) and even no/lower decrease between 2000 and 2007 AD (0 % and 4 %, respect.) (Narama et al. 2010). With 20 % annual glacial runoff (0.03 from 0.14 km³ a^{-1}), the not negligible glacier contribution to the lake is able to balance-out evaporative enrichment since 1970 AD (see δD_{C23}).

Therefore, to interpret the E/I index correctly for palaeo-hydrology reconstructions, the knowledge about catchment parameters including glaciers is a prerequisite. Further, additional studies using sediments tracking back to the Early Holocene are needed to test the applicability of recently determined transfer function of δD_{C29} and MAT to other regions in the Tian Shan and if individual site calibration are more suitable.

3.5 Conclusions

Water balance information is scarce in Central Asia especially of lakes due to the limited available climate stations and investigations. Our studies of actual (2011/12) lake hydrology and palaeo-hydrology reconstructions based on surface sediments therefore offer a significant contribution to understanding of water balance conditions in this region. Based on investigations of modern isotope hydrology of Kyrgyz lakes Chatyr Kol and Son Kol by determining isotope composition (δ^{18}O, δD) of recent meteoric-, lake-, plant-, soil- and surface sediment samples, we conclude that inflow during summer combines isotopic signals of enriched precipitation and depleted meltwater. On the other hand, the lake water isotope composition is strongly influenced by evaporative enrichment, which depends on the lake-specific hydrology. Chatyr Kol as a terminal lake experienced higher evaporation than the throughflow lake Son Kol, resulting in different LELs. The semi-quantitative expression of the water balance was applied by the E/I ratio, which is identical at both lakes between 1937 and 2008 AD. Since an asynchronous pattern after 1975 AD was detected, we conclude a similar long-term response to warming, but on short-term scale glacier meltwater input reduces the E/I value. Chatyr Kol obviously experienced this kind of buffer effect. Therefore, the understanding of the specific catchment situation as influence for the lake hydrology must be considered before lacustrine sediments can be used for palaeoclimate reconstructions. Since climatic factors like temperature, precipitation, evaporation and humidity can influence the isotopic fractionation of water isotope composition into organic molecules; the later accumulated in lacustrine sediments, detailed knowledge about these processes are required. Therefore, we compared sedimentary compound-specific δD values with meteorological temperature and precipitation data. We found highest correlation between the terrestrial δD_{C29} from Son Kol and the MAT measured at Naryn (r = 0.966, p < 0.01). Since precipitation had minor impact on terrestrial hydrogen isotopic fractionation, we conclude the temperature as main driver in arid Central Kyrgyzstan. Thus, the established transfer function MAT [°C] = 0.0437 x δD_{C29} + 10.602 could be applied in upcoming studies, when lacustrine sediments will be used for palaeoclimate reconstructions in this region.

4 Climatic imprint of the mid-latitude Westerlies in the Central Tian Shan of Kyrgyzstan and teleconnections to North Atlantic climate variability during the last 6000 years

4.1 Abstract

In general, a moderate drying trend is observed in mid-latitude ACA since the Mid-Holocene, attributed to the progressively weakening influence of the mid-latitude Westerlies on regional climate. However, as the spatio-temporal pattern of this development and the underlying climatic mechanisms are yet not fully understood, new high-resolution palaeoclimate records from this region are needed. Within this study, a sediment core from Lake Son Kol was investigated using sedimentological, (bio)-geochemical, isotopic, and palynological analyses, aiming at reconstructing regional climate development during the last 6000 years. Biogeochemical data, mainly reflecting summer moisture conditions, indicate predominantly wet conditions until 4950 cal. yr BP, succeeded by a pronounced dry interval between 4950 and 3900 cal. yr BP. In the following, a return to wet conditions and a subsequent moderate drying trend until present times are observed. This is consistent with other regional palaeoclimate records and likely reflects the gradual Late Holocene diminishment of the amount of summer moisture provided by the mid-latitude Westerlies. However, climate impact of the Westerlies was apparently not only restricted to the summer season but also significant during winter as indicated by recurrent episodes of enhanced allochthonous input through snowmelt, occurring before 6000 cal. yr BP and at 5100–4350, 3450–2850, and 1900–1500 cal. yr BP. The distinct ~1500- year periodicity of these episodes of increased winter precipitation in Central Kyrgyzstan resembles similar cyclicities observed in palaeoclimate records around the North Atlantic, likely indicating a hemispheric-scale climatic teleconnection and an impact of the NAO variability in Central Asia.

4.2 Introduction

Reliably assessing the ecosystem impact of future human-induced climate change requires a profound understanding of past natural climate variability. This is especially crucial in climatologically extreme areas, for example, at high altitudes, where the consequences of future global warming are expected to be most severe (Solomon et al. 2007). In this context, the Tian Shan in Central Asia is of particular interest, as it represents the headwaters for several large rivers (e.g. Syr Darya, Tarim), and future climate-induced water shortage there may affect human subsistence across large parts of western Central Asia. Furthermore, being located at the intercept between the influences of the mid-latitude Westerlies, the Siberian Anticyclone, and partly also the Asian monsoon system (Cheng et al. 2012), the region holds information about hemispheric-scale climatic teleconnections, necessary to understand the global climate system. However, although the Tian Shan is thus

of key importance for climate studies and various types of natural archives, for example, speleothems (Cheng et al. 2012), tree-rings (Esper et al. 2003), or loess sequences (Machalett et al. 2008) have been analyzed in this respect so far, knowledge about Holocene climate development and particularly hydrological changes in this region is still limited. For example, a moderate drying trend due to the gradual decline of moisture supplied by the Westerlies has been inferred for mid-latitude arid Central Asia since the Mid-Holocene from lake sediment records (Chen et al. 2008). Nevertheless, this might be spatially more complex as there were apparently significant differences in past climate development between the western and eastern parts of Central Asia (Rudaya et al. 2009; Kleinen et al. 2011) owed to the interplay of different climatic systems in the region. In order to provide more detailed insights into Holocene climate development in the western part of ACA, several lake sediment records (which are particularly valuable palaeoclimate archives because of the robust age control, the high temporal resolution and the variety of climate-related proxy parameters to be investigated) from NW China (Mischke and Wünnemann 2006; Wünnemann et al. 2006; Li et al. 2011; An et al. 2012a), Tajikistan (Mischke et al. 2010), Kazakhstan (Boomer et al. 2000; Sorrel et al. 2006; Huang et al. 2011), and Kyrgyzstan (Ricketts et al. 2001; Beer et al. 2007; Mathis et al. 2014) have been studied so far, but further investigations are necessary to fully disentangle the complex climatic history and interfering interplays between the different climatic systems in this region. As a part of the project CADY (*Central Asian Climate Dynamics*), aiming at reconstructing Holocene climate development in Central Asia, a sediment core from Son Kol, a lake in the Central Kyrgyz Tian Shan, was investigated within this study. The potential of this lake for regional palaeoclimate reconstructions has recently been demonstrated by Huang et al. (2012) and Mathis et al. (2014). However, as the sediment core investigated in these studies missed the last 2000 years because of coring problems, we opted for a new, more complete core and applied additional high-resolution analyses. The new sediment core, covering the last *c*. 6000 years, was investigated using sediment microfacies analysis, high-resolution μXRF element scanning and stable isotope, (bio)geochemical and pollen analyses in order to provide new, more detailed information on regional climate development since the Mid-Holocene and to shed light on climatic teleconnections, particularly the regional influence of the mid-latitude Westerlies.

4.3 Results

4.3.1 Sediment core chronology

Because of the limited number of terrestrial organic macros within the lake sediments, also several samples of aquatic material (shells, water plants, bulk sediment with unknown proportion of aquatic OM) were selected for AMS ^{14}C dating. As such material is commonly regarded to give too old radiocarbon ages because of the incorporation of dissolved, ^{14}C-depleted carbon, for example, from catchment rocks (Deevey et al. 1954; Wright 1986), a living deep-water algae (Poz-47591) from coring site D was dated to assess the recent hardwater effect and its possible impact on ^{14}C dates obtained from lacustrine materials. The obtained conventional radiocarbon age of 155 ± 30 ^{14}C yr BP (

Table **2**) shows that the recent hardwater effect is rather small. But as this might have changed through time, several cross-datings on terrestrial and aquatic samples from the same stratigraphic level in the composite profile were carried out. As a result, conventional ages obtained from aquatic material are consistently only slightly older than those from terrestrial remains with partly overlapping 2σ ranges after calibration, indicating a temporally relatively stable hardwater effect. Thus, a reservoir correction of −150 years, inferred from the age of the recent algae, was applied prior to calibration to all conventional ages derived from samples containing aquatic material (

Table **2**). According to the presence of ^{137}Cs and ^{241}Am within the topmost sediments, which are exclusively of anthropogenic origin and occur in the environment only since the mid-20th century onset of atmospheric nuclear weapon testing, it is clear that the composite profile SONK_11_D1/2 is, in contrast to the sediment core investigated by Mathis et al. (2014), complete even for modern times. However, further pinning down the chronology using ^{137}Cs was impossible as the record revealed the constant occurrence of ^{137}Cs down to a sediment depth of 9 cm (Figure 8) without distinct peaks attributable to the maximum of thermonuclear weapon testing in 1963 AD or the Chernobyl reactor accident in 1986 AD (Appleby 2002), likely owed to post-sedimentary diffusion of ^{137}Cs within the soft and water-saturated surface sediments (Davis et al. 1984; Klaminder et al. 2012). Instead, precise chronological information can be gained from ^{241}Am, which is less mobile than ^{137}Cs and has a longer half-life, making activity peaks easier detectable (Appleby et al. 1991). Accordingly, the strong ^{241}Am activity increase at 5.5 cm can be likely attributed to the onset of atmospheric nuclear weapon testing in 1950 AD at the former USSR test site Semipalatinsk, ~1000 km north of Son Kol. Alternatively, it could represent the maximum in global atmospheric nuclear weapon testing in 1958–1962 AD, but such detailed age information cannot be reliably inferred from ^{241}Am because of the low sedimentation rate and comparatively large sampling interval (0.5 cm). As the five radiocarbon ages obtained from the uppermost *c*. 20 cm of the composite profile (Poz-53029, Poz-47326, Poz-53030, Poz-52033, and Poz-53031) contradict for inexplicable reasons the reliable results of ^{241}Am dating (e.g. the sediment surface dates to *c*. 750–900 cal. yr BP) and the inferred sedimentation rate development, they were rejected from age modeling. Also, one

radiocarbon age from the base of the sediment sequence (Poz-44072) was rejected as it turned out to be *c*. 300 years older than that of another sample (Poz-48597) from the same stratigraphic level, most likely owed to re-deposition of the dated material. In consequence, the age model for composite profile SONK_11_D1/2 (Figure 8) was finally established using the remaining 22 corrected conventional radiocarbon ages (

Table **2**) as well as the chronological fix points at 5.5 cm sediment depth (first occurrence of ^{241}Am: 1950 AD) and at the sediment–water interface (date of the coring campaign: 2011 AD) as input parameters for a *P_Sequence* deposition model implemented in OxCal 4.1 (Ramsey 2008). The high agreement index A_{model} of 94.2 % proves the robustness of the chronology (Ramsey 1995, 2001), which is furthermore independently constrained by pollen analyses, revealing the first appearance of (most likely long-distance-transported) *Juglans* pollen at 44.5 cm composite depth, i.e. at *c*. 2000 cal. yr BP, which is in good agreement with the reported maximum age for the Kyrgyz walnut forests (Beer and Tinner 2008). According to the established age model, the geochemical/isotopic and biogeochemical data are multi-decadally resolved, while the resolution of the μXRF and pollen data is sub-annually and multi-centennially, respectively.

4.3.2 Microfacies and geochemical/isotopic composition of the lake sediments

The basal deposits (below 155.0 cm) in composite profile SONK_11_D1/2 are older than *c*. 6000 cal. yr BP. They consist of light gray, clay-sized endogenic carbonate mud with abundant, mostly angular sand- to gravel-sized allochthonous minerogenic detritus (quartz, feldspars, carbonates, micas) randomly scattered within the carbonate matrix, but also contain allochthonous organics, ostracod valves, and lumps of reworked micritic lake marl. Because of the chaotic sediment microfacies, this unit is interpreted as a debris flow layer. Although it was impossible to penetrate this deposit, in situ lake sediments most likely occur below (Mathis et al. 2014). Above a sharp transition at the top of this deposit, the regular pelagic sediments of composite profile SONK_11_D1/2 can be subdivided into four lithostratigraphical units (Figure 6b). Unit I (155.0–127.5 cm / 6000–5100 cal. yr BP) consists of irregularly laminated (sub-cm- to mm-scale) sediments with yellowish to light gray layers of micritic idiomorphic aragonite and calcite and brownish layers containing amorphous OM, algal material, ostracod valves, and diatom frustules. Minerogenic detritus (quartz, feldspars, micas) is abundant and randomly scattered within the sediments, reflected by strongly variable but generally high Ti and K μXRF counts (

Figure 22). C/N ratios fluctuate between 8 and 10 and $\delta^{13}C_{org}$ ranges between −19 ‰ and −25 ‰, while $\delta^{15}N$ is fairly stable (3–5 ‰). Higher detrital contents at 5500–5300 cal. yr BP are paralleled by more negative $\delta^{13}C_{org}$ values (below −27 ‰) and positive peaks in $\delta^{15}N$ (> 6 ‰) and C/N ratios (11–13). Overlying unit II (127.5–109.5 cm / 5100–4350 cal. yr BP) is characterized by homogenous, clay-sized light gray lake marl composed of endogenic calcite/aragonite with abundant ostracod valves but only very few amorphous

OM and diatom frustules. The increased abundance of finely dispersed, silt-sized (~50 μm) minerogenic detritus is reflected by strongly elevated Ti and K μXRF counts (

Figure 22). $\delta^{15}N$ values are the highest of the entire record, and two prominent peaks (up to 8–9 ‰) are paralleled by distinct negative $\delta^{13}C_{org}$ spikes (below −26 ‰). C/N ratios gradually increase from 8 to 13 within this unit. The sediment composition of unit III (109.5–79.0 cm / 4350–3250 cal. yr BP) is almost similar to unit II, but ostracod valves are less abundant and the rather dark gray lake marl reveals a gradually upward-fading sub-cm-scale light-dark lamination, owed to fluctuations in OM and carbonate contents. Although the content of finely dispersed, silt-sized minerogenic detritus is generally rather low, two short-term increases, mirrored by slightly elevated Ti and K μXRF counts, are observed at 3900–3850 and 3450–3300 cal. yr BP. C/N ratios and $\delta^{15}N$ values are in general fairly stable, but also show prominent peaks (16–20 and 6–7 ‰, respectively) parallel to the increases in minerogenic detritus. $\delta^{13}C_{org}$ is also rather stable, but shows distinct negative excursions (up to −31 ‰) synchronous to the increases in the C/N ratio, $\delta^{15}N$ values and detrital matter content. The uppermost unit IV (79.0–0.0 cm / 3250 cal. yr BP to present) consists of faintly cm-scale layered yellowish gray lake marl (aragonite and calcite) with abundant amorphous OM and frequent *Pisidium nitidum* shells. The amount of silt-sized minerogenic detritus is generally reduced, except for increases at 3250–3050, 3000–2900, 2200–2150, and 1900–1500 cal. yr BP, reflected by elevated Ti and K μXRF counts (

Figure 22). Apart from two distinct peaks at 3250–3150 and 3000–2900 cal. yr BP, C/N ratios are rather stable (11–15). $\delta^{13}C_{org}$ fluctuates between −21 ‰ and −25 ‰, but shows negative spikes concomitant to the positive C/N peaks and also at 2100 cal. yr BP. $\delta^{15}N$ also reveals distinct peaks (> 7 ‰) around 3250–3050, 3000–2850, 2250–2150, and 1900–1500 cal. yr BP.
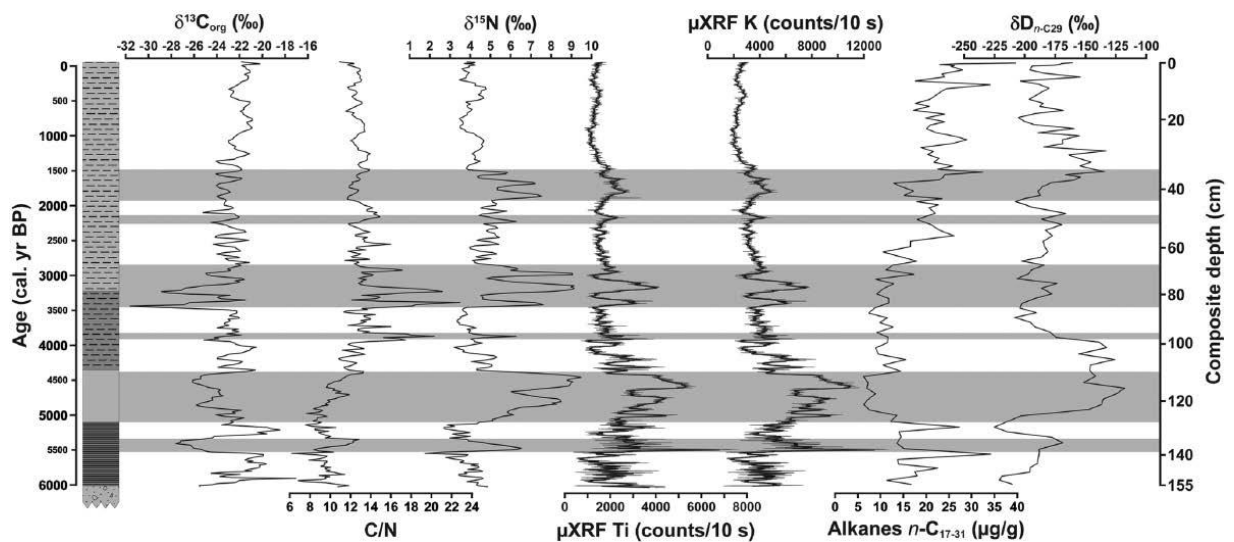
Figure 22: Results of stable isotope and (bio)-geochemical ($\delta^{13}C_{org}$, $\delta^{15}N$, C/N, Ti and K μXRF counts, total amount of *n*-alkanes *n*-C_{17-31}, δD_{C29}) analyses on the sediments of composite profile

SONK_11_D1/2 from Son Kol. The black lines in the Ti and K µXRF records represent 25-point running means. Gray bars highlight intervals of increased terrestrial input after enhanced spring snowmelt.

4.3.3 Geochemical/isotopic composition of the catchment samples

Geochemical and isotopic compositions of modern OM samples from the lake and its catchment allow characterizing the predominant sources of lake sediment OM (

Figure 23). Soils reveal a characteristic geochemical/ isotopic signature, relatively close to that of the lake sediments. While soil $\delta^{15}N$ is slightly higher (between 5.8 ‰ and 12.3 ‰) than the average of the lake sediments, $\delta^{13}C_{org}$ (−25.4 to −23.0 ‰) and C/N ratios (9 to 14) plot in a similar range. In contrast, modern terrestrial plants show comparatively low $\delta^{15}N$ (−3.3 ‰ to 6.1 ‰) and $\delta^{13}C_{org}$ values (−21.7‰ to −29.6‰), but clearly higher C/N ratios (23 to 75). Animal dung is characterized by relatively narrow ranges of $\delta^{15}N$ (2.9 to 4.2 ‰) and $\delta^{13}C_{org}$ (−27.5 ‰ to −27.9 ‰) as well as C/N ratios (25 to 28). $\delta^{15}N$ (3.2 to 4.2 ‰) and $\delta^{13}C_{org}$ values (−24.9 ‰ to −28.7 ‰) of emerged aquatic macrophytes are on average fairly similar to those of the terrestrial vegetation, while C/N ratios are distinctly lower (15 to 30). Submerged aquatic macrophytes and algae reveal $\delta^{15}N$ values of −0.3 ‰ to 8.5 ‰ and relatively low C/N ratios (11 to 26). Overall, higher $\delta^{13}C_{org}$ values (−10.0 ‰ to −19.0 ‰) clearly separate them from other materials.
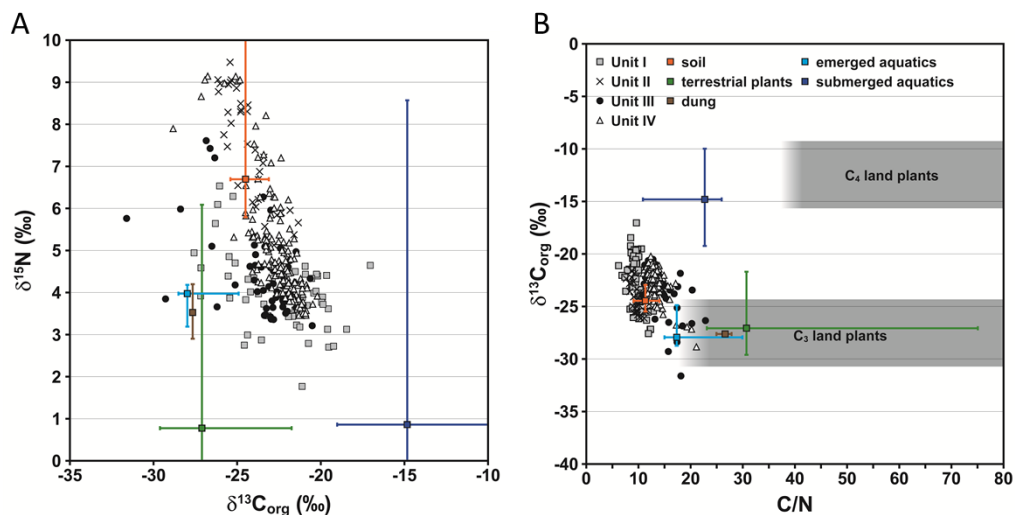
Figure 23: Geochemical and isotopic signatures (A) $\delta^{15}N$ vs $\delta^{13}C_{org}$ and (B) $\delta^{13}C_{org}$ vs C/N of the Son Kol sediments compared with those of modern organic materials collected from the lake and its catchment. The latter are given as medians (squares) with total ranges (bars). Submerged aquatics include macrophytes and algae.

4.3.4 Biogeochemistry of the lake sediments

Sediments of the composite profile SONK_11_D1/2 contain n-alkanes of variable chain length (n-C_{15} to n-C_{33}) with a clearly bimodal distribution, maximizing at n-C_{29} (6.9 ± 2.8 μg g^{-1}) and n-C_{31} (7.49 ± 3 μg g^{-1}). High fluctuations in the total amount of odd-numbered n-alkanes n-C_{17-31} characterize lithostratigraphical unit I, while δD_{C29} is strongly depleted with minimum values of about -225 ‰ (

Figure 22). Within unit II, the total amount of n-alkanes n-C_{17-31} reaches a minimum after 4950 cal. yr BP and δD_{C29} shows a strong enrichment (more than -150 ‰). Unit III is characterized by intermediate and relatively stable amounts of n-alkanes n-C_{17-31}. δD_{C29} is still enriched until about 3900 cal. yr BP, but reveals clearly depleted values (around -200 ‰) afterwards. Within unit IV, the total amount of n-alkanes n-C_{17-31} shows an overall increasing trend with clear fluctuations. δD_{C29} reveals a slight increase towards the top of the record from the uppermost part of unit III, superimposed by a short-term enrichment at 1650–950 cal. yr BP.

4.3.5 Pollen analyses

The pollen record of composite profile SONK_11_D1/2 (

Figure 23) is mainly dominated by steppe communities. Local sedge marshes and alpine meadows as well as the forest stands outside the valley are clearly underrepresented; arboreal pollen (mainly *Picea, Juniperus, Betula*), which most likely derives from long-distance eolian transport, is generally below 7 %. Throughout the record, pollen spectra show only small-scale changes, revealing a relatively stable ecosystem and timber line during the last 6000 years and confirming the vegetation development inferred for Son Kol by Mathis et al. (2014). The most notable feature of the record, separating LPAZ1 and LPAZ2, is the increase of *Artemisia* from about 40 % to 60 % at about 5000 cal. yr BP with a stable steppe community prevailing afterwards. Although the catchment is nowadays strongly influenced by livestock grazing and the presence of herding nomads in the Central Tian Shan is documented at least since the 1st millennium before Christ (Polome 1996), there is no indication for human impact throughout the pollen record.
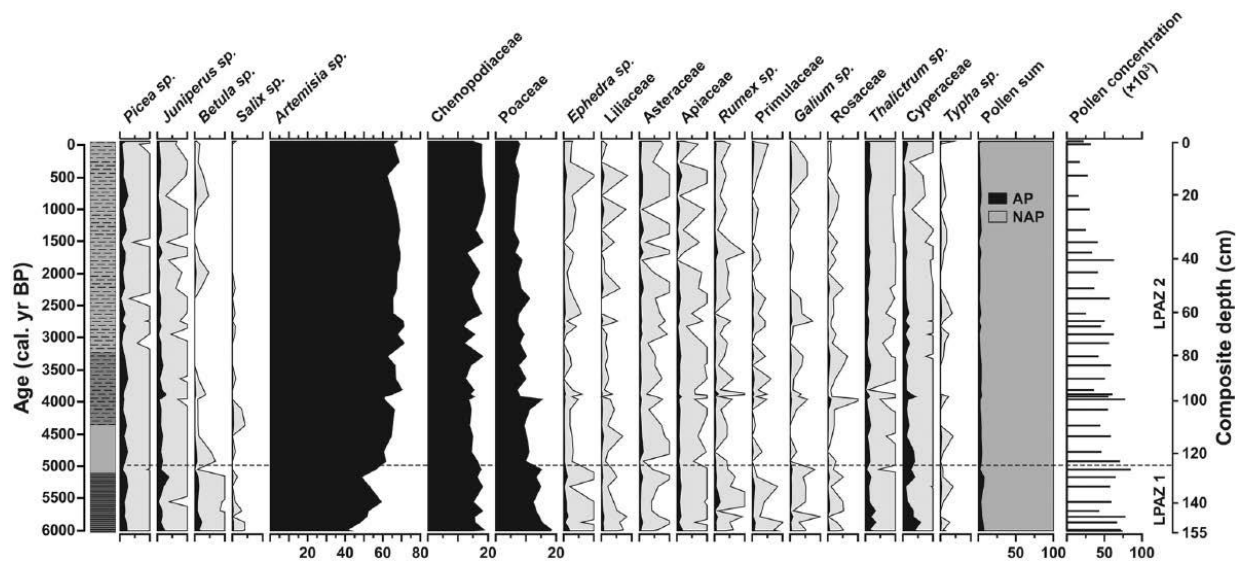
Figure 24: Pollen percentage/concentration diagram for selected taxa for composite profile SONK_11_D1/2 from Son Kol.

Pollen abundances are presented as percentages of the total pollen sum (AP + NAP), excluding aquatics and non-pollen palynomorphs. Local pollen assemblage zones (LPAZ) were determined using CONISS. The outline curves represent a 10× exaggeration.

4.4 Discussion

4.4.1 Summer moisture conditions in Central Kyrgyzstan since the Mid-Holocene

As recently shown, the δD of odd-numbered long-chain n-alkanes (e.g. n-C_{27}, n-C_{29}, and n-C_{31}), which are major constituents of the epicuticular waxes of higher terrestrial plants (Eglinton and Hamilton 1967; Maffei 1996), reflects the δD composition of precipitation during the vegetation period at a respective site, modified by changes in evapotranspiration, relative humidity, and soil moisture (Sachse et al. 2004, 2006; Smith and Freeman 2006). As high δD values are in this respect generally considered to reflect high leaf/soil evapotranspiration and thus low humidity, whereas low values correspond to relatively wet climate conditions e.g. Liu and Huang (2005), the $δD_{C29}$ record of the Son Kol sediments can be used to infer information about past summer moisture conditions. In general, the $δD_{C29}$ record confirms the previously proposed prevalence of humid conditions in mid-latitude ACA during the Mid-Holocene (at least between $c.$ 6000 and 5000 cal. yr BP) and the subsequent moderate drying trend until present times, which is thought to be caused by the gradual reduction of the intensity of the mid-latitude Westerlies and thus the amount of moisture provided during summer (Chen et al. 2008). However, as there were apparently significant differences in Holocene climate development between the western (e.g. Kyrgyzstan, Kazakhstan, Tajikistan, NW China) and eastern parts (e.g. Mongolia, NE China) of Central Asia (Rudaya et al. 2009; Kleinen et al. 2011), the Son Kol record is in

the following mainly compared with other records from the same climatic domain. Depleted δD_{C29} values between 6000 and 4950 cal. yr BP (

Figure 22) reflect an episode of predominantly humid summers at Son Kol. This coincides with indication for relatively wet climate conditions until about 5000 cal. yr BP in NW China (Mischke and Wünnemann 2006; Li et al. 2011; An et al. 2012a), Kazakhstan (Boomer et al. 2000), and Kyrgyzstan (Beer et al. 2007; Mathis et al. 2014). The humid Mid-Holocene at Son Kol was followed by a pronounced dry episode between 4950 and 3900 cal. yr BP (

Figure 22). This observation is in line with dry phases documented in NW China (Mischke and Wünnemann 2006; Wünnemann et al. 2006; Li et al. 2011; An et al. 2012a) and a phase of lowered lake-levels in SE Kyrgyzstan at about the same time (Beer et al. 2007), together proving the regional significance of this dry episode. Interestingly, it is not reflected in the Son Kol pollen record (this study and Mathis et al., 2014), which could be explained by the relative stability and climatic insensitivity of the local montane steppe ecosystem, indicating that critical precipitation thresholds for significant vegetation changes might not have been crossed during this interval. This interpretation is confirmed by the missing indication for this dry episode in other regional records (Boomer et al. 2000; Ricketts et al. 2001), showing that site-specific hydrological conditions, internal thresholds of the respective ecosystems, the sensitivity of the investigated climate proxies, and the temporal resolution and dating accuracy of the individual records are of crucial importance for identifying such climate fluctuations. Subsequent to the pronounced dry interval, a return to again more humid summers is observed around 3900 cal. yr BP at Son Kol, followed by a gradual but moderate drying trend until present. This broadly coincides with similar observations in NW China (Mischke and Wünnemann 2006; Wünnemann et al. 2006), Kazakhstan (Boomer et al. 2000), Tajikistan (Mischke et al. 2010), and Kyrgyzstan (Ricketts et al. 2001; Beer et al. 2007; Mathis et al. 2014), although the timing of the onset of the drying trend and its severity at the individual sites slightly differs, which might be owed to dating uncertainties and site characteristics. However, there is also local evidence for prevailing wet or rather fluctuating climate conditions during the Late Holocene in NW China (Rhodes et al. 1996; Liu et al. 2008b; An et al. 2012a), highlighting the spatial complexity of Late Holocene climate development in the region and the need for further investigations. Nevertheless, in summary, the overall evolution of summer moisture conditions during the last 6000 years at Son Kol with a rather wet Mid-Holocene and a subsequent moderate drying during the Late Holocene is in quite good agreement with results from other palaeoclimate records in the western part of mid-latitude ACA.

4.4.2 Phases of increased winter precipitation and hemispheric-scale climate teleconnections

In addition to the biogeochemical data, information about past environmental and climatic changes at Son Kol can also be gained from the $\delta^{13}C_{org}$, $\delta^{15}N$ and C/N composition of lake

sediment OM. Facilitated by the characteristic geochemical/isotopic signatures of the different aquatic and terrestrial organic components involved in lake sediment formation, these parameters allow to track for instance changes in environmental conditions, productivity, nutrient availability, or the origin of OM (Hollander et al. 1992; Hodell and Schelske 1998; Talbot and Laerdal 2000; Teranes and Bernasconi 2000; Talbot 2002). While $\delta^{15}N$ is in this regard a partly ambiguous proxy because of the complexity of the nitrogen cycle and the various in-lake and catchment processes and nitrogen sources involved in lake sediment OM formation (Talbot 2002), the $\delta^{13}C_{org}$ and C/N signatures of different organic materials are relatively well known. For example, freshwater phytoplankton is commonly characterized by low $\delta^{13}C_{org}$ values (−30 to −20 ‰) and C/N ratios (< 10), whereas C_3 terrestrial plants and aquatic macrophytes reveal low $\delta^{13}C_{org}$ values but high C/N ratios (> 20), and C_4 terrestrial plants are characterized by both high $\delta^{13}C_{org}$ values (more than −15 ‰) and C/N ratios (Meyers and Teranes 2002).

In general, these values are confirmed by the geochemical/isotopic signatures of modern OM samples from Son Kol and its catchment (

Figure 23). Accordingly, Son Kol sediment OM represents a complex mixture of different sources with temporally variable contributions. However, soil and terrestrial plant OM (and partly also emerged aquatics) apparently prevail as their $\delta^{15}N$, $\delta^{13}C_{org}$, and C/N signatures are most similar to those of the lake sediments (

Figure 23). This is corroborated by the predominance of the long-chain *n*-alkanes C_{29} and C_{31} within the sediments, which derive from higher terrestrial plants (Eglinton and Hamilton 1967; Maffei 1996) and thus indicate a significant contribution of terrestrial material to sediment OM. Concerning the general geochemical/ isotopic composition of the Son Kol sediments, the most striking feature are three distinct, multi-centennial phases of high $\delta^{15}N$ values at 5100–4350, 3450–2850, and 1900–1500 cal. yr BP as well as three short-term enrichments at 5500–5300, 3900–3850 and 2250–2200 cal. yr BP (

Figure 22), which are paralleled by lowered $\delta^{13}C_{org}$ values. High $\delta^{15}N$ values in the sediments could be attributed to (1) denitrification processes in an anoxic hypolimnion during periods of pronounced meromixis (Hodell and Schelske 1998; Talbot and Laerdal 2000), (2) increased aquatic productivity (Gu et al. 1996; Talbot and Laerdal 2000; Teranes and Bernasconi 2000), (3) evaporative loss of isotopically light ammonia during dry climate conditions (Talbot and Johannessen 1992), or (4) increased input of terrestrial OM (Haberzettl et al. 2005; Mayr et al. 2009). However, denitrification is unlikely to have caused elevated $\delta^{15}N$ values, as there is no sedimentological indication (e.g. varves and/or pyrite formation) for hypolimnetic anoxia within the respective intervals and sediment-dwelling ostracods (e.g. *Limnocythere inopinata, Candona neglecta*) and shells, which require well-oxygenized bottom waters, are also abundant. As evidence for a significantly deeper water body (e.g. abandoned shorelines) in the past is lacking, it is likely that the lake retained its present small depth-to-surface-area ratio at least since the Mid-Holocene and was, also in consequence of the large wind fetch, always well mixed as it is today, which is

indicated by a high O_2 saturation throughout the water column (Figure 5b) and almost no temperature stratification throughout the year. Furthermore, productivity changes can also be ruled out to have triggered high $\delta^{15}N$ values as $\delta^{15}N$ and $\delta^{13}C_{org}$ are clearly anti-correlated throughout the sediment record (

Figure 23), whereas the opposite is commonly regarded to reflect in-lake productivity changes (Hodell and Schelske 1998; Talbot and Laerdal 2000; Finlay and Kendall 2007). Finally, also evaporative loss of isotopically light ammonia during dry climate conditions is unlikely to have caused increases in $\delta^{15}N$, as there is no clear correspondence between high-$\delta^{15}N$-intervals and dry episodes reflected by the δD_{C29} record (

Figure 22).

Hence, the only reasonable explanation for elevated $\delta^{15}N$ values in the lake sediments is input of terrestrial OM, particularly soil material. This is endorsed by the high similarity between the isotopic/geochemical signatures of the soils and lake sediment OM during high-$\delta^{15}N$-intervals and also the parallel increases of $\delta^{15}N$ and Ti and K µXRF counts, the latter reflecting terrestrial minerogenic input (

Figure 22). A similar correlation observed in lake sediments from Chile has recently also been interpreted in terms of increased soil input from the catchment (Haberzettl et al. 2005). The mechanism primarily responsible for high $\delta^{15}N$ values in soils is the enrichment of ^{15}N during the mineralization/decomposition of terrestrial OM, which is influenced by several ecosystem variables, for example, climate, vegetation, soil composition, and depth as well as microbial processes (Kendall 1998; Amundson et al. 2003). The ^{15}N-enriched soil OM is thereby mainly bound to minerogenic components (besides occurring as dissolved organic/inorganic nitrogen), which are easily transported to the lake basin by catchment erosion processes. In this context, it should be mentioned that C/N ratios are in the case of Son Kol a rather ambiguous proxy for soil input. Although the catchment soils are characterized by elevated $\delta^{15}N$ values and relatively low C/N ratios (

Figure 23), lake sediment C/N ratios reveal a strongly heterogeneous response during the individual intervals of increased soil input (

Figure 22). This might be owed to variable contributions of plant OM with considerably higher C/N ratios (

Figure 23) during the individual intervals of increased allochthonous input. Concerning the transport of soil material to the lake basin, aeolian supply is rather unlikely as related deposits (loess) are generally restricted to lower altitudes, i.e. the piedmont regions of the Tian Shan (Machalett et al. 2006), and grain sizes of the detrital material within the high-$\delta^{15}N$-intervals are relatively large.

Hence, soil input should be mainly related to fluvial transport processes, namely precipitation (reflecting wetter climate conditions in summer) or meltwater runoff (reflecting increased winter snowfall). As intervals of intensified terrestrial input do not

explicitly correlate with phases of pronounced summer humidity but rather occur randomly during both dry and humid summer periods (indicated by high and low δD_{C29} values, respectively), they are consequently most likely not associated with summer precipitation but with increased winter snowfall and enhanced meltwater supply during subsequent spring thaw. This interpretation is corroborated by own field observations, revealing the perennial creeks around Son Kol almost completely desiccated during summer, although this is presently the season with the highest precipitation. Nevertheless, it should be mentioned that enhanced snowmelt and thus meltwater runoff might also be caused by increased temperatures, but since no explicitly temperature-related proxy data are available from the Son Kol sediments, this option remains speculative.

Considering also the basal debris flow in composite profile SONK_11_D1/2 as a meltwater-related deposit, distinct phases of enhanced winter precipitation in Central Kyrgyzstan occurred before *c*. 6000 and at 5100–4350, 3450–2850, and 1900–1500 cal. yr BP with an intriguing recurrence interval of ~1500 years. This closely matches a prominent low-frequency millennial-scale climate cyclicity of about 1500–1600 years observed in drift ice transport (Bond et al. 1997), ocean temperature conditions, and strength of the thermohaline circulation in the North Atlantic (Bianchi and McCave 1999; Thornalley et al. 2009), but also in many other Northern Hemisphere palaeoclimate records (Wanner et al. 2008). As recently shown, this cyclicity is not triggered by solar activity changes (Debret et al. 2007; Sorrel et al. 2012) but rather related to an ocean-internal variability of conveyor strength (Bianchi and McCave 1999). As processes in the ocean are closely coupled to changes in atmospheric conditions in the North Atlantic realm, namely, the intensity of the mid-latitude westerly jet stream, similar periodicities are also apparent in wind strength in Iceland (Jackson et al. 2005) and storm activity in northern France (Sorrel et al. 2009), as well as in the amount of winter precipitation in southwestern Norway (Bjune et al. 2005) and the western Mediterranean (Fletcher et al. 2013). Since moisture supply to Central Kyrgyzstan is mainly controlled by the strength of the mid-latitude Westerlies (Aizen et al. 1997; Bohner 2006), changes in their intensity observed in the North Atlantic realm should consequently also influence climate conditions at Son Kol. Indeed, snow-rich episodes in Central Kyrgyzstan reveal a close correspondence with millennial-scale increases in wind strength in Iceland (Jackson et al. 2005) and winter precipitation in southwestern Norway (Bjune et al. 2005), reflecting episodic intensifications of westerly atmospheric flow at high northern latitudes (Figure 25), as well as with the occurrence of drier winters and thus reduced westerly flow at lower latitudes, for example, in the western Mediterranean (Fletcher et al. 2013). This latitudinal pattern is characteristic for the present-day positive mode of the NAO (Hurrell 1995), and it thus appears that enhanced winter precipitation in the Central Tian Shan is closely coupled to a strengthening of the Westerlies during positive NAO phases. In this context, the apparent discrepancy of weakened Westerlies in the western Mediterranean but enhanced westerly flow at about the same latitude in Central Asia might be explained by a longitudinally contrasting precipitation pattern: as indicated by data reanalysis and modeling studies, the southeastern Mediterranean (Dunkeloh and

Jacobeit 2003; Black 2012) and western Central Asia (Syed et al. 2006; Syed et al. 2010) experience increased winter precipitation during positive NAO phases, while the western Mediterranean remains rather dry at these times (Fletcher et al. 2013). Hence, the ~1500-year cyclicity observed in snowfall intensity at Son Kol provides strong evidence for a significant impact of millennial-scale North Atlantic climate variability and particularly the NAO on winter precipitation conditions in Central Asia since the Mid-Holocene, a relation so far not shown for western Central Asia on longer timescales. However, as the relation between increased winter precipitation in the Tian Shan and NAO variability is still controversially debated (Aizen et al. 2001) and since also other remote influences on regional winter precipitation variability may exist (Syed et al. 2010), further studies are necessary to test the results from Son Kol and to fully understand the teleconnections exerting influence on winter precipitation variability in the western part of Central Asia.
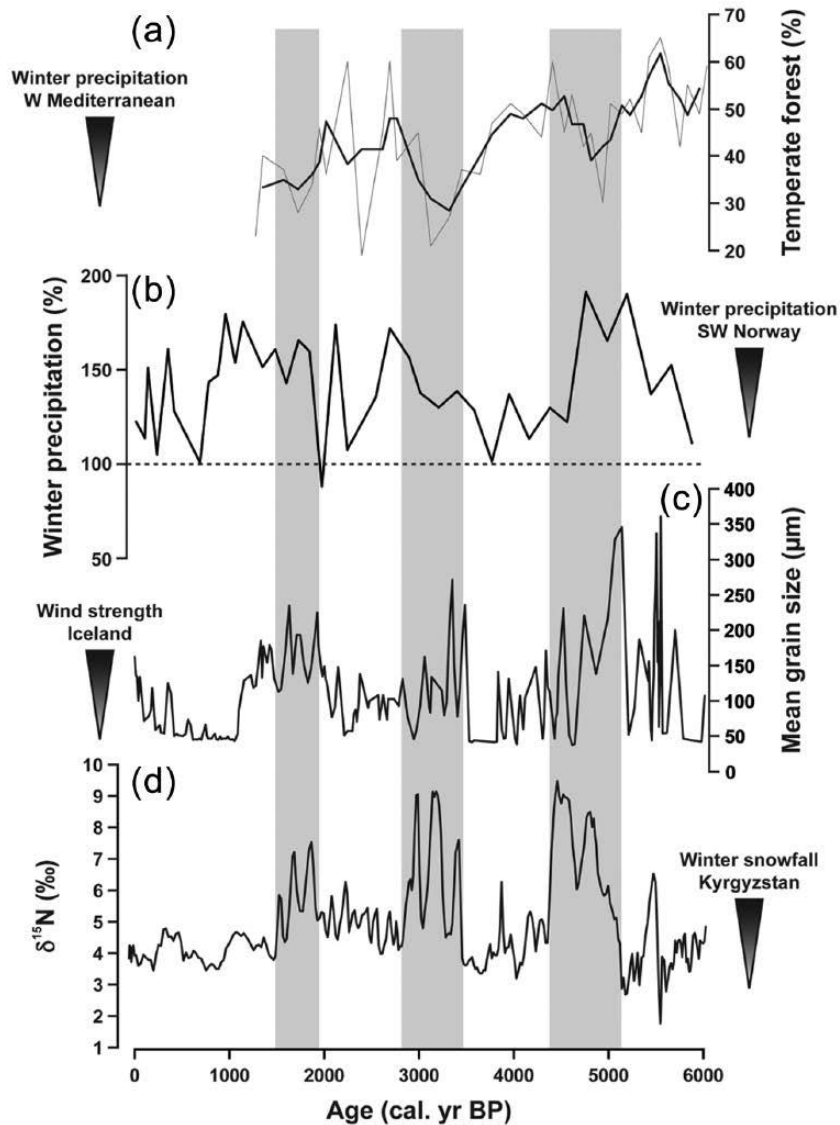
Figure 25: Hemispheric-scale comparison of climate records reflecting changes in the intensity of the wintertime Westerlies.

(a) Changes in forest composition (percentage of temperate forest taxa) in the western Mediterranean as a proxy for winter precipitation (Fletcher et al. 2013). The gray line represents the original data, while the black line is a 3-point running mean. (b) Reconstructed amount of winter precipitation in southwestern Norway compared with the present-day level (100 %) (Bjune et al. 2005). (c) Mean grain size of loess as a proxy for wind strength on Iceland (Jackson et al. 2005). (d) $\delta^{15}N$ of Son Kol sediments as a proxy for meltwater-derived input of soil material and thus snowfall intensity in Central Kyrgyzstan.

4.5 Conclusion

Multi-proxy analyses of lake sediments from Son Kol (Central Kyrgyzstan) provide evidence for a predominant influence of the mid-latitude Westerlies on Holocene moisture evolution in this region. Following a wet Mid-Holocene and a pronounced dry phase

between 4950 and 3900 cal. yr BP, a progressive but only moderate reduction of summer precipitation is observed during the Late Holocene, being in accordance with results from other regional palaeoclimate records and mainly attributable to the gradually weakening influence of the Westerlies in mid-latitude arid Central Asia throughout the Holocene. However, changes in the intensity of the Westerlies, which are directly related to climate variability in the North Atlantic realm, apparently did not only influence summer precipitation patterns but also had a substantial impact on winter climate conditions in mid-latitude ACA. This is indicated by periods of enhanced detrital input through snowmelt, reflecting increased winter snowfall brought by the Westerlies, which occurred with a distinct periodicity of ~1500 years. Synchronous low-frequency millennial-scale climate oscillations, attributed to changes in the strength and position of the westerly jet stream, have also been observed in several palaeoclimate records in the North Atlantic realm, revealing a significant hemispheric-scale teleconnection between the North Atlantic and the Central Asian climate system and a possible impact of NAO variability on winter precipitation in the Central Tian Shan. However, understanding the underlying climatic mechanisms in full detail requires further investigations and more high-resolution palaeoclimate records from the climatically sensitive region of mid-latitude Central Asia.

5 Reconstruction of glacier influence and climate changes in the Holocene at closed Lake Chatyr Kol, Tian Shan (Central Asia) using lacustrine multi-proxy analyses

5.1 Abstract

Lake Chatyr Kol in the dry inner Tian Shan (Kyrgyzstan) is a high-alpine closed lake system influenced by several glaciers and snowfields. To evaluate the spatio-temporal influence of the mid-latitude Westerlies wind system, a 6.2 m long sediment core reaching back to 11.1 cal. kyr BP was investigated. It spans almost the entire Holocene period and provides high resolution limnological and climatic information. The multi-proxy analyses include compound-specific stable hydrogen isotopic compositions of *n*-alkanes, unsaturation indices inferred from alkenones, diatoms, bulk sedimentary carbonate and organic matter stable isotope compositions, µXRF scans, revealing different conditions for the Early-, Mid- and Late Holocene. Pronounced Early Holocene glacier melting at Chatyr Kol between 10.8 and 8 cal. kyr BP is inferred from increased terrestrial minerogenic input and lake volume growth, identified by µXRF Ti scans and strongly decreased δD_{C23} values. Major driver for glacier melt was the increasing temperature triggered by maximum Northern Hemisphere summer insolation. A close climatic connection between the North Atlantic and Central Asia is also displayed by wet winters in Norway, Kyrgyzstan and North China. The interplay between the mid-latitude Westerlies and the North Atlantic Oscillation directly influences glacier behavior and lake level fluctuations in the Tian Shan and adjacent lake systems. Proxy data from Chatyr Kol sediments for the last 2000 years give evidence for alternating periods with cold/wet and warm/dry winters known as the Dark Ages Cool Period, Medieval Climate Anomaly and Little Ice Age. Warm periods in Central Asia were accompanied by low lake levels. The glacier influence and the isolated location of Lake Chatyr Kol favored rather specific limnological, but in general regionally coherent environmental responses to Holocene climatic fluctuations.

5.2 Introduction

The Holocene started at about 11.6 cal. kyr BP with a fast and significant warming from the previous cold Younger Dryas period. Maximum summer insolation in the Northern Hemisphere at the beginning of the Holocene gradually decreased to its minimum in the Late Holocene, which led to changes in global atmospheric circulation. The North Atlantic Ocean is considered as the main driver for the mid-latitude Westerlies wind system, which transports water vapor from the Atlantic via Europe to Central Asia, where water recycling at the Aral-Caspian Basin, the Mediterranean and Black Seas takes place. The heterogeneous Tian Shan Mountains in Central Asia and the neighboring ranges like Pamir provide a natural barrier to incoming moisture transported by the Westerlies, hence resulting in spatial differences in rainfall intensity between the inner and outer as well as

western and eastern ranges. The Holocene climate was characterized by spatio-temporally fluctuating conditions between cold/warm and wet/dry phases induced from the variable interplay between the Westerlies and the Siberian High. Several studies already investigated the regional Holocene climate variability using lacustrine sediments of Lake Issyk Kul in Kyrgyzstan (Ricketts et al. 2001), the Aral Sea (Sorrel et al. 2006), Lake Karakul in Tajikistan (Mischke et al. 2010) as well as Lake Karakuli (Aichner et al. 2015) and Lake Bosten (Wünnemann et al. 2006) in China. Furthermore, direct information on past hydrological changes was received from lacustrine compound-specific stable hydrogen compositions in the Tian Shan (Lauterbach et al. 2014) and Pamir (Aichner et al. 2015). It is known, that these proxies provide information on temperature (chapter 3), evaporation, precipitation as well as lake level changes (Mügler et al. 2010; Günther et al. 2013; Hu et al. 2014). In this study, a relatively isolated lake system in the southern inner Tian Shan was investigated using a multi-proxy approach to evaluate the local/regional influence and intensity of the Westerlies during the Holocene. Chatyr Kol as a closed system is additionally influenced by glacial meltwater and therefore provides important spatio-temporal information on limnological- and glacier responses to Holocene temperature- and precipitation changes. Possible biomarkers able to record temperatures are haptophyte-produced alkenones. Their temperature-sensitive unsaturation index $U_{37}^{K'}$ is already well established in marine systems (Conte et al. 2006), but for lacustrine systems a general transfer function is still lacking (Theroux et al. 2010). The occurrence of different haptophyte species in a lake strongly influences the calibration, hence making lake-specific investigations necessary. Uncertainties still exist about environmental parameters influencing alkenone production like salinity, nutrient availability, water chemistry or even ecological effects (Sikes and Sicre 2002). We therefore investigated the distribution and concentration of C_{37} and C_{38} alkenones to decipher the specific factors influencing presence/absence of haptophyte species at Chatyr Kol. In addition, the stable isotope compositions of carbonates and bulk sedimentary organic matter ($\delta^{18}O$, $\delta^{13}C$ and $\delta^{15}N$) as well as the geochemical composition of the sediments (µXRF scanning) have been investigated and their various responses to environmental changes were discussed in detail. We further wanted to evaluate the influence of glaciers in a catchment on the response to rapid climatic changes, since Chatyr Kol is one of few so far investigated Tian Shan lakes showing these conditions.

5.3 Results

Pelagic sediments of the Chak12 composite profile can be subdivided in four main units (I-IV) with unit III subdivided into III-A and III-B primarily based on lithostratigraphical characteristics; however geochemical (µXRF) and isotopic as well as biogeochemical properties discussed here allow an additional subdivision of unit II into II-A, II-B and II-C separated at 8180 and 5000 cal. yr BP, respectively.

5.3.1   Geochemical/isotopic composition of the lake sediments

The composite profile is characterized by several pairs of proxies showing significantly high correlations, namely TOC and TN (r = 0.97**), $\delta^{13}C_{org}$ and $\delta^{15}N$ (r = –0.7**) (Figure 26) as well as Ti and Al, K, Si (r = 0.86**, 0.9** and 0.91**, resp.) (Figure 27).

In unit I (623.5–567.5 cm / 11,140–10,140 cal. yr BP), consisting of laminated light-grey lake marl, TOC and TN stand out by stable but lowest values (TOC: 0.5 ± 0.2 %; TN: 0.06 ± 0.02 %). The stable carbon isotope composition of carbonates ($\delta^{13}C_{carb}$) is relatively high (mean: 1.1 ‰) and shows a similar fluctuation pattern like $\delta^{15}N$. µXRF scans show highest values for Ti of the entire composite and relatively strong fluctuations for Sr/Ca.

The lithostratigraphical unit II (567.4–131.6 cm / 10,140–2350 cal. yr BP) generally consists of laminated sediments with brownish-reddish layers indicating stable redox conditions and seasonal variability. Nevertheless, we observed strong similar fluctuations of several proxies. As a consequence of changes in biological and geochemical proxies unaffecting the sedimentological pattern at Chatyr Kol, a subdivision into section II-A to II-C was carried out.

Subunit II-A (567.4–458 cm / 10,140–8180 cal. yr BP) is characterized by slightly increasing TOC (1 to 4.6 %) and TN (0.1 to 0.4 %) values. Highest fluctuations of $\delta^{13}C_{carb}$ and $\delta^{18}O_{carb}$ with maximum (up to 7.5 ‰) and minimum (down to –4.9 ‰) values appear at 489.7 cm (8750 cal. yr BP). Their correlation is significantly negative in this subunit (r = –0.98**). Subunit II-A is also characterized by a striking decreasing trend of Ti, while Ca/Ti shows a highly variable increasing trend following the lamination pattern and sulphur shows an increasing trend (875 to 4050 counts).

The following subunit II-B (458–278.5 cm / 8180–5000 cal. yr BP) is dominated by high variations of $\delta^{15}N$ (7.4 ± 2.2 ‰), $\delta^{18}O_{carb}$ (–2.3 ± 2.5 ‰) and $\delta^{13}C_{carb}$ (1.7 ± 1.2 ‰) as well as TN (0.3 ± 0.1 %) and TOC (3.2 ± 1.1 %). In consequence, plateau-like highest values occur for $\delta^{15}N$ and $^{13}C_{carb}$ compared to other units. Surprisingly, $\delta^{13}C_{carb}$ and $\delta^{18}O_{carb}$ are significantly positive correlated this time (r = 0.7**), while $\delta^{13}C_{org}$ and $\delta^{15}N$ have their highest correlation of the entire record (r = –0.8**). At the end of subunit II-B at 305 cm (5450 cal. yr BP) consistent diatom detection with a dominance in planktonic compared to non-planktonic (benthic) diatoms can be noticed. Nevertheless, preservation of diatom shells is in bad condition. The Sr/Ca ratio calculated from µXRF scanning results shows strongly variable but highest values (0.03 ± 0.001) compared to the entire record. Obvious lamination-correlated fluctuations also appear for Mn/Fe (0.07 ± 0.02). Generally, a significantly positive correlation of S and Cl (r = 0.8**) is observed, but a short 440-year-long episode with a negative correlation due to low sulphur counts is observed from 373 to 348 cm (6660–6220 cal. yr BP).

The diatom assemblage observed in subunit II-B continues also in subunit II-C (278.5–131.6 cm / 5000–2350 cal. yr BP), accompanied by a long-term reduction of $\delta^{15}N$, $\delta^{13}C_{carb}$ and $\delta^{18}O_{carb}$, which is most characteristic for this subunit. Diatom composition abruptly

shifts at 208 cm (3715 cal. yr BP), when non-planktonic diatoms nearly completely replace planktonic diatoms. This organism shift is directly followed by a ca. 535-year-long period of higher $\delta^{15}N$ and $\delta^{13}O_{carb}$ values from 210 to 180 cm (3750 to 3215 cal. yr BP) (r = 0.7**). This excursion is not visible in $\delta^{13}C_{carb}$ values; however a slight increase during the subunit happens. Ca/Ti ratios reveal this distinct excursion too, while Ti generally increases. A stronger stepwise increase (step at ca. 206 cm) can additionally be seen in TOC (2.5 to 7.7 %), TN (0.3 to 0.8 %) and even more pronounced in total alkane values (24 to 104 μg g^{-1}). The transition to unit III causes clear changes in almost all proxies.

Lithostratigraphical units III-A (laminated grey lake marl) and III-B (laminated brownish-grey lake marl with abundant plant macros) (A: 131.5–116 cm / 2,350–2,070 cal. yr BP; B: 116–68 cm / 2070–1215 cal. yr BP) display a generally opposing behavior for all proxies except diatoms compared to the previous unit. The non-planktonic dominated diatom distribution ends at 87 cm (1550 cal. yr BP) with ongoing poor preservation of diatom shells. While $\delta^{13}C_{carb}$ and $\delta^{13}O_{carb}$ values show trends which continue in the following unit IV, $\delta^{15}N$, $\delta^{13}C_{org}$, TN and TOC display unit III as opposite record to the following unit IV. Sr/Ca as well as Ti characterize the subunit III-A with elevated values. Other μXRF scans show, compared to the previous subunit, extremely decreased values in unit III-B like Sr/Ca. However, they reach their maximum counts in the top unit IV.

The uppermost unit IV (68–0 cm / 1215 cal. yr BP to present) is characterized by homogeneous grey lake marl with abundant plant macros. S-shape proxy curves have turning points at 44 cm (790 cal. yr BP) and ~13 cm (230 cal. yr BP) with maximum Ca/Ti, minimum Sr/Ca, minimum Ti as well as high $\delta^{13}C_{org}$ values at the first point, and high Sr/Ca and Ti values as well as low $\delta^{18}O_{carb}$ values at the second point. Since sulphur becomes reduced at the end of subunit II-C it shows stable minimum counts. The upper 8 cm contain mainly planktonic diatoms under bad preservation.
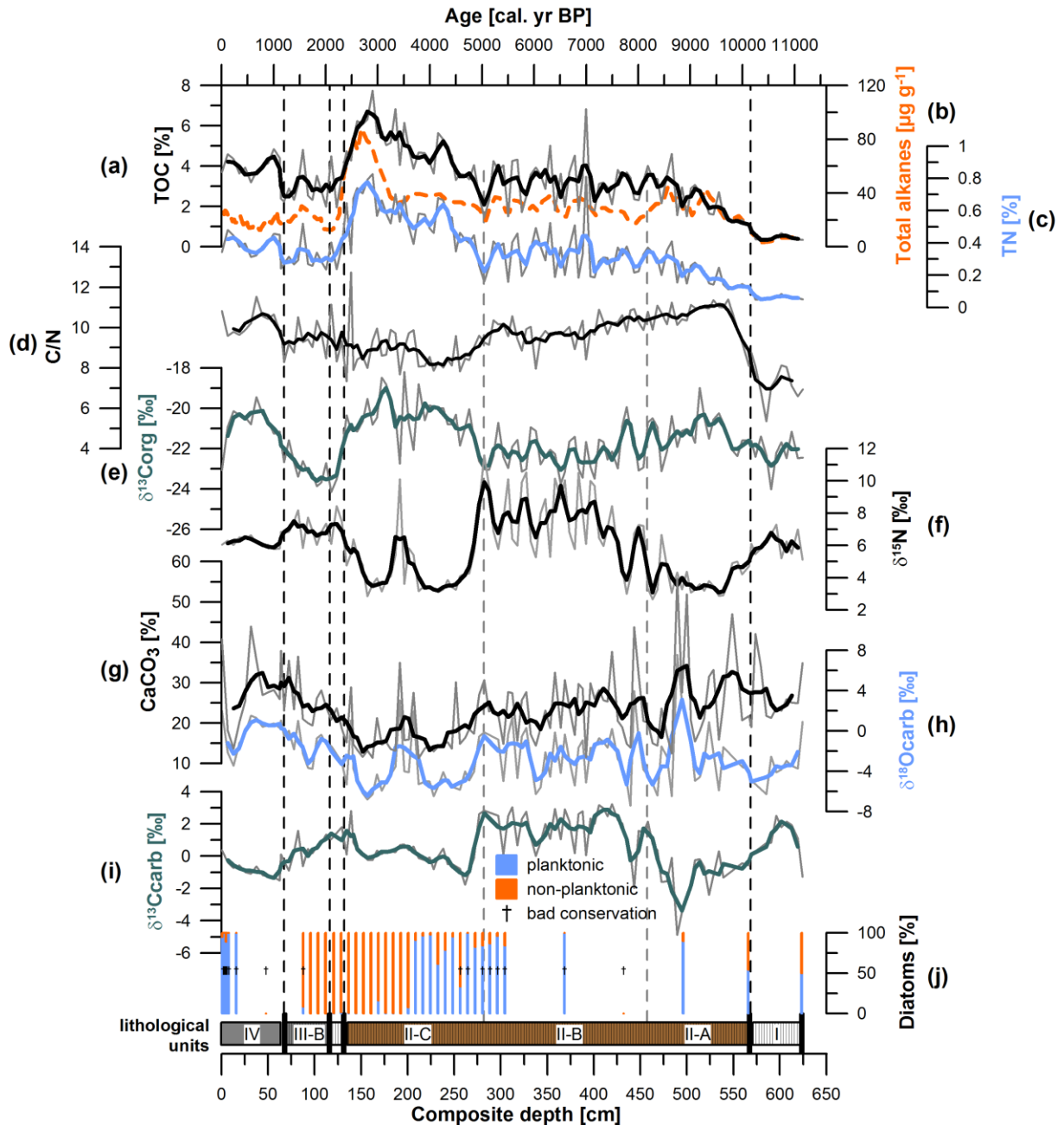
Figure 26: Results of stable isotope and geochemical analyses on the sediments of composite profile Chak12.

(a) Percentage of TOC (black line). (b) Total *n*-alkane concentration (see Figure 30, dashed orange line). (c) Percentage of TN (blue line). (d) Ratio of Total Carbon and Nitrogen (C/N). (e) Stable carbon isotope composition of organic carbon ($\delta^{13}C_{org}$, green line). (f) Stable nitrogen isotope composition ($\delta^{15}N$, black line). (g) Percentage of $CaCO_3$ (black line). (h) Stable oxygen isotope composition of carbonate ($\delta^{18}O_{carb}$, blue line). (i) Stable carbon isotope composition of carbonate ($\delta^{13}C_{carb}$, green line). (j) Relative amount [%] of planktonic (blue bars) and non-planktonic/benthic (orange bars) diatoms. Bars marked with "┼" represent bad preservation of diatoms. Dashed vertical lines represent the units subdivided by lithostratigraphical investigations.
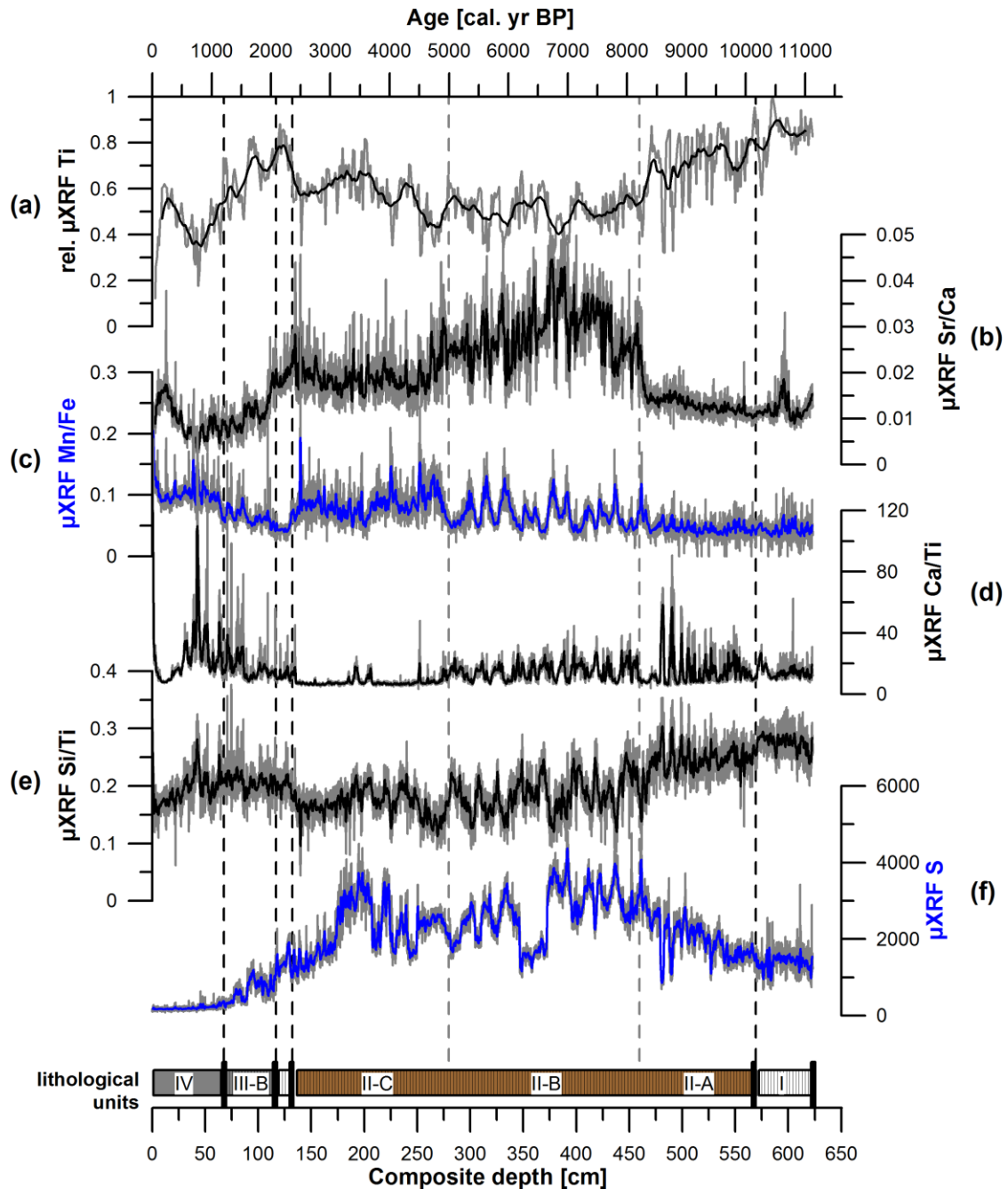
Figure 27: Results of µXRF scanning analyses on Chak12 sediments.
(a) Standardized values of Titanium (Ti). (b) Ratio of Strontium and Calcium (Sr/Ca). (c) Ratio of Manganese and Iron (Mn/Fe, blue line). (d) Ratio of Calcium and Titanium (Ca/Ti). (e) Ratio of Silicon and Titanium (Si/Ti). (f) Sulphur (S, blue line). Dashed lines represent the units subdivided by lithostratigraphical investigations.

5.3.2 Biogeochemistry of sediment core "Chak12_comp2"

5.3.2.1 *n*-Alkane distribution

Sediments of core Chak12 contain mainly odd numbered *n*–alkanes C_{17} and C_{23} to C_{31} with a changing distribution pattern within the core. According to the *n*-alkane distribution, the core contains three clusters (Figure 28A). Sediment samples combined in cluster 1 consist of odd numbered mid– and long–chain *n*–alkanes C_{23} to C_{31}, which were detected only in the upper core section from 0 to 107 cm (~1900 cal. yr BP) (unit IV/III-B). Within the entire core the total concentration of *n*–alkanes C_{17-31} ranges between 2.7 and 104 µg g^{-1} (Figure 30). In cluster 1, the mean alkane concentration is relatively low with 20 ± 5 µg g^{-1}. The most abundant cluster over a prolonged period in the core is cluster 2, which contains mainly long-chain *n*-alkanes C_{27} and C_{31}. It appears sharply after cluster 1 and dominates from 466 to 112 cm (8325–2000 cal. yr BP) (unit III-A/II-C/II-B). The alkane concentration maximizes between 156 and 136 cm (2790–2430 cal. yr BP) (84 ± 22 µg g^{-1}), while the general amount of this cluster is highly fluctuating (mean value 32 ± 19 µg g^{-1}). In the transition zone below 475 cm (< 8,490 cal. yr BP) (unit II-B), the dominance of the short-chain *n*-alkane C_{17} shown as cluster 3 appears together with cluster 2. Additionally, a decline in the alkane concentration to minimum values below 10 µg g^{-1} is visible.

5.3.2.2 Long-chain alkenone distribution

Investigations on LCAs for the composite profile reveal sections of very high alkenone concentrations, but also sections with completely missing alkenone signals (Figure 30). Alkenones are missing from the base of the sediment core until 570 cm (> 10,180 cal. yr BP) (unit I) and in the top core section above 68 cm (< 1,215 cal. yr BP) (unit IV). Between 68 and 116 cm (1215–2070 cal. yr BP) (unit III-B) the total alkenone concentration is below 50 µg g^{-1}. However, these lower values also appear sporadically in the middle part of the core (unit II). Detected alkenones in middle section show high fluctuations of their total concentrations (229 ± 278 µg g^{-1}) with maximum values of 1365 µg g^{-1}at 203 cm (3630 cal. yr BP). Considering the distribution of di-, tri- and tetra-unsaturated methyl C_{37} and ethyl C_{38} LCAs in samples with total concentrations > 50 µg g^{-1}, the core Chak12 consists of two clusters (Figure 28B). A dominance of ethyl C_{38} alkenones, mainly of tri- and tetra-unsaturated $C_{38:3}$ and $C_{38:4}$ is characteristic for cluster B, while under the same ratio of C_{38}, the dominance in cluster A is shifted to the methyl C_{37} alkenones with mainly tetra-unsaturated $C_{37:4}$ and tri-unsaturated $C_{37:3}$ compounds. Until 432 cm both clusters appear irregularly. The abundant cluster A (n = 40 of 62) appears within unit II and III-A. It is repressed remarkably by cluster B only between 294 and 220 cm (5250–3930 cal. yr BP). The relative amount of $C_{37:4}$ generally increases during the record with minor positive excursions at 460 cm (8220 cal. yr BP) and 160 cm (2860 cal. yr BP). Stratigraphically, the unsaturation index $U_{37}^{K\prime}$ shows a similar trend with increased values during the excursions. Higher $U_{38}^{K\prime}$ values only appear in subunit II-B.
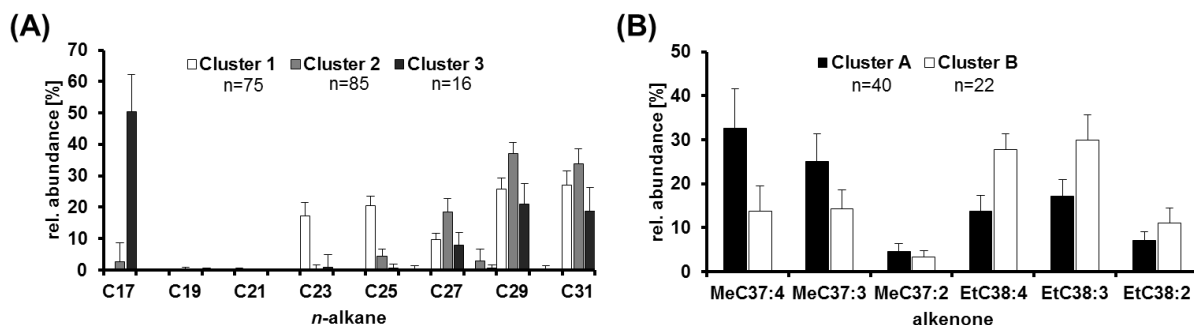
Figure 28: (A) Distribution of n-alkanes within cluster 1 to 3 in sediment composite core Chak12. Samples were classified by using the relative abundance of n–C_{17-31}. The cluster distribution shows a dominance of n–C_{17} in cluster 3, while cluster 2 contains mainly n-C_{27} to n-C_{31}. Cluster 1 is a mixture of n-alkanes C_{23} to C_{31}. (B) Distribution of di-, tri- and tetra-unsaturated methyl C_{37} and ethyl C_{38} long-chain alkenones in Chak12. Cluster A contains mainly methyl $C_{37:4}$, while cluster B is dominated by ethyl $C_{38:4}$ and $C_{38:3}$.
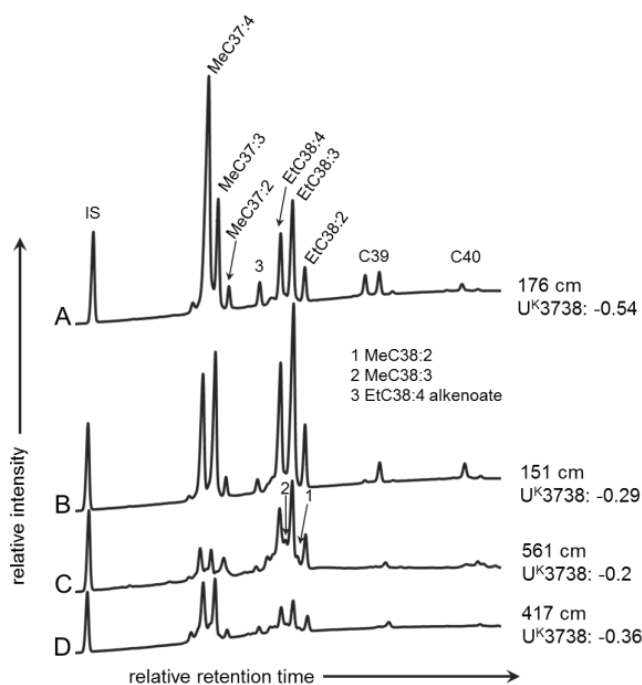
Figure 29: Examples of long-chain alkenone distribution patterns in the Chatyr Kol sediments. Gas chromatograms show dominance of (A) tetra-unsaturated methyl C_{37} and (B) tri-unsaturated ethyl C_{38} alkenones with generally high alkenone concentrations. Lower concentrated C_{38} (C) and C_{37} (D) dominated samples with detected methyl C_{38} alkenones. IS represents the Internal standard n-alkane C_{37}.

5.3.2.3 Compound-specific hydrogen isotope composition (δD)

Investigation of δD values from mid- and long-chain *n*-alkanes C_{23} and C_{29} is limited by their low concentration. Below 107 cm, where alkane cluster 2 and 3 dominate, the *n*-C_{23} concentration periodically was below the IRMS detection limit of 50 ng μl^{-1} (Figure 30). In unit I, the C_{23} concentration was even too low for any δD measurements. Therefore, highest C_{23} resolution could only be determined within cluster 1 (total core: n = 113). Instead, the sufficient amount of C_{29} within the entire core leads to δD values in higher resolution (total core: n = 174). The δD values of C_{23} range between −68 and −278 ‰, while C_{29} shows partly more depleted values between −124 and −213 ‰. In case of the core section, the δD values of C_{29} match relatively well with the alkenone concentrations. The bottom section from 623.5 to 567.5 cm (unit I) and the upper section from 68 to 0 cm (unit IV) reveal more enriched δD mean values of −147 ± 13 ‰ and −150 ± 6 ‰, respectively, compared to the unit III-B until 116 cm with only −159 ± 7 ‰. The most depleted values (−189 ± 11 ‰) appear from 131.6 to 567.4 cm (unit II). Due to relatively enriched δD values of the mid-chain alkane C_{23} from 0 to 460 cm (−140 ± 20 ‰), except a period of slightly depleted values in subunit II-A (−147 ± 26 ‰), the calculated proxy $\Delta\delta D_{C29-C23}$ follows mainly the δD_{C29} curve.
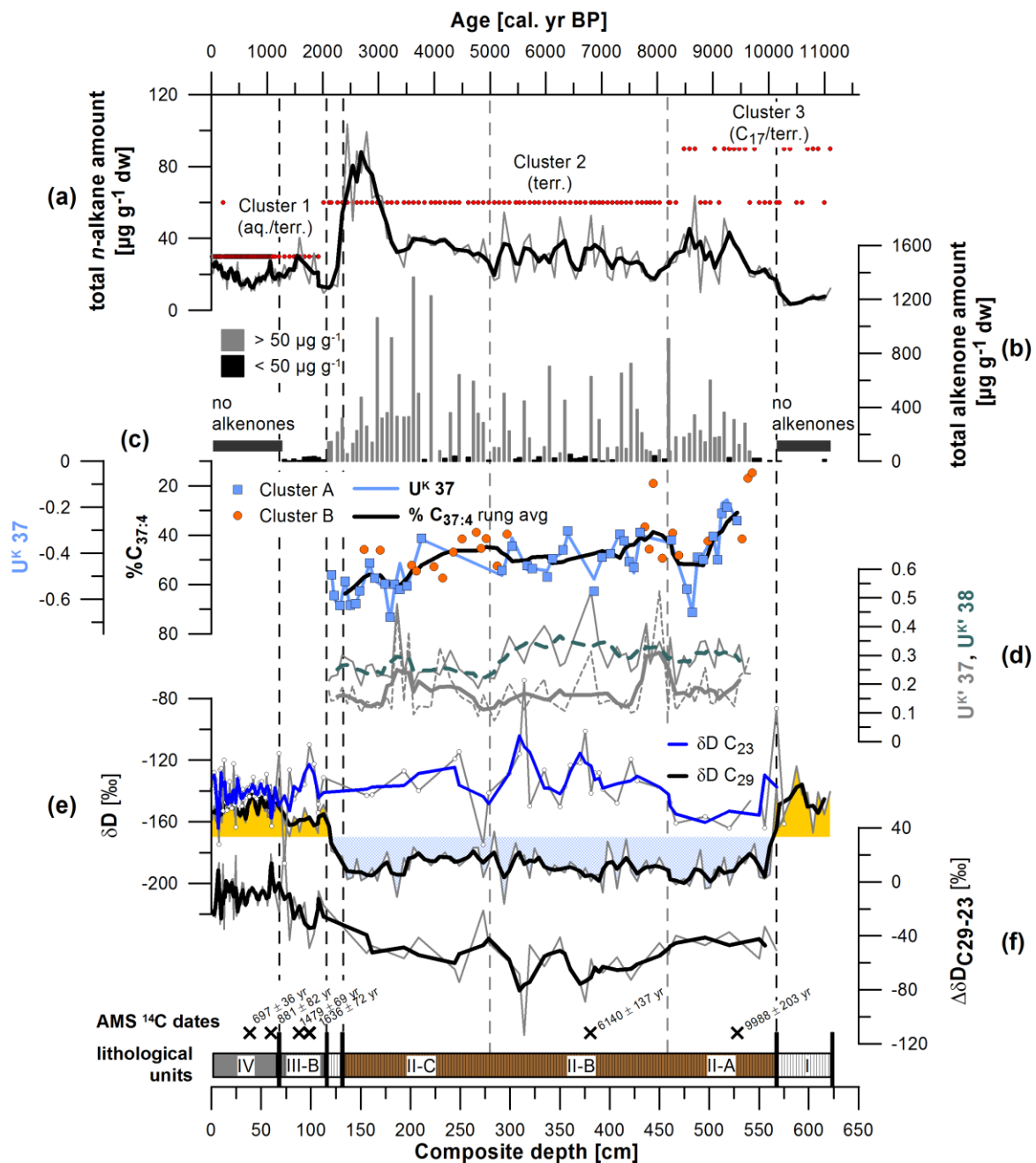
Figure 30: Biogeochemical proxies of the Chak12 composite profile.

(a) Total concentration of *n*-alkanes with cluster 1 to 3 regarding the relative distribution of chain-lengths (red circles). (b) Total concentration of alkenones (grey columns represent $> 50\ \mu g\ g^{-1}$ and black columns $< 50\ \mu g\ g^{-1}$). The absence of alkenones in unit I and IV is marked by black horizontal bars. (c) Percentage of $C_{37:4}$ alkenones to C_{37}; alkenone cluster A dominated by C_{37} is marked by blue squares and Cluster B dominated by C_{38} alkenones is marked by orange circles. The blue line represents the U^K_{37} values of cluster A. (d) Unsaturation indices $U^{K\prime}_{37}$ (grey solid line) and $U^{K\prime}_{38}$ (green dashed line). (e) Stable hydrogen isotope composition of *n*-alkane C_{23} (blue thin line) and C_{29} (black thick line). (f) Calculated $\Delta\delta D_{C29\text{-}C23}$ index. (Bottom) Six AMS ^{14}C dates are marked by "x" and 4 main lithostratigraphical units by Roman characters.

5.4 Discussion

5.4.1 Interpretation of carbonate related proxies

Oxygen isotope composition and temperature of the lake water are the driving factors controlling $\delta^{18}O$ values of carbonates (Holmes and Chivas 2002). The isotope composition of a closed water body like Chatyr Kol is mainly driven by evaporation and inflow via meltwater or precipitation. Liu et al. (2009) discovered non-linear enrichment of $\delta^{18}O_{carb}$ as salinity increases. Above a certain salinity threshold (e.g. 14 g l^{-1} at Lake Qinghai) $\delta^{18}O$ values change only very little. Consequently, if oxygen isotope composition of the lake water reaches a steady state, salinity is still able to increase due to progressive evaporation. The sensitivity of $\delta^{18}O_{carb}$ values to changes in salinity is additionally determined by the distance of the sediment core position to the surface (water depth) and to the shoreline (lake area). Deeper lake water shows higher $\delta^{18}O$ enrichment due to limited recharge by depleted surface/inflow water, while larger distances to the inflow channels also reduce the dilution with isotopic depleted meltwater of streamflow fed from precipitation. Uncertainties in the interpretation of $\delta^{18}O_{carb}$ values could be generated by different sources of bulk carbonates in lacustrine sediments. A contribution from either detrital carbonates originating from the catchment or input via aeolian dust could affect the interpretation (Liu et al. 2009), where dry deposition can exceed wet deposition in arid regions. Because lakes in arid regions experience high evaporation, the precipitation of carbonate minerals like aragonite, dolomite and calcite occurs mainly in the surface water. In addition to abiotic reasons, also biotic carbonate precipitation caused by planktonic blooms can be influenced by temperature, light and nutrient availability. Water plants and algae indirectly increase carbonate precipitation since they increase water pH due to the absorbance of CO_2 during photosynthesis. The higher salinity as response to evaporation is also reducing the amount of dissolved atmospheric CO_2 in the water, which consequently enriches $\delta^{13}C_{carb}$ (Fontes et al. 1993). Units II-B and II-C show the common synchronicity of $\delta^{13}C_{carb}$ and $\delta^{18}O_{carb}$ (Leng and Marshall 2004), while intervals below unit II-B and above unit II-C reveal asynchronous changes because extreme temperature (not precipitation) controls isotopic fractionation processes (Zhang et al. 2010). Temperature is much more controlling the fractionation of $\delta^{18}O_{carb}$ than of $\delta^{13}C_{carb}$. We observed a higher correlation between the carbonate content ($CaCO_3$) and the oxygen isotope composition of carbonates (r = 0.9**) than the carbon isotope composition (r = 0.01, p = 0.9), indicating that $\delta^{13}C_{carb}$ is additionally affected by complex biological processes at least below unit II-B and above unit II-C. Here, lower $\delta^{13}C_{carb}$ values and simultaneous high $\delta^{13}C_{org}$ can be a result of higher lake productivity, where algae and/or submerged macrophytes (see *n*-alkane cluster 1+3) preferentially use enriched dissolved CO_2 during photosynthesis. Another option is the incorporation of lighter CO_2 derived from microbial degradation of OM (Bird et al. 1991). Temperature, which influences water isotope composition and carbonate precipitation, is of secondary importance in the nowadays closed lake Chatyr Kol. Here, evaporative effects

are the overriding factors. Periods, showing high correlations between the carbon and oxygen isotope composition of the endogenic carbonates, reveal the possibility to discriminate carbonates formed in open lakes from those precipitated in closed lakes (Talbot 1990).

5.4.2 Interpretation of geochemical / elemental proxies

Large variations of µXRF scans can be attributed either to palaeoclimatic/environmental events or were caused by changes in water content and interpretation of single elements could possibly lead to wrong palaeoclimatic interpretations. Therefore, the calculation of element ratios result in more realistic information on geochemical changes (Hennekam and de Lange 2012). Scanning µXRF analysis reveal results for Al, K, Si, Pb, Co, Ti, Fe, S and Cl explained by the first principal component (PC1) as a proxy for terrigenous component of the sediment (Shanahan et al. 2009). Especially Ti, Si, K and Fe reflect detrital and minerogenic input from the shore and the catchment. Their amount is highest during unit I, indicating highest terrigenous input likely caused either by low lake volume and that the catchment reached its largest area or high erosion intensity either by wind or water.

In glacially influenced regions, advances and retreats of glaciers can have a huge potential to influence the flux of eroded material. Summer accumulation glaciers around Chatyr Kol have relatively large amounts of water constantly draining into the basin and have a larger impact on sediment composition than precipitation. Geological investigations at the At Bashy range by Glorie et al. (2011) identified the bedrock material as gneiss-schist-quartzite, ophiolite and high-pressure low-temperature metamorphites, enabling the identification of erosions by glacier advances using Ti as indicator for minerogenic input. Periods with higher Ti values and simultaneously decreasing Ca values (dilution) indicate ice advances or higher precipitation, while the opposite behavior occurs when glaciers retreat. An increase in Ca is generally correlated with increasing $CaCO_3$ and TIC contents and marks temperature increases (Fawcett et al. 2011). An possible indicator of the biogenic silica input (diatom productivity) could be the Si/Ti ratio (Stansell et al. 2010). Although diatom shell preservation is not constantly high during the core, differences between diatom productivity and preservation could be related to anoxic/oxic conditions and pH at the bottom water/surface sediment boundary. To reconstruct bottom water oxygenation in a semi-quantitative way, the Mn/Fe could be used (Naeher et al. 2013). Low Mn/Fe ratios indicate lower oxygen concentrations in the water, because Mn becomes reduced much faster than Fe under anoxic conditions. The faster oxidation of Fe under oxic conditions then leads to higher Mn/Fe ratios.

Several elements and their ratios were used as salinity indicators. One assumed lake-water salinity indicator could be Sr/Ca investigated by Zhang et al. (2009), where high ratios represent high salinities. Additional assumption about carbonate phases like calcite or aragonite precipitation could be made with x-ray diffraction (XRD) analyses. Therefore, the use of Sr/Ca as salinity proxy is possible in certain cases, but it generally describes the

water chemistry. For example, Sr/Ca depleted meltwater input from glaciers results in low lake Sr/Ca ratios (Bahr 2005).

Sulphur could be related to gypsum, pyrite or organic matter (Kristen et al. 2007). High lake productivity can increase the sulphur accumulation in the sediment (Galman et al. 2009). Lacustrine sulphur can originate from weathering of sulphur-rich rocks or from oxidation of organic sulphur from terrestrial sources (Holmer and Storkholm 2001). The sulphur deposition in sediments is mainly driven by counteracting sulphate (SO_4^{2-}) reduction and sulphide (H_2S) reoxidation. Once the freshwater amount in a lake increases rapidly, high rates of reoxidation of reduced sulphur can turn sediments from sink to a source of sulphate to the water. A lake with large areas of vegetated littoral sediments can undergo high reoxidation due to oxygen release from macrophytes.

5.4.3   Interpretation of organism-specific proxies

5.4.3.1 Diatoms

The ratio of planktonic (free-floating) and non-planktonic diatoms is an indicator of water-level changes (Vancampo and Gasse 1993). Non-planktonic forms can live on the lake bottom (benthic) and on water plants (epiphytic). Identified planktonic diatom species *Cyclotella caspia* and *Cyclotella sp*. can be defined as euplanktonic. The occurrence of these species in Tibetan lakes Bangong Co and Sumxi Co varies over a wide range of salinities, which hamper their use as salinity proxy (Wolin and Duthie 1999). A predominance of non-planktonic diatoms indicates shallow water or high light-intensity starting at 200 cm (3570 cal. yr BP) at Chatyr Kol. Non-planktonic diatoms therefore tend to be a better salinity indicator. In unit II-C predominant non-planktonic species are *Achnanthes brevipes*, *Brachysira neoexilis*, *Cocconeis placentula var. lineata*, *Navicymbula pusilla* and *Nitschia bacillum*, which prefer mesosaline conditions. Species dominating in unit III are *Cocconeis placentula* species *var. euglypta, var lineata* and *type 1*, which likely prefer lower salinities. When the lake level falls, the area of light penetration (photic zone) increases and thus favoring the non-planktonic population. However, shallow lake areas can lead to productivity-driven light limitation (Wolin and Duthie 1999).

5.4.3.2 Alkenones

Alkenone indices as palaeo-temperature proxy

The LCAs are produced by haptophyte algae in marine and lacustrine environments with 35 to 40 carbon atoms and 2 to 4 double bonds. So far, alkenones were considered to be components of haptophyte cellular membranes, where the unsaturation degree regulates the membrane fluidity (Zink et al. 2001). Recent studies have shown that their synthetization rather takes place in chloroplasts and the subsequent storage appears in cytoplasmic vesicles (Eltgroth et al. 2005). Conditions like nutrient limitation lead to an increase, while

prolonged darkness promotes the disappearance of these lipid bodies. The distribution of these di-, tri- and tetra-unsaturated methyl and ethyl ketones depends on growth temperature of their surrounding water (Brassell et al. 1986; Prahl and Wakeham 1987) and can be used as palaeo-SST proxy. Several studies defined various alkenone unsaturation indices e.g. U_{37}^K, $U_{37}^{K'}$, U_{38}^K, $U_{38}^{K'}$, U_{3738}^K to reconstruct temperatures (Brassell et al. 1986; Prahl and Wakeham 1987; Pearson et al. 2008). Investigations on alkenones from dominantly marginal marine haptophyte species (coccolithophorids) *Chrysotila lamellosa* as well as open marine species *Gephyrocapsa oceanica* and *Emiliania huxleyi* observed linear correlations with water temperature in culture experiments, marine surface sediments and even sediment-trap material (Brassell 1993; Conte et al. 1998), where an increase in temperature generally leads to a decrease in the alkenone unsaturation. Since universal calibrations for the open ocean can be applied, the application of unsaturation indices became a recognized tool in marine palaeoclimatology. In contrast, lakes need site-specific calibrations, because genetic and physiological differences between lacustrine alkenone producers result in calibrations with individual intercepts. Further evaluations reveal that too cold (< 4 °C) and too warm (> 25 °C) temperatures must be considered as thresholds for the linear relation between $U_{37}^{K'}$ and SST (Sikes and Volkman 1993). Nevertheless, the temperature dependency (i.e. slope) is generally consistent among the various alkenone calibrations, which suggests that temperature dependency (Δunsaturation / ΔT) is generally consistent among different haptophytes. Therefore, palaeo-temperature reconstructions could be applied for lacustrine systems, since the occurrence of alkenones was detected in modern and ancient lacustrine sediments in various environments ranging from saline conditions in Turkey (Thiel et al. 1997), Spain (Pearson et al. 2008), North America (Toney et al. 2010; Toney et al. 2011), Greenland (D'Andrea and Huang 2005) and China (Sun et al. 2004; Liu et al. 2006) to freshwater conditions in Europe (Cranwell 1985; Zink et al. 2001).

Rosell-Mele (1998) introduced the index % $C_{37:4}$ as potential new proxy for surface salinity, although it still has not unequivocally been proven by recent studies (Sikes and Sicre 2002; Chu et al. 2005; Liu et al. 2008a). Another explanation derived by Bendle et al. (2005), where % $C_{37:4}$ may reflect the mixing of water with autochthonous and allochthonous inputs and therefore different pools of coccolithophore assemblages. Sikes and Sicre (2002) pointed out, that this proxy is rather influenced by nutrients, light levels or growth rate rather than temperature or salinity.

Since modern climatological data from Kyrgyz stations already showed high correlations with the compound-specific stable hydrogen isotope composition from surface sediments of Chatyr Kol and Son Kol (chapter 3), correlation with lake's alkenone distribution would reinforce their use as temperature/salinity proxy. Unfortunately, degraded alkenones in the Chatyr Kol surface sediments prevent from calculation of unsaturation indices. However, surface sediments from Son Kol contain at least methyl C_{37} alkenones despite oxic conditions. We found the best relationships of U_{37}^K with the mean autumn air temperature (MAutT) (r = 0.96*; p = 0.04) [13] followed by summer temperature (r = 0.8; p = 0.18)

between 1955 and 1989 AD (Figure 31). Other studies found similar high correlations of MAutT with U^K_{3738} ($r^2 = 0.8$; $n = 13$) in endorheic Spanish lakes (Pearson et al. 2008) and with $U^{K\prime}_{37}$ ($r^2 = 0.8$; $n = 38$) in Chinese lakes (Chu et al. 2005). These findings suggest that at least in Son Kol alkenones were synthesized at certain seasons (here: autumn) of the year, which is limited to the ice-free time (May until September) and alkenone-producing organisms consequently are not adapted to spring nutrient limitation. On the other hand, we found no correlations of the % $C_{37:4}$ with annual precipitation as shown by He et al. (2013) from Lake Sugan (Qaidam Basin) between 1961 and 2009 AD.

$$\text{MAutT }_{\text{Naryn}} [°C] = 5.53 \text{ x } U^K_{37} + 7.076 \qquad\qquad [13]$$
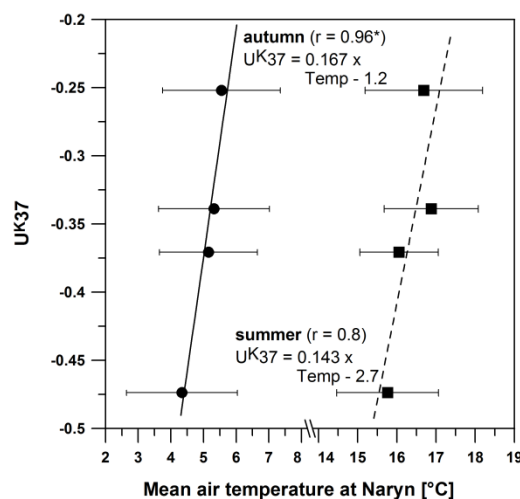
Figure 31: Scatter plot illustrating the relationship between the U^K_{37} index and mean seasonal air temperatures in autumn ($r = 0.96^*$; $p = 0.04$) and summer ($r = 0.8$; $p = 0.18$) provided from Naryn meteorological station (CAD). Error bars represent the standard deviation resulting from temperature variations within time periods.

Alkenone degradation

Not only direct response to environmental factors has to be investigated to interpret sedimentary records, but also the general physiological behavior of these organisms. Since alkenone producers are characterized as heterotrophic, they are not necessarily confined to synthesize their lipids in the photic zone. Toney et al. (2010) found that alkenone producers rose from the bottom of the lake through the water column from ice-off to early spring. The alkenones remained in equilibrium with the water temperature throughout this time despite likely light limitation. The optimum phytoplankton productivity, responsible for the flux of alkenones is highly seasonal (algae bloom) (Prahl et al. 2001). The timing of algae blooms

strongly depends on the ice-melting season and/or insolation intensity, resulting in spring or summer blooms. Here, ice cover is an important factor in lacustrine systems at higher altitude and latitude. In contrast to deeper oceans, where alkenones/coccolithophorids reach the seafloor after days (Fischer and Karakas 2009), the sinking rate at the shallow Chatyr Kol in the order of hours is of minor importance for alteration during sinking. Therefore, the total degradation in the water column is minor compared to that within the sediments (Hernandez-Sanchez et al. 2014). Additionally, aggregation of alkenones during sinking and in suspended particles could influence the efficiency of degradation processes even in lacustrine systems. Their distribution can be affected by several biotic and abiotic processes within sediments such as aerobic/anaerobic bacterial degradation, photosensitized oxidation, autoxidation, stereomutation and sulphurization (Rontani et al. 2013). Beside the non-selective degradation, a compound-specific selective degradation could possibly affect e.g. U^K_{37} values, since $C_{37:3}$ is more susceptible to degradation by aerobic bacteria and autoxidation than $C_{37:2}$ (Rontani et al. 2009). At Chatyr Kol these assumptions seem irrelevant in sedimentary units I and IV, because full degradation of alkenones prevents any calculation of unsaturation indices. Missing alkenones could be induced by redox conditions, biodegradation or simply non-occurrence of haptophytes. Other lacustrine studies explain the absence of alkenones from a core near the shoreline with lower lake levels (He et al. 2014) or interpret it with changes of haptophyte species as response of the aquatic flora to environmental changes (Schmidt et al. 2014). Toney et al. (2012) also found that haptophytes could not be cultured from enrichment cultures started from oxic lake sediments relative to anoxic lake sediments, indicating that degradation or grazing occurred in the oxic sediments preventing viable cells and/or cysts. Coring location of Chak12 and CK_S1 was at maximum water depth (20.5 m) with at least local anoxic conditions in summer 2012 AD (see water profile Figure 5), excluding the low lake level theory. An argument supporting anoxic degradation is based on the presence of stearic acid (according to similarity search at NIST 05: 66 %) eluting at alkenone retention times in Chatyr Kol surface sediment samples (CK_S1), which might have been hydrogenated from oleic acid by sedimentary bacteria under anoxic conditions (Rhead et al. 1971) (Figure 32). Surface sediments in core CK_S3 from shallower water depth (15.4 m) reveal less stearic acid possibly due to higher local affinity to oxic conditions. Since prevalence of anoxic, stratified and sulfate-reducing conditions lead to highest preservation compared to oxic conditions (Prahl et al. 1993; Teece et al. 1998; D'Andrea and Huang 2005; Toney et al. 2012), we would suspect more frequent oxic conditions in laminated unit I and unlaminated unit IV, because of less preserved alkenones. Teece et al. (1998) studied extensive degradation of MeC_{37} (up to 85 %) by heterotrophic bacteria under oxic conditions, where the $U^{K'}_{37}$ index consequently remained unchanged. The completely missing alkenones in our study contradict this degradation under oxic conditions. In addition to direct bacterial degradation the sulphurization process as a consequence of bacterial metabolism should be taken into account. Substrate-specific sulphurization leads to cross-links between inorganic sulphur species and carbon double bonds or keto-groups creating organic sulphur

compounds (OSC). Sulphurized LCAs could not be detected in the usual analytical window, and may only occur in the kerogen fraction (Koopmans et al. 1997). A partial sulphurization of di-and tri-unsaturated alkenones also does not change the $U_{37}^{K'}$ index. The dramatically reduced sulphur µXRF counts in unit IV due to possible outgassing H_2S produced by sulfate-reducing bacteria could therefore display a massive creation of OSCs (Damste et al. 1989). Thus, a high amount of H_2S may react with lipids like alkenones resulting in less remaining detectable components visible in unit IV (Figure 30). Rontani et al. (2013) describes sulphurization as an important post-depositional process under anoxic conditions, which could take 1000 to 3000 years at low temperatures (Kok et al. 2000). Surface sediments from Chatyr Kol dating back to just 70 years are therefore likely too young to be influenced by sulphurization.

A previously unexpected process of alkenone degradation could be the predation by *Gammarus alius sp. nov.*, an amphipoda recently discovered at Chatyr Kol (Sidorov 2012), which was the dominant macroinvertebrate during the field campaign in 2012 AD. This species shows a specialized morphology of the mouth parts indicating diverse feeding modes like shredder-feeding of particulate organic matter, filter-feeding, grazing of organic biofilms and sediment-feeding (MacNeil et al. 1997). Some amphipoda species even feed on diatoms and dinoflagellates from the surface of principal substrates (Keith 1969), which therefore could also be applied for haptophytes. Since fish are absent as their main predator, possibly induced by outgassing H_2S, population of *Gammarus* probably dramatically reduces the amount of viable haptophyte cells that over-winter to produce the next spring/summer bloom. However, Grice et al. (1998) did not detect noticeable changes in the alkane distribution in faecal pellets from zooplankton (copepods) feeding on *Isochrysis galbana*, but investigations on alkenone digestion are still missing.

Recent conditions at Chatyr Kol are less suitable for alkenone preservation, but the presence of an anoxic water bottom-surface layer at least during late summer should rather promote their accumulation since highest concentrations of LCAs were found in anoxic lakes (Toney et al. 2010; Toney et al. 2011). However, the unlaminated sediments in unit IV rather suggest oxic conditions during most time of the year, enabling bacteria to directly degrade and indirectly modify LCAs. Lamination, indicating long-term anoxic conditions (no bioturbation), absence of mixing and re-suspension, does not necessarily promote alkenone preservation visible in unit I and III. Furthermore, trophic conditions possibly also influence haptophyte population behavior. Most environments where haptophytes are found are oligotrophic. We therefore expect them to disappear during phases of eutrophication. Phases of increased nutrients would strengthen the diatom population, which is not constantly given during unit IV. The combination of limnological, ecological and climatological factors has to be considered when interpreting alkenone preservation especially at Chatyr Kol.
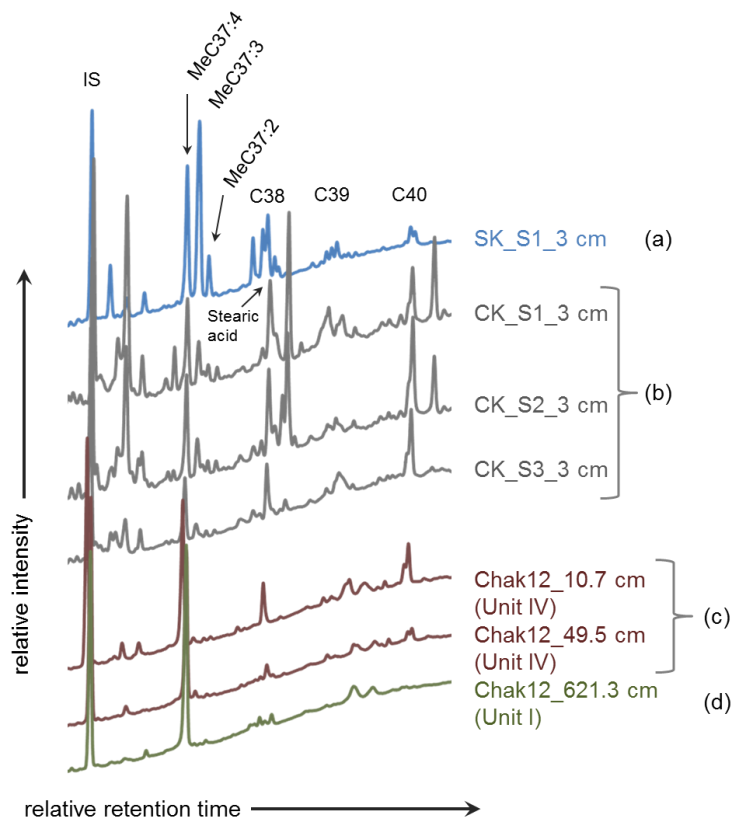
Figure 32: Chromatograms (GC-FID) showing different degrees of alkenone degradation in surface sediments from Son Kol (a) and Chatyr Kol (b), and deep core samples from Chak12 unit IV (c) and unit I (d).

Alkenone distribution produced by different haptophyte species

The detection of high alkenone concentrations in core sections of unit II possibly indicates oligotrophic conditions, particularly P limitation and high sulfate concentrations (Toney et al. 2010). The calculation of the water temperature using the U_{37}^K index with the assumption that one haptophyte species acts as single alkenone source with a certain distribution leads to wrong interpretations. Previous studies already showed that one lake could be inhabited by different species resulting in different alkenone distributions, which in turn requires different temperature calibrations. Identification of haptophyte species including taxonomic information cannot be made without investigating their genetic sequences; therefore we rather describe the differences in the LCA distribution resulting from cluster analysis. Detailed numerical differentiation results from the compositional data of tetra-unsaturated C_{37} alkenones (% $C_{37:4}$), the presence/absence of certain alkenone compounds like methyl C_{38}, and the ratio of C_{37} and C_{38} alkenones (K37/K38) (Pearson et al. 2008; Theroux et al. 2010). Since Chatyr Kol sediments contain ethyl $C_{38:4-2}$ and inconspicuous amounts of

methyl C_{38} independently from their alkenone clusters, we could exclude the marine haptophytes *Emiliania huxleyi* and *Gephyrocapsa oceanica* as the source species due to their higher methyl C_{38} amounts (Conte et al. 1998), as well as the coastal species *Isochrysis galbana* and lacustrine haptophyte *Chrysotila lamellosa* producing only ethyl $C_{38:3}$ (Rontani et al. 2004; Sun et al. 2007). Consideration of Chak12 methyl C_{37} and ethyl C_{38} alkenones results in cluster A with a dominance of methyl $C_{37:4}$, while cluster B is characterized by high proportion of ethyl $C_{38:3}$ and $C_{38:4}$. Individual indices K37/K38 and % $C_{37:4}$ of these cluster A (K37/K38 = 1.77 ± 0.56; % $C_{37:4}$ = 52.4 ± 11.1 %) and cluster B (K37/K38 = 0.5 ± 0.2; % $C_{37:4}$ = 41.8 ± 11.6 %) (Figure 33) have been compared with indices from other lakes in the USA (Theroux et al. 2010; Toney et al. 2010), Canada (Toney et al. 2011) and Greenland (D'Andrea et al. 2006), showing that alkenone composition of the US American Lake George (K37/K38 = 2; % $C_{37:4}$ = 55 %) (Theroux et al. 2010) matches best with Chatyr Kol Cluster A. Subsequent calibration (Toney et al. 2010) and culture studies (Toney et al. 2012) at Lake George successfully identified the haptophyte phylotype "Hap A" as the primary producer of a $C_{37:4}$ dominated alkenone distribution. This phylotype prefers anoxic, deep surface sediments, while the second cultured phylotype from Lake George "Hap B", dominating at ethyl $C_{38:3}$ and therefore similar to Chatyr Kol Cluster B, prefers the lake water column and shallow sediments.

We suggest, that the K37/K38 index at the first order is an indicator for the occurrence of different haptophyte species, but it is almost impossible to distinguish between them without DNA analysis (Figure 33), supported also by other studies reviewed by Pearson et al. (2008). Highest ratios (> 3) were determined in culture studies of *Isochrysis sp.*, *Isochrysis galbana* and *Chrysotila lamellosa* (Marlowe et al. 1984). Nevertheless, variations of K37/K38 could also derive from differences in nutrient concentration, physiological status of haptophytes and growth temperature (Chu et al. 2005). Other indices have usually been used as temperature proxy like U_{37}^{K}, U_{38}^{K} and U_{3738}^{K} (include $C_{37:4}/C_{38:4}$ in calculation), as well as $U_{37}^{K\prime}$ and $U_{38}^{K\prime}$ (without $C_{37:4}/C_{38:4}$), describing the degree of unsaturation of certain alkenone chain lengths. The occurrence of different LCA distributions in Chak12 is therefore triggered by two different alkenone producing haptophyte species rather than changes in temperature, salinity or nutrients. Responsible for similar significant differences of U_{37}^{K} (p = 0.0), U_{38}^{K} (p = 0.006) and U_{3738}^{K} (p = 0.002) is their connection with the relative abundance of $C_{37:4}$ (% $C_{37:4}$; p = 0.001).
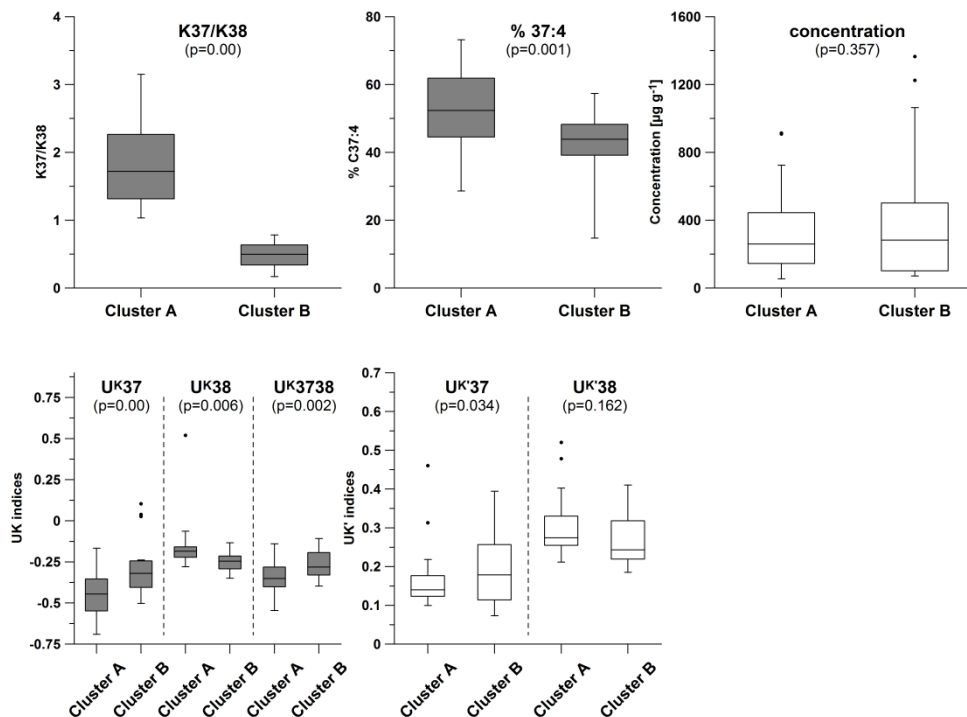
Figure 33: Box plot diagrams show ranges of certain alkenone unsaturation indices in relation to the two alkenone cluster A (C_{37} dominance) and B (C_{38} dominance).

Indices marked in dark grey are significantly different between the clusters (ANOVA, $p < 0.01$) like K37/K38, % $C_{37:4}$, U_{37}^{K}, U_{38}^{K} and U_{3738}^{K}.

5.4.4 Alkanes and their hydrogen isotope composition

As already discussed in detail (see chapter 3 and 4), terrestrial long-chain *n*-alkanes (C_{27-31}) record the isotopic signal of their source water (here: precipitation), which is mainly controlled by temperature and evaporation. δD_{C29} values generally follow MAT with enrichment under warming conditions. Nevertheless, since wet season precipitation between April and August is not necessarily positively correlated with temperature as seen in 1975 AD, a dry period under moderate temperatures may lead to an even higher isotopic enrichment. Consequently, evaporation is the main driver controlling δD_{C29} values at Tian Shan lakes. Since the Holocene isotopic variability is prominently at transitions between Early-, Mid- and Late Holocene. The Early Holocene as well as Late Holocene are characterized by enriched δD_{C29} values, thus temperature dominated the fractionation. Here, the transfer function [12] generated from Son Kol δD_{C29} data could possibly be applied. After reaching tipping points at transition periods, δD_{C29} values rapidly became depleted, indicating additional influence by precipitation complicating proxy interpretation. We suggest that even cold and dry conditions would increase δD_{C29}. The aquatic hydrogen isotope composition (δD_{C23}) recorded by macrophytes and algae represents the lake water evaporative enrichment. Higher values indicate higher evaporative enrichment of the water

under simultaneously decreased input of isotopically depleted freshwater (precipitation or meltwater) and/or higher evaporation of remaining water. On the other hand, melting of glacier under rinsing temperatures would deplete the lake water δD values and therefore result in lower δD_{C23} values. Phases with depleted values also show warmer MAutT derived by U^K_{37}, confirming the assumption of temperature induced meltwater input.

5.4.5 Reconstruction of limnological and climatic conditions at Chatyr Kol during the Late Pleistocene and Holocene

Former investigations on lake terraces, pollen, glaciers and sediments from the Chatyr Kol basin already resulted in low resolution reconstructions of glacial and climate changes beginning in the Late Pleistocene. This time interval spanning from ca. 126 to 11.7 cal. kyr BP includes the Last Glacial Maximum (LGM) representing the latest maximum expansion of ice masses and glaciers globally (see chapter 10). Palynological investigations and radiocarbon dating by Bondarev et al. (1997) and Shnitnikov (1980) have shown that the maximum glaciation at Chatyr Kol occurred between 25 and 10 cal. kyr BP. At 23 cal. kyr BP, the maximum lake filling and even lake overflow was assumed due to on-shore lake terrace dating by Romanovsky and Shatravin (2007) (Figure 34). Since then, a large regression should have taken place until the lake reached its present level at about 11.6 cal. kyr BP. According to pollen analyses on a 10 m sediment core, Romanovsky and Shatravin (2007) characterize the last 20,000 years as follows: the Late Pleistocene interval from 20 to 14.6 cal. kyr BP was humid and warm as indicated by a higher lake level. Shnitnikov (1980) investigated aquatic plant detritus at lake terraces 12–13 m between 21.5 and 16.3 cal. kyr BP. The following phase includes the transition from the Late Pleistocene to the Holocene between 14.6 and 12 cal. kyr BP until the Holocene (12 to 0 cal. kyr BP), when relatively cold and arid conditions were reached. Nevertheless, certain discrimination between the Early-, Mid- and Late Holocene showing different climatic conditions, has to be made. The transition from maximum glaciation has possibly started at around 12 cal. kyr BP, when glaciers retreated, Central Asian lakes Balkash, Issyk Kol and even Chatyr Kol were filled and pollen became more thermophyllic (Sevastianov et al. 1990). Since the Chak12 sediments were calibrated back to ca. 11.1 cal. kyr BP, they officially represent the entire Holocene. Nevertheless, ecosystem specific properties result in a delayed response to Holocene warming.
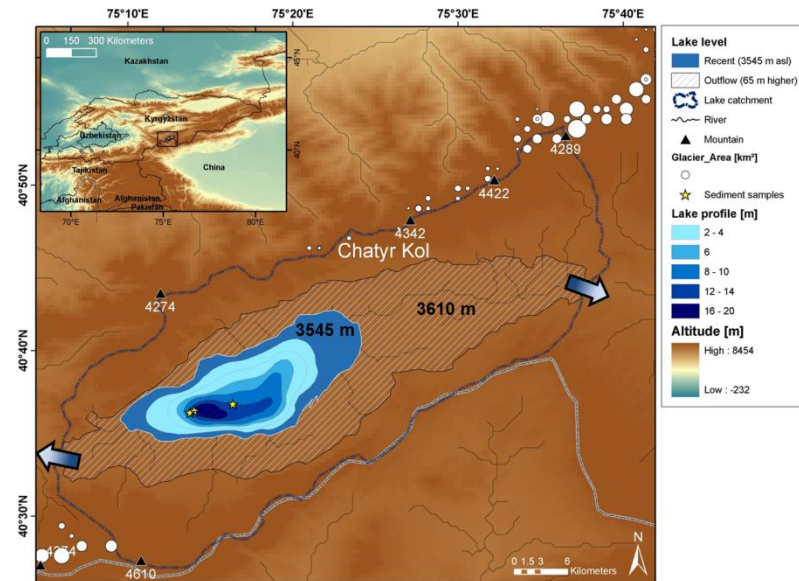
Figure 34: Lake Chatyr Kol outflow hypothesis contains a lake level of 3610 m with two outflows in the eastern and western border of the catchment.

Unit I (623.5–567.5 cm / 11,140–10,140 cal. yr BP) - Early Holocene glaciation (Influence of Late Glacial stage)

Light-grey laminated sediments of the early Holocene reveal highest Si/Ti ratios and predominantly n-C_{17} alkanes (cluster 1) produced by algae and non-planktonic diatoms, suggesting that the lowest TOC and TN contents are rather due to organic degradation in shallow-lake sediments rather than lower aquatic productivity. The summer diatom bloom in combination with mineral matter could be the reason for the formation of lamination. Highest Ti counts reflect the highest rate of terrigenous input from the larger catchment meaning that the lowest lake volume still existed until 10.1 cal. kyr BP. Climatic conditions were extremely cold and arid during summers as revealed by strongly enriched δD_{C29} values. Lower temperatures also favored long-lasting ice cover during the year, reducing the water mixing in spring and autumn, which consequently led to mainly anoxic bottom water conditions as suggested by low Mn/Fe ratios. The short ice-free seasons also hampered the haptophyte productivity and therefore the alkenone flux. Suppression of alkenone production likely occurred as a result of reduced haptophyte presence, thus producing concentrations below analytical detection limits. Similarly, haptophytes in most regions e.g. Greenland and Central North America prefer oligotrophic conditions. The high nutrients suggested by the possible diatom bloom would prevent prevalence of haptophytes. A short-term excursion to higher lake salinity is visible at ~10.7 cal. kyr BP, where higher Sr/Ca ratios and enriched $\delta^{13}C_{carb}$ values possibly indicate higher evaporation.

Unit II (567.4–131.6 cm / 10,140–2350 cal. yr BP)

Subunit II-A (567.4–458 cm / 10,140–8180 cal. yr BP) - Early Holocene deglaciation and large lake volume

This subunit shows signs of intensive deglaciation at Chatyr Kol. We detected a generally decreasing trend of Ti, indicating that the size of the catchment or erosion intensity gradually decreased. However, abruptly intensified Ti peaks possibly indicate forced erosion within meltwater channels. Consequently, lake volume rather must have been rising. Additionally, low Sr/Ca ratios indicate input of Sr/Ca depleted detrital material by meltwater, which consequently should have reduced water salinity. Since $\delta^{13}C_{carb}$ and $\delta^{18}O_{carb}$ diverge, we suggest an extreme temperature increase as the trigger for glacier melting in the catchment, which was most probably forced by maximum summer insolation at 30°N between 12 and 11 cal. kyr BP. This finding of warming can be supported by palynological data from Shnitnikov (1980), however they suggest 9 cal. kyr BP as onset of warming, but this might be related to the substantially larger dating uncertainty of this early study. The remarkably increasing Ca/Ti and $CaCO_3$ trend is an indicator of either glacier retreat or in-situ carbonate precipitation with its maximum at ~8.6 cal. kyr BP. At the same time a lake volume maximum can be inferred from strongly depleted aquatic δD_{C23} values, very low Ti counts and highest % $C_{37:4}$ values. High concentrations of $C_{37:4}$ might be related to anoxia and increasing lake depth (Toney et al. 2010) as well as increased lipid production under stress conditions, such as low water temperatures due to increased glacier meltwater contribution. A confirmation of increased lake volume could be the strong increase of the C/N ratio due to organic matter degradation within the larger water column, where N-rich components degrade faster (Yucel et al. 2010). On the other hand, this rapid increase could simply show the appearance of terrestrial vegetation (long-chain *n*-alkanes). High lake levels support the prevalence of anoxic bottom-water conditions, indicated by still low Mn/Fe ratios. Due to a higher supply of nutrients and better climatic conditions, aquatic algae productivity increased as indicated by appearing alkenones, enhanced *n*-alkane C_{17} production, highest Si/Ti ratios and enriched $\delta^{13}C_{org}$ values. Improved climatic conditions result in a greater dominance of deep-water preferring planktonic diatoms at ~8.9 cal kyr BP. At the same time the maximum of $\delta^{18}O_{carb}$ indicates maximum distance of the shoreline to the sediment core location and a generally deeper water column. According to Sevastianov et al. (1990), the lake level was 12 m higher than today at that time. Maximum $CaCO_3$ contents reflect highest carbonate precipitation, which can be triggered by enhanced algae bloom and their use of enriched dissolved CO_2 during photosynthesis. Consequently, minimum $\delta^{13}C_{carb}$ also show these complex biological processes.

Subunit II-B (458–278.5 cm / 8180–5000 cal. yr BP) – Mid-Holocene - Thermal Optimum

After the large deglaciation period inferred for subunit II-A, subunit II-B is characterized by generally higher evaporation, higher lake water salinity and lower water depth. Sharp

fluctuations appeared in ~350-year cyclicity. However, frequently appearing periods with higher *n*-alkane production (mainly terrestrial) correlate with higher amounts of alkenones, higher $\delta^{13}C_{org}$, higher Mn/Fe but also lower $\delta^{15}N$, $\delta^{18}O_{carb}$ and $\delta^{13}C_{carb}$ values, indicating conditions promoting terrestrial vegetation and also aquatic haptophyte productivity under moister and warmer climate. The minimum input of glacial meltwater or even its loss could result in highest Sr/Ca ratios. The most saline phases are visible by strongly enriched δD_{C23} values at ~6.5 and 5.5 cal. kyr BP. Since δD_{C29} values remain relatively depleted, both phases have high E/I ratios meaning high evaporation rates. Contrasting short-term phases show the same 350-year cyclicity with higher $\delta^{15}N$ values, which can explained by (1) enhanced organic matter supply to the bottom water anoxia, allowing denitrification to enrich the nitrogen isotope composition (Talbot and Laerdal 2000), by (2) evaporative loss of depleted ammonia during dryer periods since δD_{C29} values were also slightly enriched during these phases or (3) enhanced terrestrial minerogenic input as indicated by parallel high Ti counts and high $\delta^{15}N$ values. Therefore, summer evaporation and winter precipitation with the subsequent erosion of terrestrial OM during spring-melt was higher in $\delta^{15}N$-high phases, while summer humidity was higher during $\delta^{15}N$-low phases. A general trend towards fresher lake water (low salinity) is indicated by decreasing Sr/Ca and % $C_{37:4}$ values.

Subunit II-C (278.5–131.6 cm / 5000–2350 cal. yr BP) – Late Holocene

A sharp shift of climatic conditions appears at the transition to the uppermost subunit of unit II. Less obvious fluctuations of analyzed proxies within the early part of subunit II-C indicate rather moderate changes. This lower section until 3500 cal. yr BP is dominated by planktonic diatoms, preferring deeper water. Most negative $\delta^{13}C_{carb}$ and $\delta^{18}O_{carb}$ values between ~4750 and ~3770 cal. yr BP under positive correlation could be an indicator of an open lake hydrology. This abrupt opening or at least strong lake volume increase led to a depletion of δD_{C23} and favored the dominance of a second haptophyte phylotype (cluster B). Generally wet and warm conditions with more precipitation and partly more meltwater compared to the Early Holocene are inferred by depleted δD_{C29} values. Since the effective catchment decreased, precipitation had a lower potential to erode terrestrial minerogenic material (low Ti) and in particular soils (minimum $\delta^{15}N$). Alternatively, low amounts of winter snowfall and the consequently lowered meltwater input in spring could also have minimized the terrestrial minerogenic input. The wet and warm conditions during summer increased the accumulation of organic matter with rather seasonal changes of redox conditions (higher TOC and higher Mn/Fe). Haberzettl et al. (2005) argued on the basis of negative correlation between $\delta^{15}N$ and $\delta^{13}C_{org}$, that these changes rather support lake level changes than changes in productivity. Because of source signal mixing in sediments, the depletion of $\delta^{15}N$ values indicate most probably input of terrestrial plant material, which does not match with increasing $\delta^{13}C_{org}$ values (signal of submerged macrophytes).

A pronounced phase of lowered water volume appeared for ~500 years between 3770 and 3240 cal. yr BP. High amounts of $CaCO_3$, high Ca/Ti ratios and enriched $\delta^{18}O_{carb}$ values indicate increased in-lake calcite precipitation and evaporative enrichment of the surface water. This phase is a tipping point of the dominant diatom type, changing from planktonic to non-planktonic diatoms, which prefer shallower water. Water conditions and surface temperatures also supported haptophyte bloom (highest alkenone concentrations). Major changes are correlated to a sharp rise of winter snowfall, influencing the spring melt intensity (enriched $\delta^{15}N$ values and increased Ti counts).

The subsequent phase at the end of subunit II-C (3240–2700 cal. yr BP) is again characterized by a return to higher lake volume (low $CaCO_3$, $\delta^{18}O_{carb}$) due to increased summer precipitation (depleted δD_{C29}), but nevertheless low soil erosion (low $\delta^{15}N$) occurred. An additional factor controlling the prevalent diatom type and keeping non-planktonic diatoms is the nutrient limitation and temperature. The uniquely high amount of long-chain n-alkanes, TOC and TN at ~2790 cal. yr BP was probably accumulated after huge production of organic matter in the catchment, which was introduced via flooding of formerly grown vegetation in swamps and river delta. A higher macrophyte population (high $\delta^{13}C_{org}$) would support the dominance of non-planktonic diatoms if they were mostly epiphytic. To transport signals from shallower regions to the core location, other factors like wind induced currents and full-mixing were necessary. The total loss of stratification and resuspension of former oxic sediments could possibly wash in oxidized iron mineral (increased Mn/Fe).

Unit III (131.5–68 cm / 2350–1215 cal. yr BP) – Late Holocene

The shortest unit, characterized by lithostratigraphical changes from formerly laminated brownish-reddish to grey lake marl, marks the beginning of the Late Holocene with major changes of environmental and climatic conditions. According to Sevastianov et al. (1980) and Sevastianov et al. (1990) climate experienced desiccation and became drier and colder than the previous Mid-Holocene. Major indications for dramatic changes in humidity are enrichments of δD_{C29}, $\delta^{18}O_{carb}$ and $\delta^{15}N$.

Subunit III-A (131.5–116 cm / 2350–2070 cal. yr BP)

An abrupt lowering of the lake level cannot be identified for certain since Mn/Fe ratios decline to their minimum, indicating rather anoxic conditions. On the other hand, increased Ti counts support the lake-size reduction theory. Still non-planktonic diatom dominance, detected alkenones and the shift to stronger macrophyte input to the OM indicate better conditions at least for aquatic organisms. The extremely reduced terrestrial OM input shows the larger consequences of climate changes (low humidity) for the catchment. We therefore suggest that better aquatic conditions and higher input of meltwater (lower Sr/Ca) during summer would lead to enhanced phytoplankton (higher Si/Ti) and emerged

macrophyte (depleted $\delta^{13}C_{org}$) productivity, which favor the precipitation of carbonates (higher $CaCO_3$, enriched $\delta^{13}C_{carb}$) compared to the previous period. The fact that sulphur tends to be reduced in sediments since the late phase of unit II-C could be triggered by massive sulphide (H_2S) reoxidation and/or degassing, also promoted by the trend of enhanced release of oxygen from macrophytes in vegetated littoral sediments.

Subunit III-B (116–68 cm / 2070–1215 cal. yr BP) – Beginning of Recent Period

Progressive changes in environment and hydrology are primarily recognized by changes in the sediment color to brownish-grey. For the first time, terrestrial plant macros occur abundantly within the sediment, indicating significant plant growth at the sampling location or better preservation. Improved conditions for terrestrial plants must not necessarily match with optimal requirements for haptophytes and diatoms. Alkenone producing haptophytes and non-planktonic diatoms were gradually reduced until total disappearance in the following unit. A negative precipitation to evaporation balance possibly caused strong carbonate precipitation (high Ca/Ti). The carbonate to sulfate ratio in Canadian lakes, which was not measured at Chatyr Kol, indicates similar disappearance of haptophytes with evaporative balance (Toney et al. 2011). Nevertheless, TOC amount stays at very low level except for a positive excursion at ~1500 cal. yr BP with additional response in Ca/Ti, Mn/Fe and last detected diatoms.

Unit IV (68–0 cm / 1215 cal. yr BP to present)

This final unit describes more or less conditions representative for the recent climate. The still dry and cold climate of the Late Holocene caused further enrichment of terrestrial δD_{C29} values, but stable regional conditions are shown by $\delta^{15}N$ values. Yet, three limnological phases can be distinguished: (1) A striking dry phase comparable with the most recent time interval is recorded at 43 cm (~760 cal. yr BP), where strong evaporation in combination with macrophyte productivity caused increasing carbonate precipitation (highest Ca/Ti and enriched $\delta^{13}C_{org}$) and oxic conditions. A pronounced reduction of terrestrial minerogenic input (lowest Ti) as consequence of probably missing precipitation or meltwater was also detected. Sulphur content in the sediment is constantly at its minimum indirectly leading to missing alkenones (see above). (2) Afterwards, moister conditions until ~200 cal. yr BP mainly detected by higher Ti, higher Sr/Ca and low Ca/Ti, which indicate enhanced inflow by short-term moistening or melting. (3) Finally, recent climatic and limnological conditions returned to ones similar to the earlier dry phase discussed as in (1).

5.4.6 Lake level changes in the Tian Shan and Central Asia as response to the Early Holocene warming

The most obvious signs of climatic induced changes in water supply to lakes are rapid changes in lake level/volume. The topography of the catchment, i.e. slope and basin morphology, or mean residence time determines the intensity of responses to climatic changes. Thereby the internal variability in certain climate systems, either on a regional or local scale produces lake level variations which sometimes directly or indirectly occur as reaction to variations in precipitation, temperature, evaporation or other external factors. Rapid lake volume increases most likely occur after/within deglaciation phases, when a significant rise in temperature increases the melting of glaciers and snowfields. Consequently, the direct inflow amount of glacier meltwater or delayed delivery via rivers into lakes increases the transported water. Next to direct observations like lake terraces, indirect records of lake level variations can be inferred from stable isotope composition of lake water (δD, $\delta^{18}O$), aquatic organisms (e.g. ostracods, macrophytes) and inorganic components (e.g. $\delta^{13}C_{carb}$, $\delta^{18}O_{carb}$), but also from input dependent proxies (e.g. µXRF Ti).

The Early Holocene (11.7–8 cal. kyr BP) is characterized by a pronounced deglaciation visible not only at Chatyr Kol but also by a rapid temperature rise in Greenland between 12 and 10 cal. kyr BP (Alley 2000) and global sea level rise by 60 m between 11.6 and 7 cal. kyr BP (Smith et al. 2011). To emphasize the relationship between Central Asia and the North Atlantic climate system, similar responses with level changes of large water bodies west of Kyrgyzstan like the Black Sea (Balabanov 2007), the Caspian Sea (Rychagov 1997; Leroy et al. 2013) and the Aral Sea (Boomer et al. 2000) are visible at about the same time. After the Late Pleistocene lowstand, the Caspian Sea experienced a strong lake level rise from the Early Holocene due to increased post glacial meltwater input from the Pamir and Tian Shan via the Amu Darya River. A lake-highstand occurred between 10 and 7 cal. kyr BP. The Aral Sea showed increasing water level during the Early Holocene as well, but reached its maximum lake level at ca. 5 cal. kyr BP. A significant result of enhanced meltwater discharge affected the Amu Darya River at 9 cal. kyr BP, when it changed its flow path away from the Caspian Sea towards the Aral Basin in the north. Since then and until today, the Aral Sea had its water supply from two rivers, Syr Darya and Amu Darya. Later during the Mid-Holocene, the Aral Sea also discharged via the Uzboy Channel into the Caspian Sea. The connection to the Caspian Sea broke off only, when climate conditions became drier at 3.5 cal. kyr BP. Also the Black Sea experienced a transgression (11–6 cal. kyr BP) related to warming and increased precipitation. Here, the salinity increased gradually, indicating connection to the saline Mediterranean Sea. Sparse data from the largest Kyrgyz lake Issyk Kul confirm optimum local climate conditions for lake growing. According to lake terraces, higher lake levels than today appeared between 26 and 10 cal. kyr BP (Romanovsky 2002). The assumption of a freshwater open-basin system is also confirmed by Ricketts et al. (2001) for the period 8.7 to 6.9 cal. kyr BP by investigations on ostracods. Other smaller lakes especially east of the Tian Shan started to appear delayed like Bosten Lake in northwestern China at 8 cal. kyr BP (Wünnemann et al.

2006; Zhang et al. 2010) and Gun Nuur in northern Mongolia at ca 9 cal. kyr (Wang et al. 2004). The filling of Lake Bosten between 8 and 6.4 cal. kyr BP resulted from high temperature-induced glacier and snow melting in the Central Tian Shan transported via the Kaidu River. A higher lake level and simultaneously high salinity have been explained by the greater distances from fresh water inflow to the coring site (Zhang et al. 2010). Maximum lake depth was reached around 7.2 cal. kyr BP. All these changes in lake level were temperature driven, since effective moisture in Central Asia at this time was very low (Chen et al. 2008). Slightly different interpretations raised Bondarev et al. (1997), where the warming at 9 cal. kyr BP was initiated by an earlier increase in precipitation at 11–10 cal. kyr BP. These conditions promoted a small glacier advance in the inner Tian Shan (Holocene glacier maximum), followed by a recession at 8 cal. kyr BP. Finally, regional lake level changes confirm with findings at Chatyr Kol, where the extended lake volume in the Early Holocene appeared as consequence of the former maximum summer insolation in the Northern Hemisphere, increasing temperatures (detected also by U_{37}^K index) and therefore massive glacier meltwater input (Figure 35). This phenomenon can be determined as the main reason for lake volume rising of Central Asian lake systems.
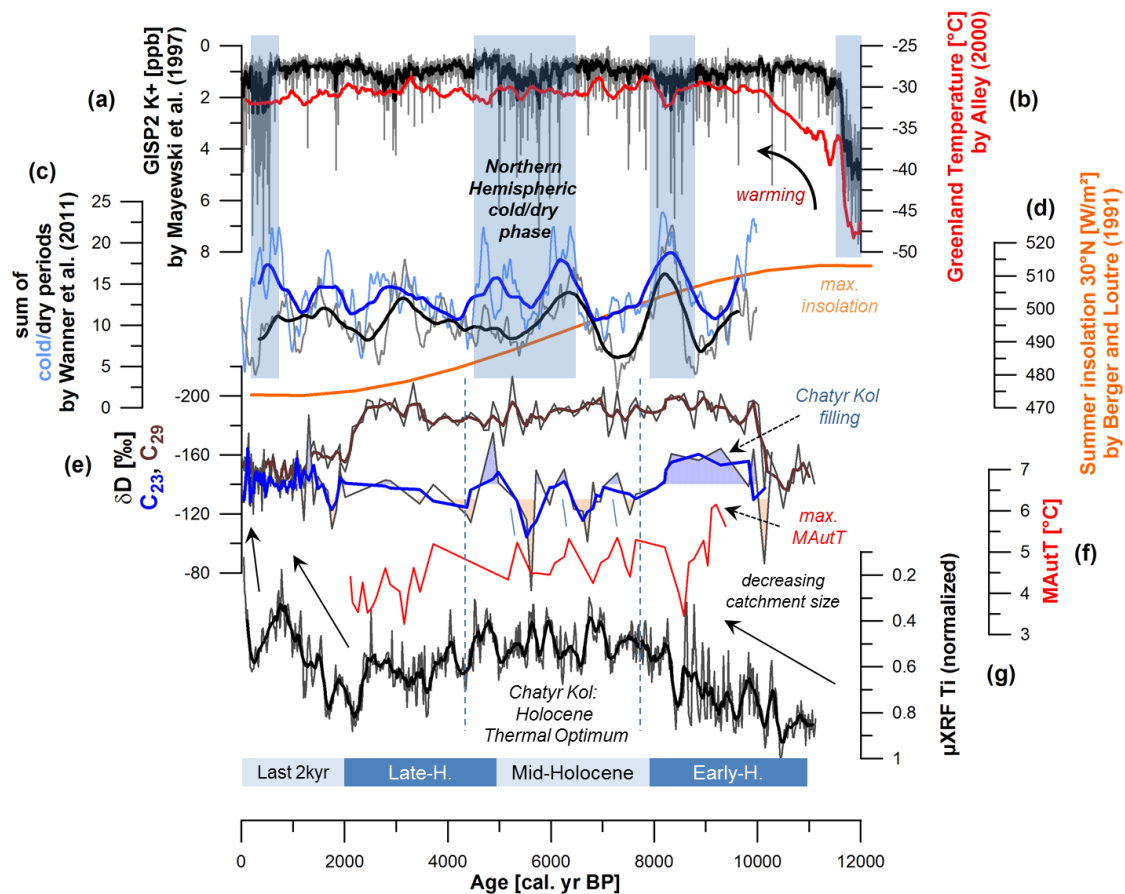
Figure 35: Early Holocene warming indicated by Greenland GISP2 proxies like (a) potassium ion concentration (K⁺) for atmospheric circulation intensity by Mayewski et al. (1997) and (b)

temperature reconstructions by Alley (2000), (c) sum of global cold and dry periods by Wanner et al. (2011), (d) summer insolation at 30°N (Berger and Loutre 1991) and by results from Chatyr Kol sedimentary record (this study) of (e) δD_{C23} (blue thick line), δD_{C29} (brown line), (f) reconstructed MAutT using $\mathbf{U_{37}^K}$ and (g) µXRF Ti.

5.4.7 Mid- and Late Holocene climate variability in Central Asia and lake level high-stands on the Tibetan Plateau

As already discussed in the previous manuscripts, δD_{C29} is a robust sedimentary proxy originating from allochthonous plant waxes, which reflects the δD composition of leaf-water influenced by temperature and evaporation during the vegetation period. As this proxy is not directly influenced by lake-internal processes, it provides independent information of regional climatic conditions. At Chatyr Kol, δD_{C29} values are strongly depleted between ~10 and 2.1 cal. kyr BP with rather minor fluctuations, indicating that the catchment, isolated by the Fergana range in the West, the Torgurat range in the South and At Bashy range in the North, was under influence of relatively stable climate conditions. The general assumption by Sevastianov et al. (1980) of a moister Mid-Holocene could be accepted at Chatyr Kol. We rather suggest that the effective moisture is the major factor for these findings, which is lower under intensified temperature-driven evaporation. The dominance of evaporation versus glacial meltwater inflow ended up in decreasing water level also of other (deep)-water basins in Central Asia. During the Mid-Holocene, the Caspian Sea had a low level from 7 to 3.5 cal kyr BP with a minimum at 3.9 cal. kyr BP (Leroy et al. 2013) and since 6.9 cal. kyr BP Lake Issyk Kul is a closed-basin system (Ricketts et al. 2001).

The lake expansion in Central Asia occurred mainly in the Early Holocene, while a temporally shifted occurrence of higher lake levels maximizing at 6 cal. kyr BP could also be detected in NE and NW Tibetan Plateau (TP) (Qin and Yu 1998). Here precipitation and effective moisture as consequence of increased monsoon circulation, but also driven by the high summer insolation, played a major role to enlarge the lakes. At least the NW TP is discussed to be in the transition zone of Westerly and IOSM influence (Yao et al. 2013). In consequence, lakes in the NW TP had their highest levels during the Mid-Holocene (8 to 5 cal. kyr BP): Lake Qinghai between 7.6 and 5.5 cal. kyr BP (Lister et al. 1991), Sumxi Co between 8.3 and 6 cal. kyr BP (Vancampo and Gasse 1993) and Bangong Co between 8.8 and 6.2 cal. kyr BP (Gasse et al. 1996).

The Late Holocene is characterized by several cold/wet and warm/dry phases with spatial and temporal variations. Chatyr Kol experienced phases of enhanced snowmelt in the spring season between 3.7 and 3.2 cal. kyr BP as well as after 2.2 cal. kyr BP, indicated by enriched $\delta^{15}N$ values and increased Ti counts. These phases match with the earlier discussed enhanced winter precipitation at Son Kol. The identified wet winter phases in Kyrgyzstan correlate with wet winters in Norway and wet summers in Central-North China (Figure 36). The origin of water vapor transport during winter and summer are most

probably the mid-latitude Westerlies. The strong intra-hemispheric connection between North-Atlantic and Central Asia is visible for example in the influence of the cold Bond event 2 between 3.5 and 2.5 cal. kyr BP causing higher winter precipitation in Norway as well as in Central Kyrgyzstan. Even beyond the Tian Shan this winter-wet phase reached Central North China (Chen et al. 2006) and the Pamir (Mischke et al. 2010) in arid Central Asia (Figure 36). Detectable duration uncertainties of such events strongly depend on the lake-individual sensitivity to climate forcing, time-resolutions and chronologies. A second pronounced wet phase, differently occurring within the records appears after ca. 2 cal. kyr BP. Best matches have been detected also in Norway, where the amount of winter precipitation significantly increased (Figure 36). Despite regional similarities during winter season, some differences occur spatially during summer times. The climate of the Late Holocene is well explored via multi-proxy investigations on lake sediments. Several studies in the Pamir Mountains investigating lakes like Karakul (Mischke et al. 2010), Karakuli (Aichner et al. 2015), Sasi Kul (Lei et al. 2014) and Kashgar (Zhao et al. 2012) show that variations in strength and pathway of Westerlies occur on very small spatial scales due to mountain heterogeneity, influencing the recorded signals.

The naturally established Late Holocene cooling trend is visible in declining summer insolation, representative for the Northern Hemisphere and the North Atlantic region. The current anthropogenic induced warming caused different responses at lake systems, where glacial-influenced systems like Chatyr Kol, Lake Bosten (Wünnemann et al. 2006) and Lake Karakul (Mischke et al. 2010), receive enhanced meltwater and could apparently rise or keep their water level balanced, while non-glacial-influenced lake systems are not able to buffer their aridification and shrink like Lake Karakuli during the last 100 years (Aichner et al. 2015).

5.4.8 Glacial activity and lake level changes in Tian Shan during the last 2000 years

During the last 2000 years three major glacial advances between 2100–1700, 1300–1100 and 700–150 cal. yr BP have been detected in the Tian Shan Mountains with minor depression of the ELA in the inner ranges compared to northwest as a reaction to spatial differences in temperature and precipitation changes (Savoskul and Solomina 1996). Lower humidity is assumed by Sevastianov et al. (1980) for the Chatyr Kol region during these cold phases compared to the warmer and moister Mid-Holocene. Nevertheless, our detailed investigations during Late Holocene detected glacial phases depicted by the Bond event 2 showing lower temperatures in the North Atlantic as well at Chatyr Kol (U_{37}^{K}) and high erosional input during spring melt, suggesting that rather cold/wet conditions occur in this region (Figure 36). This assumption can be supported by findings from warm periods like the Medieval Climate Anomaly (MCA), where less fluctuating δD_{C23} values and low lake level at Chatyr Kol (950–450 cal. yr BP), Issyk Kul (1150–450 cal. yr BP) and Balkash (1200–800 cal. yr BP) (Solomina and Alverson 2004) indicate less pronounced depleted

meltwater inflows by shrunken glaciers. Therefore, warmer periods, at least during the Late Holocene, were rather dry, which is also assumed by Chen et al. (2010) in Arid Central Asia. This summer warm and winter dry period also has been observed at Kashgar (Zhao et al. 2012), Bangong Co on the western TP (Gasse et al. 1996) and Karakul in the Pamir (Mischke et al. 2010), indicating the MCA as an over-regional phenomenon. The subsequent transgression phase with the most recent maximum cooling known as the Little Ice Age (LIA) and glacial advance affected also Issyk Kul, Balkash, Chatyr Kol and even Son Kol since 350 cal. yr BP (Shnitnikov 1980).
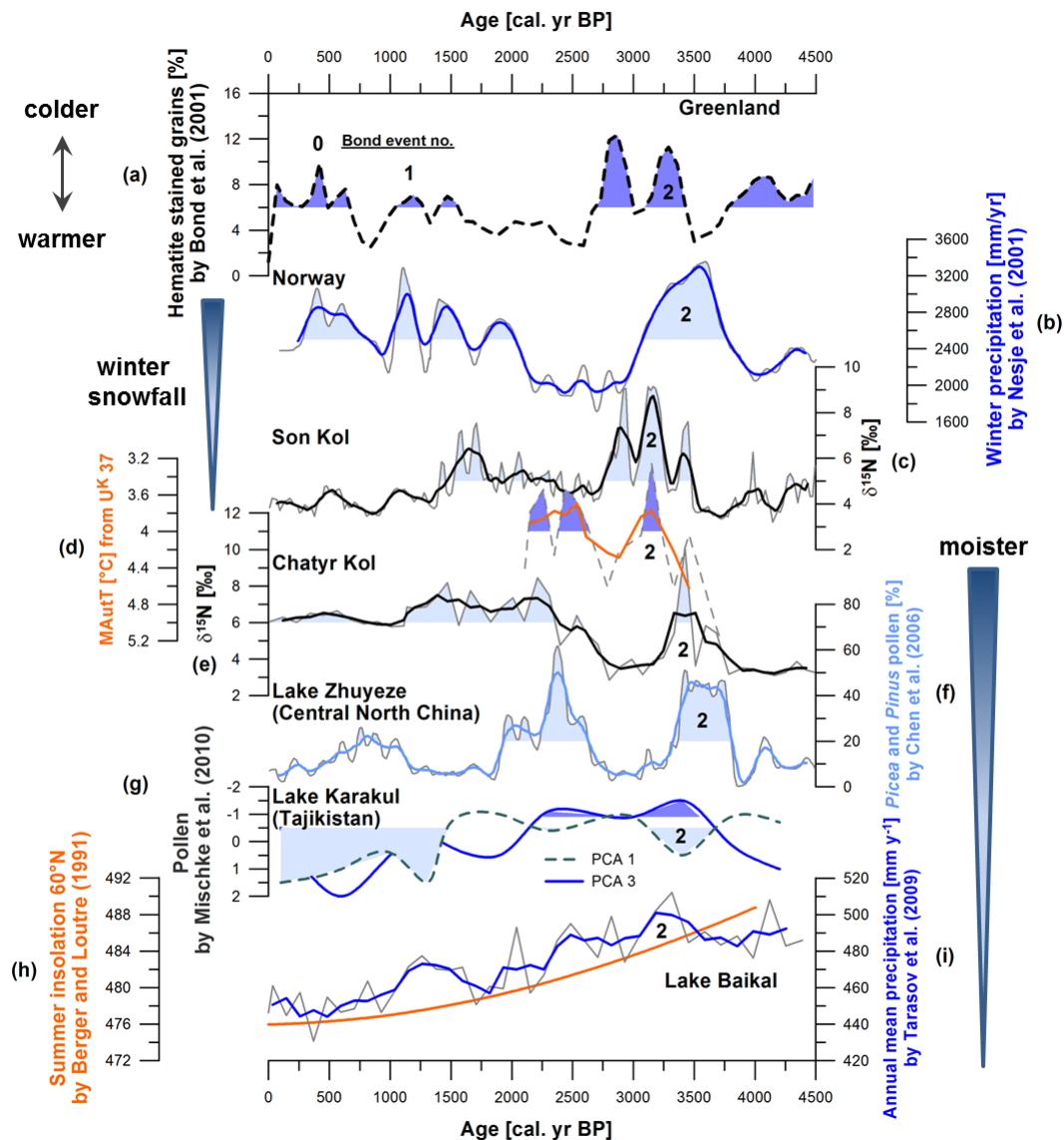
Figure 36: Comparison of Northern Hemispheric and Central Asian palaeoclimate records during the Late-Holocene.
(a) Hematite stained grains from North Atlantic sediments indicate Bond events (no. 0-2) (Bond et al. 2001), which indicate ice-rift debris in the North Atlantic. (b) Amount of winter precipitation

inferred from western Norway lacustrine sediments (Nesje et al. 2001). (c) $\delta^{15}N$ values from Lake Son Kol (chapter 4) (Lauterbach et al. 2014). (d) Reconstructed MAutT derived from U^K_{37} at Chatyr Kol. (e) $\delta^{15}N$ values from Lake Chatyr Kol (this study). (f) Percentages of *Picea* and *Pinus* pollen from Lake Zhuyeze (Chen et al. 2006). (g) Sample scores of pollen from Lake Karakul (Mischke et al. 2010), where positive PCA 1 indicates higher moisture conditions and positive PCA 3 indicates higher air temperature. (h) Summer insolation at 60°N (position of Baikal) by Berger and Loutre (1991). (i) Pollen-based mean annual precipitation at Lake Baikal (Tarasov et al. 2009). Numbers mark the Bond events.
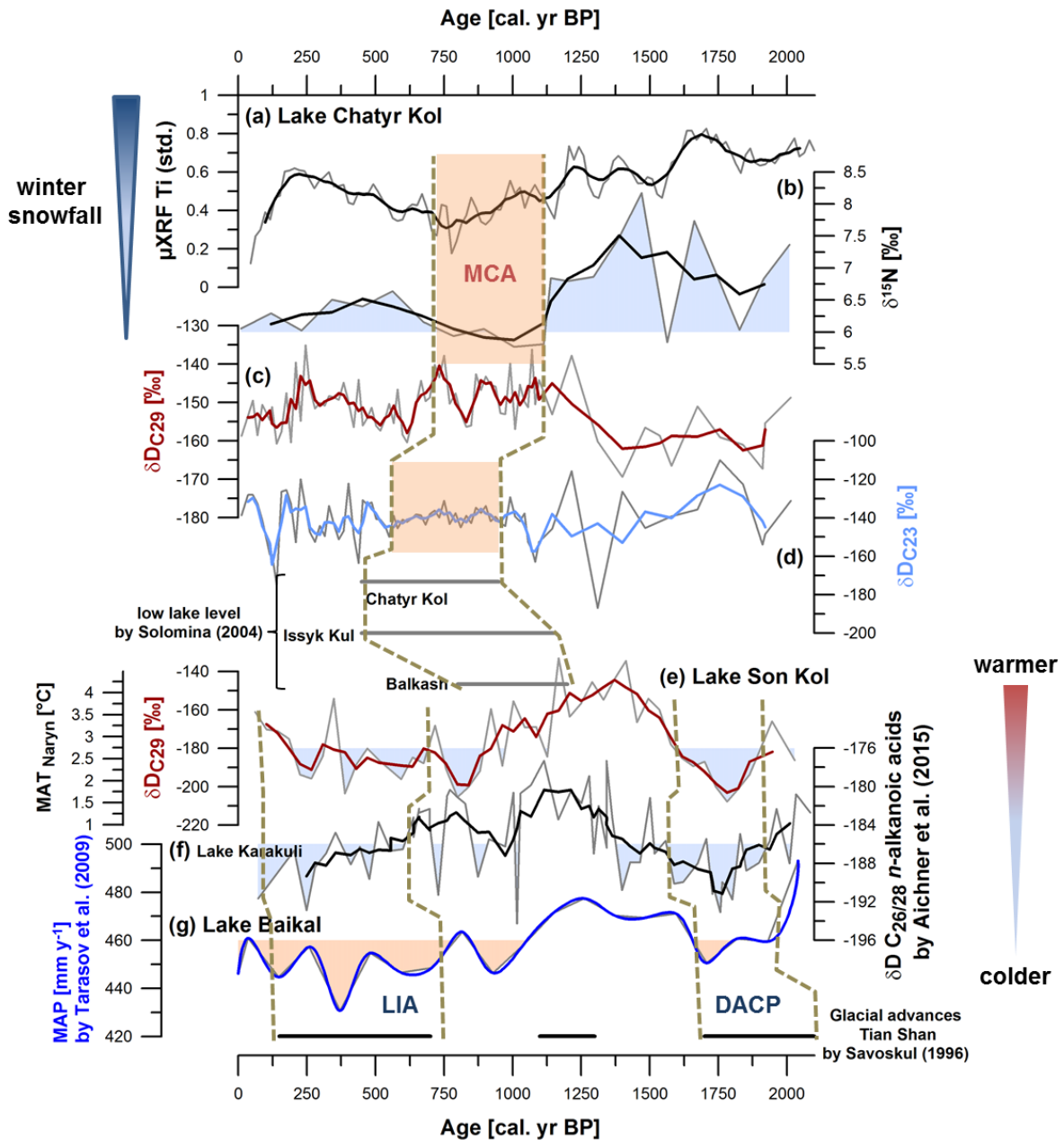
Figure 37: Comparison of regional palaeoclimate records during the last 2000 years.

A period of glacier retreat called Medieval Climate Anomaly (MCA) with reduced winter snowfall in Central Kyrgyzstan is inferred from (a) low Ti input, (b) depleted $\delta^{15}N$ values as well as (d) stable δD_{C23} values from Chatyr Kol. Terrestrial stable hydrogen isotope composition is enriched at (c) Chatyr Kol and (e) Son Kol during the MCA. Simultaneously occurring low lake levels at Chatyr Kol, Issyk Kul and Balkash were reviewed by Solomina and Alverson (2004). Glacial advances in the Tian Shan occurred during the Dark Ages Cool Period (DACP) between 2100 and 1700 cal. yr BP as well as during the Little Ice Age (LIA) between 700 and 150 cal. yr BP (Savoskul and Solomina 1996), correlating with lower mean annual air temperatures in Naryn region inferred from depleted δD_{C29} in Son Kol (e) and Karakuli sediments (f) (Aichner et al. 2015). (g) Mean annual precipitation at Lake Baikal is lower during cold periods (Tarasov et al. 2009).

5.4.9 Conclusions

Multi-proxy analyses of lake sediments from Chatyr Kol (Central Asia) provide evidences for a predominant influence of the mid-latitude Westerlies on the Holocene moisture and temperature variability. The pronounced Early Holocene warming identified in the Greenland ice core- and North Atlantic sediment records at 11.6 cal. kyr BP could also be detected by depleted aquatic δD_{C23} and higher µXRF Ti values at Chatyr Kol delayed at 10 cal. kyr BP. Responses of glaciers in the At Bashy and Torugart ranges contribute greatly to limnological and environmental variations of Chatyr Kol. Winter-wet periods like LIA between 700 and 150 cal. yr BP and Bond event 2 at around 3.3 cal. kyr BP with southwards shift of the mid-latitude Westerlies most likely forced by changes in the North Atlantic Oscillation, led to higher snowfall amounts in Kyrgyzstan and in parts of ACA. Consequently, stronger meridional temperature gradients most likely led to the increase in extreme precipitation events in all seasons (Chen et al. 2010). However, glacier-retreat periods like the Medieval Climate Anomaly at ca. 800 cal. yr BP are characterized by warm/dry conditions thus promoting lower lake levels. The isolated location of Chatyr Kol within the southern central Tian Shan has a large impact on the recorded Holocene climate variability. Terrestrial δD_{C29} values recorded major shifts at the transitions between the Early-, Mid- and Late Holocene, while intra-period fluctuations were relatively low. Enriched values during the Early- and Late Holocene indicate dry conditions strongly driven by temperature, while the Mid-Holocene (10–2 cal. kyr BP) was rather moister. The spatial differences between Central Asian palaeoclimate records can be explained by individual responses of lake systems to changes in temperature and precipitation, and changes of strength and position of the westerly jet stream. Additionally, our investigations supported the strong influence of glacier due to high water storing capacity to consistently maintain the lake system also during warm and dry periods.

6 Synthesis

6.1 Application of transfer functions to down core temperature reconstructions and possible interferences with other climate parameters

In this thesis one major objective was the evaluation of climate relevant proxies for palaeoclimate/-hydrological reconstructions in Central Asia using lake sediments. The processes affecting the recent hydrogen-isotopic composition of lipid biomarkers from phototrophic organisms need to be understood to correctly interpret recorded proxies in ancient archives.

Several transect studies across different climatic gradients (Huang et al. 2004; Sachse et al. 2004; Polissar and Freeman 2010; Garcin et al. 2012; Günther et al. 2013), investigated the influence of climate parameters like relative humidity, temperature, precipitation, evaporation on the relation between modern water and lipid biomarker isotope composition. Additional laboratory experiments investigated the influence of those and other factors like salinity and light intensity on source organisms and their compound-specific isotope composition (Englebrecht and Sachs 2005; Zhang and Sachs 2007). However, none of these studies investigated Arid Central Asia and could detect high correlations at single sites under uncontrolled conditions. The Tian Shan Mountains reveal very heterogeneous climate conditions on spatio-temporal scales with generally lower amounts of precipitation compared to monsoonal Asia. We tested the applicability of meteorological observational data of the last 90 years as alternative to transect and culture studies by comparing them with down core isotope proxy data (chapter 3). Our investigations reveal a transfer function [12] ($r = 0.97$; $p < 0.01$), which explains the isotope fractionation of terrestrial n-C$_{29}$ alkanes with the mean annual temperature variability in Central Kyrgyzstan (Figure 21).

$$\text{MAT}_{\text{Naryn}} \, [°C] = 0.0437 \text{ x } \delta D_{C29} + 10.602 \hspace{2cm} [12]$$

Here, temperature changes the terrestrial lipid δD values with 21.36 ‰ $°C^{-1}$, independently from precipitation intensity. Günther et al. (2013) found high correlations of terrestrial δD_{C29} with surface water isotope composition ($R^2 = 0.81$; $p = 0.05$), reflecting the precipitation signal on the Tibetan Plateau. Since temperature and precipitation are minor correlated during the last 90 years in Kyrgyzstan ($r = –0.2$; $p = 0.06$; $n = 79$), the variation of the precipitation isotope composition coincides with temperature variation, thus leading to highest δD values in summer and lowest values in winter in the Westerlies dominated Central Asia (Araguas-Araguas et al. 1998; Yao et al. 2013). The general warming trend observed since 1970 AD caused slight increased amounts of precipitation in some parts of the Tian Shan, but precipitation did not lead to higher influence on terrestrial hydrogen isotope fractionation than temperature. Lake Son Kol, representative for non-glacier influenced throughflow lakes, enables the palaeotemperature reconstruction using equation [12] in combination with sedimentary δD_{C29} data. However, Chatyr Kol, representative for

glacier-influenced terminal lakes, follows long-term trends rather than short-term fluctuations.

Using the equation [12] at Chatyr Kol sediments might only be possible during dry conditions, identified only for the Early Holocene and the last 2000 years (chapter 5). It seems, that once certain moisture-thresholds at a lake system with very cold and dry conditions have been exceeded, observed between 10 and 2 cal. kyr BP, clear interpretation of δD_{C29} values as proxy for MAT would not be accurate. Opposite response would be detected, because higher amounts of precipitation would cause depletion in δD values and higher temperatures lead to enriched values. For a better estimation of temperature changes, additional proxies for palaeotemperature reconstructions must be applied. To implicate alternative proxies, we used the widely established temperature-sensitive U^K_{37} index derived from haptophyte-produced alkenones. Using observational climate data, we could establish a transfer function [13] (r = 0.96; p = 0.04), enabling the reconstruction of the mean autumn air temperature in Central Kyrgyzstan (Figure 31).

$$\text{MAutT }_{\text{Naryn}} [^{\circ}C] = 5.53 \text{ x } U^K_{37} + 7.076 \qquad [13]$$

Since there is no uniform calibration of U^K_{37} indices against lake surface temperatures so far, each region needs individual calibrations noting the presence of different haptophyte species. Chatyr Kol does show at least two types of different phylotypes, which requires further DNA analysis, thus hamper the use of a single transfer function through a complete sedimentary record. Additionally, the presence/absence of alkenones can complicate down core reconstructions, since not even most recent studies were able to overcome this problem (He et al. 2014; Schmidt et al. 2014). However, we suggest possible explanations for bad preservation of alkenones and/or absence of haptophytes, which have not been supposed until now. A chain of conditions at Chatyr Kol may lead to this phenomenon. Outgassing of sedimentary H_2S would reduce the amount of fish, which support the population of amphipoda, a possible predator for haptophytes and thus reducing the preservation of alkenones. We conclude that beside climatic and limnological factors, also ecological factors could have large impact on the preservation and thus application of climate-sensitive lacustrine proxies.

The comparison of Son Kol and Chatyr Kol clarifies minor differences at climate parameters (MAT, MAP, rH) and major ones at catchment and lake characteristics (e.g. hydrology, glacial influence), but none of the detected down-core differences can be attributed to any discrepancies of sources for terrestrial and aquatic lipid biomarkers and OM, in general matching with common findings (all manuscripts). An case-example, showing inferences between local July temperatures during the Holocene explained by elevation differences, was already investigated in Sweden (Figure 38) (Larocque and Hall 2004). Even nearby lakes influenced by the same air mass show different responses, resulting in different temperature reconstructions under use of the same proxy. We conclude, that not every lacustrine record in the Tian Shan, although influenced by the mid-latitude Westerlies, record the same pattern due to unique lake characteristics. Nevertheless,

comparison of multi-proxy investigations is necessary to create large-scale reconstructions of the intensity changes and teleconnections between Westerly- and Monsoon systems in Asia.
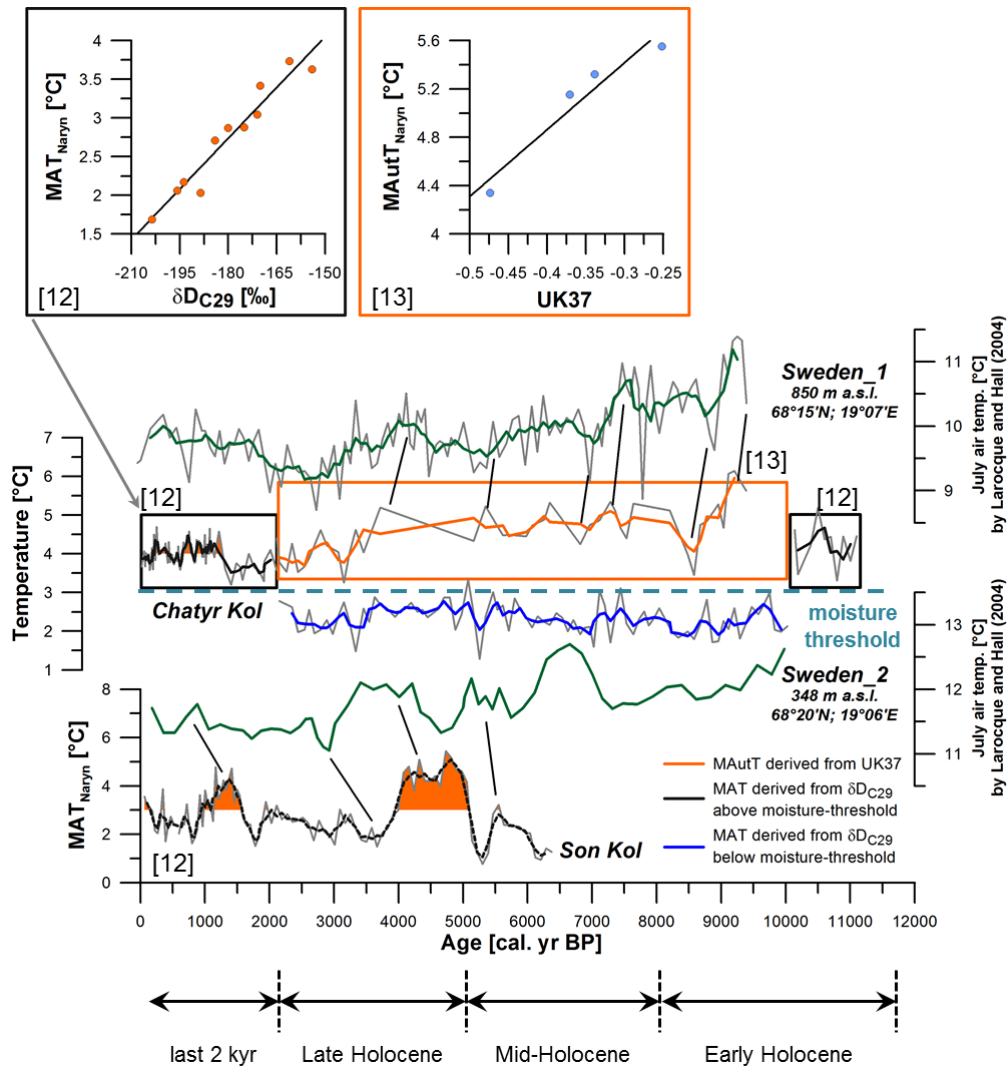
Figure 38: Application of different palaeotemperature proxies at certain moisture conditions during the Holocene in Kyrgyzstan using Chatyr Kol sediments. δD_{C29} values record the MAT properly during dry periods (black solid line/box), while higher precipitation between 10 and 2 cal. kyr BP depleted them (blue line). Therefore, an alternative transfer function with U_{37}^K, recording the MAutT, should be used during that timeframe (orange line/box). MAT reconstructions by Son Kol δD_{C29} show higher variability (dashed black line). July temperature reconstructions inferred from Chironomidae at two lakes in Sweden (1 = Lake 850; 2 = Lake Vuoskkujavri) (Larocque and Hall 2004) (green lines).

Detailed information about the lake hydrology could also be gained from aquatic δD_{C23} data, which retrace the isotope signal of the lake water [11] (Günther et al. 2013). We found higher correlations with the Standardized Precipitation Evaporation Index (SPEI) than with WET season precipitation only, indicating that the combination of temperature,

precipitation and evaporation is more likely driving the water isotope fractionation. Since SPEI data are only available for the period 1901–2011 AD and thus limiting the reconstruction on long-term scales e.g. Late Holocene, we suggest the combination of terrestrial and aquatic n-alkane δD values in the $\Delta\delta D_{C29\text{-}C23}$ proxy as an alternative for the reconstruction of evaporation and precipitation on longer timescales. However, the evaporation to inflow (E/I) ratio, highly correlated to $\Delta\delta D_{C29\text{-}C23}$ (r = −0.99; p < 0.01), offers a more quantitative calculation of the water balance under consideration of empirical and observational data (Gibson and Edwards 2002). Therefore, we suggest the application of E/I ratios, when investigating lacustrine sediments to reconstruct past lake hydrology using compound-specific stable hydrogen isotope approaches.

The multi-proxy approaches based on lipid biomarkers (n-alkanes and alkenones) and compound-specific δD values were applied to reconstruct Westerly-induced changes of past climatic and hydrological conditions at the Kyrgyz Chatyr Kol and Son Kol. However, since the Son Kol record is mainly driven by local environmental and climatic changes, and Chatyr Kol rather recorded long-term over-regional changes frequently reaching tipping points like shifts from glacial to interglacial or Late Holocene to the recent period, Chatyr Kol represents a better research location in order to evaluate the driving factors for extreme events.

Future perspectives, concerning the moisture-threshold observed mainly at Chatyr Kol, should focus on the transition periods between 10.5 and 9.5 as well as 2.5 and 1.5 cal. kyr BP either by additional lacustrine records or climate models, which could identify external or internal drivers leading to these tipping points.

6.2 Westerlies dynamics and their consequences on the glacier/lake relation in Central Asia and beyond

The research on glaciers in Central Asia during the last 20 years still has left open questions about the magnitude and spatio-temporal patterns of changes (Sorg et al. 2012; Unger-Shayesteh et al. 2013). The catchment runoff as major indicator of glacier mass storage ultimately influences the water balance of lake systems and therefore modern lake characterization can indirectly be used to evaluate glacier situation. We detected hydrological changes directly linked to large deglaciations at transitions from stadial to interstadial and even glacial to interglacial periods in Westerly-controlled lakes during the Holocene in Kyrgyzstan (chapter 5) and during the Last Glacial Maximum on the Tibetan Plateau (supplement) (Figure 39). Rising lake-level, increasing erosion of catchment material, water isotope depletion and increasing nutrient supply to aquatic organisms are only some detected consequences resulting from enhanced glacier meltwater input to a lacustrine system. Typically, deglaciation pattern lead to certain developmental stages in lakes, which, if identified, can give evidences of the catchment status. We found high

modification, possibly under the influence of glaciers, to the water isotope composition and their fractionation into organisms (

Figure 20), which needs to be known for future hydrological reconstructions. Upcoming studies should directly link annual glacier monitoring with lake water isotopic composition variability. Glaciers at Chatyr Kol catchment have not been investigated under this purpose so far.
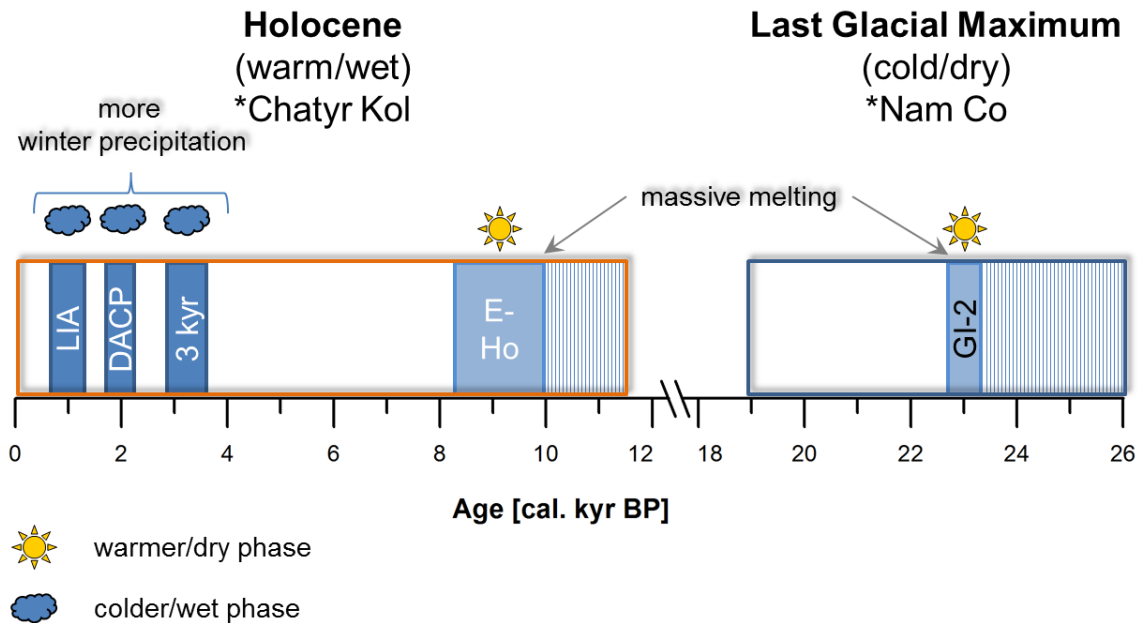
Figure 39: Scheme of enhanced meltwater phases after warming or increased winter precipitation within the LGM and Holocene. The warmer Greenland Interstadial 2 (GI-2) within the Last Glacial Maximum and the warmer Early Holocene (E-Ho) caused deglaciation at Nam Co and Chatyr Kol, respectively. Higher winter precipitation during colder periods like Little Ice Age (LIA), Dark Ages Cold Period (DACP) or the 3 kyr phase promoted higher meltwater in spring/early summer at Chatyr Kol.

Our lacustrine investigations disclosed several phases of enhanced meltwater input recorded in sedimentary proxies. The therefrom closing question is: What are the driving mechanisms of these phases and do they have the same origin? The detected warmer/dry Early Holocene at Chatyr Kol confirms with other proxy records in ACA, which detected decreased effective moisture (Feng et al. 2006; Herzschuh 2006; Chen et al. 2008; Huang et al. 2009). Climate simulations by Jin et al. (2012) suggest a relation to decreased water vapor advection due to reduced Westerly wind speed (low meridional thermal gradient) and less evaporation from the Mediterranean, Black and Caspian Seas. Minor impact was originated in Arctic ice sheet and meltwater fluxes. However, orbital forcing, decreasing the latitudinal temperature gradient and surface temperature, could explain more of the moisture signal. Similar features also accounts for the earlier cold LGM, which was indeed

promoted by minimum solar insolation but mainly forced by changes in atmospheric CO_2, with ice-sheet albedo feedbacks contributing to further cooling (Weaver et al. 1998). Abrupt appearing warm interstadials associated with warmer SSTs as consequence of increased strength of Atlantic Meridional Overturning Circulation, induced the following Post-LGM deglaciation also in Asia (Hodell et al. 2010). Warming in Asia has also been observed in palaeoclimate records in the North Atlantic realm (Alley 2000; Lowe et al. 2008), indicating a strong hemispheric-scale teleconnection between the North Atlantic and Central Asia during the Holocene and the Tibetan Plateau during the LGM. Both, the Late Glacial and the Last Glacial Maximum as precursors for the warmer Early Holocene and interstadials, led to a stronger eastward expansion of the Westerlies, thus reaching the southern Tibetan Plateau. North Atlantic teleconnections have been postulated during colder periods like the 8.2 kyr event as well, forced by weakening of the thermohaline circulation due to Laurentian meltwater inflow, leading to lower surface density and weakened deep-water formation, which than reduced the northward heat transport (Renssen et al. 2007; Wanner et al. 2011). The detected 3 kyr cooling corresponding with the Bond event 2 was possibly triggered by low solar activity forcing and amplified by the weaker thermohaline circulation (Wanner et al. 2011). The most recent cold/wet period, the LIA, originated most probably from a negative mode of the NAO (Mann et al. 2009) in combination with solar minima and tropical volcanic eruptions (Wanner et al. 2011). Generally, main triggers for cold periods could be solar irradiance, meltwater releases or even internal variability of coupled systems without external trigger. Changes in the winter Northern Hemispheric atmospheric circulation leading to stronger winter precipitation (e.g. LIA) was linked to a decrease in autumn Arctic sea ice area investigated as reaction to recently occurring events (Liu et al. 2012).

6.3 Future prospects

The alternation of stadial and interstadial periods naturally occurs due to cyclicity of hemispheric insolation changes. Since the current solar forcing is decreasing in the Northern Hemisphere, we should discover rather stadial conditions. However, anthropogenic induced global warming will continue and the effect of increasing MAT in Central Asia will have higher impact on glacial runoff than increased MAP. According to climate simulations for the future (IPCC reports), glaciers in Kyrgyzstan will reduce their area, increase their short-term and decrease their long-term runoff. In case of Chatyr Kol, lake level will rise with similar consequences than during the Early Holocene. A short-term outflow is possible, but on the long-term trend, it will possibly experience a gradual drying/lowering like already visible at Aral Sea and Lake Balkash. Nevertheless, since the down-core record did not show complete loss of water also during phases of high evaporation and low moisture, Chatyr Kol will probably not completely dry out.

7 Summary

The mid-latitude Westerlies atmospheric circulation system provides Arid Central Asia with moisture and determines the actual general climate situation in this region. Its intensity and interaction with neighboring atmospheric systems like the Asian monsoons was not stabile during the past and thus led to alternations of cold-wet and warm-dry conditions. To predict future climate and hydrological changes and manage human populations in Arid Central Asia under a global warming scenario, a better understanding of already emerged changes in the past is essential.

The general aim of this thesis was the reconstruction of the mid-latitude Westerly variability in Central Asia during the past 11,000 years using lake sediments under a multi-proxy approach. The mainly used proxies were compound-specific isotope signals of terrestrial and aquatic biomarkers. Therefore, long-term data collection from certain periods of climate changes and their provision to climate models, can be done by proxy reconstruction using high-resolution archives like lacustrine sediment-, ice core-, speleothem-, tree ring- or loess records. Since spatial-heterogeneous seasonal climate in the Tian Shan Mountains, a natural moisture-barrier, is mainly driven by different temperatures and amounts of precipitation, climate-sensitive proxies, as indicators of the variability of past environmental conditions can be used and have been analyzed using sedimentological and geochemical (gas-chromatography, mass-spectrometry) methods. Lakes, widely distributed in the Tian Shan Mountains, represent such natural archives storing these proxies. Thus, we investigated sediments from Lake Son Kol and Chatyr Kol in Kyrgyzstan. The rich variety of stored proxies enables a multi-proxy approach and thus an ideal chance to reconstruct climate, hydrological, limnological as well as environmental changes. Sedimentary records contain OM, isotopes, organisms, inorganic components and sediment lithology. Depending on the lake chemistry, hydrological character or catchment characteristic, each sedimentary record displays a unique palaeoenvironmental archive storing local and/or regional information. The geochemical investigation of the OM, which contains molecular biomarkers like *n*-alkanes derived from phototrophic organisms, and alkenones derived from haptophytes (microphytoplancton), reveals biological adjustments to climate/environmental changes. Compound-specific stable hydrogen isotope signals, recorded in terrestrial and aquatic *n*-alkanes, can be used to decipher the past water isotope signal and thus the lake water balance and/or moisture condition. Bulk isotope data (δ^{15}N, δ^{13}C) recorded limnological responses to catchment/environmental changes. The correct interpretation of investigated proxies requires an understanding of origin of individual biomarkers and the processes affecting for example the hydrogen-isotope composition of them. Therefore, we compared sedimentary data with recent catchment vegetation studies and instrumental climatic data bases. The following results improve the understanding of climate impact on biomarkers and their hydrogen isotope signal in Kyrgyzstan:

- The biotic sources of terrestrial *n*-alkanes C_{29} are terrestrial higher plants and of aquatic *n*-alkanes C_{23} submerged water plants and phototrophic algae confirming with previous studies. This indicates that Kyrgyz sedimentary organic matter and especially *n*-alkane composition was derived by comparable sources than other sites under different conditions. Thus the *n*-alkane distribution can be applied as palaeoenvironmental proxy and allows comparisons with other sites globally on spatial/temporal scales.

- The hydrogen isotope composition of terrestrial *n*-C_{29} (δD_{C29}) correlates best with mean annual air temperature ($r = 0.97$, $p < 0.01$). This indicates that isotopic fractionation in this terrestrial system strongly depends on temperature rather than precipitation. The impact by precipitation is only noticeable above certain moisture thresholds in this dry region.

- The lake water isotope signal is more enriched at the terminal Chatyr Kol than the throughflow Son Kol, indicating that lake hydrology primary controls the effect of apparent evaporation. However, glacier meltwater input at Chatyr Kol counteracts to evaporation, thus hiding real evaporative enrichment. Consequently, the aquatic *n*-alkanes C_{23} retraces the isotope signal of the lake water modified by evaporation and glacier meltwater.

- The isotopic difference between *n*-C_{29} and *n*-C_{23} ($\Delta\delta D_{C29-C23}$), implemented in the calculation of the evaporation to inflow (E/I) ratio, can be used to describe the water balance is a semi-quantitative way. The E/I ratio of the glacier-influenced Chatyr Kol and the non-glacier-influenced Son Kol diverged since 1975 AD, indicating that recent warming and glacier runoff caused different catchment reactions. Consequently, palaeohydrological reconstructions have to consider various catchment parameters.

- The haptophyte-derived alkenone unsaturation index (U^K_{37}) correlates best with the mean autumn air temperature and can be used as additional palaeotemperature proxy in Kyrgyzstan. The combination of U^K_{37} and δD_{C29} enables robust down-core palaeotemperature reconstructions.

Finally, previous findings were applied to long-term sedimentary records of Son Kol and Chatyr Kol to reconstruct the Westerlies-forced hydrological and environmental changes in the last 11,000 years. This multi-proxy study provides further insides into the spatio-temporal Westerlies variability in Central Asia mainly during the Holocene:

- The Early Holocene warming, detected already Greenland and Central Asia could also be identified at Chatyr Kol. The warming, identified by U^K_{37} caused glacier meltwater input, which was responsible for a lake volume rise, visible in water isotope signal (δD_{C23}) and increased minerogenic input (μXRF Ti).

- Cold and wet periods like the Little Ice Age (LIA), the Dark Ages Cool Period (DACP) and the 3 kyr period could be detected by using δD_{C23}, δD_{C29}, U^K_{37}, Ti and

δ^{15}N. Characteristic enhanced winter precipitation and thus promoted summer melting have been suggested.

- We provide supporting evidences for an exclusive influence of the Westerlies in Kyrgyzstan and thus Central Asia during the Holocene. The Westerly variability was rather driven by North Atlantic Oscillation changes, which in turn are controlled by solar radiation, meltwater releases or other external factors.

This thesis supported the importance and reliability of biomarkers (*n*-alkanes, alkenones) as palaeoclimate and palaeoenvironmental proxies, but also demonstrated the importance of additional proxies and parameters (glacier), which are essential for a realistic reconstruction using lake sediments. Multi-proxy studies should be applied in every upcoming lake investigation, since catchment and lake reveal heterogeneous properties and thus requiring primarily individual interpretations.

8 Zusammenfassung

Die Westwinde der mittleren geographischen Breiten, die sogenannten Westerlies, versorgen Zentralasien mit Feuchtigkeit und bestimmen somit die aktuelle klimatische Situation. Aufgrund der variablen Intensität und Interaktion der Westerlies mit benachbarten atmosphärischen Zirkulationssystemen wie den asiatischen Monsunen, war die klimatische Situation in der holozänen Vergangenheit durch wechselnde Phasen mit kalt-feuchten und warm-trockenen Bedingungen geprägt. Um zukünftige klimatische und hydrologische Änderungen besser vorhersagen und die menschliche Bevölkerung in Zentralasien in Bezug auf das globale Erwärmungs-Szenario vorbereiten zu können, ist ein besseres Verständnis über die bereits zuvor im Quartär abgelaufenen Änderungen durch Erwärmung unerlässlich.

Das Ziel dieser Dissertation war die Intensitäts-Rekonstruktion der Westerlies in Zentralasien der letzten 11.000 Jahre mittels Seesedimenten unter der Verwendung eines Multi-Indikator-Ansatzes. Die hauptsächlich untersuchten Indikatoren, sogenannte Proxies, waren substanz-spezifische Isotopensignale der terrestrischen und aquatischen molekularen Biomarker. Die Ermittlung von Daten bestimmter Zeitabschnitte und deren spätere Bereitstellung für Klimamodelle kann durch die Verwendung von zeitlich hoch-aufgelösten natürlichen Archiven wie Seesedimenten, Eiskernen, Stalagmiten, Baumringen oder Lößprofilen erfolgen, die zum Beispiel Klimaparameter indirekt in Proxies aufgezeichnet haben. Da das räumlich-heterogene saisonale Klima im Tian Shan-Gebirge, eine natürliche Barriere für angelieferte Feuchtigkeit in Zentralasien, vor allem von unterschiedlichen Temperaturen und Niederschlagsmengen geprägt ist, bieten sich besonders klima-sensitive Proxies als Indikatoren für die vergangene Variabilität der Umweltbedingungen an und wurden in dieser Arbeit mittels sedimentologischen und geochemischen (z.B. Gas-Chromatographie, Massenspektrometrie) Methoden analysiert. Seen stellen außerordentlich vielseitige Archive dar und sind auch im zentralen kirgisischen Tian Shan-Gebirge vorzufinden. Daher wurden in dieser Arbeit der Son Kol und der Chatyr Kol für die Probenahme und spätere systematische Analyse gezielt ausgewählt. Die hohe Diversität an gespeicherten Proxies ermöglicht eine ideale Möglichkeit, Änderungen des Klimas, der Hydrologie, der Limnologie und sogar der Umwelt zu rekonstruieren. Sedimentäre Ablagerungen enthalten organische und anorganischen Komponenten, Isotope, Organismen und lithologische Merkmale. In Abhängigkeit seines Chemismus, Hydrologie oder Einzugsgebietes, zeichnet jeder See spezifische lokale und/oder regionale Informationen im Sediment auf. Die geochemische Untersuchung der organischen Substanz, besonders sogenannter molekularer Biomarker wie *n*-Alkane, die von phototrophen Organismen synthetisiert werden, und Alkenone aus Kalkalgen, offenbart Informationen über biologische Anpassungen an klimatische und umweltbedingte Veränderungen. Substanz-spezifische stabile Wasserstoffisotopensignale der terrestrischen und aquatischen *n*-Alkane wurden in dieser Arbeit verwendet, um Niederschlags- und Seewasserisotopensignaturen zu

ermitteln und anschließend die Feuchtigkeitssituation oder Wasserbilanz zu rekonstruieren. Des Weiteren eignen sich Bulkisotopendaten (δ^{15}N, δ^{13}C) für die Rekonstruktion von limnologischen Reaktionen auf veränderte Bedingungen im Einzugsgebiet.

Die richtige Interpretation der untersuchten Proxies erfordert Verständnis zum einen über die Herkunft und die Modifizierung der einzelnen Biomarker und zum anderen die dafür verantwortlichen Prozesse, die beispielsweise die Wasserstoffisotopenzusammensetzung verändern. Daher wurden Sedimentdaten mit Vegetationsstudien der Einzugsgebiete und mit instrumentellen klimatischen Datenbanken verglichen. Die folgenden Ergebnisse sollen zum verbesserten Verständnis der Auswirkungen von Klimaänderungen auf Biomarker und deren Wasserstoffisotopensignale in Zentral Asien beitragen:

- Die biotischen Quellen des sedimentären n-Alkan C_{29} sind terrestrische höhere Pflanzen und die des sedimentären n-Alkan C_{23} sind Unterwasserpflanzen und phototrophe Algen. Unsere Untersuchungen bestätigen Erkenntnisse aus früheren Studien und beweisen, dass kirgisisches sedimentäres organisches Material und insbesondere deren n-Alkan-Zusammensetzung mit vergleichbaren Quellen anderer Untersuchungsgebiete, jedoch anderer Umweltbedingungen übereinstimmen. Somit kann die n-Alkanverteilung als Paläoumwelt-Proxy eingesetzt werden und ermöglicht Vergleiche mit anderen Standorten weltweit auf räumlich / zeitlichen Skalen.

- Die Wasserstoffisotopenzusammensetzung vom terrestrischen n-C_{29} (δD_{C29}) korreliert am besten mit der mittleren Jahreslufttemperatur (r = 0,97, p < 0,01). Dies zeigt, dass die Isotopenfraktionierung in diesem terrestrischen System stärker von der Temperatur als vom Niederschlag abhängt. Die Einflüsse des Niederschlages sind nur oberhalb bestimmter Feuchtigkeits-Schwellenwerte in dieser trockenen Region erkennbar.

- Die Anreichung mit Deuterium ist deutlich höher im Seewasser des geschlossenen Chatyr Kol im Vergleich zum offenen Son Kol. Dies deutet darauf hin, dass die Hydrologie eines Sees primär durch offensichtliche Evaporation gesteuert wird. Dennoch, schließt die Isotopensignatur des Seewassers den Eintrag von abgereichertem Gletscherschmelzwasser am Chatyr Kol mit ein und verbirgt so die höhere tatsächliche Evaporation. Folglich zeichnen die δD Werte des aquatischen n-C_{23} das Isotopensignal des Seewassers auf, das jedoch durch Verdunstung und Gletscherschmelzwasser modifiziert wurde.

- Die isotopische Differenz zwischen n-C_{29} und n-C_{23} ($\Delta\delta D_{C29-C23}$), einbezogen in die Berechnung des Evaporation zu Zufluss Verhältnisses (E/I), kann verwendet werden, um die Wasserbilanz in semi-quantitativer Weise zu beschreiben. Das E/I-Verhältnis des Gletscher-beeinflussten Chatyr Kol's und des Nicht-Gletscher-beeinflussten Son Kol's weicht seit 1975 AD voneinander ab, das anzeigt, dass die jüngste Erwärmung und Gletscherschmelze verschiedene Reaktionen in Einzugsgebieten verursacht. Folglich müssen paläohydrologische Rekonstruktionen verschiedene Parameter des Einzugsgebietes berücksichtigen.

- Der von Kalkalgen abgeleitete Alkenon-Sättigungs Index (U_{37}^K) korreliert am besten mit der mittleren Herbst-Lufttemperatur (r = 0.96, p = 0.04) und kann als zusätzlicher Paläotemperatur-Proxy in Kirgisistan eingesetzt werden. Die Kombination von U_{37}^K und δD_{C29} ermöglicht somit robuste Sedimentkern-basierte Paläotemperatur-Rekonstruktionen.

Anschließend wurden diese Ergebnisse auf weiter zurückreichende Sedimentkerne des Son Kol und Chatyr Kol angewandt, um die Westerlies-bedingten hydrologischen und ökologischen Änderungen der letzten 11.000 Jahre zu rekonstruieren. Diese Multi-Proxy-Studie liefert weitere Einsichten in die räumlich-zeitliche Variabilität der Westerlies in Zentralasien vor allem während des Holozäns:

- Die Früh-Holozäne Erwärmung, bereits in Eiskernarchiven in Grönland detektiert, konnte auch im Chatyr Kol identifiziert werden. Die Erwärmung, nachgewiesen durch den U_{37}^K Index, verursachte erhöhten Eintrag von Gletscherschmelzwasser und schließlich Zunahme des Seevolumens, angezeigt durch abgereichertes Seewasser-Isotopensignal (δD_{C23}) und erhöhten minerogenen Eintrag (μXRF Ti).
- Kalte und feuchtere Perioden wie die kleine Eiszeit (LIA), die Mittelalter-Kälteperiode (DACP) und die 3000 BP Periode konnten mithilfe von δD_{C23}, δD_{C29}, U_{37}^K, Ti und $\delta^{15}N$ nachgewiesen werden. Charakteristisch erhöhte Winterniederschläge und damit begünstigte Sommerschmelze können diesen Perioden zugewiesen werden.
- Diese Arbeit liefert unterstützende Beweise für einen exklusiven Einfluss der Westerlies in Kirgisistan und Zentralasien während des Holozäns. Die Westerlies-Variabilität wurde vielmehr durch Änderungen in der nordatlantischen Oszillation (NAO) bestimmt, die wiederum durch solare Einstrahlung, Schmelzwasser-Einträge oder andere externe Faktoren gesteuert wurde.

Diese Arbeit unterstützt die Bedeutung und Zuverlässigkeit der Biomarker (*n*-Alkane, Alkenone) als Paläoklima- und Umwelt-Proxies, zeigt aber auch, wie wichtig zusätzliche Proxies und Parameter (Gletscher) für eine realistische Rekonstruktion mit Seesedimenten sind. Multi-Proxy-Studien sollten in jeder zukünftigen See-Untersuchung angewandt werden, da jedes Einzugsgebiet und sein See individuelle Eigenschaften aufzeigt und somit in erster Linie individuelle Interpretationen erfordert.

9 References

Academy_of_Science_of_the_Kyrgyz_SSR (1987) Atlas of the Kyrgyz Soviet Socialistic Republic. Volume 1: Natural conditions and resources. State Agency for Cartography and Geodesy, Central Directorate for Geodesy and Cartography, Council of Ministers of the USSR doi:

Ageta Y and Higuchi K (1984) Estimation of mass balance components of a summer-accumulation type glacier in the Nepal Himalaya. Geografiska Annaler Series a-Physical Geography 66:249-255

Aichner B, Feakins SJ, Lee JE, Herzschuh U and Liu X (2015) High-resolution leaf wax carbon and hydrogen isotopic record of the late Holocene paleoclimate in arid Central Asia. CliPa 11:619-633

Aichner B, Herzschuh U and Wilkes H (2010a) Influence of aquatic macrophytes on the stable carbon isotopic signatures of sedimentary organic matter in lakes on the Tibetan Plateau. Org Geochem 41:706-718

Aichner B, Herzschuh U, Wilkes H, Vieth A and Bohner J (2010b) delta D values of n-alkanes in Tibetan lake sediments and aquatic macrophytes - A surface sediment study and application to a 16 ka record from Lake Koucha. Org Geochem 41:779-790

Aichner B, Wilkes H, Herzschuh U, Mischke S and Zhang CJ (2010c) Biomarker and compound-specific delta C-13 evidence for changing environmental conditions and carbon limitation at Lake Koucha, eastern Tibetan Plateau. J Paleolimnol 43:873-899

Aizen EM, Aizen VB, Melack JM, Nakamura T and Ohta T (2001) Precipitation and atmospheric circulation patterns at mid-latitudes of Asia. IJCli 21:535-556

Aizen VB, Aizen EM, Joswiak DR, Fujita K, Takeuchi N and Nikitin SA (2006) Climatic and atmospheric circulation pattern variability from ice-core isotope/geochemistry records (Altai, Tien Shan and Tibet). In: E MosleyThompson and LG Thompson (eds), Annals of Glaciology, Vol 43, 2006, pp 49-60

Aizen VB, Aizen EM and Melack JM (1995) Climate, snow cover, glaciers, and runoff in the Tien-Shan, Central-Asia. Water Resour Bull 31:1113-1129

Aizen VB, Aizen EM, Melack JM and Dozier J (1997) Climatic and hydrologic changes in the Tien Shan, Central Asia. J Clim 10:1393-1404

Alley RB (2000) The Younger Dryas cold interval as viewed from central Greenland. Quat Sci Rev 19:213-226

Allison GB (1982) The relationship between o-18 and deuterium in water in sand columns undergoing evaporation. J Hydrol 55:163-169

Allison GB, Barnes CJ and Hughes MW (1983) The distribution of deuterium and 18O in dry soils. J Hydrol 64:377-397

Allison GB and Hughes MW (1983) The use of natural tracers as indicators of soil-water movement in a temperate semi-arid region. J Hydrol 60:157-173

Amundson R, Austin AT, Schuur EAG, Yoo K, Matzek V, Kendall C, Uebersax A, Brenner D and Baisden WT (2003) Global patterns of the isotopic composition of soil and plant nitrogen. Global Biogeochem Cycles 17

An C-B, Lu Y, Zhao J, Tao S, Dong W, Li H, Jin M and Wang Z (2012a) A high-resolution record of Holocene environmental and climatic changes from Lake Balikun (Xinjiang, China): Implications for central Asia. Holocene 22:43-52

An ZS, Colman SM, Zhou WJ, Li XQ, Brown ET, Jull AJT, Cai YJ, Huang YS, Lu XF, Chang H, Song YG, Sun YB, Xu H, Liu WG, Jin ZD, Liu XD, Cheng P, Liu Y, Ai L, Li XZ, Liu XJ, Yan LB, Shi ZG, Wang XL, Wu F, Qiang XK, Dong JB, Lu FY and Xu XW (2012b) Interplay between the Westerlies and Asian monsoon recorded in Lake Qinghai sediments since 32 ka. Scientific Reports 2

Andersen KK, Azuma N, Barnola JM, Bigler M, Biscaye P, Caillon N, Chappellaz J, Clausen HB, DahlJensen D, Fischer H, Fluckiger J, Fritzsche D, Fujii Y, Goto-Azuma K, Gronvold K, Gundestrup NS, Hansson M, Huber C, Hvidberg CS, Johnsen SJ, Jonsell U, Jouzel J, Kipfstuhl S, Landais A, Leuenberger M, Lorrain R, Masson-Delmotte V, Miller H, Motoyama H, Narita H, Popp T, Rasmussen SO, Raynaud D, Rothlisberger R, Ruth U, Samyn D, Schwander J, Shoji H, Siggard-Andersen ML, Steffensen JP, Stocker T, Sveinbjornsdottir AE, Svensson A, Takata M, Tison JL, Thorsteinsson T, Watanabe O, Wilhelms F, White JWC and Project NGIC (2004) High-resolution record of Northern Hemisphere climate extending into the last interglacial period. Nature 431:147-151

Appleby PG (2002) Chronostratigraphic techniques in recent sediments. Tracking Environmental Change Using Lake Sediments, Vol 1: Basin Analysis, Coring, and Chronological Techniques 1:171-203

Appleby PG, Richardson N and Nolan PJ (1991) 241Am dating of lake-sediments. Hydrobiologia 214:35-42

Araguas-Araguas L, Froehlich K and Rozanski K (1998) Stable isotope composition of precipitation over southeast Asia. J Geophys Res-Atmos 103:28721-28742

Araguasaraguas L, Rozanski K, Gonfiantini R and Louvat D (1995) Isotope effects accompanying vacuum extraction of soil-water for stable-isotope analyses. J Hydrol 168:159-171

Bahr A (2005) Late Glacial to Holocene Paleoenvironemental Evolution of the Black Sea. Dissertation doi:

Balabanov IP (2007) Holocene sea-level changes of the Black Sea. In Yanko-Hombach et al (eds): The Black Sea Flood Question doi:711-730

Barbour MM and Farquhar GD (2000) Relative humidity- and ABA-induced variation in carbon and oxygen isotope ratios of cotton leaves. Plant Cell Environ 23:473-485

Barnes CJ and Allison GB (1988) Tracing of water-movement in the unsaturated zone using stable isotopes of hydrogen and oxygen. J Hydrol 100:143-176

Barrows TT and Juggins S (2005) Sea-surface temperatures around the Australian margin and Indian ocean during the last glacial maximum. Quat Sci Rev 24:1017-1047

Battarbee RW and Kneen MJ (1982) The use of electronically counted microspheres in absolute diatom analysis. Limnol Oceanogr 27:184-188

Beer R, Heiri O and Tinner W (2007) Vegetation history, fire history and lake development recorded for 6300 years by pollen, charcoal, loss on ignition and chironomids at a small lake in southern Kyrgyzstan (Alay Range, Central Asia). Holocene 17:977-985

Beer R and Tinner W (2008) Four thousand years of vegetation and fire history in the spruce forests of northern Kyrgyzstan (Kungey Alatau, Central Asia). Vegetation History and Archaeobotany 17:629-638

Begueria S, Vicente-Serrano SM, Reig F and Latorre B (2014) Standardized precipitation evapotranspiration index (SPEI) revisited: parameter fitting, evapotranspiration models, tools, datasets and drought monitoring. IJCli 34:3001-3023

Bendle J, Rosell-Mele A and Ziveri P (2005) Variability of unusual distributions of alkenones in the surface waters of the Nordic seas. Paleoceanography 20

Berger A and Loutre MF (1991) Insolation values for the climate of the last 10 million years. Quat Sci Rev 10:297-317

Bergmann J, Friedel P and LKleeberg R (1998) BGME - A new fundamental parameters based Rietveld program for laboratory X-ray sources, it`s use in quantitative analysis and structure investigations. CPD Newsletter 20:5-8

Beug H-J (2004) Leitfaden der Pollenbestimmung für Mitteleuropa und angrenzende Gebiete. Verlag Dr Friedrich Pfeil doi:

Bianchi GG and McCave IN (1999) Holocene periodicity in North Atlantic climate and deep-ocean flow south of Iceland. Nature 397:515-517

Bird MI, Chivas AR, Radnell CJ and Burton HR (1991) Sedimentological and stable-isotope evolution of lakes in the Vestfold Hills, Antarctica. Palaeogeogr, Palaeoclimatol, Palaeoecol 84:109-130

Bjune AE, Bakke J, Nesje A and Birks HJB (2005) Holocene mean July temperature and winter precipitation in western Norway inferred from palynological and glaciological lake-sediment proxies. Holocene 15:177-189

Black E (2012) The influence of the North Atlantic Oscillation and European circulation regimes on the daily to interannual variability of winter precipitation in Israel. IJCli 32:1654-1664

Bohner J (2006) General climatic controls and topoclimatic variations in Central and High Asia. Boreas 35:279-295

Bolch T, Yao T, Kang S, Buchroithner MF, Scherer D, Maussion F, Huintjes E and Schneider C (2010) A glacier inventory for the western Nyainqentanglha Range and the Nam Co Basin, Tibet, and glacier changes 1976-2009. Cryosphere 4:419-433

Bond G, Kromer B, Beer J, Muscheler R, Evans MN, Showers W, Hoffmann S, Lotti-Bond R, Hajdas I and Bonani G (2001) Persistent solar influence on north Atlantic climate during the Holocene. Science 294:2130-2136

Bond G, Showers W, Cheseby M, Lotti R, Almasi P, deMenocal P, Priore P, Cullen H, Hajdas I and Bonani G (1997) A pervasive millennial-scale cycle in North Atlantic Holocene and glacial climates. Science 278:1257-1266

Bondarev LG, Gobedzhishvili RG and Solomina ON (1997) Fluctuations of local glaciers in the southern ranges of the former USSR: 18,000-8000 BP. Quat Int 38-9:103-108

Boomer I, Aladin H, Plotnikov I and Whatley R (2000) The palaeolimnology of the Aral Sea: a review. Quat Sci Rev 19:1259-1278

Bowen GJ and Revenaugh J (2003) Interpolating the isotopic composition of modern meteoric precipitation. Water Resour Res 39

Brassell SC (1993) Applications of biomarkers for delineating marine paleoclimatic fluctuations during the Pleistocene. Top Geobiol 11:699-738

Brassell SC, Eglinton G, Marlowe IT, Pflaumann U and Sarnthein M (1986) Molecular stratigraphy - a new tool for climatic assessment. Nature 320:129-133

Brauer A, Endres C and Negendank JFW (1999) Lateglacial calendar year chronology based on annually laminated sediments from Lake Meerfelder Maar, Germany. Quat Int 61:17-25

Buslov MM, De Grave J, Bataleva EAV and Batalev VY (2007) Cenozoic tectonic and geodynamic evolution of the Kyrgyz Tien Shan Mountains: A review of geological, thermochronological and geophysical data. JAESc 29:205-214

Castaneda IS and Schouten S (2011) A review of molecular organic proxies for examining modern and ancient lacustrine environments. Quat Sci Rev 30:2851-2891

Chabangborn A, Brandefelt J and Wohlfarth B (2014) Asian monsoon climate during the Last Glacial Maximum: palaeo-data-model comparisons. Boreas 43:220-242

Chen B, Xu XD, Yang S and Zhang W (2012) On the origin and destination of atmospheric moisture and air mass over the Tibetan Plateau. Theor Appl Climatol 110:423-435

Chen F-H, Chen J-H, Holmes J, Boomer I, Austin P, Gates JB, Wang N-L, Brooks SJ and Zhang J-W (2010) Moisture changes over the last millennium in arid central Asia: a review, synthesis and comparison with monsoon region. Quat Sci Rev 29:1055-1068

Chen F-H, Cheng B, Zhao Y, Zhu Y and Madsen DB (2006) Holocene environmental change inferred from a high-resolution pollen record, Lake Zhuyeze, arid China. Holocene 16:675-684

Chen F, Yuan Y-j, Chen F-H, Wei W-s, Yu S-l, Chen X-j, Fan Z-a, Zhang R-b, Zhang T-w, Shang H-m and Qin L (2013) A 426-year drought history for Western Tian Shan, Central Asia, inferred from tree rings and linkages to the North Atlantic and Indo-West Pacific Oceans. Holocene 23:1095-1104

Chen FH, Yu ZC, Yang ML, Ito E, Wang SM, Madsen DB, Huang XZ, Zhao Y, Sato T, Birks HJB, Boomer I, Chen JH, An CB and Wunnemann B (2008) Holocene moisture evolution in arid central Asia and its out-of-phase relationship with Asian monsoon history. Quat Sci Rev 27:351-364

Cheng H, Zhang PZ, Spoetl C, Edwards RL, Cai YJ, Zhang DZ, Sang WC, Tan M and An ZS (2012) The climatic cyclicity in semiarid-arid central Asia over the past 500,000 years. Geophys Res Lett 39

Chimner RA and Cooper DJ (2004) Using stable oxygen isotopes to quantify the water source used for transpiration by native shrubs in the San Luis Valley, Colorado USA. Plant Soil 260:225-236

Chu GQ, Sun Q, Li SQ, Zheng MP, Jia XX, Lu CF, Liu JQ and Liu TS (2005) Long-chain alkenone distributions and temperature dependence in lacustrine surface sediments from China. Geochim Cosmochim Acta 69:4985-5003

Clark I and Fritz P (1997) Environmental Isotopes in Hydrogeology. doi:

Clark PU, Dyke AS, Shakun JD, Carlson AE, Clark J, Wohlfarth B, Mitrovica JX, Hostetler SW and McCabe AM (2009) The Last Glacial Maximum. Science 325:710-714

Conte MH, Sicre MA, Ruhlemann C, Weber JC, Schulte S, Schulz-Bull D and Blanz T (2006) Global temperature calibration of the alkenone unsaturation index (UK37') in surface waters and comparison with surface sediments. Geochemistry Geophysics Geosystems 7

Conte MH, Thompson A, Lesley D and Harris RP (1998) Genetic and physiological influences on the alkenone/alkenoate versus growth temperature relationship in Emiliania huxleyi and Gephyrocapsa oceanica. Geochim Cosmochim Acta 62:51-68

Craig H (1961) Isotopic variations in meteoric waters. Science 133:1702-&

Craig H and Gordon L (1965) Deuterium and oxygen-18 in the ocean and the marine atmosphere, in Stable Isotopes in Oceanographic Studies and Paleotemperatures. Spoleto doi:9-130

Cranwell PA (1985) Long-chain unsaturated-ketones in recent lacustrine sediments. Geochim Cosmochim Acta 49:1545-1551

Croudace IW, Rindby A and Rothwell RG (2006) ITRAX: description and evaluation of a new multi-function X-ray core scanner. New Techniques in Sediment Core Analysis 267:51-63

D'Andrea WJ and Huang Y (2005) Long chain alkenones in Greenland lake sediments: Low delta C-13 values and exceptional abundance. Org Geochem 36:1234-1241

D'Andrea WJ, Lage M, Martiny JBH, Laatsch AD, Amaral-Zettler LA, Sogin ML and Huang Y (2006) Alkenone producers inferred from well-preserved 18S rDNA in Greenland lake sediments. Journal of Geophysical Research-Biogeosciences 111

Damste JSS, Rijpstra WIC, Deleeuw JW and Schenck PA (1989) The occurrence and identification of series of organic sulfur-compounds in oils and sediment extracts .2. Their presence in samples from hypersaline and non-hypersaline paleoenvironments and possible application as source, palaeoenvironmental and maturity indicators. Geochim Cosmochim Acta 53:1323-1341

Dansgaard W (1964) Stable isotopes in precipitation. Tell 16:436-468

Daut G, Mäusbacher R, Baade J, Gleixner G, Kroemer E, Mügler I, Wallner J, Wang J and Zhu L (2010) Late Quaternary hydrological changes inferred from lake level fluctuations of Nam Co (Tibetan Plateau, China). Quat Int 218:86-93

Davis RB, Hess CT, Norton SA, Hanson DW, Hoagland KD and Anderson DS (1984) Cs-137 and pb-210 dating of sediments from soft-water lakes in new england (USA) and scandinavia, a failure of cs-137 dating. Chem Geol 44:151-185

De Grave J, Glorie S, Buslov MM, Izmer A, Fournier-Carrie A, Batalev VY, Vanhaecke F, Elburg M and Van den Haute P (2011) The thermo-tectonic history of the Song-Kul plateau, Kyrgyz Tien Shan: Constraints by apatite and titanite thermochronometry and zircon U/Pb dating. Gondwana Res 20:745-763

Debret M, Bout-Roumazeilles V, Grousset F, Desmet M, McManus JF, Massei N, Sebag D, Petit JR, Copard Y and Trentesaux A (2007) The origin of the 1500-year climate cycles in Holocene North-Atlantic records. CliPa 3:569-575

Deevey ES, Gross MS, Hutchinson GE and Kraybill HL (1954) The natural C14 contents of materials from hard-water lakes. Proc Natl Acad Sci U S A 40:285-288

Doberschütz S, Frenzel P, Haberzettl T, Kasper T, Wang J, Zhu L, Daut G, Schwalb A and Mäusbacher R (2014) Monsoonal forcing of Holocene paleoenvironmental change on the central Tibetan Plateau inferred using a sediment record from Lake Nam Co (Xizang, China). J Paleolimnol 51:253-266

Dongmann G, Nurnberg HW, Forstel H and Wagener K (1974) Enrichment of H218O in leaves of transpiring plants. Radiat Environ Biophys 11:41-52

Duan Y, Wu BX, Xu L, He JX and Sun T (2011) Characterisation of n-alkanes and their hydrogen isotopic composition in sediments from Lake Qinghai, China. Org Geochem 42:720-726

Dunkeloh A and Jacobeit J (2003) Circulation dynamics of Mediterranean precipitation variability 1948-98. IJCli 23:1843-1866

Edwards TWD, Wolfe BB, Gibson JJ and Hammarlund D (2004) Use of water isotope tracers in high latitude hydrology and paleohydrology. In: R Pienitz, MSV Douglas, JP Smol, R Pienitz, MSV Douglas and JP Smol (eds), Long-Term Environmental Change in Arctic and Antarctic Lakes

Eglinton G and Hamilton RJ (1967) Leaf epicuticular waxes. Science 156:1322-&

Ehleringer JR and Dawson TE (1992) Water-uptake by plants - perspectives from stable isotope composition. Plant Cell Environ 15:1073-1082

Ehleringer JR, Roden J and Dawson TE (2000) Assessing ecosystem-level water relations through stable isotope ratio analyses. Springer-Verlag GmbH and Co. KG, Heidelberger Platz 3, D-14197, Berlin, Germany 175 Fifth Avenue, New York, NY, 10010-7858, USA, 181-198 pp

Eltgroth ML, Watwood RL and Wolfe GV (2005) Production and cellular localization of neutral long-chain lipids in the haptophyte algae Isochrysis galbana and Emiliania huxleyi. J Phycol 41:1000-1009

Englebrecht AC and Sachs JP (2005) Determination of sediment provenance at drift sites using hydrogen isotopes and unsaturation ratios in alkenones. Geochim Cosmochim Acta 69:4253-4265

Esper J, Schweingruber FH and Winiger M (2002) 1300 years of climatic history for Western Central Asia inferred from tree-rings. Holocene 12:267-277

Esper J, Shiyatov SG, Mazepa VS, Wilson RJS, Graybill DA and Funkhouser G (2003) Temperature-sensitive Tien Shan tree ring chronologies show multi-centennial growth trends. ClDy 21:699-706

Falatkova K, Sobr M, Kocum J and Jansky B (2014) Hydrological regime of adygine lake, Tien Shan, Kyrgyzstan. Geografie 119:320-341

Fawcett PJ, Werne JP, Anderson RS, Heikoop JM, Brown ET, Berke MA, Smith SJ, Goff F, Donohoo-Hurley L, Cisneros-Dozal LM, Schouten S, Damste JSS, Huang Y, Toney J, Fessenden J, WoldeGabriel G, Atudorei V, Geissman JW and Allen CD (2011) Extended megadroughts in the southwestern United States during Pleistocene interglacials. Nature 470:518-521

Feng ZD, An CB and Wang HB (2006) Holocene climatic and environmental changes in the arid and semi-arid areas of China: a review. Holocene 16:119-130

Ficken KJ, Li B, Swain DL and Eglinton G (2000) An n-alkane proxy for the sedimentary input of submerged/floating freshwater aquatic macrophytes. Org Geochem 31:745-749

Finlay JC and Kendall C (2007) Stable isotope tracing of temporal and spatial variability in organic matter sources to freshwater ecosystems, 283-333 pp

Fischer G and Karakas G (2009) Sinking rates and ballast composition of particles in the Atlantic Ocean: implications for the organic carbon fluxes to the deep ocean. Biogeosciences 6:85-102

Flanagan LB, Bain JF and Ehleringer JR (1991) Stable oxygen and hydrogen isotope composition of leaf water in c3 and c4 plant-species under field conditions. Oecologia 88:394-400

Fletcher WJ, Debret M and Goni MFS (2013) Mid-Holocene emergence of a low-frequency millennial oscillation in western Mediterranean climate: Implications for past dynamics of the North Atlantic atmospheric westerlies. Holocene 23:153-166

Fontes JC, Melieres F, Gibert E, Qing L and Gasse F (1993) Stable-isotope and radiocarbon balances of two Tibetan lakes (Sumxi Co, Longmu Co) from 13,000-BP. Quat Sci Rev 12:875-887

Fritz P and Fontes JC (1980) Handbook of environmental isotope geochemistry. Vol.1. The terrestrial environment, A, xii+546 pp-xii+546 pp pp

Galman V, Rydberg J, Shchukarev A, Sjoberg S, Martinez-Cortizas A, Bindler R and Renberg I (2009) The role of iron and sulfur in the visual appearance of lake sediment varves. J Paleolimnol 42:141-153

Gao L, Hou JZ, Toney J, MacDonald D and Huang Y (2011) Mathematical modeling of the aquatic macrophyte inputs of mid-chain n-alkyl lipids to lake sediments: Implications for interpreting compound specific hydrogen isotopic records. Geochim Cosmochim Acta 75:3781-3791

Garcin Y, Schwab VF, Gleixner G, Kahmen A, Todou G, Sene O, Onana J-M, Achoundong G and Sachse D (2012) Hydrogen isotope ratios of lacustrine sedimentary n-alkanes as proxies of tropical African hydrology: Insights from a calibration transect across Cameroon. Geochim Cosmochim Acta 79:106-126

Gasse F, Fontes JC, VanCampo E and Wei K (1996) Holocene environmental changes in Bangong Co basin (western Tibet) .4. Discussion and conclusions. Palaeogeogr Palaeoclimatol Palaeoecol 120:79-92

Gat JR and Gonfiantini R (1981) Stable Isotope Hydrology. Deuterium and Oxygen in the Water Cycle. IAEA doi:

Gat JR and Levy Y (1978) Isotope hydrology of inland sabkhas in bardawil area, sinai. Limnol Oceanogr 23:841-850

Gazis C and Feng XH (2004) A stable isotope study of soil water: evidence for mixing and preferential flow paths. Geoderma 119:97-111

Gehre M, Geilmann H, Richter J, Werner RA and Brand WA (2004) Continuous flow H-2/H-1 and and(18)O/O-16 analysis of water samples with dual inlet precision. Rapid Commun Mass Spectrom 18:2650-2660

Gelpi E, Schneide.H, Mann J and Oro J (1970) Lipids of geochemical significance in microscopic algae .1. hydrocarbons of geochemical significance in microscopic algae. Phytochemistry 9:603-&

Gibson JJ, Birks SJ and Edwards TWD (2008) Global prediction of delta(A) and delta(2)H-delta(18)O evaporation slopes for lakes and soil water accounting for seasonality. Global Biogeochem Cycles 22

Gibson JJ and Edwards TWD (2002) Regional water balance trends and evaporation-transpiration partitioning from a stable isotope survey of lakes in northern Canada. Global Biogeochem Cycles 16

Gibson JJ, Edwards TWD, Birks SJ, St Amour NA, Buhay WM, McEachern P, Wolfe BB and Peters DL (2005) Progress in isotope tracer hydrology in Canada. HyPr 19:303-327

Gibson JJ, Prepas EE and McEachern P (2002) Quantitative comparison of lake throughflow, residency, and catchment runoff using stable isotopes: modelling and results from a regional survey of Boreal lakes. J Hydrol 262:128-144

Giese E, Mossig I, Rybski D and Bunde A (2007) Long-term analysis of air temperature trends in Central Asia. Erdkunde 61:186-202

Glorie S, De Grave J, Buslov MM, Zhimulev FI, Stockli DF, Batalev VY, Izmer A, Van den Haute P, Vanhaecke F and Elburg MA (2011) Tectonic history of the Kyrgyz South Tien Shan (Atbashi-Inylchek) suture zone: The role of inherited structures during deformation-propagation. Tecto 30

Grice K, Breteler W, Schouten S, Grossi V, de Leeuw JW and Damste JSS (1998) Effects of zooplankton herbivory on biomarker proxy records. Paleoceanography 13:686-693

Grimalt J and Albaiges J (1987) Sources and occurence of C12-C22 n-alkane distributions with even carbon-number preference in sedimentary environments. Geochim Cosmochim Acta 51:1379-1384

Gu BH, Schelske CL and Brenner M (1996) Relationship between sediment and plankton isotope ratios (delta C-13 and delta N-15) and primary productivity in Florida lakes. Can J Fish Aquat Sci 53:875-883

Günther F, Aichner B, Siegwolf R, Xu B, Yao T and Gleixner G (2013) A synthesis of hydrogen isotope variability and its hydrological significance at the Qinghai-Tibetan Plateau. Quat Int 313:3-16

Günther F, Mügler I, Mäusbacher R, Daut G, Leopold K, Gerstmann UC, Xu B, Yao T and Gleixner G (2011) Response of delta D values of sedimentary n-alkanes to variations in source water isotope signals and climate proxies at lake Nam Co, Tibetan Plateau. Quat Int 236:82-90

Günther F, Witt R, Schouten S, Mäusbacher R, Daut G, Zhu L, Xu B, Yao T and Gleixner G (2015) Quaternary ecological responses and impact of the Indian Ocean Summer Monsoon at Nam Co, Southern Tibetan Plateau. Quat Sci Rev 112:66-77

Haberzettl T, Fey M, Lucke A, Maidana N, Mayr C, Ohlendorf C, Schabitz F, Schleser GH, Wille M and Zolitschka B (2005) Climatically induced lake level changes during the last two millennia as reflected in sediments of Laguna Potrok Aike, southern Patagonia (Santa Cruz, Argentina). J Paleolimnol 33:283-302

Hammer O, Harper DAT and Ryan PD (2001) PAST: paleontological statistics software package for education and data analysis. Palaeontol Electron 4:Unpaginated-Unpaginated

He Y, Zhao C, Wang Z, Wang H, Song M, Liu W and Liu Z (2013) Late Holocene coupled moisture and temperature changes on the northern Tibetan Plateau. Quat Sci Rev 80:47-57

He Y, Zheng Y, Pan A, Zhao C, Sun Y, Song M, Zheng Z and Liu Z (2014) Biomarker-based reconstructions of Holocene lake-level changes at Lake Gahai on the northeastern Tibetan Plateau. Holocene 24:405-412

Hennekam R and de Lange G (2012) X-ray fluorescence core scanning of wet marine sediments: methods to improve quality and reproducibility of high-resolution paleoenvironmental records. Limnology and Oceanography-Methods 10:991-1003

Hernandez-Sanchez MT, LaRowe DE, Deng F, Homoky WB, Browning TJ, Martin P, Mills RA and Pancost RD (2014) Further insights into how sediment redox status controls the preservation and composition of sedimentary biomarkers. Org Geochem 76:220-234

Herrmann M, Lu XM, Berking J, Schütt B, Yao TD and Mosbrugger V (2010) Reconstructing Holocene vegetation and climate history of Nam Co area (Tibet), using pollen and other palynomorphs. Quat Int 218:45-57

Herzschuh U (2006) Palaeo-moisture evolution in monsoonal Central Asia during the last 50,000 years. Quat Sci Rev 25:163-178

Hodell DA, Evans HF, Channell JET and Curtis JH (2010) Phase relationships of North Atlantic ice-rafted debris and surface-deep climate proxies during the last glacial period. Quat Sci Rev 29:3875-3886

Hodell DA and Schelske CL (1998) Production, sedimentation, and isotopic composition of organic matter in Lake Ontario. Limnol Oceanogr 43:200-214

Hollander DJ, McKenzie JA and Lotenhaven H (1992) A 200-year sedimentary record of progressive eutrophication in lake greifen (switzerland) - implications for the origin of organic-carbon-rich sediments. Geology 20:825-828

Holmer M and Storkholm P (2001) Sulphate reduction and sulphur cycling in lake sediments: a review. Freshwat Biol 46:431-451

Holmes JA and Chivas AR (2002) Ostracod shell chemistry - Overview. Ostracoda: Applications in Quaternary Research 131:185-204

Hou J, D'Andrea WJ and Liu Z (2012) The influence of 14C reservoir age on interpretation of paleolimnological records from the Tibetan Plateau. Quat Sci Rev 48:67-79

Hou JZ, D'Andrea WJ and Huang YS (2008) Can sedimentary leaf waxes record D/H ratios of continental precipitation? Field, model, and experimental assessments. Geochim Cosmochim Acta 72:3503-3517

Hu X, Zhu L, Wang Y, Wang J, Peng P, Ma Q, Hu J and Lin X (2014) Climatic significance of n-alkanes and their compound-specific delta D values from lake surface sediments on the Southwestern Tibetan Plateau. Chin Sci Bull 59:3022-3033

Huang W, Chen J, Zhang X, Feng S and Chen F (2015) Definition of the core zone of the "westerlies-dominated climatic regime", and its controlling factors during the instrumental period. Sci China-Earth Sci 58:676-684

Huang X, Oberhaensli H, von Suchodoletz H and Sorrel P (2011) Dust deposition in the Aral Sea: implications for changes in atmospheric circulation in central Asia during the past 2000 years. Quat Sci Rev 30:3661-3674

Huang X, Oberhänsli H and Mathis M (2012) A Holocene lacustrine record of Lake Sonkul: Hydro-climatic changes in central Asia and possible interactions between Westerlies and Asian monsoon. EGU General Assembly 2012 14

Huang XZ, Chen FH, Fan YX and Yang ML (2009) Dry late-glacial and early Holocene climate in arid central Asia indicated by lithological and palynological evidence from Bosten Lake, China. Quat Int 194:19-27

Huang YS, Shuman B, Wang Y and Webb T (2004) Hydrogen isotope ratios of individual lipids in lake sediments as novel tracers of climatic and environmental change: a surface sediment test. J Paleolimnol 31:363-375

Hughes PDG, P.L.; Ehlers, J. (2013) Timing of glaciation during the last glacial cycle: evaluating the concept of a global 'Last Glacial Maximum'. Earth-Sci Rev 125:171-198

Hurrell JW (1995) Decadal trends in the north-atlantic oscillation - regional temperatures and precipitation. Science 269:676-679

Hurrell JW and Deser C (2009) North Atlantic climate variability: The role of the North Atlantic Oscillation. J Mar Syst 78:28-41

Ingraham NL (1998) Isotopic variations in precipitation. Isotope Tracers in Catchment Hydrology doi:87-118

Jackson MG, Oskarsson N, Tronnes RG, McManus JF, Oppo DW, Gronvold K, Hart SR and Sachs JP (2005) Holocene loess deposition in Iceland: Evidence for millennial-scale atmosphere-ocean coupling in the North Atlantic. Geology 33:509-512

Jin L, Chen F, Morrill C, Otto-Bliesner BL and Rosenbloom N (2012) Causes of early Holocene desertification in arid central Asia. ClDy 38:1577-1591

Johnsen SJ, Clausen HB, Dansgaard W, Gundestrup NS, Hammer CU, Andersen U, Andersen KK, Hvidberg CS, DahlJensen D, Steffensen JP, Shoji H, Sveinbjornsdottir AE, White J, Jouzel J and Fisher D (1997) The delta O-18 record along the Greenland Ice Core Project deep ice core and the problem of possible Eemian climatic instability. J Geophys Res-Oceans 102:26397-26410

Jonsson CE, Leng MJ, Rosqvist GC, Seibert J and Arrowsmith C (2009) Stable oxygen and hydrogen isotopes in sub-Arctic lake waters from northern Sweden. J Hydrol 376:143-151

Kahmen A, Simonin K, Tu KP, Merchant A, Callister A, Siegwolf R, Dawson TE and Arndt SK (2008) Effects of environmental parameters, leaf physiological properties and leaf water relations on leaf water delta(18)O enrichment in different Eucalyptus species. Plant Cell Environ 31:738-751

Kalbe L and Werner H (1974) Das Sediment des Kummerower Sees. Untersuchungen des Chemismus und der Diatomeenflora. Int Rev Hydrobiol 59:755-782

Karthe D, Chalov S and Borchardt D (2015) Water resources and their management in central Asia in the early twenty first century: status, challenges and future prospects. Environ Earth Sci 73:487-499

Kasper T, Haberzettl T, Wang J, Daut G, Zhu L and Mäusbacher R (2015) Hydrological variations on the Central Tibetan Plateau since the Last Glacial Maximum and their teleconnection to inter-regional and hemispheric climate variations. J Quat Sci 30:70-78

Keith DE (1969) Aspects of feeding in caprella-californica and caprella-equalibra amphipoda tunicates sponges bryozoa algae association diatoms dinoflagellates suctorians crustaceans detritus diet. Crustaceana (Leiden) 16:119-124

Kendall C (1998) Tracing nitrogen sources and cycling in catchments. Isotope Tracers in Catchment Hydrology doi:519-576

Klaminder J, Appleby P, Crook P and Renberg I (2012) Post-deposition diffusion of 137Cs in lake sediment: Implications for radiocaesium dating. Sedim 59:2259-2267

Kleinen T, Tarasov P, Brovkin V, Andreev A and Stebich M (2011) Comparison of modeled and reconstructed changes in forest cover through the past 8000 years: Eurasian perspective. Holocene 21:723-734

Kok MD, Rijpstra WIC, Robertson L, Volkman JK and Damste JSS (2000) Early steroid sulfurisation in surface sediments of a permanently stratified lake (Ace Lake, Antarctica). Geochim Cosmochim Acta 64:1425-1436

Koopmans MP, SchaefferReiss C, DeLeeuw JW, Lewan MD, Maxwell JR, Schaeffer P and Damste JSS (1997) Sulphur and oxygen sequestration of n-C37 and n-C38 unsaturated ketones in an immature kerogen and the release of their carbon skeletons during early stages of thermal maturation. Geochim Cosmochim Acta 61:2397-2408

Koppes M, Gillespie AR, Burke RM, Thompson SC and Stone J (2008) Late Quaternary glaciation in the Kyrgyz Tien Shan. Quat Sci Rev 27:846-866

Kriegel D, Mayer C, Hagg W, Vorogushyn S, Duethmann D, Gafurov A and Farinotti D (2013) Changes in glacierisation, climate and runoff in the second half of the 20th century in the Naryn basin, Central Asia. Global Planet Change 110:51-61

Kristen I, Fuhrmann A, Thorpe J, Roehl U, Wilkes H and Oberhaensli H (2007) Hydrological changes in southern Africa over the last 200 Ka as recorded in lake sediments from the Tswaing impact crater. S Afr J Geol 110:311-326

Lambeck K, Yokoyama Y and Purcell T (2002) Into and out of the Last Glacial Maximum: sea-level change during Oxygen Isotope Stages 3 and 2. Quat Sci Rev 21:343-360

Larocque I and Hall RI (2004) Holocene temperature estimates and chironomid community composition in the Abisko,Valley, northern Sweden. Quat Sci Rev 23:2453-2465

Lauterbach S, Witt R, Plessen B, Dulski P, Prasad S, Mingram J, Gleixner G, Hettler-Riedel S, Stebich M, Schnetger B, Schwalb A and Schwarz A (2014) Climatic imprint of the mid-latitude Westerlies in the Central Tian Shan of Kyrgyzstan and teleconnections to North Atlantic climate variability during the last 6000 years. The Holocene 24:970-984

Lehner B, Verdin K and Jarvis A (2006) HydroSHEDS Technical Documentation. doi:

Lei Y, Tian L, Bird BW, Hou J, Ding L, Oimahmadov I and Gadoev M (2014) A 2540-year record of moisture variations derived from lacustrine sediment (Sasikul Lake) on the Pamir Plateau. Holocene 24:761-770

Leng MJ and Marshall JD (2004) Palaeoclimate interpretation of stable isotope data from lake sediment archives. Quat Sci Rev 23:811-831

Leroy SAG, Kakroodi AA, Kroonenberg S, Lahijani HK, Alimohammadian H and Nigarov A (2013) Holocene vegetation history and sea level changes in the SE corner of the Caspian Sea: relevance to SW Asia climate. Quat Sci Rev 70:28-47

Li MH, Kang SC, Zhu LP, You QL, Zhang QG and Wang JB (2008) Mineralogy and geochemistry of the Holocene lacustrine sediments in Nam Co, Tibet. Quat Int 187:105-116

Li X, Zhao K, Dodson J and Zhou X (2011) Moisture dynamics in central Asia for the last 15 kyr: new evidence from Yili Valley, Xinjiang, NW China. Quat Sci Rev 30:3457-3466

Lin X, Zhu L, Wang Y, Wang J, Xie M, Ju J, Mäubacher R and Schwalb A (2008) Environmental changes reflected by n-alkanes of lake core in Nam Co on the Tibetan Plateau since 8.4 kaBP. Chin Sci Bull 53:3051-3057

Lioubimtseva E, Cole R, Adams JM and Kapustin G (2005) Impacts of climate and land-cover changes in arid lands of Central Asia. J Arid Environ 62:285-308

Lister GS, Kelts K, Zao CK, Yu JQ and Niessen F (1991) Lake Qinghai, China - closed-basin lake levels and the oxygen isotope record for ostracoda since the latest pleistocene. Palaeogeogr Palaeoclimatol Palaeoecol 84:141-162

Liu J, Curry JA, Wang H, Song M and Horton RM (2012) Impact of declining Arctic sea ice on winter snowfall. Proc Natl Acad Sci U S A 109:4074-4079

Liu J, Kang S, Gong T and Lu A (2010) Growth of a high-elevation large inland lake, associated with climate change and permafrost degradation in Tibet. Hydrol Earth Syst Sci 14:481-489

Liu W, Li X, Zhang L, An Z and Xu L (2009) Evaluation of oxygen isotopes in carbonate as an indicator of lake evolution in arid areas: The modern Qinghai Lake, Qinghai-Tibet Plateau. Chem Geol 268:126-136

Liu W, Liu Z, Fu M and An Z (2008a) Distribution of the C-37 tetra-unsaturated alkenone in Lake Qinghai, China: A potential lake salinity indicator. Geochim Cosmochim Acta 72:988-997

Liu WG and Huang YS (2005) Compound specific D/H ratios and molecular distributions of higher plant leaf waxes as novel pale oenvironmental indicators in the Chinese Loess Plateau. Org Geochem 36:851-860

Liu X, Herzschuh U, Shen J, Jiang Q and Xiao X (2008b) Holocene environmental and climatic changes inferred from Wulungu Lake in northern Xinjiang, China. Quatern Res 70:412-425

Liu Z, Henderson ACG and Huang Y (2006) Alkenone-based reconstruction of late-Holocene surface temperature and salinity changes in Lake Qinghai, China. Geophys Res Lett 33

Lowe JJ, Rasmussen SO, Bjorck S, Hoek WZ, Steffensen JP, Walker MJC, Yu ZC and Grp I (2008) Synchronisation of palaeoenvironmental events in the North Atlantic region during the Last Termination: a revised protocol recommended by the INTIMATE group. Quat Sci Rev 27:6-17

Machalett B, Frechen M, Hambach U, Oches EA, Zoller L and Markovic SB (2006) The loess sequence from Remisowka (northern boundary of the Tien Shan Mountains, Kazakhstan) - Part I: Luminescence dating. Quat Int 152:192-201

Machalett B, Oches EA, Frechen M, Zoeller L, Hambach U, Mavlyanova NG, Markovic SB and Endlicher W (2008) Aeolian dust dynamics in central Asia during the Pleistocene: Driven by the long-term migration, seasonality, and permanency of the Asiatic polar front. Geochemistry Geophysics Geosystems 9

MacNeil C, Dick JT and Elwood RW (1997) The trophic ecology of freshwater Gammarus spp. (Crustacea: Amphipoda): Problems and perspectives concerning the functional feeding group concept. Biol Rev Camb Philos Soc 72:349-364

Maffei M (1996) Chemotaxonomic significance of leaf wax n-Alkanes in the Umbelliferae, Cruciferae and Leguminosae (subf papilionoideae). Biochem Syst Ecol 24:531-545

Mahesh BS and Banakar VK (2014) Change in the intensity of low-salinity water inflow from the Bay of Bengal into the Eastern Arabian Sea from the Last Glacial Maximum to the Holocene: Implications for monsoon variations. Palaeogeogr Palaeoclimatol Palaeoecol 397:31-37

Mann ME, Zhang Z, Rutherford S, Bradley RS, Hughes MK, Shindell D, Ammann C, Faluvegi G and Ni F (2009) Global Signatures and Dynamical Origins of the Little Ice Age and Medieval Climate Anomaly. Science 326:1256-1260

Marlowe IT, Green JC, Neal AC, Brassell SC, Eglinton G and Course PA (1984) Long-chain (n-c37-c39) alkenones in the prymnesiophyceae - distribution of alkenones and other lipids and their taxonomic significance. Br Phycol J 19:203-216

Mathis M, Sorrel P, Klotz S, Huang X and Oberhaensli H (2014) Regional vegetation patterns at lake Son Kul reveal Holocene climatic variability in central Tien Shan (Kyrgyzstan, Central Asia). Quat Sci Rev 89:169-185

Mayewski PA, Meeker LD, Twickler MS, Whitlow S, Yang QZ, Lyons WB and Prentice M (1997) Major features and forcing of high-latitude northern hemisphere atmospheric circulation using a 110,000-year-long glaciochemical series. J Geophys Res-Oceans 102:26345-26366

Mayr C, Luecke A, Maidana NI, Wille M, Haberzettl T, Corbella H, Ohlendorf C, Schaebitz F, Fey M, Janssen S and Zolitschka B (2009) Isotopic fingerprints on lacustrine organic matter from Laguna Potrok Aike (southern Patagonia, Argentina) reflect environmental changes during the last 16,000 years. J Paleolimnol 42:81-102

Meyer H, Schonicke L, Wand U, Hubberten HW and Friedrichsen H (2000) Isotope studies of hydrogen and oxygen in ground ice - Experiences with the equilibration technique. Isotopes Environ Health Stud 36:133-149

Meyers PA (2003) Applications of organic geochemistry to paleolimnological reconstructions: a summary of examples from the Laurentian Great Lakes. Org Geochem 34:261-289

Meyers PA and Lallier-Verges E (1999) Lacustrine sedimentary organic matter records of Late Quaternary paleoclimates. J Paleolimnol 21:345-372

Meyers PA and Teranes JL (2002) Sediment organic matter. Tracking Environmental Change Using Lake Sediments, Vol 2: Physical and Geochemical Methods 2:239-269

Mischke S, Rajabov I, Mustaeva N, Zhang CJ, Herzschuh U, Boomer I, Brown ET, Andersen N, Myrbo A, Ito E and Schudack ME (2010) Modern hydrology and late Holocene history of Lake Karakul, eastern Pamirs (Tajikistan): A reconnaissance study. Palaeogeogr Palaeoclimatol Palaeoecol 289:10-24

Mischke S and Wünnemann B (2006) The Holocene salinity history of Bosten Lake (Xinjiang, China) inferred from ostracod species assemblages and shell chemistry: Possible palaeoclimatic implications. Quat Int 154:100-112

Mix AC, Bard E and Schneider R (2001) Environmental processes of the ice age: land, oceans, glaciers (EPILOG). Quat Sci Rev 20:627-657

Moreno A, Stoll H, Jimenez-Sanchez M, Cacho I, Valero-Garces B, Ito E and Edwards RL (2010) A speleothem record of glacial (25-11.6 kyr BP) rapid climatic changes from northern Iberian Peninsula. Global Planet Change 71:218-231

Morris BL, George Darling WG, Gooddy DC, Litvak RG, Neumann I, Nemaltseva EJ and Poddubnaia I (2006) Assessing the extent of induced leakage to an urban aquifer using environmental tracers: an example from Bishkek, capital of Kyrgyzstan, Central Asia. HydJ 14:225-243

Mügler I, Gleixner G, Günther F, Mäusbacher R, Daut G, Schütt B, Berking J, Schwalb A, Schwark L, Xu B, Yao T, Zhu L and Yi C (2010) A multi-proxy approach to reconstruct hydrological changes and Holocene climate development of Nam Co, Central Tibet. J Paleolimnol 43:625-648

Mügler I, Sachse D, Werner M, Xu BQ, Wu GJ, Yao TD and Gleixner G (2008) Effect of lake evaporation on delta D values of lacustrine n-alkanes: A comparison of Nam Co (Tibetan Plateau) and Holzmaar (Germany). Org Geochem 39:711-729

Naeher S, Gilli A, North RP, Hamann Y and Schubert CJ (2013) Tracing bottom water oxygenation with sedimentary Mn/Fe ratios in Lake Zurich, Switzerland. Chem Geol 352:125-133

Narama C, Kaab A, Duishonakunov M and Abdrakhmatov K (2010) Spatial variability of recent glacier area changes in the Tien Shan Mountains, Central Asia, using Corona (similar to 1970), Landsat (similar to 2000), and ALOS (similar to 2007) satellite data. Global Planet Change 71:42-54

Nesje A, Matthews JA, Dahl SO, Berrisford MS and Andersson C (2001) Holocene glacier fluctuations of Flatebreen and winter-precipitation changes in the Jostedalsbreen region, western Norway, based on glaciolacustrine sediment records. Holocene 11:267-280

Oleary MH (1981) Carbon isotope fractionation in plants. Phytochemistry 20:553-567

Pearson EJ, Juggins S and Farrimond P (2008) Distribution and significance of long-chain alkenones as salinity and temperature indicators in Spanish saline lake sediments. Geochim Cosmochim Acta 72:4035-4046

Pham SV, Leavitt PR, McGowan S, Wissel B and Wassenaar LI (2009) Spatial and temporal variability of prairie lake hydrology as revealed using stable isotopes of hydrogen and oxygen. Limnol Oceanogr 54:101-118

Polissar PJ and Freeman KH (2010) Effects of aridity and vegetation on plant-wax delta D in modern lake sediments. Geochim Cosmochim Acta 74:5785-5797

Polissar PJ, Freeman KH, Rowley DB, McInerney FA and Currie BS (2009) Paleoaltimetry of the Tibetan Plateau from D/H ratios of lipid biomarkers. Earth Planet Sci Lett 287:64-76

Polome EC (1996) Nomads of the Eurasian steppes in the early Iron Age - DavisKimball,J, Bashilov,VA, Yablonsky,LT. Journal of Indo-European Studies 24:433-434

Prahl FG, Collier RB, Dymond J, Lyle M and Sparrow MA (1993) A biomarker perspective on prymnesiophyte productivity in the northeast pacific-ocean. Deep-Sea Research Part I-Oceanographic Research Papers 40:2061-2076

Prahl FG, Pilskaln CH and Sparrow MA (2001) Seasonal record for alkenones in sedimentary particles from the Gulf of Maine. Deep-Sea Research Part I-Oceanographic Research Papers 48:515-528

Prahl FG and Wakeham SG (1987) Calibration of unsaturation patterns in long-chain ketone compositions for paleotemperature assessment. Nature 330:367-369

Qin BQ and Yu G (1998) Implications of lake level variations at 6 ka and 18 ka in mainland Asia. Global Planet Change 18:59-72

Rach O, Brauer A, Wilkes H and Sachse D (2014) Delayed hydrological response to Greenland cooling at the onset of the Younger Dryas in western Europe. Nat Geosci 7:109-112

Ramsey CB (2009) Bayesian analysis of radiocarbon dates. Radiocarbon 51:337-360

Ramsey CB (2008) Deposition models for chronological records. Quat Sci Rev 27:42-60

Ramsey CB (2001) Development of the radiocarbon calibration program. Radiocarbon 43:355-363

Ramsey CB (1995) Radiocarbon calibration and analysis of stratigraphy: The OxCal program. Radiocarbon 37:425-430

Ran M and Feng Z (2013) Holocene moisture variations across China and driving mechanisms: A synthesis of climatic records. Quat Int 313:179-193

Rao Z, Jia G, Qiang M and Zhao Y (2014) Assessment of the difference between mid- and long chain compound specific delta Dn-alkanes values in lacustrine sediments as a paleoclimatic indicator. Org Geochem 76:104-117

Rao ZG, Wu Y, Zhu ZY, Jia GD and Henderson A (2011) Is the maximum carbon number of long-chain n-alkanes an indicator of grassland or forest? Evidence from surface soils and modern plants. Chin Sci Bull 56:1714-1720

Rasmussen SO, Selerstad IK, Andersen KK, Bigler M, Dahl-Jensen D and Johnsen SJ (2008) Synchronization of the NGRIP, GRIP, and GISP2 ice cores across MIS 2 and palaeoclimatic implications. Quat Sci Rev 27:18-28

Reille M (1992) Pollen et Spores d'Europe et d'Afrique du Nord. CNRS doi:

Reimer PJ, Baillie MGL, Bard E, Bayliss A, Beck JW, Blackwell PG, Ramsey CB, Buck CE, Burr GS, Edwards RL, Friedrich M, Grootes PM, Guilderson TP, Hajdas I, Heaton TJ, Hogg AG, Hughen KA, Kaiser KF, Kromer B, McCormac FG, Manning SW, Reimer RW, Richards DA, Southon JR, Talamo S, Turney CSM, van der Plicht J and Weyhenmeye CE (2009) Intcal09 and marine09 radiocarbon age calibration curves, 0-50,000 years cal bp. Radiocarbon 51:1111-1150

Renssen H, Goosse H and Fichefet T (2007) Simulation of Holocene cooling events in a coupled climate model. Quat Sci Rev 26:2019-2029

Rhead MM, Eglinton G, Draffan GH and England PJ (1971) Conversion of oleic acid to saturated fatty acids in severn estuary sediments. Nature 232:327-&

Rhodes TE, Gasse F, Lin RF, Fontes JC, Wei KQ, Bertrand P, Gibert E, Melieres F, Tucholka P, Wang ZX and Cheng ZY (1996) A late Pleistocene-Holocene lacustrine record from Lake

Manas, Zunggar (northern Xinjiang, western China). Palaeogeogr Palaeoclimatol Palaeoecol 120:105-121

Ricketts RD, Johnson TC, Brown ET, Rasmussen KA and Romanovsky VV (2001) The Holocene paleolimnology of Lake Issyk-Kul, Kyrgyzstan: trace element and stable isotope composition of ostracodes. Palaeogeogr Palaeoclimatol Palaeoecol 176:207-227

Romanovsky VV (2007) Climate, Glaciers, Lakes of Tien Shan: Journey of the past. doi:168

Romanovsky VV (2002) Water level variations and water balance of Lake Issyk-Kul. In: J Klerkx and B Imanackunov (eds), Lake Issyk-Kul: Its Natural Environment, pp 45-57

Romanovsky VV and Shatravin VI (2007) Reconstruction of glacial and climate changes in the Late Pleistocene and Holocene based on the studies of closed alpine lakes in Tien-Shan and Pamir. doi:

Rontani JF, Beker B and Volkman JK (2004) Long-chain alkenones and related compounds in the benthic haptophyte Chrysotila lamellosa Anand HAP 17. Phytochemistry 65:117-126

Rontani JF, Volkman JK, Prahl FG and Wakeham SG (2013) Biotic and abiotic degradation of alkenones and implications for U-37(K ') paleoproxy applications: A review. Org Geochem 59:95-113

Rontani JF, Zabeti N and Wakeham SG (2009) The fate of marine lipids: Biotic vs. abiotic degradation of particulate sterols and alkenones in the Northwestern Mediterranean Sea. Mar Chem 113:9-18

Rosell-Mele A (1998) Interhemispheric appraisal of the value of alkenone indices as temperature and salinity proxies in high-latitude locations. Paleoceanography 13:694-703

Rothe J and Gleixner G (2000) Do stable isotopes reflect the food web development in regenerating ecosystems? Isotopes Environ Health Stud 36:285-301

Rudaya N, Tarasov P, Dorofeyuk N, Solovieva N, Kalugin I, Andreev A, Daryin A, Diekmann B, Riedel F, Tserendash N and Wagner M (2009) Holocene environments and climate in the Mongolian Altai reconstructed from the Hoton-Nur pollen and diatom records: a step towards better understanding climate dynamics in Central Asia. Quat Sci Rev 28:540-554

Rychagov GI (1997) Holocene oscillations of the Caspian Sea, and forecasts based on palaeogeographical reconstructions. Quat Int 41-2:167-172

Sachse D, Billault I, Bowen GJ, Chikaraishi Y, Dawson TE, Feakins SJ, Freeman KH, Magill CR, McInerney FA, van der Meer MTJ, Polissar P, Robins RJ, Sachs JP, Schmidt HL, Sessions AL, White JWC, West JB and Kahmen A (2012) Molecular Paleohydrology: Interpreting the Hydrogen- Isotopic Composition of Lipid Biomarkers from Photosynthesizing Organisms. Annual Review of Earth and Planetary Sciences, Vol 40 40:221-249

Sachse D, Kahmen A and Gleixner G (2009) Significant seasonal variation in the hydrogen isotopic composition of leaf-wax lipids for two deciduous tree ecosystems (Fagus sylvativa and Acer pseudoplatanus). Org Geochem 40:732-742

Sachse D, Radke J and Gleixner G (2006) delta D values of individual n-alkanes from terrestrial plants along a climatic gradient - Implications for the sedimentary biomarker record. Org Geochem 37:469-483

Sachse D, Radke J and Gleixner G (2004) Hydrogen isotope ratios of recent lacustrine sedimentary n-alkanes record modern climate variability. Geochim Cosmochim Acta 68:4877-4889

Sato T, Tsujimura M, Yamanaka T, Iwasaki H, Sugimoto A, Sugita M, Kimura F, Davaa G and Oyunbaatar D (2007) Water sources in semiarid northeast Asia as revealed by field observations and isotope transport model. J Geophys Res-Atmos 112

Savoskul OS and Solomina ON (1996) Late-Holocene glacier variations in the frontal and inner ranges of the Tian Shan, central Asia. Holocene 6:25-35

Schmidt F, Oberhänsli H and Wilkes H (2014) Biocoenosis response to hydrological variability in Southern Africa during the last 84 ka BP: A study of lipid biomarkers and compound-specific stable carbon and hydrogen isotopes from the hypersaline Lake Tswaing. Global Planet Change 112:92-104

Schütt B, Berking J, Frechen M, Frenzel P, Schwalb A and Wrozyna C (2010) Late Quaternary transition from lacustrine to a fluvio-lacustrine environment in the north-western Nam Co, Tibetan Plateau, China. Quat Int 218:104-117

Schwark L, Zink K and Lechterbeck J (2002) Reconstruction of postglacial to early Holocene vegetation history in terrestrial Central Europe via cuticular lipid biomarkers and pollen records from lake sediments. Geology 30:463-466

Sevastianov DV, Berdovskaya GN and Lijva AA (1990) Evolution of the mountain lakes in Middle Asia in Late Pleistocene time. Proceedings of the All-Union Geographical Society 122:1-337

Sevastianov DV, Berdovskaya GN, Liyva AA and Shnitnikov AV (1980) The lakes of Tian Shan and their history (in Russian). doi:150-210

Shanahan TM, Overpeck JT, Anchukaitis KJ, Beck JW, Cole JE, Dettman DL, Peck JA, Scholz CA and King JW (2009) Atlantic Forcing of Persistent Drought in West Africa. Science 324:377-380

Shi Y (2002) Characteristics of late Quaternary monsoonal glaciation on the Tibetan Plateau and in East Asia. Quat Int 97-8:79-91

Shnitnikov AV (1980) Lakes of the Tian Shan and Their History. doi:

Shnitnikov AV, Lijva AA, Berdovskaya GN and Sevastianov DV (1978) Paleo limnology of chatyrkel lake tien-shan. Pol Arch Hydrobiol 25:383-390

Sidorov DA (2012) Two new species of freshwater amphipods (Crustacea: Gammaridae) from Central Asia, with comments on the unusual upper lip morphology. Zootaxa 3317:1-24

Siegfried T, Bernauer T, Guiennet R, Sellars S, Robertson AW, Mankin J, Bauer-Gottwein P and Yakovlev A (2012) Will climate change exacerbate water stress in Central Asia? Clim Change 112:881-899

Sikes EL and Sicre MA (2002) Relationship of the tetra-unsaturated C-37 alkenone to salinity and temperature: Implications for paleoproxy applications. Geochemistry Geophysics Geosystems 3

Sikes EL and Volkman JK (1993) Calibration of alkenone unsaturation ratios (u-37(k')) for paleotemperature estimation in cold polar waters. Geochim Cosmochim Acta 57:1883-1889

Slemmons KEH, Saros JE and Simon K (2013) The influence of glacial meltwater on alpine aquatic ecosystems: a review. Environ Sci Process Impacts 15:1794-1806

Smith DE, Harrison S, Firth CR and Jordan JT (2011) The early Holocene sea level rise. Quat Sci Rev 30:1846-1860

Smith FA and Freeman KH (2006) Influence of physiology and climate on delta D of leaf wax n-alkanes from C-3 and C-4 grasses. Geochim Cosmochim Acta 70:1172-1187

Solomina O and Alverson K (2004) High latitude Eurasian paleoenvironments: introduction and synthesis. Palaeogeogr Palaeoclimatol Palaeoecol 209:1-18

Solomon S, Qin D and Manning M (2007) Climate Change 2007: The Physical Science Basis, 1-996 pp

Sorg A, Bolch T, Stoffel M, Solomina O and Beniston M (2012) Climate change impacts on glaciers and runoff in Tien Shan (Central Asia). Nature Climate Change 2:725-731

Sorrel P, Debret M, Billeaud I, Jaccard SL, McManus JF and Tessier B (2012) Persistent non-solar forcing of Holocene storm dynamics in coastal sedimentary archives. Nat Geosci 5:892-896

Sorrel P, Popescu SM, Head MJ, Suc JP, Klotz S and Oberhansli H (2006) Hydrographic development of the Aral Sea during the last 2000 years based on a quantitative analysis of dinoflagellate cysts. Palaeogeogr Palaeoclimatol Palaeoecol 234:304-327

Sorrel P, Tessier B, Demory F, Delsinne N and Mouaze D (2009) Evidence for millennial-scale climatic events in the sedimentary infilling of a macrotidal estuarine system, the Seine estuary (NW France). Quat Sci Rev 28:499-516

Spotl C and Vennemann TW (2003) Continuous-flow isotope ratio mass spectrometric analysis of carbonate minerals. Rapid Commun Mass Spectrom 17:1004-1006

Stansell ND, Abbott MB, Rull V, Rodbell DT, Bezada M and Montoya E (2010) Abrupt Younger Dryas cooling in the northern tropics recorded in lake sediments from the Venezuelan Andes. Earth Planet Sci Lett 293:154-163

Stocker TF, Qin D, Plattner GK, Tignor MMB, Allen SK, Boschung J, Nauels A, Xia Y, Bex V and Midgley PM (2013) IPCC, 2013: Summary for Policymakers. Climate Change 2013: The Physical Science Basis

Stockmarr J (1971) Calcium tablets with spores used in absolute pollen analysis. Pollen et Spores 13:615-621

Stuiver M and Grootes PM (2000) GISP2 oxygen isotope ratios. Quatern Res 53:277-283

Sun D, Chu GQ, Li SQ, Lu CF and Zheng MP (2004) Long-chain alkenones in sulfate lakes and its paleoclimatic implications. Chin Sci Bull 49:2082-2086

Sun Q, Chu G, Liu G, Li S and Wang X (2007) Calibration of alkenone unsaturation index with growth temperature for a lacustrine species, Chrysotila lamellosa (Haptophyceae). Org Geochem 38:1226-1234

Sun YB, Clemens SC, Morrill C, Lin XP, Wang XL and An ZS (2012) Influence of Atlantic meridional overturning circulation on the East Asian winter monsoon. Nat Geosci 5:46-49

Syed FS, Giorgi F, Pal JS and Keay K (2010) Regional climate model simulation of winter climate over Central-Southwest Asia, with emphasis on NAO and ENSO effects. IJCli 30:220-235

Syed FS, Giorgi F, Pal JS and King MP (2006) Effect of remote forcings on the winter precipitation of central southwest Asia part 1: observations. Theor Appl Climatol 86:147-160

Taft JB, Phillippe LR, Dietrich CH and Robertson KR (2011) Grassland composition, structure, and diversity patterns along major environmental gradients in the Central Tien Shan. Plant Ecol 212:1349-1361

Talbot MR (2002) Nitrogen isotopes in palaeolimnology. Tracking Environmental Change Using Lake Sediments, Vol 2: Physical and Geochemical Methods 2:401-439

Talbot MR (1990) A review of the paleohydrological interpretation of carbon and oxygen isotopic-ratios in primary lacustrine carbonates. Chem Geol 80:261-279

Talbot MR and Johannessen T (1992) A high-resolution paleoclimatic record for the last 27,500 years in tropical west africa from the carbon and nitrogen isotopic composition of lacustrine organic-matter. Earth Planet Sci Lett 110:23-37

Talbot MR and Laerdal T (2000) The Late Pleistocene-Holocene palaeolimnology of Lake Victoria, East Africa, based upon elemental and isotopic analyses of sedimentary organic matter. J Paleolimnol 23:141-164

Tarasov PE, Bezrukova EV and Krivonogov SK (2009) Late Glacial and Holocene changes in vegetation cover and climate in southern Siberia derived from a 15 kyr long pollen record from Lake Kotokel. CliPa 5:285-295

Teece MA, Getliff JM, Leftley JW, Parkes RJ and Maxwell JR (1998) Microbial degradation of the marine prymnesiophyte Emiliania huxleyi under oxic and anoxic conditions as a model for early diagenesis: long chain alkadienes, alkenones and alkyl alkenoates. Org Geochem 29:863-880

Teranes JL and Bernasconi SM (2000) The record of nitrate utilization and productivity limitation provided by delta N-15 values in lake organic matter - A study of sediment trap and core sediments from Baldeggersee, Switzerland. Limnol Oceanogr 45:801-813

Theroux S, D'Andrea WJ, Toney J, Amaral-Zettler L and Huang Y (2010) Phylogenetic diversity and evolutionary relatedness of alkenone-producing haptophyte algae in lakes: Implications for continental paleotemperature reconstructions. Earth Planet Sci Lett 300:311-320

Thiel V, Jenisch A, Landmann G, Reimer A and Michaelis W (1997) Unusual distributions of long-chain alkenones and tetrahymanol from the highly alkaline Lake Van, Turkey. Geochim Cosmochim Acta 61:2053-2064

Thornalley DJR, Elderfield H and McCave IN (2009) Holocene oscillations in temperature and salinity of the surface subpolar North Atlantic. Nature 457:711-714

Toney JL, Huang Y, Fritz SC, Baker PA, Grimm E and Nyren P (2010) Climatic and environmental controls on the occurrence and distributions of long chain alkenones in lakes of the interior United States. Geochim Cosmochim Acta 74:1563-1578

Toney JL, Leavitt PR and Huang Y (2011) Alkenones are common in prairie lakes of interior Canada. Org Geochem 42:707-712

Toney JL, Theroux S, Andersen RA, Coleman A, Amaral-Zettler L and Huang Y (2012) Culturing of the first 37:4 predominant lacustrine haptophyte: Geochemical, biochemical, and genetic implications. Geochim Cosmochim Acta 78:51-64

Trenberth K, Jones PD, Ambenje P, Bojariu R, Easterling D, Klein Tank A, Parker D, Rahimzadeh F, Renwick JA, Rusticucci M, Soden B and Zhai P (2007) Observations: surface and atmospheric climate change. Cambridge Univ Press, New York, 1-996 pp

Tyler JJ, Leng MJ and Arrowsmith C (2007) Seasonality and the isotope hydrology of Lochnagar, a Scottish mountain lake: implications for palaeoclimate research. Holocene 17:717-727

Unger-Shayesteh K, Vorogushyn S, Farinotti D, Gafurov A, Duethmann D, Mandychev A and Merz B (2013) What do we know about past changes in the water cycle of Central Asian headwaters? A review. Global Planet Change 110:4-25

Vancampo E and Gasse F (1993) Pollen-inferred and diatom-inferred climatic and hydrological changes in sumxi co basin (western tibet) since 13,000 yr bp. Quatern Res 39:300-313

Vandenberghe J, Renssen H, van Huissteden K, Nugteren G, Konert M, Lu H, Dodonov A and Buylaert J-P (2006) Penetration of Atlantic westerly winds into Central and East Asia. Quat Sci Rev 25:2380-2389

Vicente-Serrano SM, Begueria S and Lopez-Moreno JI (2010) A Multiscalar Drought Index Sensitive to Global Warming: The Standardized Precipitation Evapotranspiration Index. J Clim 23:1696-1718

Wang R, Yang XD, Langdon P and Zhang EL (2011) Limnological responses to warming on the Xizang Plateau, Tibet, over the past 200 years. J Paleolimnol 45:257-271

Wang WG, Feng ZD, Lee XQ, Zhang HC, Ma YZ, An CB and Guo LL (2004) Holocene abrupt climate shifts recorded in Gun Nuur lake core, northern Mongolia. Chin Sci Bull 49:520-526

Wang X, Feng L, Zhang F and Ding Z (2008) On-line measurements of delta N-15 in biological fluids by a modified continuous-flow elemental analyzer with an isotope-ratio mass spectrometer. Rapid Commun Mass Spectrom 22:1196-1202

Wang Y and Sessions AL (2008) Memory Effects in Compound-Specific D/H Analysis by Gas Chromatography/Pyrolysis/Isotope-Ratio Mass Spectrometry. Anal Chem 80:9162-9170

Wang YJ, Cheng H, Edwards RL, An ZS, Wu JY, Shen CC and Dorale JA (2001) A high-resolution absolute-dated Late Pleistocene monsoon record from Hulu Cave, China. Science 294:2345-2348

Wanner H, Beer J, Butikofer J, Crowley TJ, Cubasch U, Fluckiger J, Goosse H, Grosjean M, Joos F, Kaplan JO, Kuttel M, Muller SA, Prentice IC, Solomina O, Stocker TF, Tarasov P, Wagner M and Widmann M (2008) Mid- to Late Holocene climate change: an overview. Quat Sci Rev 27:1791-1828

Wanner H, Solomina O, Grosjean M, Ritz SP and Jetel M (2011) Structure and origin of Holocene cold events. Quat Sci Rev 30:3109-3123

Weaver AJ, Eby M, Augustus FF and Wiebe EC (1998) Simulated influence of carbon dioxide, orbital forcing and ice sheets on the climate of the Last Glacial Maximum. Nature 394:847-853

Werner RA and Brand WA (2001) Referencing strategies and techniques in stable isotope ratio analysis. Rapid Commun Mass Spectrom 15:501-519

Williams MW and Konovalov VG (2008) Central Asia Temperature and Precipitation Data, 1879-2003. National Snow & Ice Data Center 9.7

Witt R, Günther F, Lauterbach S, Kasper T, Mäusbacher R, Yao T and Gleixner G (2015) Biogeochemical evidence for freshwater periods during the Last Glacial Maximum recorded in lake sediments from Nam Co, southern-central Tibetan Plateau. J Paleolimnol doi:

Wolin JA and Duthie HC (1999) Diatoms as indicators of water level change in freshwater lakes, 183-202 pp

Wright HE (1986) Handbook of holocene paleoecology and palaeohydrology - berglund,be. Science 233:482-482

Wünnemann B, Mischke S and Chen FH (2006) A Holocene sedimentary record from Bosten Lake, China. Palaeogeogr Palaeoclimatol Palaeoecol 234:223-238

Xia ZH, Xu BQ, Mügler I, Wu GJ, Gleixner G, Sachse D and Zhu LP (2008) Hydrogen isotope ratios of terrigenous n-alkanes in lacustrine surface sediment of the Tibetan Plateau record the precipitation signal. Geochem J 42:331-338

Yao T, Masson-Delmotte V, Gao J, Yu W, Yang X, Risi C, Sturm C, Werner M, Zhao H, He Y, Ren W, Tian L, Shi C and Hou S (2013) A review of climatic controls on delta o-18 in precipitation over the tibetan plateau: Observations and simulations. Rev Geophys 51

Yao TD, Thompson LG, Shi YF, Qin DH, Jiao KQ, Yang ZH, Tian LD and Thompson EM (1997) Climate variation since the last interglaciation recorded in the Guliya ice core. Sci China Ser D-Earth Sci 40:662-668

Yao TD, Xu BQ and Pu JC (2001) Climatic changes on orbital and sub-orbital time scale recorded by the Guliya ice core in Tibetan Plateau. Sci China Ser D-Earth Sci 44:360-368

Yucel M, Konovalov SK, Moore TS, Janzen CP and Luther GW, III (2010) Sulfur speciation in the upper Black Sea sediments. Chem Geol 269:364-375

Zech M, Pedentchouk N, Buggle B, Leiber K, Kalbitz K, Markovic SB and Glaser B (2011) Effect of leaf litter degradation and seasonality on D/H isotope ratios of n-alkane biomarkers. Geochim Cosmochim Acta 75:4917-4928

Zhang C, Feng Z, Yang Q, Gou X and Sun F (2010) Holocene environmental variations recorded by organic-related and carbonate-related proxies of the lacustrine sediments from Bosten Lake, northwestern China. Holocene 20:363-373

Zhang C, Mischke S, Zheng M, Prokopenk A, Guo F and Feng Z (2009) Carbon and Oxygen Isotopic Composition of Surface-Sediment Carbonate in Bosten Lake (Xinjiang, China) and its Controlling Factors. Acta Geologica Sinica-English Edition 83:386-395

Zhang Z and Sachs JP (2007) Hydrogen isotope fractionation in freshwater algae: I. Variations among lipids and species. Org Geochem 38:582-608

Zhao K, Li X, Dodson J, Atahan P, Zhou X and Bertuch F (2012) Climatic variations over the last 4000 cal yr BP in the western margin of the Tarim Basin, Xinjiang, reconstructed from pollen data. Palaeogeogr Palaeoclimatol Palaeoecol 321:16-23

Zhao MX, Dupont L, Eglinton G and Teece M (2003) n-alkane and pollen reconstruction of terrestrial climate and vegetation for NW Africa over the last 160 kyr. Org Geochem 34:131-143

Zhou S, Kang S, Chen F and Joswiak DR (2013) Water balance observations reveal significant subsurface water seepage from Lake Nam Co, south-central Tibetan Plateau. J Hydrol 491:89-99

Zhu DG, Meng XG, Zhao XT, Shao ZG, Xu ZF, Yang CB, Ma ZB, Wu ZG, Wu ZH and Wang JP (2004) Evolution of an ancient large lake in the southeast of the northern Tibetan Plateau. Acta Geologica Sinica-English Edition 78:982-992

Zhu LP, Xie MP and Wu YH (2010) Quantitative analysis of lake area variations and the influence factors from 1971 to 2004 in the Nam Co basin of the Tibetan Plateau. Chin Sci Bull 55:1294-1303

Zink KG, Leythaeuser D, Melkonian M and Schwark L (2001) Temperature dependency of long-chain alkenone distributions in Recent to fossil limnic sediments and in lake waters. Geochim Cosmochim Acta 65:253-265

10 Supplement

Additional Manuscript: Biogeochemical evidence for freshwater periods during the Last Glacial Maximum recorded in lake sediments from Nam Co, southern-central Tibetan Plateau

Abstract

Improved knowledge on deglaciation processes during the termination of the Last Glacial Maximum (LGM) at the Tibetan Plateau can provide important information for the understanding of deglaciations in climate sensitive high–altitude ecosystems. However, only little knowledge is available on this time interval, as most lacustrine records from the Tibetan Plateau are younger than 19,000 years. The present study focused on a lake sediment record from Nam Co (southern–central Tibetan Plateau) covering the interval from ~ 23.7 to 20.9 cal. kyr BP. We analyzed the distribution and the compound specific hydrogen isotope composition (δD) of sedimentary n–alkanes as well as the bulk sediment TOC, TN, $\delta^{13}C_{org}$ and $\delta^{15}N$ composition to reconstruct lake system development. Pronounced changes of environmental conditions between ~ 21.6 and 21.1 cal. kyr BP as well as between 23.1 and 22.5 cal. kyr BP (Greenland Interstadial 2) are inferred from increased aquatic n–alkane amounts and decreased $\delta D_{n–C23}$ values within these time intervals, respectively. Freshwater inputs that most likely resulting from enhanced glacier melting caused these changes. Our results suggest that mountain glacier retreat on the Tibetan Plateau started earlier than previously assumed. The necessary thawing energy was probably provided by temperature changes caused by the reorganizations of atmospheric circulations, which have been also recorded in Greenland ice records.

Introduction

Global climate change and the associated temperature increase particularly affect high–altitude freshwater resources by glacier melting, increased evaporation and loss of water storing capacity. In this regard, the Tibetan Plateau with the world`s third largest amount of glaciers as well as numerous lakes represents a key region of interest as it is the main freshwater source area for millions of people in Asia. For example, Nam Co, the second largest Tibetan lake, which is located close to a large glaciated area on the southern–central Tibetan Plateau, already shows a distinct response to current warming (Bolch et al. 2010). Hence, investigating large–scale climatic changes in the Nam Co region during different climatic conditions, e.g. the Last Glacial Maximum (LGM) can contribute to the understanding of typical developmental stages during deglaciation and thus help to conceive environmental changes that the region is experiencing nowadays and under continued warming in the future.

Due to the more equatorial position of the Intertropical Convergence Zone during the LGM (Chabangborn et al. 2014; Günther et al. 2015), the Indian Ocean Summer Monsoon (IOSM), which nowadays provide moist air masses to the Tibetan Plateau, was much weaker (Barrows and Juggins 2005). As a consequence, the winter monsoon in the interior of the Tibetan Plateau, which is related to the interplay of the Siberian High and the mid–latitude Westerlies, is assumed to have been stronger due to a weaker thermal contrast between the Asian continent and the ocean (Shi 2002). The resulting dominance of colder and dryer air masses may have caused a decrease in annual precipitation from 1000 to 200 mm, which forced the expansion of extreme continental cold glaciers during the LGM, resulting in a 15-times larger glacier extent on the Tibetan Plateau than today (Shi 2002). Globally, the LGM is characterized by a larger extent of ice sheets (Mix et al. 2001), lower sea levels and air temperatures of 6 to 9 °C lower than today (Lambeck et al. 2002; Shi 2002). Although the LGM is generally defined from 26 to 19 cal. kyr BP (Clark et al. 2009), the related maximum extent of glaciated areas reveals large spatial and temporal differences (Hughes 2013). The Greenland ice core records, as the most investigated climate archives, already detected rapid climatic events within the LGM (Lowe et al. 2008). Deglaciation on the Tibetan Plateau, especially in the Nam Co region is thought to have occurred only between 16 and 18 kyr BP, similar to the deglaciation on the Southern Hemisphere and thus later than in other regions (Clark et al. 2009). The precise timing of deglaciation in this area as well as local environmental changes during this period are still matter of debate (Clark et al. 2009; Hou et al. 2012).

Although the distribution of *n*–alkanes and their stable hydrogen isotope composition (δD) have previously been successfully used to reconstruct Holocene environmental and climatic changes (e.g. humidity and temperature) at Nam Co (Xia et al. 2008; Mügler et al. 2010), such analyses have not been applied to LGM sedimentary records so far. While sedimentary *n*–alkane distribution reflects sources of organic matter input, the *n*–alkane isotopic composition retrace the signal of their source water and can thus be used to e.g. differentiate between meltwater and precipitation water (Aichner et al. 2010b; Günther et al. 2013; Hu et al. 2014). Within the present study, biogeochemical analyses of the distribution and δD composition of sedimentary *n*–alkanes as well as bulk sediment geochemical analyses ($\delta^{13}C_{org}$, $\delta^{15}N$, TOC, TN) were applied to sediments of the late LGM (23.7 to 20.9 cal. kyr BP) from Nam Co. These investigations aim at characterizing environmental changes during this time at Nam Co and to transfer the results to a larger scale of the Tibetan Plateau. It will help to understand the possible regional climatic characteristics during the transition from full glacial conditions to a deglaciation stage in a climatically sensitive region. In particular, our investigations focused on (1) reconstructing lake development and changes in climate and biomass productivity during this period, and (2) clarifying whether continuous ice cover persisted during this interval and, if not, which processes provided thawing energy to the lake system.

Study area

Lake Nam Co is located in the southern–central part of the Tibetan Plateau (30°30`–30°56`N, 90°16`–91°03`E) at an elevation of 4722 m a.s.l. (Lin et al. 2008; Schütt et al. 2010) (Supp. Figure 1). The lake has a size of approximately 70 x 30 km (surface area ~ 2015 km² in 2004; (Zhu et al. 2010), a maximum water depth of 99 m (Daut et al. 2010) and a catchment area of about 10,600 km² (Wang et al. 2011). The recent climatic character at Nam Co is semi–arid to semi–humid continental (Mügler et al. 2010) with a mean annual evaporation of 790 mm for the total lake surface and 320 mm for the catchment (Li et al. 2008). Most of the local precipitation is delivered by the IOSM during summer, whereas during winter, cold and dry air masses of the Westerlies and the Siberian High prevail (Chen et al. 2012). The mean annual precipitation varies between 300 and 500 mm (Zhu et al. 2004) and the mean annual air temperature is –1 °C (Schütt et al. 2010). As the Nam Co basin is closed (Schütt et al. 2010), the water balance is mainly controlled by evaporation, precipitation and inflow, but partly also influenced in a negative way by seepage of lake water into groundwater (Zhou et al. 2013). The presently positive water balance is caused by enhanced input of glacial meltwater from the Nyainqentanglha mountain range in the south of Nam Co, which is due to recently rising temperature (Liu et al. 2010). Vegetation within the catchment is adapted to high–altitude climatic conditions and dominated by alpine meadow and steppe grasses such as *Kobresia sp*., *Stipa sp*., *Artemisia sp*., *Oxytropis sp*., *Morina sp*. and *Carex sp.* (Mügler et al. 2008).
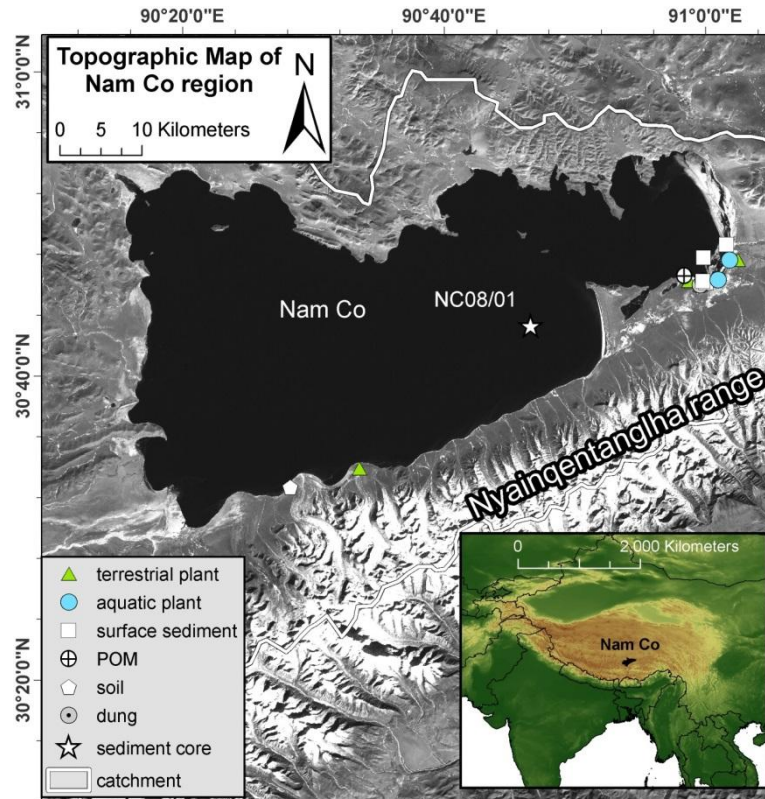
Supp. Figure 1: Location map of Nam Co, southern–central Tibet.
Satellite image obtained from www.landsat.org. The location of sediment core NC 08/01 in the south–eastern basin is marked by a star. Locations of different plant, surface sediment, soil and particulate organic matter (POM) samples are marked by symbols explained in the legend. Nam Co catchment location at the lower Asia map is marked in black.

Materials and Methods

Field Sampling

In 2008, a 10.4 m long composite sediment core (NC 08/01) was recovered from the south–eastern basin of Nam Co (30°44'14.7"N, 90°47'25.2"E, 93 m water depth, Supp. Figure 1) using a piston corer with a diameter of 90 mm (UWITEC, Mondsee, Austria). This study focuses on the lowermost part of the sediment core (6.60 to 10.38 m composite depth). This core section was sampled at a 5–cm interval with ~12 g dry sediment for each sample. Additionally, surface sediment samples were taken in 2009 by using a HTH gravity corer with 6.6 cm internal diameter (Pylonex, Luneå, Sweden). From these cores, the uppermost 1 cm was sampled. For further analyses all samples were freeze dried (P25, Piatkowski, Munich, Germany) and homogenized.

Terrestrial plants (e.g. *Carex*, *Kobresia*, *Stipa*, *Leontopodium, Potentilla* and *Dasiphora parvifolia*) were taken from the eastern/southern Nam Co catchment and submerged macrophytes (*Potamogeton*) were taken from 2 to 5 m water depth at the eastern Nam Co basin in 2009. For each specific plant sample several individuals were mixed. In addition,

dung from different herbivores was collected representing the digested residue of plant matter. Catchment soil samples were taken from two different depth intervals (0–5 cm and 5–10 cm) and sieved over 2–mm meshes. All soil, plant and dung samples were air–dried in the field and transported in paper bags. Particulate organic matter (POM) was filtered from the lake water depth of 15 m by using a filtration system with a glass fibre filter of 1 μm pore size to adsorb finer particles and two pre–filters of 50 and 10 μm to hold coarser particles.

Chronology of Nam Co sediment core NC 08/01

The chronology of the complete NC 08/01 sediment core is based on 24 AMS ^{14}C ages (Beta Analytics, Miami, USA) obtained from bulk sediment samples (Doberschütz et al. 2014; Kasper et al. 2015) using calibrated median ages of the 2σ distribution provided by OxCal 4.1.7 (Ramsey 1995). The investigated core section between 6.60 and 10.38 m includes 5 AMS ^{14}C ages (Supp. Figure 2) (Kasper et al. 2015). A reservoir effect of 1,420 ^{14}C years was inferred from the age of the sediment–water interface of the sediment core and was subtracted from all radiocarbon ages prior to calibration (Doberschütz et al. 2014). The interval investigated in this study covers a time span of 2.8 kyr between 23.7 and 20.9 cal. kyr BP. The mean sediment accumulation rate (SAR) in this section of the sediment record is 1.7 mm a^{-1}.
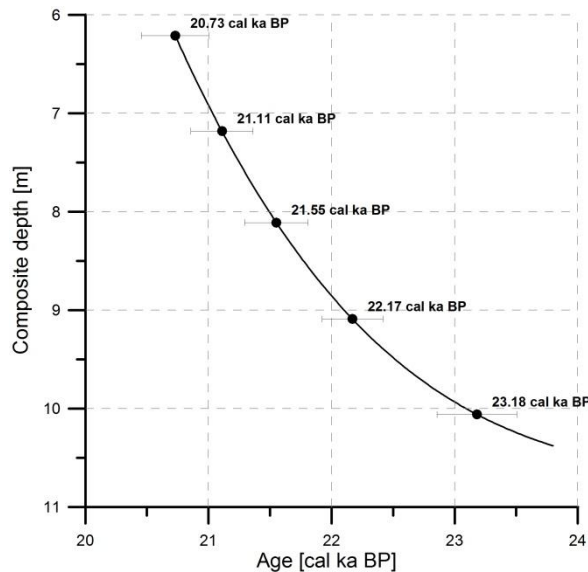
Supp. Figure 2: Chronology of Nam Co sediment core NC 08/01 for the investigated interval as established from the calibrated median ages of 5 radiocarbon dates from bulk sediment samples (Kasper et al. 2015). Error bars represent the 2σ uncertainty range.

Measurement of sediment $\delta^{13}C_{org}$, $\delta^{15}N$, TOC and TN

For geochemical analyses, homogenized aliquots of the dry sediment were weighed in tin capsules (~4 mg for C, ~80 mg for N). Inorganic carbon was removed by adding H_2SO_3 stepwise until 120 µl in total (Steinbeiss et al. 2008) prior to measuring the content of total organic carbon (TOC) and the stable carbon isotope composition ($\delta^{13}C_{org}$) of the organic fraction. TOC and $\delta^{13}C_{org}$ as well as the total nitrogen content (TN) and the stable nitrogen isotope composition ($\delta^{15}N$) were determined in separate runs with a coupled EA–IRMS system (EA: NA 1100 CN–EA, CE Instruments, Milan, Italy; IRMS: Delta C with Delta [Plus] ion source, Finnigan MAT, Bremen, Germany). Each sample was measured in duplicate, to verify sample homogeneity (analytical precision: $\delta^{13}C_{org} = \pm\, 0.12$ ‰; $\delta^{15}N = \pm\, 0.12$ ‰). Working standards were acetanilide ($\delta^{13}C = -29.8$ ‰, $\delta^{15}N = -1.5$ ‰) and caffeine ($\delta^{13}C = -40.2$ ‰, $\delta^{15}N = -15.5$ ‰) calibrated against the international standards IAEA–N1 and NBS–22. The $\delta^{13}C$ and $\delta^{15}N$ compositions are reported in the conventional δ–notation relative to the Vienna Pee Dee Belemnite (V–PDB) and atmospheric (AIR) nitrogen standards (Werner and Brand 2001).

Analysis of sedimentary and plant n–alkanes

Lipid extractions were performed on 6-g of dry core sediment and 2-g of dry surface sediment, plant material (all plant parts were used), dung and soil using an accelerated solvent extractor (ASE 200, DIONEX Corp., Sunnyvale, USA). The ASE was operated at 100 °C and 138 bar for 15-min in 2 cycles using a 9:1 (v/v) solvent mixture of dichloromethane and methanol. HCl–activated copper (15 % HCl) was added to remove elemental sulphur. The total lipid extract was then separated using solid phase extraction on silica gel (0.040 – 0.063 mm mesh; Merck, Darmstadt, Germany) according to Sachse et al. (2006). The n–alkane (aliphatic) fraction was eluted with 80 ml n–hexane.

Identification and quantification of n–alkanes from the sediment core samples was accomplished using a GC–FID system (TRACE GC 2000, CE Instruments, Thermo Quest, Rodano, Italy) with a DB–1MS column (30 m length, 0.25 mm ID, 0.25 µm film thickness; Agilent Technologies, Santa Clara, USA) by comparing peak areas and retention times with an external n–alkane standard mixture (n–C_{10} to n–C_{34}). The PTV–injector was operated in splitless mode with an initial temperature of 45 °C for 0.1 min and then heated to 300 °C with 14.5 °C s^{-1} for 3 min. The temperature of the GC oven was held at 90 °C for 1 min, raised to 300 °C at 10 °C min^{-1}, kept constant for 9 min and finally increased with 30 °C min^{-1} to 335 °C and held there for 3 min. Helium was used as carrier gas at constant flow of 2 ml min^{-1}. The FID was operated at constantly 300 °C and with gas flows of 40, 45 and 450 ml min^{-1}, for synthetic air, hydrogen and nitrogen, respectively.

The n–alkane concentrations of recent plant, soil, dung and sediment samples were measured in a GC–FID system (HP 6890, Agilent Technologies, Santa Clara, USA) with an Agilent 19091B–115 column (50 m length, 0.32 mm ID, 0.52 µm film thickness, Agilent

Technologies, Santa Clara, USA). Here the injector was operated in split mode with a ratio of 10:1 and a constant temperature of 280 °C. The oven programme started at 80 °C and was kept constant for 1 min before increasing with 10 °C min^{-1} to 300 °C. After 11 min, the oven heated up with 30 °C min^{-1} to 330 °C and kept constant for 5 min. Each sample was measured in triplicate. The results are expressed as ng g^{-1} dry weight.

To discriminate between the input of fresh and digested allochthonous plant material, the Carbon Preference Index (CPI) for n–C$_{17}$ to n–C$_{31}$, which expresses the ratio of n–alkanes with an odd number of carbon atoms relative to those with an even number, was calculated according to:

$$CPI_{17-31} = 0.5 \times ((\Sigma_{odd}\ C_{15-29}) / (\Sigma_{even}\ C_{16-30})) + ((\Sigma_{odd}\ C_{17-31}) / (\Sigma_{even}\ C_{16-30})). \qquad [14]$$

The average chain length (ACL) was calculated according to:

$$ACL_{17-31} = \Sigma\ (C_n \times n) / \Sigma C_n. \qquad [15]$$

Cluster analysis of the sedimentary n–alkane distribution was performed with the PASW statistics 18 software, using K–means clustering. Different sources of lacustrine n–alkanes were visualized by principal component analysis (PCA) using SigmaPlot 10 software.

Measurement of δD of n–alkanes

Stable hydrogen isotope ratios (δD) were analyzed using a coupled GC–IRMS system. Due to very low n–alkane concentrations (< 250 ng g^{-1}), 3–4 sediment samples had to be pooled together. According to the age-depth model, this pooling results in mean δD values spreading over a range from ~ 80-years in the younger section till ~ 200-years in the bottom section. The combined samples were injected into a GC system (HP5890 Series II, Agilent Technologies, Böblingen, Germany) equipped with a BP1 column (60 m, 0.32 mm ID, 0.50 μm film thickness; SGE GmbH, Darmstadt, Germany). The injector was operated at a constant temperature of 280 °C in splitless mode. The oven was maintained for 1 min at 60 °C, heated with 10 °C min^{-1} to 300 °C and was kept constant for 28.5 min. The final ramp heated with 20 °C min^{-1} to 340 °C and was kept constant for 3 min. The column flow was constant at 2 ml min^{-1}. 5 % of the gas flow was transferred to an ion trap mass spectrometer (GCQ Thermo Electron, San Jose, USA) to identify mass fragments and 95 % went to an isotope ratio mass spectrometer (Delta^{plus}XL, Finnigan MAT, Bremen, Germany). The δD composition was determined three times for each sample and reported in the conventional δ–notation relative to the Vienna Standard Mean Ocean Water (VSMOW). A general offset calculation was accomplished using H$_2$ reference gas with

known isotopic composition and correcting measured δD values from a standard mixture containing several *n*–alkanes (*n*–C$_{10}$ to *n*–C$_{34}$). Outliers were eliminated using Peirce`s criterion. The mean standard deviation for the standard triplicates was 5.2 ‰. Consequently, no drift correction was applied. The H$_3^+$ factor was determined on a daily basis and stayed constant within the analytical error at 11.44 (SD = 0.52; n = 9) during the measurement period.

Polissar et al. (2009) already pointed out that for low concentrated Tibetan samples additional concentration dependent corrections are necessary. We calibrated our GC-IRMS system using standard mixtures in five different concentrations (5 to 200 ng µl^{-1}). The δD values increased logarithmically (*n*–C$_{23-31}$: R² = 0.91 to 0.99) below a concentration of 100 ng µl^{-1}. As the majority of samples were below this limit, a concentration dependent correction was applied (Wang et al. 2008; Wang and Sessions 2008). This correction decreased the δD values of small peaks between 2.3 and 4.3 ‰. However, the correction did not change the significance of differences between the data points in the time series.

Results

δ^{13}Corg, δ^{15}N, TOC and TN of catchment samples and lake sediments

Soil geochemical values (n = 2) are close to that of lake sediments with mean δ^{13}C$_{org}$ of − 24.9 ‰ and TOC/TN ratios of 7.7 ± 0.5 (Supp. Figure 3). Modern terrestrial plant samples (n = 3) reveal clearly higher TOC/TN ratios (21 ± 5), while δ^{13}C$_{org}$ values plot in the same range like soils and sediments (–25 ± 2 ‰). In contrast, submerged macrophyte samples of *Potamogeton* (n = 2) show highest values for δ^{13}C$_{org}$ (–6.4 ± 0.6 ‰) and for the TOC/TN ratio (28 ± 7). The highest enrichment in δ^{15}N was determined in the NC08/01 sediments (n = 78; 7.8 ± 0.5 ‰), showing a significant difference (p < 0.05) with recent aquatic macrophytes (5.1 ± 1.9 ‰), terrestrial plants (4.4 ± 2.3 ‰) and soil samples (2.9 ± 1.2 ‰).

In the lower part of the investigated core section (10.38 to 8.75 m / 23.7 to 22.0 cal. kyr BP) δ^{13}C$_{org}$ and δ^{15}N show no clear trends with mean values of –26.4 ± 0.7 ‰ and 8 ± 0.4 ‰, respectively (Supp. Figure 7 A, B). Within the upper unit (8.75 to 6.60 m / 22.0 to 20.9 cal. kyr BP) δ^{13}C$_{org}$ values increase from –27.5 to –24 ‰. δ^{15}N values reveal a decreasing trend from 8.6 to 6.6 ‰. Both proxies have a significant negative correlation (R^2 = 0.4, p < 0.01). The mean content as well as the variability of TOC (0.42 ± 0.05 %) is much higher than these of TN (0.05 ± 0.003 %). Hence, the TOC/TN ratio (7.9 ± 0.8) is mainly influenced by changes of TOC contents (Supp. Figure 7 C, D, E). The lower unit is characterized by a mean TOC/TN ratio of 7.3 ± 0.6, whereas the upper part of the investigated section shows a higher mean value (8.4 ± 0.7) due to increasing TOC contents. Between 22.4 and 22.0 cal. kyr BP, TOC and TN reach lowest values, leading to relatively low mean TOC/TN ratios (7 ± 0.5).
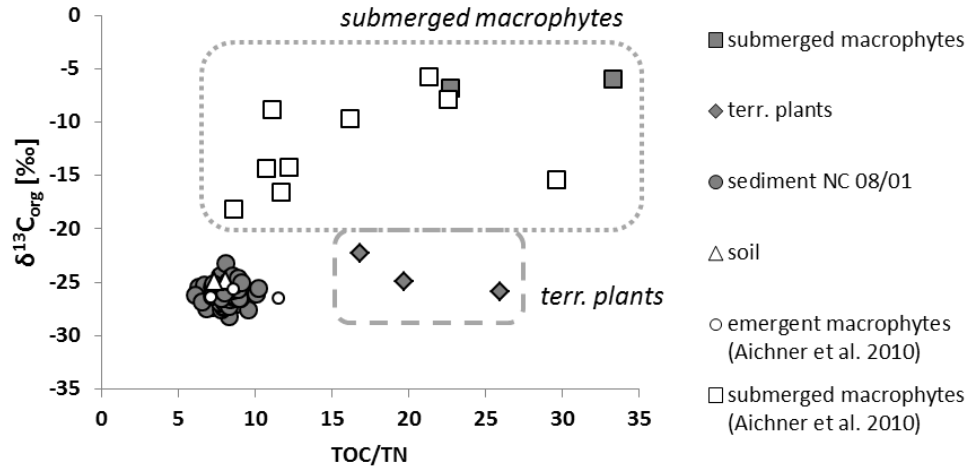
Supp. Figure 3: Sources of organic matter according to the $\delta^{13}C_{org}$ composition and TOC/TN ratio. The composition of the sediments from core NC 08/01 indicates a predominant contribution of aquatic organic matter. Compositions of additional macrophytes are given after Aichner et al. (2010b).

Distribution and concentration of *n*–alkanes

Catchment (soils, terrestrial and aquatic plants, dung, POM) and surface sediment samples

The composition of *n*–alkanes in terrestrial plant samples, but also in dung as decomposition products of terrestrial plants and soil biomass reveals an increasing predominance of long–chain *n*–alkanes n–$C_{29/31}$ (ACL = 29, 29.8 and 29.9, respectively) with a clear odd/even preference (Supp. Figure 4). The odd/even preference is also visible in the aquatic plants, although mid–chain *n*–alkanes n–$C_{23/25}$ (ACL = 23.7) are dominant. This bimodal distribution of long– and mid–chain *n*–alkanes within plant biomass is also reflected in the Nam Co surface sediments (ACL = 25.9), showing the generally high contribution of plant material to lacustrine OM. POM within the lake water is characterized by an *n*–alkane distribution between n–C_{15} and n–C_{25} (ACL = 21.1), a low CPI (1.5) and therefore no odd/even predominance.
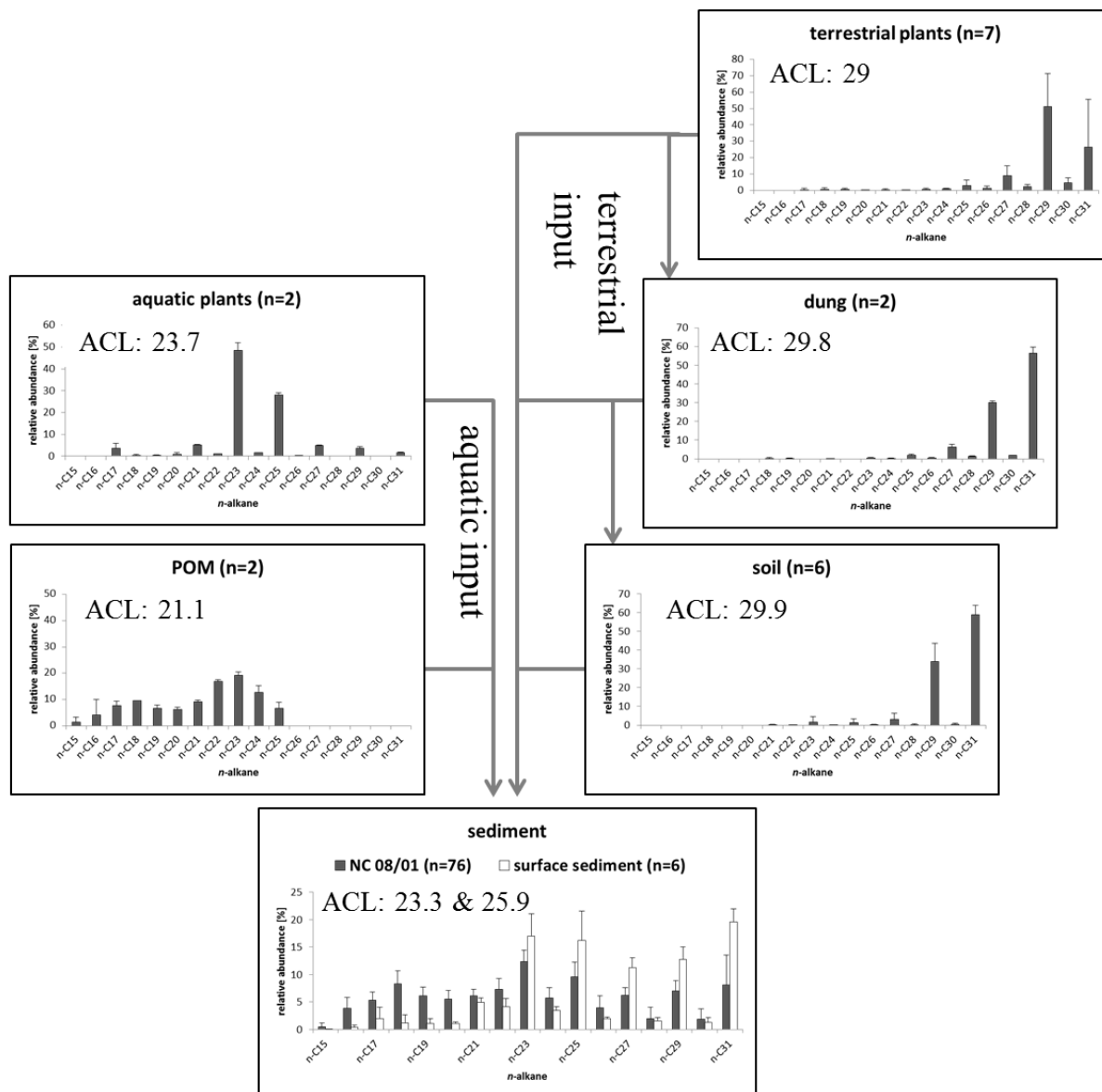
Supp. Figure 4: Relative abundance and distribution of *n*–alkanes and calculated Average Chain Length (ACL) for *n*–alkanes *n*–C_{17-31} in recent terrestrial (soil, terrestrial plants, dung) and aquatic (aquatic plants, particulate organic matter (POM) samples as sources for lake sediment samples (recent, core NC 08/01) at Nam Co.
Error bars represent the sample variability.

Sediment core NC 08/01

Sediments of core NC 08/01 contain *n*–alkanes *n*–C_{15} to *n*–C_{31} with a mainly bimodal distribution, maximizing at *n*–C_{23} (104 ng g^{-1}), followed by *n*–C_{25} (82 ng g^{-1}) and *n*–C_{31} (73 ng g^{-1}) (Supp. Figure 4 and Supp. Figure 6). The total concentration of *n*–alkanes *n*–C_{15-31} ranges between 300 and 1700 ng g^{-1}. The mid– and long–chain *n*–alkanes reveal an

odd/even preference, while n–alkanes $< n$–C_{21} have higher even carbon numbered n–alkane amounts. The aquatic biomarker n–C_{23} and the terrestrial n–C_{31} show similar concentration variability (mean value $= 111 \pm 40$ ng g^{-1}; 78 ± 39 ng g^{-1}), compared to the terrestrial biomarker n–C_{29} (mean value $= 63 \pm 22$ ng g^{-1}). n-C_{23} and n-C_{29} show minimum concentrations at ~ 21.7 cal. kyr BP, while n-C_{31} could not even be detected at $\sim$22.5 cal. kyr BP. Maximum concentrations appear at 23.6 (n-C_{31}) and ~ 21.3 cal. kyr BP (n-C_{23}) (Supp. Figure 7 H, I).

A principal component analysis (PCA) of the relative n–alkane distribution from sediments of core NC 08/01 as well as surface sediments, terrestrial and aquatic plants, dung, soil and POM visualizes the different sources of lacustrine OM (Supp. Figure 5). The n–alkane C_{29} has a strong positive loading on Axis 1 (57.6 %), while short– to mid–chain n–alkanes $C_{16–25}$ have negative loadings. The terrestrial signal consists of terrestrial plants, dung and soil, where the former ones are mainly controlled by long–chain n–alkanes C_{29} and soils are stronger controlled by n–C_{31}. Generally they are clearly separated from the aquatic signal, consisting of aquatic plants, surface sediments and POM.
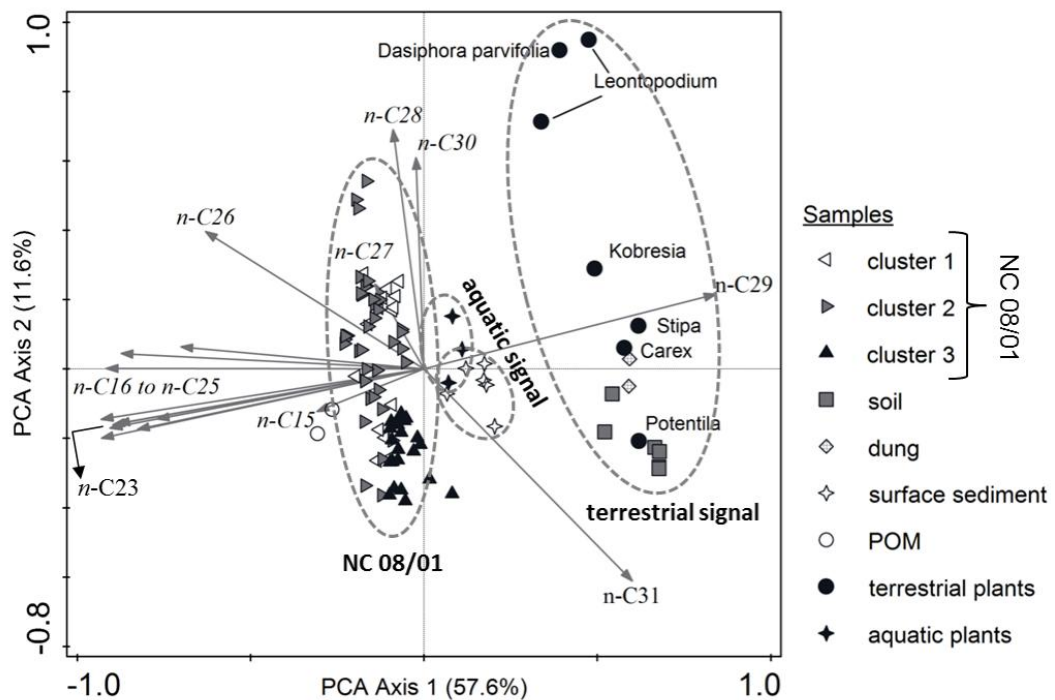
Supp. Figure 5: PCA of Nam Co sediment core NC 08/01 (3 clusters), surface sediments, different aquatic and terrestrial end members (plants, soil, dung and POM) illustrate sources of lacustrine organic matter.

According to the n–alkane distribution, the core can be separated into three clusters using cluster analysis (Supp. Figure 6). Sediment samples combined in cluster I (microbial) point

out no odd/even predominance of *n*–alkane chain length and thus a very low CPI (1.4). This cluster is very characteristic for period 2 and 5. Sediments in cluster II and III are dominated by odd mid– and long–chain *n*–alkanes. While samples in cluster II (aquatic) show high abundances of the mid–chain *n*–alkanes *n*–C_{23} and *n*–C_{25}, the dominance in cluster III (terrestrial) is shifted towards odd carbon numbers ≥ *n*–C_{23}, particularly towards *n*–C_{31}. The CPI for cluster II and III is 2.3 and 3.3, respectively. Both clusters do not show any difference in the abundance of short–chain *n*–alkanes ≤ *n*–C_{22}. Cluster II is characterized by a decreasing abundance with increasing *n*-alkane chain length > *n*-C_{22}, while cluster III reveals a shift towards an increasing trend at *n*-alkanes > *n*-C_{29}.
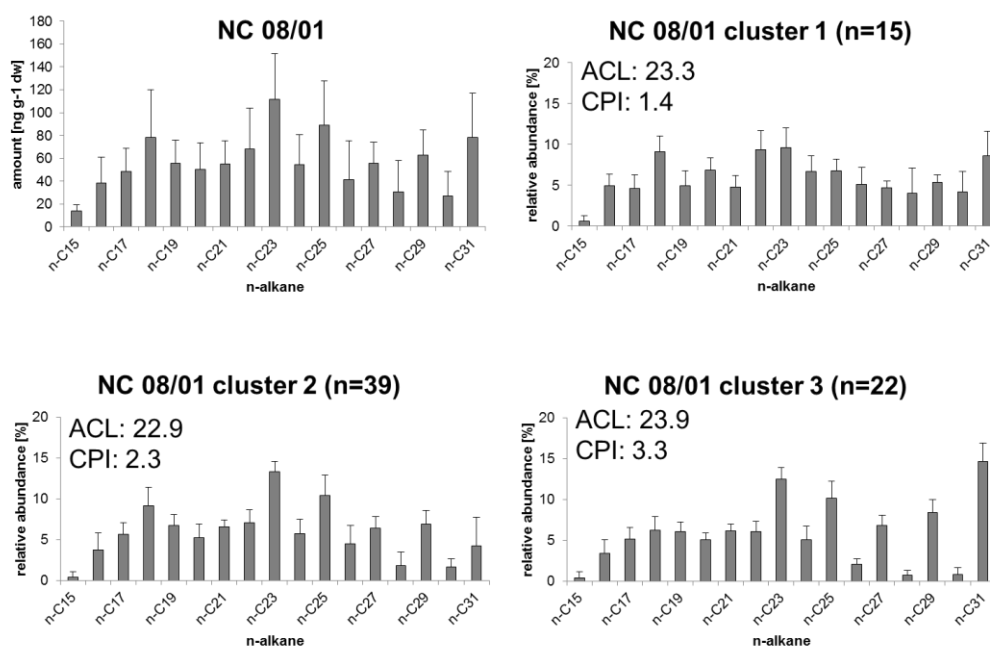
Supp. Figure 6: Distribution of *n*-alkanes within clusters I to III of NC 08/01.
Samples were classified by using the relative abundance of *n*–C_{15-31}. The cluster distribution depends on the Carbon Preference Index (CPI), which increases with higher cluster number. Error bars represent the variability over the core.

δD values of *n*–alkanes in lake sediments

δD data of the most abundant aquatic *n*–alkane *n*–C_{23} (δD$_{n–C23}$) in the Nam Co LGM sediments show three sections while two of them recording a mean value of −156 ± 48 ‰ at the bottom and the upper part (Supp. Figure 7 J). During the upper part, two excursions appear with enriched values at ~ 21.4 and 21 cal. kyr BP. Nevertheless, such single events should not be overestimated due to measurement uncertainties. The other section differs significantly (p < 0.01, Tukey HSD) from the surrounding ones by a drop in the mean to -376 ± 49 ‰ between 23.1 and 22.4 cal. kyr BP. A rather moderate decrease is maintained

by the terrestrial n–C$_{29}$ above 22 cal. kyr BP (–200 till -350 ‰) prior to a rapid enrichment in the youngest part of the core (Fig. 3 K). Due to low biomarker concentrations, continuous and interpretable δD records could not be derived for 960-years from n-C$_{29}$ between ~23 and 22.2 cal. kyr BP. Even a nearly 300-year long data gap occurred for n-C$_{23}$ between 22.47 and 22.17 cal. kyr BP.

Identification of lake periods

The investigated core interval can be subdivided into seven periods (1–7) according to variations in the bulk geochemical data, n–alkane distribution and δD values (Supp. Figure 7). Period 1 (23.7 to 23.1 cal. kyr BP) shows high fluctuations of odd– and even–numbered n–alkanes, while the CPI decreases from 4.7 to 3.1. Stable hydrogen isotopic values of aquatic alkanes n-C$_{23}$ stay constant (–164 ± 6 ‰), while n-C$_{29}$ slightly increases. Period 2 (23.1 to 22.5 cal. kyr BP) is characterized by strong depleted δD$_{C23}$ values (down to –450 ‰) and the first appearance of alkane cluster I. The following period 3 (22.5 to 22.0 cal. kyr BP) is characterized by relatively stable and low concentrated n–alkanes, resulting in mean CPI values of 2.7 ± 0.5. Additionally, δ^{15}N values obviously decrease for the first time. Period 4 (22.0 to 21.6 cal. kyr BP) reveals the lowest concentrations of n-C$_{23}$ and C$_{29}$. Subsequently, the CPI reaches its maximum at 21.7 cal. kyr BP due to the dominance of odd–numbered n–alkanes, while even–numbered n–alkanes reach minimum concentrations. From this period onwards δD$_{C29}$ values generally decrease, while δD$_{C23}$ starts to fluctuate around its mean value like period 1. Furthermore, δ^{15}N values start do decrease, while δ^{13}C values slightly increase. During period 5 (21.6 to 21.4 cal. kyr BP), the amount of even–numbered n–alkanes increases rapidly, leading to the lowest CPI values. Period 6 (21.4 to 21.1 cal. kyr BP) displays the highest concentrations of odd–numbered n–alkanes, especially n–C$_{23}$. Until the end of period 7 (21.1 to 20.9 cal. kyr BP) the CPI ranges around 2.4, while the amount of n–alkanes slightly decreases. Additionally, the terrestrial δD$_{C29}$ signal shows its tipping point back to enriched values. Cluster II, representing the aquatic signal, mainly dominates during the periods 3, 4, 6 and 7, while cluster III, reflecting the terrestrial signal, is distinctive during periods 1 to 4, and cluster I (microbial signal) dominates during period 5.
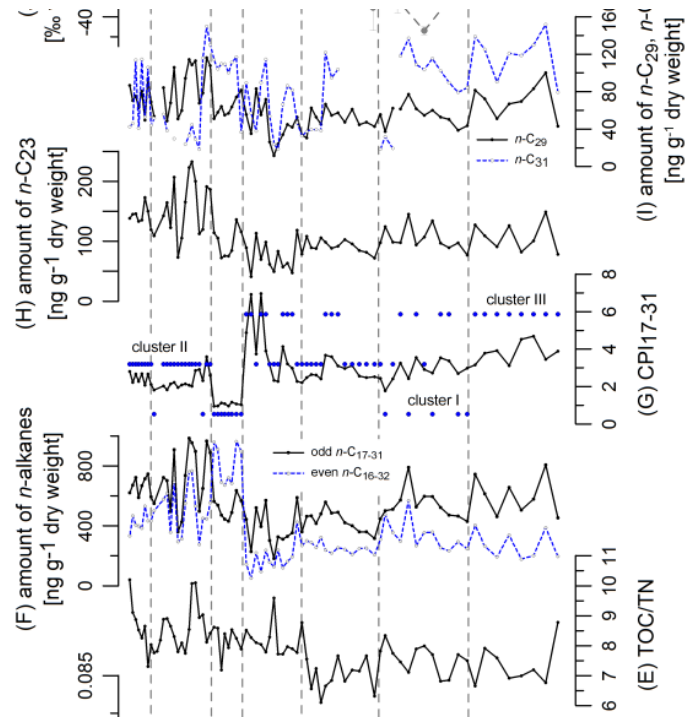
Supp. Figure 7: Proxy records for sediment core NC 08/01 between 23.7 and 20.9 cal. kyr BP. (A) $\delta^{13}C_{org}$ of bulk sediment, (B) $\delta^{15}N$ of bulk sediment, (C) TOC content of bulk sediment, (D) TN content of bulk sediment, (E) TOC/TN ratio, (F) amount of odd– numbered n–alkanes (n–$C_{17–31}$) and even–numbered n–alkanes (n–$C_{16–32}$), (G) calculated Carbon Preference Index (CPI) for n–alkanes n–$C_{17–31}$ (solid line) and alkane cluster I – III (blue dots), (H) amount of n–alkane n–C_{23}, (I) amount of n–alkane n–C_{29} (solid black line) and n–C_{31} (dashed blue line), (J) δD of n–C_{23} and (K) δD of n–C_{29}, where grey dots represent samples below 50 ng μl^{-1} and blue dots samples above 50 ng μl^{-1}, (L) mean sediment accumulation rate (Kasper et al. 2015). Error bars indicate the standard deviation.

Discussion

$\delta^{13}Corg$, $\delta^{15}N$, TOC and TN

$\delta^{13}C_{org}$ values of terrestrial C_3 plants typically range around –28 ‰, while those of C_4 plants are clearly higher (~ –14 ‰, (Oleary 1981). Hence, relatively low $\delta^{13}C_{org}$ values of OM in the Nam Co sediment samples (–26 ± 1 ‰) could reflect a predominance of C_3 plant material during the LGM. Similar values (–22 to –26 ‰) are documented throughout the Holocene at Nam Co (Mügler et al. 2010), indicating rather no changes in plant material since the LGM. Recent palynological and botanical studies also defined this high-alpine region as C_3 dominated with *Kobresia schoenoides*, *Kobresia pygmaea*, *Morina*, *Oxytropis*, *Stipa*, *Artemisia* and *Poa* (Mügler et al. 2008; Herrmann et al. 2010). However, as lacustrine algae and aquatic macrophytes (emergent, submerged) also use the C_3 pathway with $\delta^{13}C_{org}$ values ranging between –26 and –6 ‰ (Aichner et al. 2010a), $\delta^{13}C_{org}$ alone should not be used to distinguish between terrestrial and aquatic C_3 plants. A combined interpretation with the TOC/TN ratio, which is independent of the photosynthetic pathway,

could generally be used to better assess the sources of OM (Meyers and Lallier-Verges 1999). Anyhow, some arguments reduce the benefit of these proxies for detailed paleoenvironmental reconstructions: first, due to rather constant and low TN values during the LGM, the TOC/TN ratio is mainly driven by TOC, which diminish its validity for these sediments. Second, $\delta^{13}C_{org}$ and TOC/TN ratios of aquatic macrophytes from Nam Co and other Tibetan lakes (Aichner et al. 2010a) reveal a broader range with higher values, making it hard to detect terrestrial signals if macrophyte contribution is high. Nevertheless, the influence of aquatic material in Nam Co is (1) highly diverse under high abundance of these sources and (2) confirmed by the *n*-alkane signature. As the LGM sediments of Nam Co are largely characterized by TOC/TN ratios < 10, sedimentary OM was apparently mainly produced by algae and macrophytes, but in certain periods also by terrestrial material like soil (see alkane distribution). The subsequent drop of $\delta^{13}C_{org}$ values at 22.0 cal. kyr BP potentially reflects the reaction to a lowering in salinity due to increased precipitation (see discussion δD_{n-C29}), whereas the following trend back to higher $\delta^{13}C_{org}$ values is likely owed to increased aquatic productivity (submerged macrophytes) (Aichner et al. 2010c) as a consequence of higher nutrient supply by glacial meltwater and precipitation input (Slemmons et al. 2013) (see discussion on amount of $n–C_{23}$).

Further paleoenvironmental information can be derived from trends in the stable nitrogen isotopic composition as an indicator of ecosystem regeneration (Rothe and Gleixner 2000). Since the mean $\delta^{15}N$ value of 8 ± 0.4 ‰ in the oldest Nam Co sediments till 22.5 cal. kyr BP (periods 1 and 2) is higher than known values of recent organic material, this could indicate rather an unproductive ecosystem using mainly old recycled nitrogen. The still enriched values in the following periods show however a decreasing trend to a more abundant nitrogen supply as the lake system starts to regenerate under influence of terrestrial and aquatic OM. Furthermore, the amount of TN reflects the trophic status of the aquatic system. Lower temperatures can decrease the decomposition rate and therefore reduce the deposition of TN within the system. At Nam Co the amount of TN is rather stable with a mean value of 0.05 ± 0.003 %, which is very low compared to the Holocene variability (~ 0.2 %) (Doberschütz et al. 2014), indicating general reduced productivity and decomposition rates and therefore low deposition of nitrogen into OM during the LGM.

Sources and composition of sedimentary *n*–alkanes

In general, the distribution and total amount of *n*–alkanes in lake sediments is an indicator for biomass productivity and/or the grade of degradation in a lake system or its catchment, enabling the identification of the relative contribution of autochthonous and allochthonous OM (Eglinton and Hamilton 1967; Gelpi et al. 1970; Grimalt and Albaiges 1987; Ficken et al. 2000). It can be used for the reconstruction of relative temperature and precipitation (Lin et al. 2008), although large lakes like Nam Co are assumed to react rather slow to climatic changes. Main factors influencing the biomass productivity of aquatic plants are temperature, sunlight intensity, nutrient supply and the availability of dissolved inorganic

carbon (Lin et al. 2008). The dominant aquatic n–alkane n–C_{23} within the recent samples as well as within the sediments of Nam Co can be used as a proxy for lake water conditions (Günther et al. 2013). The total amount of n–alkanes in the Nam Co sediments between 23.7 and 20.9 cal. kyr BP is clearly lower (900 ± 360 ng g^{-1}) than in the recent surface sediments (3 to 28 µg g^{-1}) and during the Late Holocene (7 to 28 µg g^{-1}) (Günther et al. 2011), indicating limited biomass production due to colder and dryer climatic conditions during the LGM. Despite the lower biomass production, the distribution of short–, mid– and long–chain even– and odd–numbered n–alkanes enables distinguishing vegetation type and source changes.

To identify the typical sources of short–, mid– and long–chain n–alkanes, investigations of different organic materials from the lake and its catchment are necessary. As shown by Eglinton and Hamilton (1967), terrestrial vascular plants preferentially synthesize long–chain odd–numbered n–alkanes n–C_{27-33}, which is confirmed by the n–alkane composition of plant samples from the Nam Co catchment. Although n–C_{29} has previously been interpreted as an indicator for tree vegetation (Schwark et al. 2002), it must be considered to represent herbaceous terrestrial vegetation at Nam Co because it is mainly found in alpine meadows and steppe grasses dominating the local treeless vegetation. Nevertheless, a clear discrimination between the signal of woody and herbaceous plants is not possible due to mixing effects of different sources within the lake sediment (Rao et al. 2011). On the other hand, n-C_{29} was also found to higher proportion in emergent macrophyte species *Hippuris* and minor abundance in submerged plants (*Potamogeton*, *Batrachium*), with more affinity to shallower lakes experiencing dryer conditions (Ficken et al. 2000; Aichner et al. 2010a).

After grazing and subsequent digestion by herbivores, the plant n–alkane distribution is mainly unaffected in their dominance of n–C_{29} and n–C_{31}. Following the nutrition cycle, digested material is retained on the soil where the same n–alkane signature prevails. The input of terrestrial material into the sediment is mainly influenced by the degree of grazing, which entails mobilization of plant material, as well as the strength of aeolian and fluvial transport. Zhao et al. (2003) characterized dust input as the major mechanism transporting terrestrial n–alkanes into a lake system. This aeolian transport is assumed to be stronger in glacial times than during warm and humid periods. In contrast, mid–chain odd–numbered n–alkanes C_{21-25} are mainly produced by submerged and floating aquatic plants (Ficken et al. 2000; Aichner et al. 2010a), which is also confirmed by analyses of aquatic plants from Nam Co. Gao et al. (2011) could show that up to 97 % of the mid-chain n-alkane C_{23} in sediments is derived from floating and submerged macrophytes. Furthermore, photosynthetic bacteria and algae synthesize mainly short–chain odd–numbered n–alkanes C_{15-19} with a dominance at n–C_{17} (Gelpi et al. 1970). In addition, some microorganisms produce even–numbered n–alkanes C_{12-22} (Grimalt and Albaiges 1987), which is consistent with analyses of POM from Nam Co, reflecting a mixture of mid–chain n–alkanes from aquatic plants and short–chain n–alkanes n–C_{17-21} derived from algae and/or microbes.

In case of the incorporation of allochthonous organic material from the catchment in lake sediments, the *n*–alkane composition can be altered in two directions. While fresh, undegraded plant material is characterized by a high odd/even preference of *n*–alkanes and consequently high CPI values (cluster III), OM degraded by soil microorganisms reveals a very low odd/even preference and no chain length preference (Zech et al. 2011). In consequence, high input of microbially degraded soil OM decreases the sediment CPI (cluster I), while intermediate CPI values (cluster II) are characteristic for mainly aquatic–plant–derived OM. In general, the sedimentary OM composition of the investigated core section is stronger influenced by short– to mid–chain *n*–alkanes compared to long–chain *n*–alkanes, resulting in a closer similarity to the aquatic and POM signal compared to the terrestrial signal. Regarding the uncertainty due to mixing processes from heterogeneous OM sources, additional benefit should be taken from compound specific stable hydrogen compositions to interpret changes in the ecosystem.

Hydrogen source for sedimentary *n*–alkanes

The δD composition of *n*–alkanes from Tibetan lake sediments has recently been shown to provide information about biological sources (Duan et al. 2011) as well as about past environmental and hydrological changes (Mügler et al. 2010; Günther et al. 2011). This is mainly related to the fact, that *n*–alkane synthesizing organisms utilize their ambient water as primary hydrogen source: hence, aquatic organisms and macrophytes use the lake water, whereas terrestrial plants mainly utilize meteoric water. Previous studies revealed that the isotopic composition of the lake water, which is reflected by the δD of the aquatic mid–chain *n*–alkane C_{23}, is modified by evaporation (Günther et al. 2013), while the isotopic composition of the precipitation/inflow, reflected by the δD of the terrestrial long–chain *n*–alkane C_{29} is modified by meteorological conditions like evapotranspiration and relative moisture (Mügler et al. 2008; Xia et al. 2008; Hu et al. 2014). In consequence, δD_{n-C23} and δD_{n-C29} can be used as proxies for aquatic and terrestrial hydrological changes, as well as for investigating lake–level changes (Mügler et al. 2008; Mügler et al. 2010). Further, the comparison of the terrestrial and aquatic δD values can be used to distinguish between large–scale precipitation changes and inflow events. In case of Nam Co, it has been shown that depleted δD_{n-C29} values are assumed to reflect a higher influence of monsoonal rainfall, whereas enriched δD_{n-C29} values display an increased influence of continental moisture sources (e.g. Westerlies) or convective precipitation after evaporation from the lake itself (Mügler et al. 2010). The trend to depleted δD_{n-C29} values starting at ~ 22 cal. kyr BP could therefore be interpreted as a general change to wetter conditions resulting in decreased evapotranspiration. In contrast, depleted δD_{n-C23} values may reflect the input of isotopically depleted water (e.g. meltwater from winter snowfall), while enriched δD_{n-C23} values likely indicate increased evaporation during summer. Considering this, the strong depletion within period 2 (23.1 to 22.5 cal. kyr BP) could point to a first lake filling by meltwater during the LGM, while δD_{n-C29} data are missing as indication for still under-representative terrestrial vegetation. In consequence, compound–specific δD values of the different *n*–alkanes are used to differentiate between freshwater input from meltwater and precipitation. Throughout the LGM part of the Nam Co sediment record, the aquatic *n*–C_{23} is more enriched in deuterium compared to the terrestrial *n*–C_{29}. This is typical for closed lakes under arid conditions with a negative water balance (Mügler et al. 2008).

Local palaeoenvironmental reconstruction

Period 1 (23.7–23.1 cal. kyr BP)

The first period of the investigated sequence is characterized by high fluctuations in the amount of odd–numbered *n*–alkanes, probably caused by a strong sensitivity of the likely small and shallow lake to changes in nutrient supply (Kasper et al. 2015). According to the dominant terrestrial cluster III, lake sediment was almost exclusively influenced by fresh material from macrophytes (emergent, submerged) as well as soil/dung (mainly *n*–C_{31}). Slight changes in temperature and water supply would result in a larger response of a

shallow lake under glacial conditions. The slight increase in TOC and TN in correspondence with a fairly stable TOC/TN ratio implies increased decomposition and thus enhanced accumulation of nitrogen within the OM due to periodically warmer conditions. Nevertheless, these changes in temperatures additionally supported by slightly decreased δD_{n-C29} values did not influence the lake water isotopic signal to a great extent, which is inferred by stable δD_{n-C23} values, since Nam Co has not reached typical lake behavior.

Period 2 (23.1–22.5 cal. kyr BP)

This shows a pronounced lake response to climatic changes. A remarkable drop in the δD_{n-C23} down to strongly depleted values suggests high input of meltwater from the neighboring Nyainqentanglha mountain range at an early stage of deglaciation, where Lake Nam Co still was very small and shallow. If the winter precipitation would have been increased, a thick and long-lasting snow cover would suppress the anyhow sparse terrestrial vegetation and not even meltwater during summer could provide enough moisture to support their n-$C_{29/31}$ biosynthesis. In consequence, due to the low amount of the terrestrial biomarker, no detailed isotopic information on terrestrial hydrologic conditions could be gained for this timeframe and even further. The first occurrence of alkane cluster I supports the appearance of periodically smaller erosion events limited to meltwater streams.

Period 3 (22.5–22.0 cal. kyr BP)

Since the lake reached its first main freshwater pulse, the climatic situation in period 3 shifted to the driest and coldest conditions within the investigated interval. Limited production of OM as a result of cold climate conditions is also reflected by low amounts of n–alkanes within the sediments, inhibiting the reliable determination of the δD of aquatic and terrestrial biomarkers for most of this period. The pronounced reduction of terrestrial OM input via lowered erosion and/or productivity is inferred by missing C_{31} n-alkanes. The major input was derived by aquatic organisms reflected by the cluster II. Still low TOC/TN ratios and decreased $\delta^{15}N$ values point to a further dominance of aquatic OM from likely emergent macrophytes. However, decreasing amounts of TOC and TN may reflect reduced intra–lake productivity and a reduced deposition of OM maybe due to climatic cooling.

Period 4 (22.0–21.6 cal. kyr BP)

During period 4, the starting trend to a higher TOC content and therefore higher TOC/TN ratios as well as decreased $\delta^{13}C_{org}$ and $\delta^{15}N$ values indicating enhanced input of organic material. Additionally, lowest amounts of even–numbered n–alkanes and consequently maximum CPI values suggest the input of fresh material. This increased input is probably related to higher rates of precipitation indicated by the beginning trend to depleted δD_{n-C29}

values at 22.0 cal. kyr BP. Changes in the lake water isotopic signal ($\delta D_{n–C23}$) are not significant, reflecting a rather attenuated response level. However, increasing TOC contents in combination with decreasing amounts of n-alkanes seems to be inconsistent. Nevertheless, the lowest amounts of $n–C_{23}$ and of $n–C_{29}$ indicate rather cold conditions, which should have reduced biomass productivity in the lake and the catchment.

Period 5 (21.6–21.4 cal. kyr BP)

Period 5 is characterized by the highest amounts of even–numbered n–alkanes as well as high $n–C_{31}$ input, originating from degraded soil and dung OM. The significant contribution of reworked material lowers the CPI value to ~1 (cluster I). Low CPI values are in accordance with decreasing $\delta^{15}N$ values, reflecting a continuously rising supply of terrestrial OM to the lake. This likely reflects erosional processes in the catchment, probably triggered by enhanced runoff due to increased precipitation and/or melting glaciers. As the $\delta D_{n–C23}$ values rather fluctuate around the mean and simultaneously $\delta D_{n–C29}$ values continue decreasing, enhanced precipitation generating erosion events under warmer and wetter conditions apparently started at 21.6 cal. kyr BP, which is in agreement with increased input of microbially degraded soil material. Since the terrestrial vegetation is yet not fully developed, precipitation unhindered erodes soil material, which is visible in increased sediment accumulation rates (Supp. Figure 7 L)

Period 6 (21.4–21.0 cal. kyr BP)

The significant environmental change initiated during period 5 is carried on in period 6 reflected by the rising amount of the aquatic $n–C_{23}$. This strong increase in biomass production of mainly aquatic macrophytes ($n–C_{23}$), likely induced by enhanced mixing and nutrient supply by freshwater input (Slemmons et al. 2013) can be supported by rather depleted $\delta D_{n–C23}$ values and strong enriched $\delta^{13}C$ values. An enrichment in $\delta D_{n–C29}$ values show that the isotopic composition of precipitation changed to dryer conditions. Consequently, the low $\delta D_{n–C23}$ values are likely related to inflow of glacial meltwater rather than to the input of isotopically light rainwater. Additionally, input by terrestrial n-C_{31} decreased even to missing data.

Period 7 (21.0–20.9 cal. kyr BP)

Considerable high variability in almost all proxies suggests a system with pronounced climate variability during the short period 7. $\delta^{13}C_{org}$, $\delta^{15}N$ and TOC reached maxima values for $\delta^{13}C_{org}$ and TOC as well as minimum values for $\delta^{15}N$ during this period at 20.9 cal. kyr BP. This may indicate rather high intra–lake biomass productivity, dominating the contribution to sedimentary OM, and high nutrient availability due to additional input of organic material. Thus this period can be characterized by climate conditions similar to

those of period 1. In addition, enriched $\delta D_{n–C29}$ values also suggest a shift back to arid conditions with decreased amounts of precipitation.

Although the onset of mountain glacier retreat on the Tibetan Plateau is generally believed to have occurred only between 16 and 18 ka BP, our results indicate that first retreat events likely occurred already at 23 cal. kyr BP in the Nam Co region. This might be related to increasing temperatures, which most likely have affected glaciers in the Nyainqentanglha mountain range south of Nam Co. Meltwater runoff was probably confined to river channels as the input of reworked soil OM was rather limited, illustrated by moderate CPI values. Since the catchment vegetation was not fully developed, precipitation influenced sediment accumulation rates to higher extent during the LGM. Changing climatic conditions like temperature and precipitation fluctuations are displayed by cyclic variations of *n*–alkane amounts during this interval and initiated the gradual formation of a larger lake.

Regional palaeoclimate comparison

The Nam Co sediment record can be compared with some palaeoclimate relevant records like Greenland ice cores, Hulu Cave stalagmites (east China), Lake Qinghai sediments (northern Tibetan Plateau) and the East Arabian Sea sediments to reveal the connection of the regional climate evolution on the Tibetan Plateau to changes at the northern hemisphere (Supp. Figure 8). Primary driving force for long–term climatic variations is supposed to be solar irradiation forced by Earth–orbital periods, which influences global atmospheric circulation. The main driving air mass at Nam Co during the LGM and also the one responsible for abrupt climate changes on the northern Tibetan Plateau (e.g. Lake Qinghai) is the mid–latitude Westerlies wind system, which is directly controlled by the Atlantic meridonal overturning circulation (Sun et al. 2012). However, changes in the atmospheric circulation on centennial– to millennial time scales are not explainable with solar irradiation changes (Yao et al. 2001). Two of such relatively abrupt circulation changes during the LGM caused the cold Heinrich-2 event (H-2) and the subsequent warm Greenland Interstadial 2 (GI–2) (Supp. Figure 8). The cold/dry and dust–rich H-2 event is clearly recorded between 23.5 and 24.3 cal. kyr BP in the NGRIP, GRIP and GISP2 Greenland ice core records (Rasmussen et al. 2008) as well as in Hulu Cave between 23.6 and 24.4 cal. kyr BP (Wang et al. 2001), in Lake Qinghai sediments between 23.5 and 24.1 cal. kyr BP (An et al. 2012b) and in the East Arabian Sea Surface Temperature (SST) from 23.3 to 24.2 cal. kyr BP (Mahesh and Banakar 2014). This indicates an intra–hemispheric coupling of climatic events in Greenland and Asia, which can be explained by intensified Westerlies as a consequence of a cold and ice–covered North Atlantic Ocean (An et al. 2012b). It is possible that at ~23.5 cal. kyr BP the shallow Nam Co, which was characterized by a highly fluctuating stage (period 1), had been influenced by the cold and dry H-2 event. However, since the general climate conditions at the shallow Nam Co during that time were anyway dry and cold, evidences from compound specific data do not support

the H-2 onset. The subsequent warmer GI–2 is also visible in the other records starting at 23.5 ± 0.2 cal. kyr BP. During the period 2 a significant response is indicated by depleted δD_{n-C23} values, indicating increased meltwater input due to warmer conditions. The impact of the warmer GI-2 event was less severe on the sparse catchment vegetation at the possible background of too short thawing seasons and therefore regeneration phases. Previous studies (Yao et al. 1997) suggest, that the Tibetan Plateau and hence also the Nam Co region reacts more sensitively to climate changes than Greenland. However, a second freshwater period was detected at Nam Co, starting at 22.0 cal. kyr BP in the middle of the colder Greenland Stadial 2c event (GS-2c), which is in slight agreement with the GISP2 and GRIP records. After reaching a certain threshold of energy in the system, the amount of precipitation or temperature affects the input of nutrients and/or melting. With this promotion Nam Co went through several developmental stages from glacial condition to a deglaciation stage. These freshwater periods at Nam Co could be precursors for the onset or strengthening of the IOSM during the LGM. Abruptly increasing temperatures would have reduced the snow cover on the Tibetan Plateau and therefore increase surface temperature and radiative heating. Consequently, if warming of the Indian Ocean was synchronous with the deglaciation of continental ice sheets, the abrupt freshwater event at Nam Co could be a sign of an early deglaciation pulse on the southern Tibetan Plateau probably forced by weakening of the winter monsoon and a stronger summer monsoon.
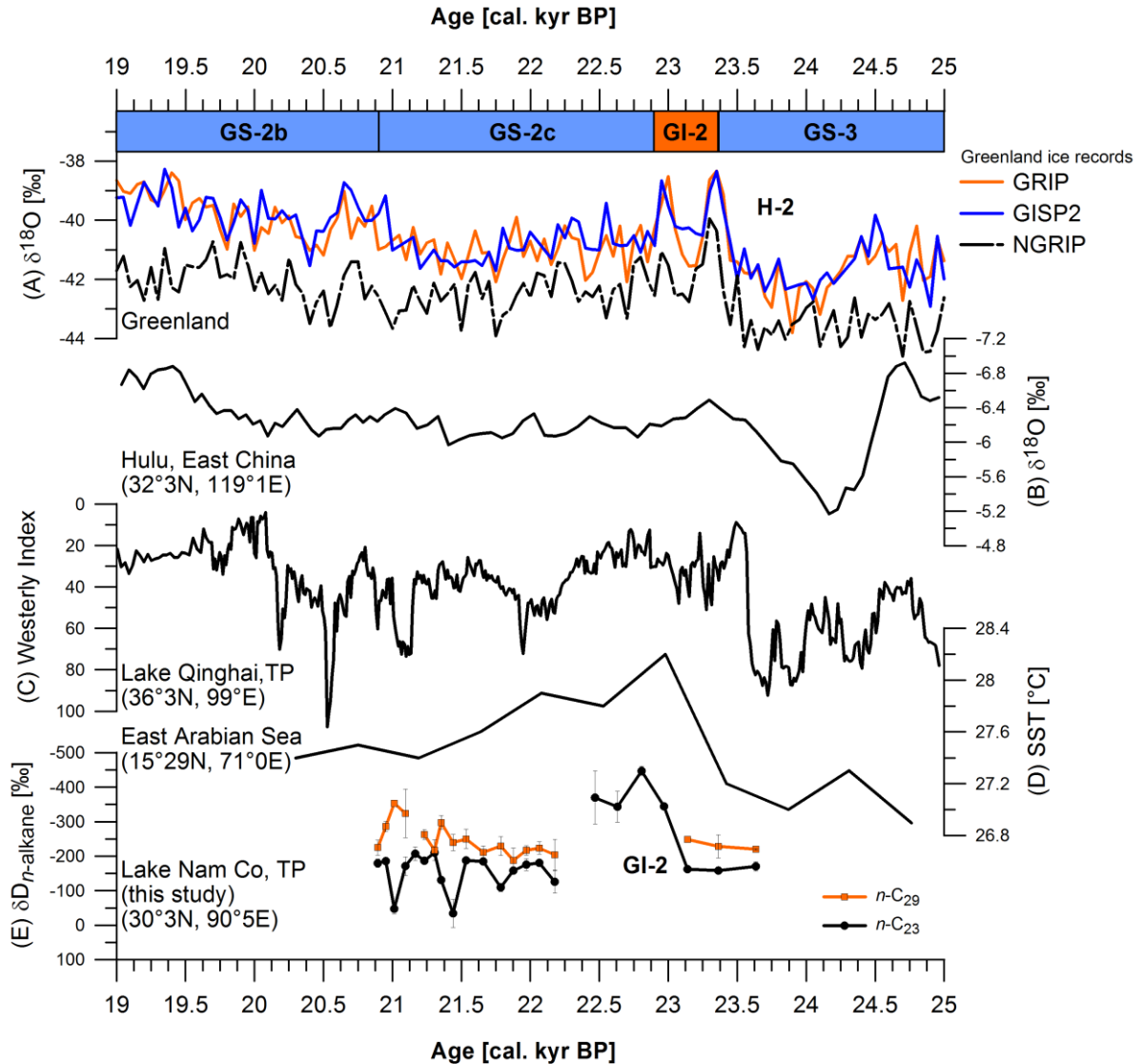
Supp. Figure 8: Comparison of proxy records from different locations between 19 and 25 cal. kyr BP. Greenland Stadials (GS-2b, GS-2c) and Greenland Interstadial 2 (GI-2) following Lowe et al. (2008). Heinrich-2 event (H-2) is marked following Moreno et al. (2010). (A) δ^{18}O from three Greenland ice cores matched by Rasmussen et al. (2008): GRIP (Johnsen et al. 1997), GISP2 (Stuiver and Grootes 2000) and NGRIP (Andersen et al. 2004), (B) δ^{18}O of stalagmites from Hulu Cave, eastern China (Wang et al. 2001), (C) Lake Qinghai Westerlies climate index from flux of > 25 μm sediment fraction (An et al. 2012b), (D) Sea surface temperature calculated from Mg/Ca ratios of planktic foraminifer *G. sacculifer* in the East Arabian Sea (Mahesh and Banakar 2014), (E) δD_{n-C23} and δD_{n-C29} of *n*–alkanes of sediment core NC 08/01 from Nam Co, southern–central Tibet (this study).

Conclusions

The sediment record from Nam Co, southern–central Tibetan Plateau, reflects typical early stages of deglaciation in a climate sensitive high-altitude region during the LGM. Evidences for two distinct freshwater periods were found using stable hydrogen isotope composition, n–alkane distribution and concentration as well as bulk sediment TOC, TN, $\delta^{13}C_{org}$ and $\delta^{15}N$ composition between 23.7 and 20.9 cal. kyr BP. Lake system and catchment development as response to intra-hemispheric climate events were described by seven reconstructed periods at Nam Co. Additionally, this study aimed at investigating whether Nam Co was continuously ice–covered during the LGM, and, if not, which factors provided thawing energy. Compared to the Holocene, colder and dryer conditions during the LGM strongly suppressed terrestrial vegetation. Periodically erosion events led to highest sediment accumulation rates until catchment growth prevented for excessive erosion to the shallow Nam Co. Major OM was produced by aquatic organisms, recording isotopic signal of lake water. Coldest conditions are inferred between 22.5 and 22.0 cal. kyr BP. However, even during this period ice cover was temporarily interrupted by short thawing seasons during the summers. High amounts of even numbered n–alkanes indicate increased erosional input of soil material into the lake between 21.6 and 21.4 cal. kyr BP. More obvious environmental changes occurred after 23.1 cal. kyr BP with the influence of the warmer Greenland Interstadial-2 event leading to strongly depleted δD_{n-C23} values, while δD_{n-C29} values remained rather enriched. This likely indicates meltwater inflow from the Nyainqentanglha mountain range. A second freshwater period induced by increased precipitation was detected by changes in n-alkane distribution and depleted terrestrial δD_{n-C29} values starting at 22.0 cal. kyr BP. This period is characterized by several developmental stages of deglaciation in the middle of the colder Greenland Stadial 2c event. On millennial time–scale, environmental changes are supposed to have been caused by a slightly intensified IOSM and attenuated Westerlies during winter. Apparently, the first evidence of deglaciation at Nam Co was preceded by at least two earlier glacier melting phases between 23.1 and 21.1 cal. kyr BP within the warmer Greenland Interstadial 2 and colder Greenland Stadial 2c events.

Supplement Figures
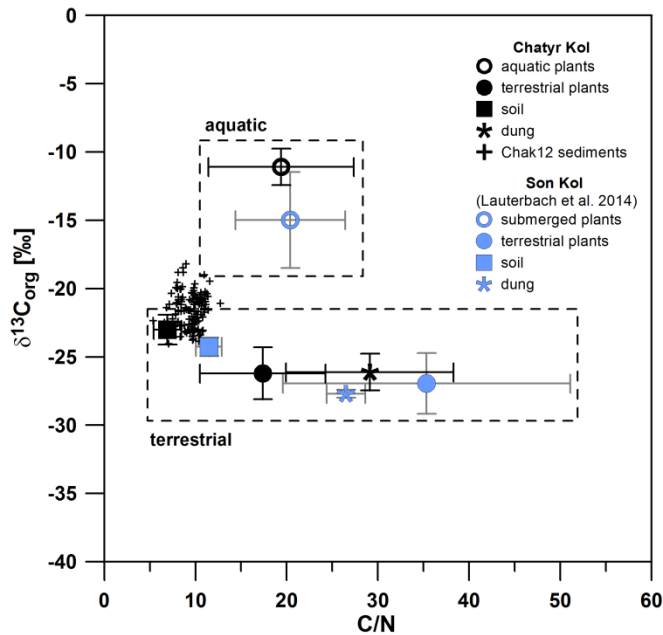
Supp. Figure 9: Geochemical and isotopic signatures $\delta^{13}C_{org}$ and C/N of the Chatyr Kol sediments (+) in comparison with those of modern organic materials collected from Son Kol (blue symbols) and Chatyr Kol (black symbols) lake and catchment.
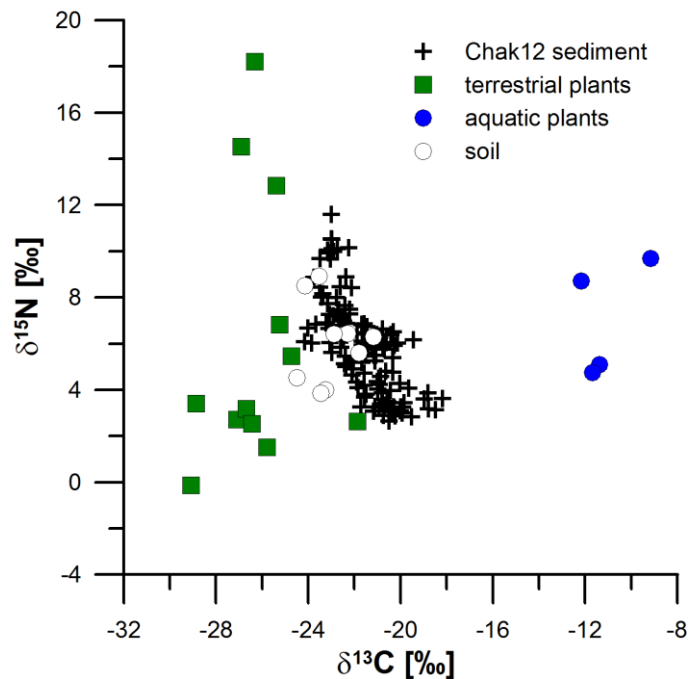
Supp. Figure 10: Isotopic signatures $\delta^{15}N$ and $\delta^{13}C_{org}$ of Chatyr Kol sediments in comparison with those of modern catchment samples.

Supplement Tables

Supp. Table 1: Relevant Glaciers and Snowfields in the catchment of Lake Chatyr Kol based on the World Glacier Inventory by WGMS and NSIDC updated 2012.

ID	Latitude N	Longitude E	Range	Class	Form	Source nourishment	max Elevation [m]	mean Elevation [m]	min Elevation [m]	Snowline Elevation [m]	Snowline Date [year]	Total area [km²]	max Length [km]	Orientation Accumulation
1	40.88	75.56	At Bashy	Valley Glacier	Simple Basin	Snow	4,320	4,020	3,720	4,320	1962	0.6	1.7	N
2	40.87	75.56	At Bashy	Mountain Glacier	Niche	Snow	4,360	4,190	4,020			0.1	0.4	N
3	40.85	75.54	At Bashy	Mountain Glacier	Niche	Snow	4,280	4,130	3,980			0.1	0.4	NE
4	40.85	75.53	At Bashy	Mountain Glacier	Niche	Snow	4,400	4,250	4,100			0.2	0.7	N
5	40.84	75.53	At Bashy	Mountain Glacier	Cirque	Snow	4,320	4,095	3,870	4,120	1962	0.4	1	N
6	40.83	75.51	At Bashy	Mountain Glacier	Niche	Snow	4,320	4,130	3,940			0.2	0.6	NW
7	40.83	75.5	At Bashy	Mountain Glacier	Cirque	Snow	4,320	4,100	3,880	4,040	1962	0.4	0.9	N
8	40.82	75.5	At Bashy	Mountain Glacier	Niche	Snow	4,280	4,120	3,960			0.2	0.6	NW
9	40.82	75.47	At Bashy	Mountain Glacier	Niche	Snow	4,280	4,040	3,800			0.3	0.8	N
10	40.81	75.47	At Bashy	Mountain Glacier	Cirque	Snow	4,320	4,140	3,960			0.2	0.6	NW
11	40.81	75.46	At Bashy	Mountain Glacier	Simple Basin	Snow	4,360	4,140	3,920			0.5	1.1	N
12	40.81	75.46	At Bashy	Mountain Glacier	Cirque	Snow	4,510	4,235	3,960			0.4	1.1	N
13	40.81	75.45	At Bashy	Mountain Glacier	Niche	Snow	4,340	4,150	3,960			0.1	0.5	N
14	40.79	75.44	At Bashy	Snowfield	Niche	Snow	4,120	4,080	4,040			0.1	0.2	N
15	40.78	75.39	At Bashy	Mountain Glacier	Niche	Snow	4,080	3,960	3,840			0.2	0.4	NW
16	40.77	75.36	At Bashy	Snowfield	Niche	Snow	4,080	3,910	3,740			0.2	0.3	N
17	40.77	75.36	At Bashy	Mountain Glacier	Niche	Snow	4,360	4,160	3,960			0.1	0.4	N
18	40.77	75.35	At Bashy	Mountain Glacier	Cirque	Snow	4,280	4,110	3,940			0.2	0.5	N
19	40.47	75.15	Torgurat	Valley Glacier	Simple Basin	Snow	4,400	4,220	4,040			1.4	2	N
20	40.87	75.57	At Bashy	Valley Glacier	Simple Basin	Snow	4,400	4,200	4,000	4,140	1967	0.8	1.2	SE
21	40.88	75.58	At Bashy	Valley Glacier	Simple Basin	Snow	4,460	4,280	4,100	4,200	1967	1	1.3	SE
22	40.88	75.6	At Bashy	Valley Glacier	Simple Basin	Snow	4,760	4,430	4,100	4,210	1967	1	1.5	SE

Supp. Table 2: Lake site characteristics of global transect study from Kyrgyzstan (this study), Tibetan Plateau (Günther et al. 2013), Europe (Sachse et al. 2004) and Cameroon (Garcin et al. 2012). Site codes are displayed in

Figure 20.

reference	area	site code	MAT [°C]	MAP [mm yr⁻¹]	altitude [m a.s.l.]	water depth [m]	lake area km²	δD n-C₂₃ [‰]	δD n-C₂₉ [‰]	δD29-23 [‰]	ε C₂₃/source [‰]	ε C₂₉/source [‰]	δDlake [‰]	δDmet [‰]
Günther et al. 2013	Tibet	Nam Co	0	281	4718	99	1962	-173	-221	-48	-107	-111	-74.1	-123.9
Günther et al. 2013	Tibet	Tangra Yumco	0.7	315	4718	213	835	-184	-211	-27	-116	-81	-77.1	-141.6
Günther et al. 2013	Tibet	Taro Co	1	190	4549	95	450	-192	-219	-27	-131	-109	-70	-123.7
Günther et al. 2013	Tibet	Kunggyu Co	3.6	125	4570	25	50	-182	-239	-57	-128	-95	-62.2	-158.5
Günther et al. 2013	Tibet	Songmuxa Co	-1.5	70	5070	12	23	-135	-196	-61	-84	-142	-55.4	-63.5
Günther et al. 2013	Tibet	Lungmu Co	-1.5	70	4798	64	100	-80	-209	-129	-63	-154	-17.9	-64.9
this study	Kyrgyzstan	Chatyr Kol	-5.6	237	3545	20	159	-135	-153	-18	-125	-131	-11.0	-76
this study	Kyrgyzstan	Son Kol	-1.85	382	3016	13	283	-113	-179	-66	-81.7	-174	-35.0	-79
Sachse et al. 2004	SWE	KEI	-2	450	428	2	0.01	-234	-230	4	-136	-130	-96.6	-114.1
Sachse et al. 2004	FIN	SOD003	-0.3	529	178	4.7	0.01	-235	-215	20		-118	-103.7	-103.9
Sachse et al. 2004	FIN	SOD007	-0.3	529	293	10.7	0.36	-268	-227	41	-182	-136		-105.2
Sachse et al. 2004	FIN	HYY	3.5	640	149	13.3	0.84	-218	-205	13	-138	-124	-81.1	-92.9
Sachse et al. 2004	FIN	SYR			156	8.5	0.3	-207	-207	0	-128	-127	-86.5	-91.4
Sachse et al. 2004	FIN	LAM	3.6	619	151	44.9	13.42	-272	-205	67	-199	-125	-73.7	-91.3
Sachse et al. 2004	GER	HZM	10.5	1042	436	24	0.058	-225	-198	27	-175	-147	-47.1	-60.1
Sachse et al. 2004	ITA	MEZ	13.1	1030	466	30.4	0.445	-164	-167	-3	-124	-128	-3.5	-45.7
Garcin et al. 2012	Cameroon	MORA	27.2	540	438	1.5	0.1	-165	-170	-5	-175	-146	12.4	-27.6
Garcin et al. 2012	Cameroon	RHUM	22.7	970	1028	3	1.3	-203	-167	36	-203	-145	-0.7	-26
Garcin et al. 2012	Cameroon	MAMG	26.3	1560	322	5	0.6	-115	-156	-41	-120	-141	5.6	-17.9
Garcin et al. 2012	Cameroon	TIZO	21.9	1450	1155	45	7	-163	-155	8	-182	-142	22.8	-15.6
Garcin et al. 2012	Cameroon	TABE	21.7	1450	1161	62	10	-156	-167	-11	-166	-154	11.4	-15.6
Garcin et al. 2012	Cameroon	ASSO	23	1740	896	3	141	-120	-154	-34	-116	-141	-4.7	-14.9
Garcin et al. 2012	Cameroon	MANE	16	2700	1911	165	35	-160	-185	-25	-155	-152	-6.1	-60.1
Garcin et al. 2012	Cameroon	DEBU	25.7	11700	70	16	7	-154	-153	1	-147	-146	-8.7	-8.4
Garcin et al. 2012	Cameroon	OSSA	26.3	2900	17	6	3700	-191	-147	44	-182	-136	-11.9	-12.6

MAT = mean annual temperature
MAP = mean annual precipitation

Selbstständigkeitserklärung

Ich erkläre, dass ich die vorliegende Arbeit selbstständig und unter Verwendung der angegebenen Hilfsmittel, persönlichen Mitteilungen und Quellen angefertigt habe.

Ort, Datum

Roman Witt